Vietnam National University Ho Chi Minh City

University Of Sciences

Faculty of Physics and Engineering Physics

Department of Oceanology, Meteorology and Hydrology

Thesis

Topic:

ANALYSIS OF THE IMPACT OF EQUATORIAL ROSSBY WAVE ON TROPICAL CYCLONE ACTIVITY IN NOTHERN WEST PACIFIC OCEAN

Student: DANG DONG PHA

Advisor: MSc. LE THI XUAN LAN

Reviewer: Prof. VO LUONG HONG PHUOC

HO CHI MINH CITY, 07/2019

ACKNOWLEDGEMENT

I would like to sincerely express my gratitude to Master Le Thi Xuan Lan for dedicating time to guide and assist me in completing this thesis. The knowledge and experience that she has imparted are valuable assets for my future.

I am extremely grateful to the professors of the University of Natural Sciences, especially those of the Department of Oceanography, Meteorology and Hydrology, for imparting knowledge and lessons on character throughout my four years of study.

I would like to thank my family for always creating the most favorable conditions and supporting me.

I thank my classmates of class 15HDH for accompanying and helping me in the learning process.

Sincere thanks to all!

ABSTRACT

ANALYSIS OF THE IMPACT OF EQUATORIAL ROSSBY WAVE ON TROPICAL CYCLONE ACTIVITY IN NORTHERN WEST PACIFIC OCEAN

Equatorial Rossby wave plays a crucial role in tropical cyclone activity in the Northern West Pacific basin. The study of these equatorially trapped, tropical waves is fundamental to understand tropical dynamics and tropical cyclone genesis. In the Pacific typhoon season 2018, there were 29 tropical storms and typhoons which were investigated to evaluate the effect of equatorial Rossby wave on them by OLR maps and diagrams, synoptic charts as well as satellite images. In addition, Madden – Julian oscillation and El Nino Southern Oscillation are also used to analyze their contributions on tropical cyclones. The results show that the impact of equatorial Rossby waves on tropical cyclones genesis in the cases of typhoon Sanba and Pabuk.

TABLE OF CONTENTS

LIST OF FIGURES

LIST OF TABLES

LIST OF ABBREVIATIONS

^{0}E	East longitude
^{0}N	North latitude
^{0}S	South latitude
^{0}W	West longitude
TD	Tropical depression
BoM	Bureau of Meteorology
ENSO	El Nino – Southern Oscillation
JMA	Japan Meteorological Agency
JTWC	Joint Typhoon Warning Center
Kts	Knots
MC	Maritime Continent
MIT	Massachusetts Institute of Technology
MJO	Madden – Julian Oscillation
NOAA	National Oceanic and Atmospheric Administration
OLR	Outgoing Longwave Radiation
RMM	Real-time Multivariate MJO Index
WMO	World Meteorological Organization
TC	Tropical cyclones

INTRODUCTION

The Pacific Ocean is the largest ocean on the planet, bordering Asia, America, Australia, and the Southern Pole. The Northwest Pacific is considered the largest typhoon hotspot on the globe, with many devastating typhoons forming in the region. The 2018 Northwest Pacific typhoon season was more active than usual with 29 typhoons, half of which were major and 7 were super typhoons. The world witnessed a significant number of typhoons affecting Japan and China, while Vietnam was hit by 13 typhoons and tropical depressions causing tens of thousands of billions of dongs in damages. Therefore, monitoring the activity of tropical cyclones in the East Sea and the Northwest Pacific is of great importance in predicting and mitigating the impact of natural disasters in Vietnam.

Thanks to the advancement of science and technology and understanding of the global climate system, scientists around the world can predict storms on a seasonal scale. Seasonal storm prediction is carried out through statistical, dynamic, or a combination of statistical and dynamic methods. Many large atmospheric research centers have applied these methods to the Northwestern Pacific Ocean. Examples of statistical methods include Hong Kong University (China) and the Tropical Storm Warning Center (UK). Dynamic methods are applied at the European Centre for Medium-Range Weather Forecasts (ECMWF) and the International Climate and Society Institute (USA) [17]. In Vietnam, seasonal storm forecasting is mainly based on statistical methods combined with large-scale atmospheric circulation analysis, such as El Nino-Southern Oscillation (ENSO).

The Northwestern Pacific Ocean is influenced by large-scale oceanic and atmospheric circulations, including equatorial waves such as Rossby waves, which propagate westward due to the Earth's rotation. These slow-moving waves often lead to prolonged weather patterns. Recent studies have explored the interaction between Rossby waves and tropical cyclone activity, and have identified Rossby waves as the second most common factor in the formation of tropical cyclones in the Northwestern Pacific, after the monsoon. However, there is still limited research on this topic in Vietnam, which is why the chosen topic is to analyze the impact of Equatorial Rossby waves on tropical cyclone activity in the Northwestern Pacific.

This study aims to initially explore the impact of Rossby waves on the formation of tropical cyclones through the long-wave radiation field in different phases. The research results may serve as a basis for further in-depth analysis in the future. The thesis consists of three chapters:

- Chapter I: Overview of the Rossby waves and tropical cyclones
- Chapter II: Overview of the study area and methodology
- Chapter III: Results.

CHAPTER I. OVERVIEW OF THE EQUATORIAL ROSSBY WAVES AND TROPICAL CYCLONE

I.1. Overview of the Equatorial Rossby waves

I.1.1. Brief history of discovery

Rossby waves, also known as planetary waves, are a natural phenomenon in both the atmosphere and the ocean due to the effect of the Earth's rotation. They were first discovered by the Swedish meteorologist Carl-Gustaf Arvid Rossby.

Rossby's research in the 1930s and 1940s originated from a long-range forecasting project at the Massachusetts Institute of Technology (MIT) in collaboration with the US Weather Bureau. The project involved weekly drawing of 7-day and 5-day mean sea-level pressure charts in the Northern Hemisphere, as well as entropy contours and pressure at 3 km altitude in North America. These mean charts assumed that the averaging process, at least in part, eliminated noise in pressure distributions associated with fast-moving waves. The charts were dominated by large pressure centers, showing the statistical position of anticyclones and cyclones at sea level. Although these large pressure centers had been known for a long time, it was not until the 1930s that high-quality data was available to allow a systematic study of their relationship to westward propagating long waves in the upper layers. Rossby clarified the dynamics of planetary waves and found a simple formula for propagation speed, a result of years of statistical analysis of charts at MIT by him and his colleagues.

In 1945, Rossby made a breakthrough in the development of planetary wave theory. Instead of considering simple harmonic waves, he focused on wave trains with acceptable amplitude, period, and wavelength distribution. Assuming the number of wave crests and troughs is conserved, he derived general equations to determine how energy distribution and wavelength should change over time. Rossby showed that these changes are controlled by group velocity, especially in the case of planetary waves, where the energy of a local source can be transmitted downstream at a super-infinite speed.

In the late 1940s, the first electronic computers were invented, and this was also a time when planetary wave experts did not make significant progress due to the complexity of the atmosphere. In 1949, Charney and Eliassen proposed a one-dimensional Rossby wave model synthesized from initial data. Although this was a small step, it surpassed the threshold of nonlinear equations [4].

I.1.2. The theory of Equatorial waves

The shallow water equation system governing independent vertical motion of a layer of incompressible, homogeneous fluid on a rotating sphere is also known as the Laplace's tidal equations. The shallow water equation system can be derived from the mathematical separation of horizontal and vertical elements that vary over time in the flow stream of the complete primitive equations.

Matsuno examined the linearized, inviscid shallow water equation system in a state of rest [2]. The Coriolis coefficient f is assumed to be linearly proportional to the distance from the equator ($f = \beta y$). The equations include:

$$\begin{cases} \dfrac{\partial u_l}{\partial t} - \beta y v_l = -\dfrac{\partial \phi_l}{\partial x} & (1.1) \\ \dfrac{\partial v_l}{\partial t} + \beta y u_l = -\dfrac{\partial \phi_l}{\partial y} & (1.2) \\ \dfrac{\partial \phi_l}{\partial t} + g h_e \left(\dfrac{\partial u_l}{\partial x} + \dfrac{\partial v_l}{\partial y} \right) = 0 & (1.3) \end{cases}$$

with u_l and v_l being the wind speed in the eastward and northward directions, ϕ_l being the geopotential, g being the acceleration due to gravity, and h_e being the depth of the unstratified fluid layer, equations (1.1) and (1.2) are momentum equations, equation (1.3) is the mass continuity equation, linking the changes in geopotential to the stratification. The subscript l denotes the three-dimensional atmospheric motion.

The system of equations has a solution of the form:

$$\begin{pmatrix} u_l \\ v_l \\ \phi_l \end{pmatrix} = \begin{pmatrix} \hat{u}(y) \\ \hat{v}(y) \\ \hat{\phi}(y) \end{pmatrix} \exp\left[i(kx - \omega t)\right] \quad (1.4)$$

where k is the zonal wavenumber and ω is the frequency.

Rearranging the terms and substituting yields a second-order partial differential equation in $\hat{v}$:

$$\frac{d^2\hat{v}}{dy^2} + \left(\frac{\omega^2}{gh_e} - k^2 - \frac{k}{\omega}\beta - \frac{\beta^2 y^2}{gh_e}\right)\hat{v} = 0 \qquad (1.5)$$

The solution of equation (1.5) decays with increasing distance from the equator, so the constants in the second term in the parentheses must satisfy:

$$\frac{\sqrt{gh_e}}{\beta}\left(\frac{\omega^2}{gh_e} - k^2 - \frac{k}{\omega}\beta\right) = 2n + 1, \qquad n = 0, 1, 2, \ldots \qquad (1.6)$$

Equation (1.6) describes the relationship between ω and k for each integer value of n, and thus determines the meridional dispersion relation of the waves.

I.1.3. Rossby wave in the atmosphere

According to the National Weather Service of the United States, Rossby waves in the atmosphere are formed as a result of the distribution of Earth's geography. Rossby waves transport heat from the tropics to the poles and bring cold air from the poles to the tropics to maintain the balance of the atmosphere. They also help determine the location of jet streams and mark the path of surface low-pressure systems. The slow movement of the waves often leads to prolonged weather patterns. In the atmosphere, there are two main types of Rossby waves: gravity waves and planetary waves [20].

I.1.3.1. The gravity Rossby wave

The vortices centered on the equatorial axis of the central Pacific Ocean correspond to gravity waves, but when the abnormal waves propagate westward, they move away from the vortices and then head northwest towards the Philippines. These chains are often observed from disturbances originating from western Pacific equatorial waves. Gravity waves are relatively fast and dominate the upper level of the atmosphere, especially the lower layer. Gravity waves also contribute to the formation of clockwise vortices in the Pacific Ocean. Thanks to satellite cloud images, gravity waves can be identified by the cumulonimbus clusters formed asymmetrically across the equator in the central and western Pacific regions [14].

I.1.3.2. The Equatorial Rossby wave

Equatorial Rossby waves create alternating high and low pressure systems that are symmetric across the equator. Faster winds are associated with Rossby waves nearer to the equator. As a result, in both hemispheres, there is a persistent low-level divergence between the eastern low pressure and the western high pressure, leading to descending air and fair weather in these regions. Conversely, there is a low-level convergence between the eastern high pressure and the western low pressure, leading to convection. Equatorial Rossby waves propagate from east to west, at speeds of 10-20 m/s for dry waves and 5-7 m/s for moist waves. The distance between adjacent gyres varies from 4000 to 10000 km. Equatorial Rossby waves can be detected through satellite cloud imagery, with a low pressure gyre in the Northern Hemisphere and a low pressure gyre in the Southern Hemisphere symmetric across the equator. In some cases, both low pressure gyres can develop into tropical cyclones and eventually become twin typhoons. Figure I.2 illustrates the appearance of equatorial Rossby waves through a pair of symmetric convective cloud clusters across the equator in Southeast Asia and the central Pacific on October 7, 2002 at 00 UTC.

I.1.4. Rossby wave in the ocean

Unlike ocean surface waves, Rossby waves are enormous waves that ripple through the ocean, spanning hundreds of kilometers and traveling westward. The large scale of Rossby waves significantly impacts Earth's climate. Along with sea level rise and the influence of El Nino, Rossby waves in the ocean contribute to high tides and flooding in some coastal areas around the world.

Rossby waves have a fairly complex motion. The horizontal velocity of Rossby waves and the time it takes for them to travel along the ocean depend on latitude. In the Pacific Ocean, waves at low latitudes (near the equator) can take months to several years to complete their journey. Waves formed farther from the equator can take 10 to 20 years to move. The vertical motion of Rossby waves is small near the surface and larger at depth. The changes in vertical motion are quite abrupt: the normal motion of water near the surface is around 10 cm, while at depth this number is 1000 times greater. In other words, for a wave with a height of 10 cm at the ocean surface, the height of the wave at depth can

be up to 100 m. Because the vertical motion of Rossby waves at the surface is quite small and cannot be observed with the naked eye, scientists must use satellites to detect wave patterns [20].

I.2. Overview of Tropical cyclone

I.2.1. Definition and classfication

A tropical cyclone (TC) is a low-pressure system with a moderate scale, developing and operating mainly over tropical waters, not accompanied by fronts, and with the strongest winds near the center. TCs have a counterclockwise circulation system, characterized by closed isobars that almost encircle a low-pressure center.

The World Meteorological Organization (WMO) classifies tropical cyclones based on the average wind speed. Average wind speed is the average speed of wind blowing over 10 minutes (surface wind average) or the average wind speed over 1 minute at a height of 10 m or estimated according to the Beaufort scale. Based on this definition, tropical cyclones are divided into:

- Tropical depression: a TC with the maximum sustained winds of 33 knots (17.1 m/s, corresponds to level 6 - 7) or less near the center.
- Tropical storm: the maximum sustained winds of 34 – 47 knots (17.2 – 24.4 m/s, level 8 – 9) near the center.
- Severe tropical storm: the maximum sustained winds of 48 – 63 knots (24.5 – 32.6 m/s, level 10 - 11) near the center.
- Typhoon: the maximum sustained winds of 64 knots (more than 32.7 m/s, above level 12) or more near the center.

In addition, small-scale synoptic tropical cyclones without fronts develop over tropical or subtropical ocean areas with increased convection and light winds at the surface, known as tropical disturbances [10].

I.2.2. Genesis conditions

In 1956, Palmen proposed three basic conditions for the formation of a storm:

a) A storm can only form and develop over open oceans and seas with sea surface temperatures greater than 26.5°C. At that point, the air mass near the surface can rise to a height of about 10-12 km, becoming warmer and more humid than the surrounding environment. In addition, higher temperatures ensure a strong evaporation rate, which provides latent heat (the energy released from water vapor in the air) for the storm system.

b) Unlike other disturbances, the rotating motion is a fundamental part of the circulation of a typhoon. Therefore, the Coriolis parameter must have a sufficiently large value to create rotation. A typhoon cannot form and develop in the region between 5°S-5°N, where the Coriolis force is too weak to balance the pressure gradient force of the low-pressure areas to create counterclockwise rotation.

c) The weak vertical wind shear is necessary to ensure the initial concentration of moist air into the developing storm area during the early stages of a storm formation. In the Northwestern Pacific, the smallest value of the meridional wind shear is less than 5 knots over a very broad range from 25°N to 35°N. In other areas, the wind shear is larger, sometimes reaching 30 to 40 knots.

In addition to the three conditions for the formation of a typhoon, Riehl (1984) also added two conditions necessary for the formation of a typhoon, which are the existence of turbulence in the surface layer of the atmosphere and wind shear in the upper layer above the turbulence in the surface layer.

The presence of a high-altitude wind shear over the low-level turbulence causes mixing and convergence in the surface layer of the atmosphere. This explains the interaction between cumulus convection and large-scale motion. The area of cumulus clouds in the turbulence heats the air by releasing latent heat of condensation. This heating reduces surface pressure and enhances low-level convergence due to mixing in the surface layer of the atmosphere. This convergence creates towering cumulus clouds that further increase latent heat of condensation and further reduce surface pressure. These processes repeat and reinforce each other, promoting the development of a typhoon.

I.2.3. Tropical cyclone structure

Tropical cyclone is a mesoscale system with a very complex structure and undergoes different stages of development. Generally, the meteorological characteristics of a mature storm are described as follows: [1]

I.2.3.1. Pressure field

When a TC reaches its mature stage, the central surface air pressure drops to its lowest point, averaging 950-960 mb. The air pressure within the storm does not decrease evenly from outside to inside, but rather decreases more rapidly as it moves towards the center, similar to the counterclockwise rotation of the storm. Especially in the central region of the storm, within a diameter of about 100 km, the air pressure gradient is very steep. At the center of the storm, within a radius of 20-30 km, the air pressure gradient approaches 0. Therefore, on a pressure chart at meteorological stations where the storm passes through, a funnel-shaped pattern is observed.

I.2.3.2. Wind field

At low altitude, the wind in a storm blows in a counterclockwise direction and converges towards the center. From outside to inside, the circulation of the storm can be divided into three different regions:

a) The outer region: This is the outermost region of the storm with a radius of 300-500 km, measured from the closed isobaric contour (or where the wind speed reaches level 6) to where the wind speed reaches its maximum. In this region, the closer to the center of the storm, the higher the wind speed.

b) The eyewall: This is a ring-shaped region surrounding the center of the storm, with an average thickness of 10-20 km. This is the region with the highest wind speed and the greatest convergence of wind, so convective clouds develop strongly and rainfall is also the heaviest.

c) The center (also known as the eye of the storm): This is the innermost region with an average radius of 15-30 km, with some storms having a radius of up to 90 km. In this region, because the air pressure gradient decreases suddenly to nearly 0, the wind also decreases suddenly, only a light wind or even calm wind.

I.2.3.3. Vertical velocity

On a large scale (the whole storm system), the area within the eye of the storm can be considered as an area of updrafts, while the outer edge of the storm is an area of downdrafts. If we consider smaller scales (from the edge of the eye to the edge of the storm), the vertical motion within the storm is also very complex. The vertical motion within the storm can be divided into three areas:

a) The outer region: there is strong convergence of warm, moist air at low levels that rises. The cooling process causes the hot water vapor to condense, and latent heat is released. The dynamic and thermal conditions make the air unstable and it rises strongly. The updraft velocity is about 10-30 m/s.

b) The storm's wall: at low levels, the wind blows counterclockwise and converges towards the center of the storm, with increasing convergence as it approaches the center. However, wind convergence does not occur uniformly around the storm, but only in some bands of rotating clouds. Therefore, the updrafts also only appear strongly in those bands. Between the bands of rotating clouds are areas of downdrafts.

c) The center: due to the centrifugal force, the air in the central area of the storm expands and converges towards the storm wall, so the air density and pressure here are very low, resulting in a downdraft from the top to the surface. The boundary of the central area of the storm can be considered as the interface between the downdraft area in the middle and the strong updraft area around it. Therefore, the central area of the storm is not a cylindrical shape, but a funnel shape, with a wider upper part and a narrower lower part, suitable for the periodic motion at the upper part and the strong convergence at the lower part of the storm wind. The downdraft in the central area of the storm is much smaller than the updraft around it. Therefore, the descending air cannot compensate for the periodic airflow, resulting in a very low pressure in the center of the storm compared to the surrounding area.

I.2.3.4. Thermal field

A strong typhoon has a hot core of air that rises from below to high altitudes. In the outer region of the typhoon, the temperature is generally not much different from the

environment. As moving towards the center, the temperature increases significantly, and the isothermal surface rises significantly. The heating of the air is due to the latent heat of condensation, which enhances convective motion. Thus, the latent heat of condensation is converted into potential energy, and some of the potential energy is then converted into kinetic energy of the typhoon. In the center of the typhoon, the descending air makes the air heat up adiabatically, so the temperature here increases the most. The descending air also makes the air much drier. However, at the surface, in the central and nearby areas, the temperature is somewhat lower than the average value due to the direct influence of rain.

I.2.3.5. Clouds

The main cloud system of a hurricane consists of several bands of swirling clouds that spiral into the center of the storm. These bands are formed from many strong cumulus clouds that are closely linked and arranged in a clear pattern. Near the center of the hurricane, these bands converge into a dense, swirling mass of clouds, often referred to as the central cloud region. The center of this cloud mass is the eye of the storm. In strong hurricanes with wind speeds over 30 m/s, the sinking air in the center of the storm can dissolve the clouds there, revealing a narrow, cloud-free area at the center of the storm with an average diameter of 30-50 km (the eye of the storm).

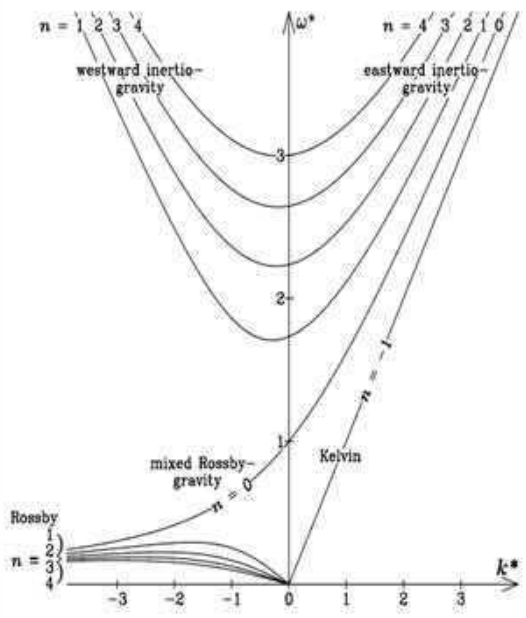

Figure I. 1. Dispersion curve of the equatorial waves [2]

With k^* and ω^* being the non-dimensional forms of wavenumber and frequency, $\omega^* \equiv \omega/(\beta\sqrt{gh_l})^{1/2}$, $k^* \equiv k/(\sqrt{gh_l}/\beta)^{1/2}$. The curves represent the equatorial Rossby waves, gravity waves, Kelvin waves, and internal waves in westward moving flows with zonal wavenumber n ranging from 0 to 4. Equatorial Rossby waves have negative zonal wavenumbers, so they propagate from east to west.

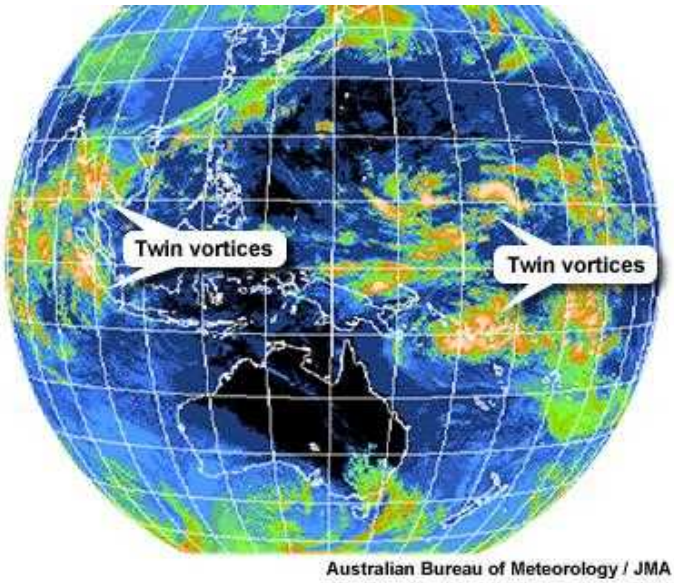

Figure I. 2. A pair of vortices that are symmetrical about the equator showing the presence of Rossby waves in satellite cloud images at 00 UTC on October 7, 2002 [14]

CHAPTER II. OVERVIEW OF THE STUDY AREA AND METHODOLOGY

II.1. The study area

II.1.1. The Northwest Pacific

The Northwest Pacific region is located between the equator and latitude 60°N, stretching from longitude 100°E to 180°E, including the South China Sea. The TC formed and operated in this area are warned by the Japan Meteorological Agency (JMA). This is the most active typhoon area in the world, accounting for one-third of all typhoons globally each year. The TC activity peaks in the period from mid to late summer, when the surface temperature difference between the ocean and the land is the greatest. Tropical cyclones affect East Asia, Southeast Asia, and islands in the Pacific. The coast of China is the place where the most typhoons make landfall in the world. The Philippines is the country that suffers the most severe impacts, experiencing nearly 20 typhoons per year, including 8-9 direct landfalling ones [13].

II.1.2. Climate variability in the Northwest Pacific

II.1.2.1. El Nino - Southern Oscillation

El Nino - Southern Oscillation (ENSO) are oscillations due to the interaction between the ocean and atmosphere in the tropical region of the Pacific Ocean. ENSO consists of three oscillation phases: neutral, El Nino (warm ENSO), and La Nina (cold ENSO). During the neutral phase, the trade winds blow from east to west across the surface of the Pacific, carrying warm, moist air and warm water to the west and keeping the central Pacific relatively cool. The thermocline in the west is deeper than in the east. The upward motion of air in the west and downward motion in the east with easterly winds at the surface is called the Walker circulation. During the El Nino phase, the trade winds weaken or even reverse, causing the central and eastern Pacific to become warmer. As a result, the amount of rainfall on the east coast of the Pacific (Peru, Kiribati) increases and the west coast (Australia, Southeast Asia) becomes drier. During the La Nina phase, the Walker circulation strengthens with enhanced upwelling on the west coast and strong trade winds.

La Nina is associated with increased rainfall on the west coast and drought on the east coast.

ENSO is quantified through the Southern Oscillation Index (SOI), which is calculated based on the distribution of sea surface temperature and atmospheric pressure fluctuations between two stations in the Southern Hemisphere, namely Tahiti (to the east) and Darwin (to the west):[6]

$$SOI = 10 \times \frac{P_{diff} - P_{diffav}}{SD(P_{diff})} \quad (2.1)$$

where:

- P_{diff} = monthly averaged sea level pressure at Tahiti – monthly averaged sea level pressure at Darwin
- P_{diffav} = average of P_{diff}
- $SD(P_{diff})$ = standard deviation of P_{diff}

The SOI has negative values during El Nino and positive values during La Nina. In addition to the SOI, the Oceanic Nino Index (ONI) is also used to determine the timing and intensity of each ENSO phase. The ONI is the standard used by the US National Oceanic and Atmospheric Administration (NOAA) to define El Nino and La Nina in the central equatorial Pacific region. It is defined as the three-month running mean of sea surface temperature anomalies in the Nino 3.4 region (between 5°N and 5°S, 120°W and 170°W). The ENSO phases are defined as five consecutive three-month periods with anomalies higher than +0.5°C for warm phases and lower than -0.5°C for cold phases. The thresholds are divided into four intensity levels: weak (anomaly SST between 0.5°C and 0.9°C), moderate (1.0°C to 1.4°C), strong (1.5°C to 1.9°C), and very strong (greater than 2°C) for both phases. The ONI ranges from -0.5°C to +0.5°C are considered neutral phase [18].

II.1.2.2. Madden – Julian Oscillation

The Madden-Julian Oscillation (MJO) is a tropical oscillation with a time scale ranging from weeks to months. The MJO is characterized by the eastward movement of clusters of clouds and rainfall near the equator, typically repeating with a period of 30 to 60 days and a speed of approximately 4-8 m/s. The MJO plays an important role in controlling the

intraseasonal oscillation of the tropical region. The activity of the MJO is characterized by an area of increased convective transmission to the east, starting from the tropical region of the western Indian Ocean and then moving to the western tropical region of the Pacific. When convection shows signs of weakening and ends at longitude 1800E, the winds of the MJO continue to move through the eastern tropical Pacific, South America, and the Atlantic.

The convective signals of MJO are often limited to the Indian Ocean and the Pacific due to the unstable nature of convection that can only be sustained over warm sea surfaces. However, MJO signals can still be detected in other tropical regions, with different meteorological fields such as sea surface temperature. The convective activity of MJO in the Maritime Continent (an area that includes Indonesia, Borneo, New Guinea, the Philippines, the Malay Peninsula, and the surrounding seas) is weaker than in the surrounding oceans. This is mainly due to the strong diurnal heating over land, which causes a clear diurnal cycle in convective activity, leading to moisture and energy competition with MJO. In addition, the obstruction of terrain to low-level moisture convergence and surface evaporation is significantly reduced on land, affecting the intensity of MJO in the aforementioned region. The development of MJO monitoring and tracking is driven by the research needs of MJO. Many time-based indices have been developed to monitor MJO activity, with the Real-time Multivariate MJO (RMM) index being the most widely used. RMM studies have been developed and conducted at the Australian Bureau of Meteorology (BoM), which can efficiently display and extract atmospheric variability related to MJO.

Initially, the data set for the period 1979-2001 was filtered to remove low-frequency oscillations such as the time-mean field, the three zonal harmonics of the seasonal cycle, the interannual variability (ENSO), the 10-day variability, and the removal of the 120-day mean value of each day. The daily anomalies after filtering were averaged by latitude in the range from 15°N to 15°S on both sides of the equator. The meteorological fields were normalized by the global variance of each field before being subject to orthogonalization.

After orthogonalization, the first and second EOF1 and EOF2 account for a total of 25% of the variability of the original dataset, while the third EOF3 only accounts for 6.1%. The

first orthogonal space shows enhanced convection over the Maritime Continent with low-level westerly anomalies covering the Indian Ocean and Maritime Continent, while easterly anomalies dominate over the western Pacific. The second orthogonal space describes a state of enhanced tropical convergence located over the western Pacific. The state of the MJO is determined as a point in the 2-dimensional space of the RMM1 and RMM2 indices.

The vertical axis represents the values of RMM1, and the horizontal axis represents the values of RMM2. The 2-dimensional space is divided into 8 regions, labeled in order from phase 1 to phase 8. These phases represent the relative positions of the MJO convective envelope: phases 2 and 3 correspond to the Indian Ocean, phases 4 and 5 correspond to the Maritime Continent, phases 6 and 7 correspond to the western Pacific, and phases 8 and 1 correspond to the western hemisphere and Africa. The pairs of RMM1 and RMM2 values for a given day determine the MJO activity for that day. The positions of subsequent days are connected together. It can be seen that many consecutive days move counterclockwise around the origin. This indicates a systematic eastward movement of the MJO. The larger amplitude circles represent periods of strong MJO activity, while weak MJO activity appears as random motions around the origin.

The MJO intensity is calculated as

$$RMM = \sqrt{{RMM_1}^2 + {RMM_2}^2} \qquad (2.2)$$

Days with RMM > 1 are considered days with strong MJO activity. Conversely, RMM < 1 corresponds to weak MJO activity. The stronger the MJO, the farther the point is from the origin in the spatial diagram. RMM2 has a delay of about 10-15 days compared to RMM1. The maximum lag correlation coefficient between RMM1 and RMM2 is 0.56 at a lag of 9 days. This lag correlation coefficient is higher than those obtained in previous studies. The high correlation coefficient at long lags suggests the predictability of this index.[8]

The RMM time series and MJO chart were obtained from the BoM website. The RMM values and MJO phases are determined daily from 1974 to present. The RMM1 axis is the horizontal axis, while the RMM2 axis is the vertical axis. The chart is divided into eight wedges corresponding to the eight phases of the MJO. Each day's RMM1 and RMM2

values are represented as a point on the chart, with days of weak MJO activity within the center circle (RMM < 1). For the 3-month MJO chart, the first month is marked in red, the second in green, and the last in blue (Figure II.1).

II.1.3. Characteristics of TC activity over the Northwest Pacific

The Pacific Ocean has two areas where tropical cyclones (TC) are most active: the Northeast and Northwest regions. Globally, TCs occur least frequently in May and most frequently in September. November is the only month when all basins across the world are active. In the Northwest Pacific Ocean, TCs are least frequent in February and March, and most frequent in September. [22] The peak of TC activity in this region occurs at the end of summer, which can be explained by the slow absorption of heat by the ocean, resulting in the highest sea surface temperature at the end of summer and creating favorable conditions for TC formation and development.

In addition to the condition of sea surface temperature, meteorologists also pay attention to the influence of circulation factors in the formation of tropical cyclones. Ritchie and Holland (1999) conducted a statistical study of 199 cases of TC formation in the period 1984-1992 (excluding 1989) in the Northwest Pacific Ocean. The research team classified five large-scale circulation features in the formation of TCs, including monsoon shear line, monsoon convergence zone, monsoon gyre, eastward waves, and Rossby wave energy dispersion from preexisting anticyclones. [11]

The impacts of typhoons in this region are closely monitored as most storms tend to make landfall in countries that are centers of the world economy and finance, such as China, South Korea, and Japan. Additionally, typhoons cause significant damage to developing countries such as the Philippines and Vietnam, as well as threaten the existence of Pacific islands. Typhoon Haiyan in 2013, when it made landfall in the Philippines, caused huge losses, with the city of Tacloban almost completely flattened and still unable to fully recover from the devastation. Although it did not make landfall in Vietnam, Typhoon Haiyan still caused significant damage due to the storm's circulation. In addition, the Northwest Pacific region has important maritime shipping routes, and strong typhoons can disrupt the passage of vessels through this area.

In the context of climate change, the formation of storms in the Northwest Pacific has become more unpredictable than ever before. Global warming plays an important role in the formation of strong storms. In addition to an increase in intensity, the trajectory of storms has also undergone significant changes. According to Wang et al. (2011), during the period from 1965 to 2009, the impact of storms tended to decrease in the South China Sea and increase in the vicinity of East Asia, and global warming is linked to these results [7].

II.2. Data

II.2.1. Outgoing Longwave Radiation

Outgoing Longwave Radiation (OLR) is the energy radiated by the Earth into space in the form of low-energy infrared radiation. The energy transport conveyed by OLR is measured in units of W/m^2. OLR is a very important component of the Earth's energy balance. In an ideal state, the total longwave radiation emitted by the atmosphere is exactly balanced by the total shortwave radiation absorbed from the Sun. As a result, the average temperature of the Earth remains stable. OLR is affected by clouds and dust in the atmosphere. Clouds tend to block longwave radiation, resulting in low OLR flux.

OLR is a useful data in monitoring the convective component of the equatorial convective wave. OLR can be used to represent the degree of convection in the tropical region. An anomalous negative OLR value indicates an enhancement of convection, whereas an anomalous positive OLR value is associated with the suppression of convection. However, OLR values do not represent rainfall in the region. Today, OLR is measured by many artificial satellites since 1957, including Nimbus-6, Nimbus-7, NOAA-9, NOAA-10, and so on. The daily average OLR data in this thesis is taken from the climate data of the National Oceanic and Atmospheric Administration (NOAA) with a global resolution of 10x10 square degrees. The data was collected from 1979 to the present [19].

II.2.2. Tropical cyclone data

The data on the formation location of tropical cyclones (TCs) is obtained from the Joint Typhoon Warning Center (JTWC). The JTWC is a joint agency of the US Navy and Air Force, headquartered in Hawaii. The JTWC is responsible for issuing tropical cyclone

warning bulletins in the Northwest Pacific, South Pacific, and Indian Ocean regions. Other TC data is obtained from the JMA best track dataset. Information on TCs in the JMA dataset includes position, intensity, direction of movement, central pressure, and the minimum and maximum radius of strong winds at 30 kts and 50 kts. The JMA provides typhoon data from 1951 to present [24].

II.3. Space – time spectra analysis

Spectral analysis in space-time is a useful method for studying the propagation along latitudes of waves because it separates the data dependent on time and longitude into a data domain of wave number and frequency for waves propagating to the east and west directions [3].

Assuming that the domain of the data in space and time is along the longitude (x) and is limited by time $(0 < t < T)$. For convenience, frequency is denoted by ω and wavenumber is denoted by k.

The space-time sequence $W(x,t)$ is expanded into a Fourier series

$$W(x,t) = Re \sum_{k,\omega} \widehat{W}_{k,\omega} e^{i(kx+\omega t)} + \widehat{W}_{k,-\omega} e^{i(kx-\omega t)} \tag{2.3}$$

where $\widehat{W}_{k,\omega}$ is a two-dimensional complex transformation defined by

$$2\widehat{W}_{k,\omega} = \frac{1}{\pi T} \int_0^T \left[\int_0^{2\pi} W(x,t) \right] e^{-i\omega t}\, dt \tag{2.4}$$

with a positive k, a negative frequency represents a westward propagation while a positive frequency corresponds to a eastward propagation.

The energy spectrum $P_{k,\omega}$ is defined as the variance of the Fourier component of (2.1) given by

$$P_{k,\omega}(W) = \frac{1}{2} \langle \left| \widehat{W}_{k,\omega} \right|^2 \rangle \tag{2.5}$$

II.4. Wheeler – Kiladis filter

To clarify the relationship between OLR and tropical waves, Wheeler and Kiladis used the spectral analysis method based on wave number and frequency [9]. Initially, 10 OLR

time series data over a period of 90 days were collected by shifting every 30 days from the start date of the data series. Each data series was detrended and the mean was subtracted using the least squares method. Next, the Hanning window function was used to smooth the data to reduce errors in spectrum estimation. For each data series, the fast Fourier transform was applied to both the longitude and time dimensions to calculate the wave-number-frequency spectrum (or space-time spectrum).

With the obtained 10 spectrum, the symmetric and asymmetric component is determined as:

$$OLR(\varphi) = OLRA(\varphi) + OLRS(\varphi) \tag{2.6}$$

$$OLRS(\varphi) = \frac{OLR(\varphi) + OLR(-\varphi)}{2} \tag{2.7}$$

$$OLRA(\varphi) = \frac{OLR(\varphi) - OLR(-\varphi)}{2} \tag{2.8}$$

where:

- $OLR(\varphi)$: the function OLR with latitudes φ
- $OLRS(\varphi)$: the symmetric component
- $OLRA(\varphi)$: the asymmetric component

The background spectrum is calculated by taking the average of OLRA and OLRS and is smoothed multiple times using a 1-2-1 weighted filter in both frequency and wavenumber:

$$R(\omega) = \frac{1}{2} + \frac{1}{2} cos\ cos\ (\omega \Delta t)\ , 0 < \omega < \frac{\pi}{\Delta t} \tag{2.9}$$

The enhanced wave spectra as a function of wave number and frequency are obtained by taking the symmetric (or asymmetric) component of the wave spectra divided by the background spectra. The results of the two components help determine the characteristics of each type of equatorial wave. For example, gravity waves are asymmetric waves and therefore only appear in the asymmetric radiation component (Figure II.2). In contrast,

Kelvin waves, Rossby equatorial waves, and the MJO oscillation are found in the symmetric component (Figure II.3).

After determining the relationship between frequency-wave number and energy of each type of equatorial wave in the OLR spectrum, each type of wave is filtered out from the spectrum and its spatial distribution is shown on a map (Figure II.4). To illustrate the movement of equatorial waves over time, a Hovmoller diagram is used by taking the average OLR values along each latitude in the range of 5°N-15°N, combined with filtering from the frequency-wave number spectrum (Figure II.5).

II.5. Data processing procedure

The data processing procedure for analyzing the correlation between Rossby wave activity and typhoons is described in Figure II.3. First, global SST is displayed on a map to clarify the initial conditions in typhoon formation. In the next step, OLR data is represented in two forms: a map (establishing the distribution on the global space) and a Hovmoller diagram (illustrating the movement of Rossby waves over time). In addition to Rossby waves, MJO is also considered through the RMM index diagram. Finally, synoptic maps at the surface, 850 mb, and 500 mb, as well as satellite cloud images, are used to identify the synoptic signatures of Rossby waves. All these factors will evaluate the role of Rossby waves and the influence of MJO in each case through qualitative analysis.

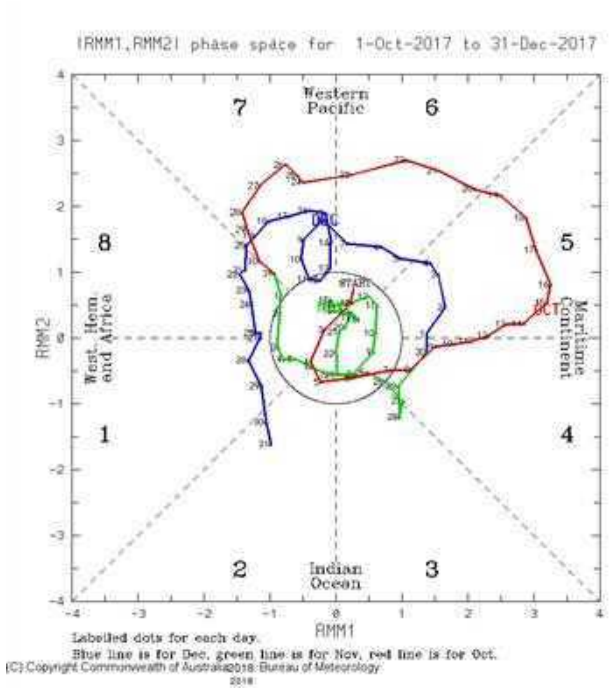

Figure II. 1. RMM temporal evolution from October 1st to December 31th, 2017

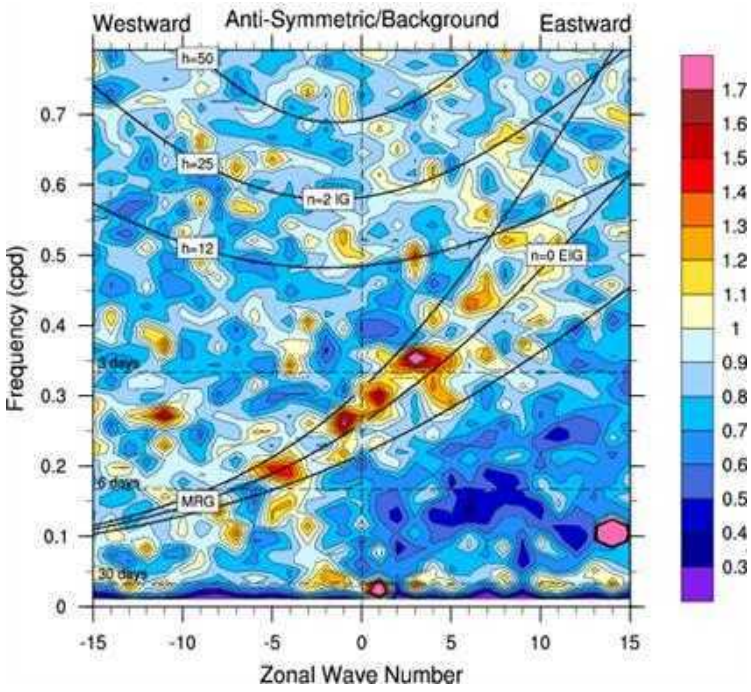

Figure II. 2. Frequency spectrum - wave number of OLR asymmetric component [9]

The black curves represent the dispersion curves of gravity and internal gravity Rossby waves propagating westward at depths of 12, 25, and 50 meters and zonal wavenumbers of 0, 1, and 2. The horizontal axis represents the zonal wavenumber, and the vertical axis represents the frequency in cycles per day. The spectra are colored with red indicating higher energy levels.

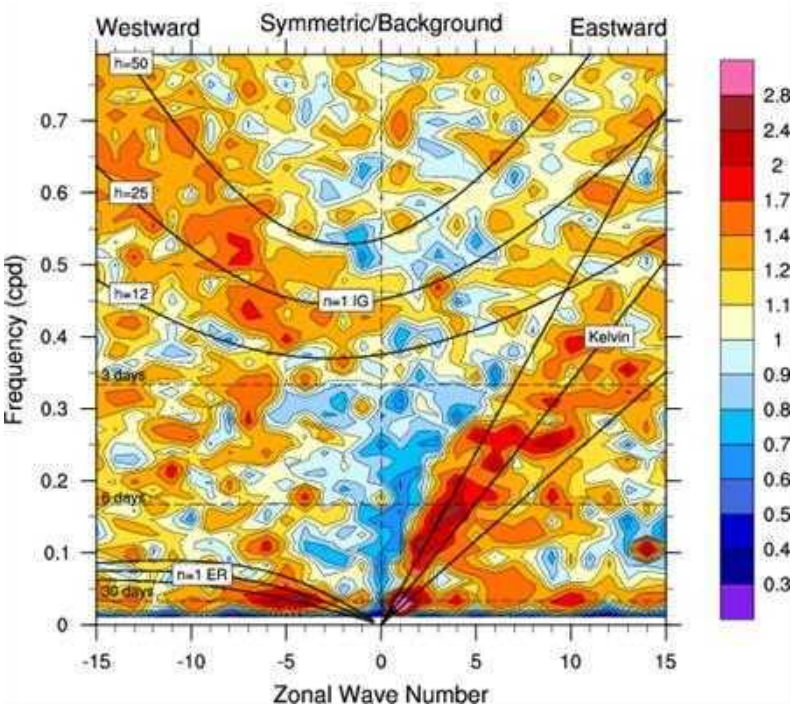

Figure II. 3. Frequency spectrum - wave number of OLR symmetric component

The notions are similar to Figure II.2, but for Inertial gravity waves, equatorial waves, and Kelvin waves.

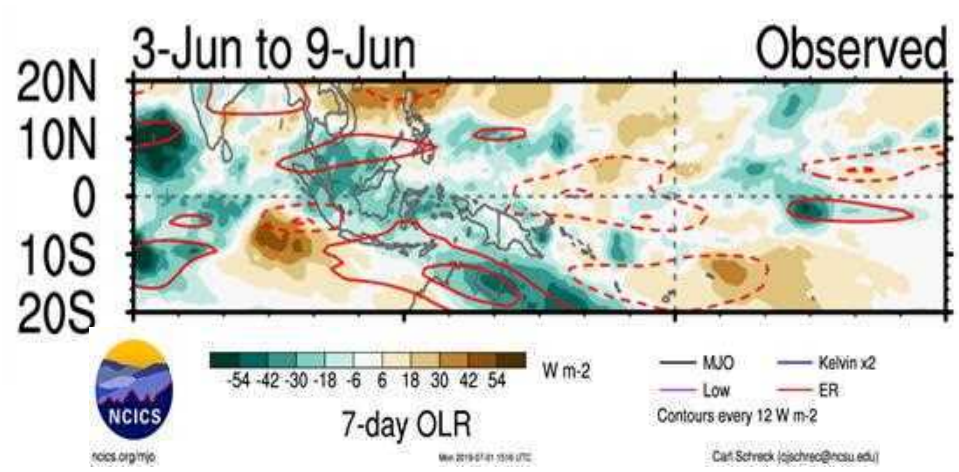

Figure II. 4. Spatial distribution of equatorial Rossby waves from June 3-9, 2019[19]

The distribution of Rossby waves in the Pacific and Indian Oceans is illustrated by the red lines within the range of 10°S – 20°N based on 7-day OLR data. According to convention, solid lines represent Rossby waves propagating over negative OLR (dark color) and dashed lines represent Rossby waves propagating over positive OLR (light color).

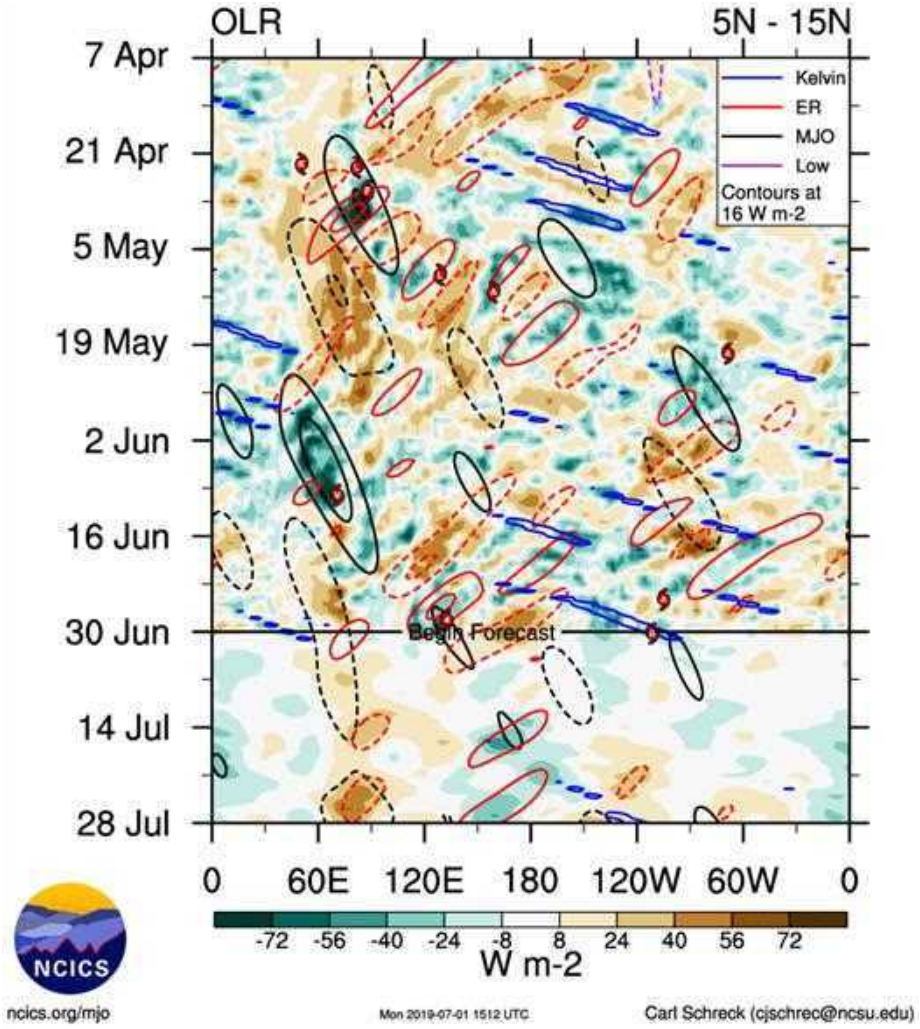

Figure II. 5. Hovmoller diagram for equatorial waves and MJO [8]

The time axis is shown from top to bottom. The notation is similar to Figure II.4, in addition to Rossby waves, there are Kelvin waves (blue), MJO (black), and low-frequency waves (purple). The location and formation time of storms are indicated by red swirls with the first letter of the storm name. This map can forecast the movement of zonal waves, starting from the "Begin Forecast" line.

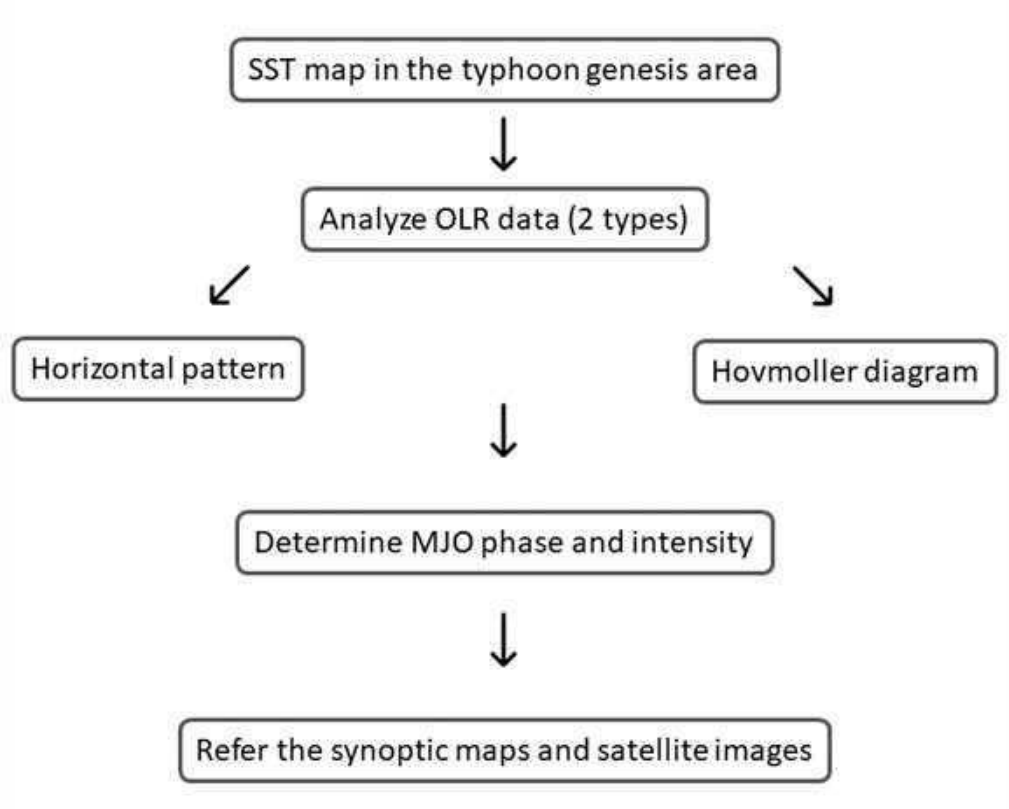

Figure II. 6. Data processing procedure

CHAPTER III. RESLUTS

III.1. Large scale circulation in 2018

III.1.1. El Nino – southern oscillation

Understanding the impact of ENSO on the equatorial waves is crucial not only for improving the prediction of tropical and extra-tropical weather within a few days but also for climate prediction. The development of ENSO in 2018 is shown through the ONI index, which is calculated as the average over three consecutive months. Figure III.1 shows that 2018 was a year when both El Nino and La Nina operated at weak intensities. La Nina was weak for the first 4 months of the year, then gradually weakened and shifted to the El Nino phase from May, and strengthened from September to December. Therefore, ENSO in 2018 did not significantly affect the activity of equatorial waves and the formation of tropical cyclones in the Northwestern Pacific Ocean.

III.1.2. Madden – Julian Oscillation

The movement of the MJO in each phase increases convection in the area it passes through and promotes the formation of tropical cyclones. In some cases, the activity of the MJO in an area plays a role in the formation of shorter and faster-moving equatorial waves. Overall, the MJO is most active in the western Pacific Ocean during the first two months of the year and weakens in March (Figure III.3). In the next phase, the MJO exists in Africa and the Indian Ocean (April), with average intensity in May and weakening in June (Figure III.4). In July, the MJO has a period of increased intensity in the Maritime Continent but quickly weakens in August-September (Figure III.5). In the last period of the year, the MJO shows signs of strengthening in October-November and is active in the Maritime Continent from the second half of December (Figure III.6).

In 2018, there were a total of 87 days of MJO activity in the western Pacific (24% frequency), of which 66 days were strong activity (amplitude greater than 1) with a frequency of 18%. For the Maritime Continent, there were a total of 111 days of MJO activity (30%), with 62 days of strong intensity (17%) (Figure III.2). The dominance of the MJO over the western Pacific and Maritime Continent areas has had significant impacts on

the activity of tropical cyclones. Especially in the last months of the year, the MJO is located in the southern South China Sea, increasing convection in the offshore area and affecting the weather on land.

III.2. Overview of the 2018 storm season and case studies

The analyzed storms include 28 storms that formed over the Northwest Pacific Ocean in 2018 and the first storm of 2019, Pabuk, which was a remnant of the 2018 storm season. The impact of Rossby waves on the storms is based on Hovmoller diagrams of Outgoing Longwave Radiation (OLR) (Appendices A, B, C). Of the 29 storms, 10 were formed due to the influence of Rossby waves, and the characteristics of these storms are presented in Table III.1. In 2018, Rossby waves were active from September to December, while they were almost inactive from June to August. From January to May, Rossby waves appeared on average once per month (Appendices A, B, C).

In the 2018 storm season, although only one-third of the storms were formed due to the influence of Rossby waves, 70% of them reached the category of super typhoons, and some strong storms formed at unusual times and in low-latitude regions.

Table III.1. Statistics of storms affected by Rossby waves in typhoon season 2018

No	Name	Formation time (mm/yy)	Intensification
1	Sanba	02/2018	Typhoon
2	Jelawat	03/2018	Super typhoon
3	Maliksi	06/2018	Strong typhoon
4	Prapiroon	06/2018	Super typhoon
5	Cimaron	08/2018	Super typhoon
6	Mangkhut	09/2018	Super typhoon
7	Kongrong	09/2018	Super typhoon
8	Yutu	10/2018	Super typhoon
9	Manyi	11/2018	Super typhoon
10	Pabuk	01/2019	Typhoon

The analyzed storms below include Typhoon Sanba (February 2018), Typhoon Mangkhut (September 2018), and Typhoon Pabuk (January 2019). The formation of each storm was more or less influenced by Rossby waves and other circulations.

III.2.1. Sanba

Typhoon Sanba, also known as Typhoon Basyang in the Philippines, was a relatively weak tropical cyclone that affected the southern Philippines in February 2018. Initially, a tropical depression formed near Chuuk Island on February 8. The depression moved westward and intensified into Typhoon Sanba on February 11. Sanba made landfall in the northeastern part of Mindanao on February 13 and weakened into a tropical depression a day later before dissipating over the Philippine Sea.

Typhoon Sanba was a characteristic storm influenced by the Rossby waves interacting with the symmetric tropical cyclone system across the equator. The equatorial Rossby waves can transfer vorticity energy into the Southern Hemisphere monsoon trough, enhancing convection and providing favorable conditions for typhoon formation. In addition, during the typhoon's formation period, the MJO was active over the western Pacific, potentially contributing to the storm's development through increased convection.

Typhoon Sanba formed over the tropical waters east of the Philippines. During the period from February 10th to February 17th, the average SST in this area was above 27°C, reaching up to 30°C in some places, which is ideal for typhoon formation. (Figure III.9)

On the map, a region of long-wave radiation existed in the area of longitude 150°E from February 1st to February 9th, indicating a strong development of convergence in that area. In addition, a Rossby wave appeared from February 1st to February 16th, moving from 160°E to 110°E (Figure III.10). In the Pacific region, from February 3rd to February 5th, a Rossby wave appeared over a large area stretching from 140°E to 180°E, covering from the equator up to 20°N, accompanied by a region of negative OLR. From February 6th to February 8th, the Rossby wave strengthened and moved westward, which was also the preexisting disturbance period of Typhoon Sanba in that region. From February 9th to February 11th, the Rossby wave continued to move westward over the waters east of the Philippines and gradually developed into a symmetrical wave across the equator. From February 12th to February 15th, the Northern Hemisphere Rossby wave acted over the Philippines, while the remaining part of the wave continued to strengthen in the Southern Hemisphere. From February 16th to February 18th, the Northern Hemisphere Rossby wave

weakened and moved into the South China Sea, while the remaining part developed into a Kelvin wave operating over the waters of Australia. (Figure III.11)

In addition to the above maps, the thesis also used synoptic maps at different levels to identify the signs of Rossby waves. On the surface synoptic map of February 7th, 2018, a tropical low-pressure area existed near longitude 150°E, and the 850 mb level showed the appearance of a symmetrical pair of cyclones across the equator in the above-mentioned area (Figure III.12). This is an important sign in detecting the activity of Rossby waves. This symmetrical low-pressure pair did not develop into the 500 mb level but instead formed a convergence zone centered at 15°S-125°E. (Figure III.13).

From February 8th to 10th, the tropical depression moved slowly to the west and intensified into a typhoon on February 11th. At this time, the Rossby wave had developed relatively completely, helping to enhance the convection of the typhoon. The symmetric pair of low-pressure systems across the equator is clearly seen on the surface synoptic map (Figure III.14). The symmetric cloud system generated by the pair of low-pressure systems is also depicted in the satellite cloud image (Figure III.15).

III.2.2. Mangkhut

Typhoon Mangkhut, or Ompong as it is known in the Philippines, was a super typhoon that caused extensive damage to the islands of Guam, the Philippines, and the South China Sea in mid-September 2018. Mangkhut was the strongest storm to make landfall in the Philippines since Super Typhoon Haiyan in 2013, and also the strongest typhoon to affect Hong Kong since 1983.

On September 5th, 2018, the JTWC began monitoring a tropical disturbance near the international date line. The system continued to develop and was classified by JMA as a tropical depression on September 7th. The tropical depression gradually intensified into a typhoon and was named Mangkhut. Mangkhut reached super typhoon status on September 9th. A wide eye of the storm, 18 km in diameter, was observed on satellite imagery as it approached the Northern Mariana Islands and Guam, with sustained winds of up to 165 km/h (46 m/s - category 14) at 12:00 UTC on September 10th. According to JMA, the central pressure of the storm was 905 mb and the sustained winds for 10 minutes reached

205 km/h (57 m/s - category 17) at 18:00 UTC on September 11th. Meanwhile, the JTWC assessed that Mangkhut reached its maximum intensity on September 12th with sustained winds for 1 minute reaching 285 km/h (79 m/s - above category 17). The typhoon made landfall for the first time in Baggao, Cagayan province, Philippines at 18:00 UTC on September 14th. Mangkhut weakened as it passed through the mountainous region of Luzon Island, continued to move into the South China Sea on September 15th, and made its second landfall on the coast of Jiangmen, Guangdong, China at 9:00 UTC on September 16th with sustained winds for 2 minutes reaching 160 km/h (45 m/s - category 14). After making landfall, the typhoon weakened into a tropical depression and dissipated over Guangxi province at the end of September 17th.

Typhoon Mangkhut formed over the equatorial waters of the Pacific Ocean near longitude 180°E. The sea surface temperature in this area from 4/9 to 11/9 was quite high, ranging from 27°C to 30°C, which is ideal for the formation of a typhoon (Figure III.18). During most of September 2018, the Madden-Julian Oscillation (MJO) was weak and only strengthened over the western hemisphere and Africa at the end of the month, so its impact on the formation of Typhoon Mangkhut was not significant. On the Hovmöller diagram, a Rossby wave formed near longitude 180°E in early September 2018. This was a long-lasting wave that persisted until September 20 and extended to longitude 60°E. At the time of Typhoon Mangkhut's formation, the negative radiation anomaly in this area did not persist for a long time (Figure III.19).

At the end of August and beginning of September 2018, a Rossby wave formed in the eastern region of the International Date Line over an area of negative radiation. From September 2nd to 4th, the Rossby wave developed into two symmetrical parts across the equator. By September 7th, the northern part had strengthened, creating favorable conditions for the formation of Typhoon Mangkhut. Meanwhile, the southern hemisphere Rossby wave remained active for the next three days before gradually weakening and disappearing. The remaining Rossby wave continued to expand and move westward. However, its direction did not coincide with the path of Typhoon Mangkhut and shifted southward. On September 17th, the Rossby wave was active in the southern part of the South China Sea (Figure III.20).

Due to the development of the Rossby wave in the region near the 180°E longitude, it cannot be detected by ground synoptic maps or high-altitude maps of Thailand. Instead, the Rossby wave can be detected through increased convection due to satellite cloud images. Figure III.13 shows the cloud area caused by Typhoon Mangkhut when it made landfall in China and the cloud area in the southern part of the South China Sea caused by the activity of the Rossby wave at 12:00 UTC on September 16, 2018 (Figure III.21).

III.2.3. Pabuk

Typhoon Pabuk was the earliest-forming storm in 2019 in both the Northwest Pacific and North Indian Ocean regions. It formed in late 2018 over the South China Sea and continued into 2019, moving into the Indian Ocean before dissipating into a tropical low. The estimated damages caused by Typhoon Pabuk were around 151 million USD. It was a weak storm but had a fairly unusual timing and location of formation.

On December 28, 2018, a tropical disturbance formed in the southern region of the South China Sea, absorbing the remnants of Typhoon Usman on December 30. By December 31, both the JTWC and JMA had classified the area of low pressure as a tropical depression. At 6:00 UTC on January 1, 2019, the tropical depression intensified into a named storm, Pabuk, according to the JMA, becoming the earliest-forming storm in the Pacific ever recorded. Pabuk continued to move slowly westward, about 650 km southeast of Ho Chi Minh City. Pabuk strengthened over the next two days and accelerated into the Gulf of Thailand on January 3. On January 4, Pabuk made landfall in Pak Phanang district, Nakhon Si Thammarat province at 5:45 UTC. By 12:00 UTC, the JMA issued its final warning on Pabuk as it moved into the Indian Ocean. Over the next few days, Pabuk moved west-northwestward before dissipating into a remnant low on January 7 and vanishing in the Indian Ocean on January 8.

Typhoon Pabuk formed over warm ocean waters. The average sea surface temperature in the South China Sea from December 30, 2018 to January 4, 2019 was consistently around 27°C, which is suitable for the formation and development of typhoons (Figure III.24). During the formation of Typhoon Pabuk, the Madden-Julian Oscillation (MJO) was active with above-average intensity over the Maritime Continent region. The MJO

contributed to the formation of the monsoon trough over the Coral Sea (Australia) and increased convection over the southern South China Sea region.

On the map, a Rossby wave formed near the 150°W in early December 2018 and moved to the 100°E on January 6, 2019 (Figure III.25). This is a long-lived Rossby wave, contributing to the formation of the 30°W tropical depression and Typhoon Pabuk. Satellite cloud images and synoptic surface maps show signs of the equatorial Rossby wave due to the appearance of a pair of symmetric low-pressure systems across the equator at 110°E (Figure III.26-27). The symmetric anticyclonic swirls across the equator develop up to 850 mb, along with the appearance of a pair of symmetric anticyclonic swirls at the 135°E-140°E (Figure III.28). The low-pressure system develops up to 500 mb (Figure III.29).

On the map, a Rossby wave formed in the negative radiation region east of the Philippines from 19-21/12, creating a tropical depression at 30°W but did not last long. The Rossby wave moved westward, and on the southern hemisphere, a wave formed stretching from 170°E to 110°E from 28-30/12. By 31/12, the Rossby wave structure was relatively complete, including two symmetrical components across the equator (Figure III.30). The activity of the Rossby wave during this period played a significant role in the formation of Typhoon Pabuk. The Rossby wave continued to move westward, passing the Malay Peninsula and entering the Indian Ocean, coinciding with the path of Typhoon Pabuk.

CONCLUSION AND DISCUSSION

The research topic used statistical and qualitative analysis to investigate the relationship between the activity of equatorial Rossby waves and tropical cyclones in the Northwest Pacific in 2018. The analyzed tropical cyclones included Typhoon Sanba, Super Typhoon Mangkhut, and Typhoon Pabuk. The study delved into the influence of Rossby waves on the formation of these cyclones during different stages. In addition, large-scale circulation patterns in the study area were discussed and evaluated through widely used charts and indices. By analyzing the long-wave radiation field OLR, equatorial Rossby wave packets were identified in terms of position and intensity to clarify their correlation with tropical cyclones.

Based on the results obtained from this thesis, it is found that the equatorial Rossby waves have a clear relationship with the activity of tropical cyclones in the Northwest Pacific. The analysis results show the presence of Rossby waves in areas with negative outgoing longwave radiation, which enhances convection. These waves are formed in the region near the date line and move slowly to the west. For large-scale circulation, although the activity of ENSO is known to have an impact on Rossby waves, the weak intensity of ENSO in 2018 did not cause significant effects. The impacts of MJO and Rossby waves were examined for each typhoon.

In general, the three selected storms for analysis formed over warm ocean waters with ideal temperatures. Typhoon Sanba appeared in February, which is a fairly unusual time for a typhoon in the Pacific. The precursor tropical depression of Typhoon Sanba was energized by Rossby waves, increasing its rotation and strengthening it into a typhoon. During its early formation phase, the MJO was also active over the western Pacific, contributing to increased convection and fueling the storm's development. Typhoon Mangkhut, which occurred in September, was a very strong storm with devastating destructive power. It formed off the coast of the Pacific with the presence of Rossby waves during its initial phase. Typhoon Mangkhut was a typical typhoon of the Pacific typhoon season, forming over warm ocean waters and moving westward. During the existence of Super Typhoon Mangkhut, the MJO was weak and did not cause significant impact. Finally, Typhoon Pabuk formed at the end of 2018 with relatively weak intensity.

However, typhoon Pabuk had a very unusual time and location of formation. Typhoon Pabuk intensified from a tropical depression located quite close to the equator in the southwestern waters of the Philippines. In December 2018, a continuous Rossby wave contributed to the formation of a tropical depression at 30W, which did not intensify into a typhoon but its dissipation significantly contributed latent heat energy to Typhoon Pabuk. During that period, the Madden-Julian Oscillation (MJO) had strong intensity in the Maritime Continent region, which increased convection. The MJO, along with the Rossby wave, created favorable dynamic conditions for the rare formation of Typhoon Pabuk in the region.

The analyses and results on forecasting the formation of offshore Pacific storms, especially those intensifying in the South China Sea, are important for early warnings of low latitude storms like Typhoon Pabuk through observations of Rossby waves. From this, we can take measures to prevent and mitigate natural disasters both at sea and on land.

The data and charts in this thesis were referenced from reputable research centers, providing visual and easily accessible information. Government agencies can use this dataset to improve the accuracy of their weather forecasts. In the future, if possible, I will conduct a deeper qualitative and quantitative analysis of the correlation between Rossby waves and tropical cyclones in the Pacific.

REFERENCES

Vietnamese Document

[1] Trần Công Minh (2003), *Giáo trình khí tượng nhiệt đới*. Hà Nội: NXB DHQG Hà Nội.

English Documents

[2] Matsuno, T. (1966), Quasi-geostrophic motions in the equatorial area, *Journal of the Meteorological Society of Japan. Ser. II*, vol. 44, pp. 25-43.

[3] Hayashi, Y. (1982), Space-time spectral analysis and its applications to atmospheric waves, *Journal of the Meteorological Society of Japan. Ser. II*, vol. 60, pp. 156-171.

[4] Platzman, G. W. (1968), The Rossby wave, *Quarterly Journal of the Royal Meteorological Society*, vol. 94, pp. 225-248.

[5] Schreck III, C. J., Molinari, J., and Aiyyer, A. (2012), A global view of equatorial waves and tropical cyclogenesis, *Monthly Weather Review*, vol. 140, pp. 774-788.

[6] Troup, A. J. (1965), The 'southern oscillation', *Quarterly Journal of the Royal Meteorological Society*, vol. 91, pp. 490-506.

[7] Wang, R., Wu, L., and Wang, C. (2011), Typhoon track changes associated with global warming, *Journal of Climate*, vol. 24, pp. 3748-3752.

[8] Wheeler, M. and Hendon, H. H. (2004), An all-season real-time multivariate MJO index: Development of an index for monitoring and prediction, *Monthly Weather Review*, vol. 132, pp. 1917-1932.

[9] Wheeler, M. and Kiladis, G. N. (1999), Convectively coupled equatorial waves: Analysis of clouds and temperature in the wavenumber–frequency domain, *Journal of the Atmospheric Sciences*, vol. 56, pp. 374-399.

[10] WMO (2008), *Typhoon commitee operational manual: Meteorological component*, Switzerland

[11] Yoshida, R. and Ishikawa, H. (2013), Environmental factors contributing to tropical cyclone genesis over the western North Pacific, *Monthly Weather Review*, vol. 141, pp. 451-467.

Internet sources

[12] http://agora.ex.nii.ac.jp/digital-typhoon/index.html.en.

[13] http://bagong.pagasa.dost.gov.ph/climate/tropical-cyclone-information.

[14] http://kejian1.cmatc.cn/vod/comet/tropical/MJO_EqWaves/.

[15] http://www.bom.gov.au/climate/mjo/.

[16] http://www.bom.gov.au/climate/mjo/graphics/rmm.74toRealtime.txt.

[17] https://cyclone.wmo.int/pdf/Chapter-Seven.pdf.

[18] https://ggweather.com/enso/oni.htm.

[19] https://ncics.org/portfolio/monitor/mjo/.

[20] https://oceanservice.noaa.gov/facts/rossby-wave.html.

[21] https://tmd.go.th/en/weather_map.php.

[22] https://www.aoml.noaa.gov/hrd/tcfaq/E10.html.

[23] https://www.esrl.noaa.gov/psd/map/clim/sst.shtml.

[24] https://www.jma.go.jp/jma/jma-eng/jma-center/rsmc-hp-pub-eg/besttrack.html.

[25] https://www.ssec.wisc.edu/data/comp/ir/.

APPENDIXES

UNIVERSITY OF SCIENCE,
VIETNAM NATIONAL UNIVERSITY HO CHI MINH CITY
Physics & Engineering Physics Faculty
Department of Oceanology, Meteorology and Hydrology

SOCIALIST REPUBLIC OF VIETNAM
Independence – Freedom – Happiness
--o0o---

GRADUATION THESIS COURSE REVIEWS

Student: Dang Dong Pha

Title: **Analysis the impact of equatorial rossby wave on tropical cyclone activity in northern west pacific ocean**

Field of Oceanology, major: Meteorology

Reviewer: (Full name, Academic title, Degree) MSc. Le Thi Xuan Lan

Working agency: Southern Regional Hydrometeorological Center

Role:

☒ Supervisor ☐ Reviewer

Comments and evaluation of graduation thesis:

1. **Scientific significance**:

Equatorial Rossby waves play an important role in the formation and development of tropical cyclones in the Northwest Pacific Ocean. Understanding the tropical equator is an important foundation in studying tropical cyclone dynamics.

The activities of storms and tropical depressions in the western Pacific Ocean and the East Sea are related to weather developments in our country, research on storm abnormalities, early recognition and prediction of formation and development. The development of tropical storms and depressions is important in forecasting and warning of natural disasters, in order to contribute to ensuring security, economy and especially the lives of millions of people living along the coast and operating at sea. Analyzing this data helps students have a practical and applied research direction in natural disaster forecasting and prevention. The topic is highly scientific.

2. **Content**:

The report includes an introduction, chapter 1 is an overview of Rossby waves and tropical cyclones consisting of 10 pages. Chapter 2 provides an overview of the Pacific Northwest research area, data sources, space-time spectrum analysis methods, Wheeler - Kiladis filtering method and data processing procedures including 12 pages. Chapter 3 is the main research part: analysis to evaluate the impact of Rossby waves, Madden - Julian oscillations, ENSO on storm formation including 25 pages, conclusion and analysis section.

In the overview sections, students refer to many documents and this is also a new research direction, so students do not mention domestic research. Mainly, because the thesis writing time is not yet at the peak of Rossby, MJO... Consider development potential. Although only analyzing 3 storms, including 2 out-of-season storms, it still clearly shows the impact of Rossby waves, MJO, OLR on storm activity quite clearly, especially with out-of-season storms, forming in Low latitudes are potentially dangerous for Vietnam. This research is only the first step, the students' limitation is that they do not have enough time with more storms and other data sources to have more objective comments to increase the application value in forecasting. early storm.

The student proactively proposed this research direction, had a serious working attitude, and complied with the schedule and opinions of the instructor. During the process of writing the thesis, students are quite bold in coming up with new ideas in research to make the thesis complete, even though it is not easy to get data on the sea. Reference documents show that students have put in a lot of effort, have a fairly good level of English, and have quite complete knowledge of storms and waves from Rossby and MJP.

3. Form:

The layout of the topic is reasonable.

The report is quite coherent, easy to understand, clear illustrations, relatively complete statistical tables and maps, with few spelling errors.

Appendices and references are clear.

4. Conclusion:

The thesis meets the requirements of a university graduation thesis.

We respectfully request the thesis grading committee to approve the thesis with points: 10/10

City. Ho Chi Minh, July 12th 2015

REVIEWERS

Le Thi Xuan Lan

UNIVERSITY OF SCIENCE,
VIETNAM NATIONAL UNIVERSITY HO CHI MINH CITY
Physics & Engineering Physics Faculty
Department of Oceanology, Meteorology and Hydrology

SOCIALIST REPUBLIC OF VIETNAM
Independence – Freedom – Happiness
--o0o---

GRADUATION THESIS COURSE REVIEWS

Student: Dang Dong Pha

Title: **Analysis the impact of equatorial rossby wave on tropical cyclone activity in northern west pacific ocean**

Field of Oceanology, major: Meteorology

Reviewer: (Full name, Academic title, Degree) Asso. Prof., PhD. Vo Luong Hong Phuoc.....

Working agency: University of Science, Ho Chi Minh City, Vietnam. Vietnam National University-Ho Chi Minh City, Vietnam

Role:

☐ Supervisor ☒ Reviewer

Comments and evaluation of graduation thesis:

1. **Scientific significance**:

Has scientific significance

2. **Content**:

Includes 3 chapters: Introduction, Introduction, Conclusion, 53 pages

Summary: satisfactory, should say assessment

English symbols: should be translated

Chapter 1: Overview of Rossby waves and tropical cyclones

There should be drawings

Chapter 2: Overview of the research area and research methods

Presentation meets requirements

Chapter 3: Analysis of 2018 results with 3 storm cases

Storm Kelvan wave Rossby

3. **Form**:

There should be drawings

4. **Conclusion: Does the thesis meet the requirements of a university graduation thesis?**

The thesis meets the requirements of a university graduation thesis

We respectfully request the thesis grading committee to approve the thesis with points:10/10

City. Ho Chi Minh, July 12th 2015

REVIEWERS

Vo Luong Hong Phuoc

Vietnam National University, Ho Chi Minh City

University of Science - VNUHCM

Physics - Physic Engineering College

Oceanology – Meteorology – Hydrology Department

Bachelor Thesis

Topic:

THE CALCULATED MODELING OF WAVE HEIGHT THRESHOLD AFFECTING ON THE CORAL BOTTOM

Student: **NGUYỄN THỊ TỐ VÂN**

Supervisor: PGS. TS. VÕ LƯƠNG HỒNG PHƯỚC

HO CHI MINH CITY, 07/2019

SUMMARY

MÔ HÌNH TÍNH TOÁN NGƯỠNG ĐỘ CAO SÓNG TÁC ĐỘNG ĐẾN CHÂN SAN HÔ

Rạn san hô hiện đang là một trong những vấn đề cấp bách được quan tâm hàng đầu trên thế giới nói chung và cả Việt Nam nói riêng vì số lượng chúng đang giảm dần do các nguyên nhân như ô nhiễm đại dương, nóng lên toàn cầu hay các thiên tai (như bão, lốc xoáy…). Nghiên cứu này là bước đầu tìm hiểu các tác động cơ học của sóng do bão gây ra ảnh hưởng đến chân san hô. Dựa vào các tính toán động lực học của sóng do bão và san hô, mô hình được xây dựng nhằm tính ngưỡng độ cao sóng cho các cá thể san hô tạo rạn có hình khối cầu hay khối bán cầu lý tưởng trong trường hợp chu kỳ sóng dài và ngắn khác nhau. Mô hình còn được áp dụng tính toán tại khu vực vịnh Vân Phong – Bến Gỏi (tỉnh Khánh Hòa) trong hai cơn bão Mirinae (2009) và Damrey (2017). Kết quả cho thấy độ cao sóng do bão gây ra ngoài thực tế hầu như không vượt qua ngưỡng độ cao sóng đã được tính toán. Kết quả tính toán khá phù hợp với điều kiện thực tế của san hô khi gặp bão.

THE CALCULATED MODELING OF WAVE HEIGHT THRESHOLD AFFECTING ON THE CORAL BOTTOM

Coral reefs is currently a top concern in the world in general and in Vietnam in particular because their number is decreasing due to different causes such as ocean pollution, global warming or natural disasters (storms, tornadoes, etc.). This study aims to understand the mechanical effects of waves caused by storms affecting on the coral bottom. Based on hydrodynamic mathematics of storm induced waves and corals, the model is built to calculate the thresholds of the wave height for reef-shaped individuals with ideal spherical or hemispherical shapes in different cases of long and short waves. The model is also applied in the area of Van Phong bay - Ben Goi (Khanh Hoa province) in two cases of Typhoon Mirinae (2009) and Typhoon Damrey (2017). The results show that the actual wave height caused by the storm hardly exceeds the calculated wave height threshold. These results are quite consistent with the actual conditions of the coral when facing the storm.

CONTENT

LIST OF FIGURES

LIST OF TABLES

OPENING

Coral reefs are one of the most diverse ecosystems, providing a unique habitat for numerous marine species. However, the global extent of coral reefs has always been limited, accounting for only 0.1% of the area in the world's oceans. Unfortunately, this area is shrinking further due to various factors such as pollution, overexploitation, global warming, and natural disasters like storms and hurricanes, all of which can impact the structure of coral reefs. Therefore, this dissertation aims to initially investigate the influence of storm waves on the base of coral reefs. Coral reefs are predominantly examined in two common forms: spherical-shaped colonies (such as the *Porites* genus) and idealized hemispherical shapes (such as *Diploastrea heliopora* species). Based on the hydrodynamic equations developed by Massel and Done (1993), this research constructs a computational model to calculate wave height thresholds during storms that could overturn an individual coral colony with specific dimensions at constant depths. Additionally, the study calculates the flow velocity around the coral and considers the erosion of the coral head. Furthermore, the model is applied for calculations in the Van Phong – Ben Goi bay (Khanh Hoa province) during two typhoons, Mirinae (2009) and Damrey (2017), to analyze and assess the extent of coral damage in the computational model compared to real-world observations.

Contents:

Chapter 1: Introduction.

Chapter 2: Calculated model of wave height threshold affecting on the coral bottom.

Chapter 3: Results.

Chapter 4: Application of calculated model of wave height threshold in Van Phong Ben Goi bay area.

CHAPTER 1: INTRODUCTION

I.1 INTRODUCTION ABOUT CORAL REEF

Coral is a group of very small cylindrical organisms with tentacles at the top, used for capturing prey in aquatic environments, and classified under the Coral (Anthozoa) class of the Phylum Cnidaria in the taxonomic system. Coral is divided into three main groups: hard coral, soft coral, and horn coral. Among them, many species of hard coral have the ability to form reefs and are called reef-building corals. Reef-building corals are only found in shallow and warm sea regions. Even in ideal conditions, reef-building corals grow very slowly. Among these corals, the skeletal structure of block-like coral only grows a few millimeters per year, while branching coral grows very rapidly (up to 150 mm or more in a year). Over centuries and millennia, the growth of these corals forms massive limestone structures - these are coral reefs. [1].

Coral reefs, also known as tropical rainforests of the ocean, are a vibrant ecosystem of the ocean. Although they cover only 0.1% of the world's oceans, they are the habitat for at least 25% of marine species, including fish, mollusks, crustaceans, and more [14] The types of coral reefs include [1]: *fringing reef, platform reef, barrier reef, atoll.*

Natural environmental factors govern the distribution of coral including *light, temperature, sedimentation, salinity, tidal range and wave*. In the context of this study, only the impact of waves on two types of spherical-shaped corals (*Porites* and *Diploastrea heliopora*) is being considered among the factors mentioned above.

I.2 PORITES

Porites is a genus of hard coral, also known as stony coral. They belong to the SPS (Small Polyp Stony) category, which means they have small polyps. Porites corals come in various forms, including boulder and branching shapes. However, for the

convenience of computational modeling, this thesis focuses only on Porites in the boulder form, idealized as spherical with a specific diameter (Figure 1.1). Species within the *Porites* genus are widespread and diverse, found in coral reefs worldwide. In Vietnam, *Porites* can be found in most coral reefs extending from the north to the south. *Porites* also dominate the Pandora reef system within the Great Barrier Reef. Additionally, Porites corals come in various sizes, with small coral heads ranging from 2 to 10 cm in diameter commonly found in coral assemblages. Larger coral heads with diameters of 2 to 10 meters are rarer and typically exist at depths of approximately 6 to 12 meters. In closed reef systems with minimal dynamic disturbances, *Porites*, especially large Porites heads (around 5 meters in diameter), tend to thrive and grow. [2].

Despite their richness in species, distribution, and size, Porites corals also have limitations that restrict their occurrence and growth. Being a type of stony coral, they share the stringent environmental requirements common to all corals. Additionally, Porites in the boulder form grows at an exceptionally slow rate, approximately 0.1 to 0.5 cm per year [2]. Juvenile or immature Porites individuals are at high risk of mortality due to various factors, such as predation by coral-eating crown-of-thorns starfish or competition with other coral species in the community [2]. These challenges are compounded by the potential damage caused by storms and wave action.

I.3 DIPLOASTREA HELIOPORA

Diploastrea heliopora, also known as brain coral or honeycomb coral, is the last remaining species of the *Diploastrea* genus, a type of stony coral (Figure 1.2). This species can form dome-shaped colonies, sometimes exceeding 1 meter in height, with smooth surfaces and typically appearing in cream or gray-brown colors, occasionally tinged with green [20]. It is commonly found in the Indian and Western Pacific Oceans, including the waters around Vietnam. According to a study by Vo Si Tuan

and colleagues (2006), this species is present in most Vietnamese coastal regions, with the exception of the Gulf of Tonkin [1]. *Diploastrea heliopora* is relatively abundant in specific regions but less common in others. Its already limited distribution, combined with contemporary threats such as pollution, ocean acidification, and rising global temperatures, has led to a decreasing population, and it has been listed as "near threatened" on the International Union for Conservation of Nature (IUCN) Red List [20]. Due to its scarcity and limited distribution, information about *Diploastrea heliopora* is less extensive compared to other coral species, such as those in the *Porites* genus.

I.4 STUDIES ON THE IMPACT OF HYDRODYNAMICS ON CORALS

I.4.1 Studies in Vietnam

There are not many coral studies in Vietnam, with most of them being research projects conducted by Vo Si Tuan and colleagues (2006) [1], from the Institute of Oceanography in Nha Trang. In their work, the authors provide a clear inventory of the number of species throughout the entire territory of Vietnam. Additionally, they provide detailed descriptions of coral reef characteristics in various regions of the country. However, most domestic studies primarily focus on statistical data and assess the current status of coral reefs to propose conservation measures. There have been very few, if any, projects or research topics that delve into the detailed hydrodynamic factors within coral reef areas.

Figure 1.1 An individual coral of *Porites* Solida (a species belonging to the genus *Porites*) [15]

Figure 1.2 Coral *Diploastrea Heliopora* taken by Veron, Charlie (J.E.N.) [19]

I.4.2 International studies

There is a wealth of research literature on the impact of hydrodynamics on corals. One notable study is by Massel and Done (1993), who investigated the effects of tidal bore turbulence on large coral blocks in the Great Barrier Reef [6]. They used meteorological data and hydrodynamic formulas to analyze the risk and predict the consequences of tidal bore events on coral blocks in different regions within the Great Barrier Reef. Specifically, they examined the forces generated by waves and calculated the wave height thresholds that could affect corals. [6].

Mireille L. Harmelin-Vivien (1994) conducted a study to assess the impact of storms and cyclones on coral reefs. Specifically, the study examined various types of damage caused by cyclones, including mechanical destruction, changes in sedimentation, increased turbidity, salinity fluctuations, and alterations in sea level. The research also explored both direct and indirect effects of cyclones on coral reef morphology, sedimentation, community structure, and nutrient exchange [3]. According to studies by Done and colleagues (1986), Done (1982), and Rogers (1992), the impact of cyclones on coral reefs is characterized by the following factors [3]:

- Diversity of Mixing Parameters
- Variability in Timing and Mechanisms of Cyclones.
- Variation in the Degree of Coral Reef Structure Affected.
- Spatial Scale of Damage.

Harris D. L. and colleagues (2018) conducted a study on the crucial role of coral reefs in coastal protection against wave impacts in the context of current sea-level rise. They selected three coral reef study areas in Moorea (Tiahura, Ha'apiti, and Temae) and one reef in Tahiti (Teahupo'o) and presented calculations and predictions extending to the year 2100. They used the Xbeach 1D model, which was adjusted to

calculate and run Monte Carlo simulations for wave height after passing through complex coral reef structures, which can influence shoreline erosion. The results of their scenarios indicated that, with the current rate of sea-level rise coupled with coral reef structure loss, there is a significant increase in wave height compared to the present conditions. This study highlights the importance of coral reefs in providing natural coastal protection and the potential implications of their degradation in the face of rising sea levels. [4].

Tristan Salles and colleagues (2018) presented the 1-D pyReef - Core version 1.0, SFM carbonate model used to simulate straight-up coral reef sequences equivalent to cores found in actual drill cores. This model serves as a basis for studying the relationship between biological processes (meaning the functional interactions of coral assemblages) related to coral reef development and the changes in environmental factors (such as sea level, tectonics, ocean temperature, pH, and nutrients). The significance of this method lies in its ability to incorporate the dynamics of coral communities into the coral reef growth model and understand the responses of coral reefs to environmental perturbations over time scales ranging from hundreds to thousands of years in the context of coral reefs. Exploring these intermediate time scales is crucial for a better understanding of the sustainable growth responses of corals when faced with expected long-term climate and environmental changes affecting coral reefs in the future [9].

CHƯƠNG II: CALCULATED MODEL OF WAVE HEIGHT THRESHOLD AFFECTING ON THE CORAL BOTTOM

II.1 INTRODUCTION

To calculate the impact of waves on an ideal spherical or hemispherical coral individual with a specific diameter at defined depths, you need to consider the forces acting on it and the force balance, as illustrated in Figure 2.1. Following the perspective of Massel and Done (1993), the forces transmitted by waves to coral reefs and corals are a function of the components of orbital velocity u and horizontal acceleration a generated by waves with wave height H and wave period T_p [6].

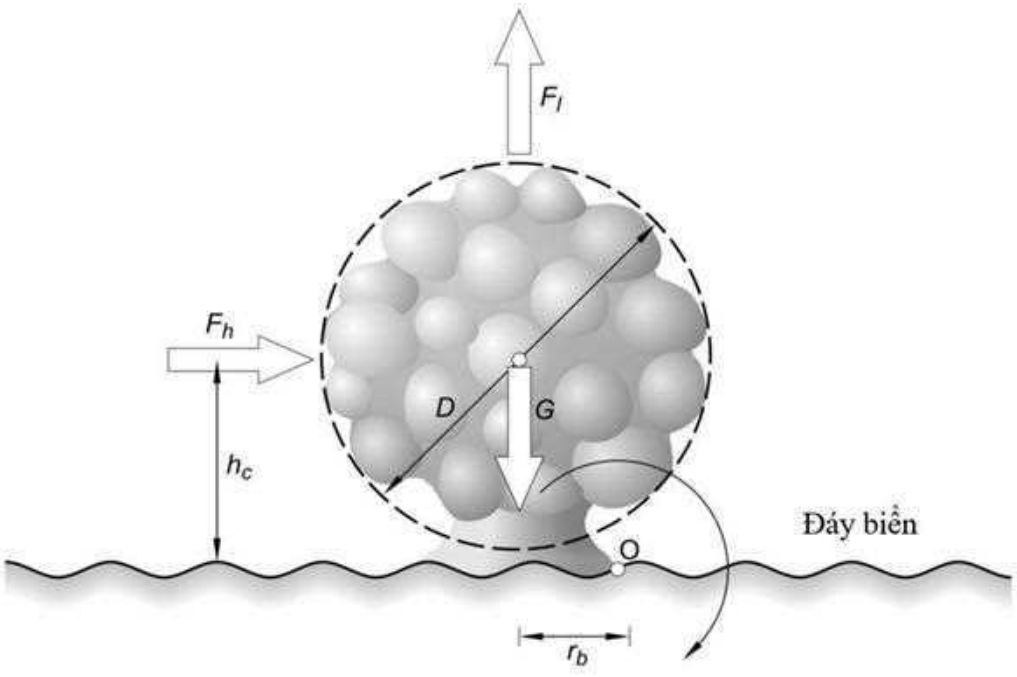

Figure 2.1 The forces acting on a spherical coral [7]

Trong đó:

- F_h: Total horizontal force (N).
- F_l: Lift force (N).
- G: Coral gravitation (N).
- D: Diameter of the coral head (m).
- h_c: Distance from the center of the spherical coral to the reef surface (m).
- r_b: Radius of the base of the coral bottom (m).

II.2 IMPACTING FORCES

Based on Figure 2.1, we assume that the waves will exert an impact on the coral model horizontally, moving from left to right. From there, we can analyze the forces exerted by the waves and break them down into three components of force:

II.2.1 Inertial Force F_i

The inertial force (**Fi**) acting horizontally can be expressed as follows:

$$\boldsymbol{F_i} = C_m \rho_w V a \, \boldsymbol{i_x} \tag{2.1}$$

Where:

- C_m: is the inertial coefficient, which depends on the shape of the coral and the Reynolds number $\boldsymbol{Re} = \frac{uD}{\nu}$)
- ρ_w: sea water density (kg/m^3)
- V: is the volume displaced by the coral (m^3)
- a: acceleration (m/s^2)
- $\mathbf{i_x}$: the unit vector along the x-direction

Based on the concept of kinetic energy [6], you can express the inertial force (Fi) as follows:

$$\boldsymbol{F_i} = \frac{51}{24}\pi\rho_w \left(\frac{D}{2}\right)^3 a\, \boldsymbol{i_x} = 1.57\rho_w V a\, \boldsymbol{i_x} \quad (2.2)$$

II.2.2 The drag force F_d

The drag force $\mathbf{F_d}$ generated by the current and waves, also acts horizontally

$$\boldsymbol{F_d} = \frac{1}{2}\rho_w C_d \pi \left(\frac{D}{2}\right)^2 |u|u\, \boldsymbol{i_x} \quad (2.3)$$

Where:

- u: velocity of wave-induced current (m/s).
- C_d: drag coefficient

II.2.3 Lift force F_l

Lift force $\mathbf{F_l}$: created by the flow around the asymmetric sphere, resulting in a net force [6].

$$\boldsymbol{F_l} = \frac{1}{2}\rho_w C_l \pi \left(\frac{D}{2}\right)^2 u^2\, \boldsymbol{i_z} \quad (2.4)$$

Where:

- C_l: lift coefficient
- $\mathbf{i_z}$: The unit vector in the direction perpendicular to the coral plane along the z-axis perpendicular to the reef plane.

II.2.4 The total force due to wave:

From the three force components, we obtain the equation for the total wave-induced force as follows:

$$\boldsymbol{F} = \boldsymbol{F_i} + \boldsymbol{F_d} + \boldsymbol{F_l} \tag{2.5}$$

$$\Leftrightarrow \boldsymbol{F} = \left[\frac{51}{24}\pi\rho_w\left(\frac{D}{2}\right)^3 a + \frac{1}{2}\pi\rho_w C_d\left(\frac{D}{2}\right)^2 |u|u\right]\boldsymbol{i_x} + \frac{1}{2}\pi\rho_w C_l\left(\frac{D}{2}\right)^2 u^2\boldsymbol{i_z} \tag{2.6}$$

II.2.5 Gravitational force of coral G

In addition to the wave-induced forces, the main force acting on the coral is its weight or gravitational force (G). Other forces related to the coral's adhesion to the substrate are neglected, and it can be expressed as follows:

$$G = \frac{4}{3}\pi(\rho_s - \rho_w)g\left(\frac{D}{2}\right)^3 \tag{2.7}$$

Where:

ρ_s: skeleton density of the coral (kg/m^3)

II.3 THE BALANCE OF TOTAL FORCES

Based on the shape of the coral block, the problem is divided into two cases:

II.3.1 Spherical coral (*Porites*):

For the spherical coral Figure 2.1a, we consider that the coral will tip over from the substrate at point O1. The equation for the equilibrium condition is written as follows [6]:

$$F_x(t)\frac{D}{2} \geq F_v(t)r_b \tag{2.8}$$

Inequality (2.8) is based on the formula for moment of force, where

- F_x (t) represents the total horizontal force acting on the largest cross-sectional area of the coral head with the lever arm being the radius of the coral head $\left(\frac{D}{2}\right)$.
- F_v (t) is the total vertical force acting on the bottom surface of the coral block with the lever arm being the radius of the coral bottom r_b.

Replace the equations for the forces:

- Horizontal: F_i, from (2.2) and F_d, from (2.3)
- Vertical: F_l, from (2.4) và G, from (2.7)

Into equation (2.8) we have:

$$(F_d + F_i)\frac{D}{2} = (G - F_l)r_b \tag{2.9}$$

$$\Leftrightarrow \frac{1}{2}\rho_w C_d \pi \left(\frac{D}{2}\right)^3 |u|u + \frac{51}{24}\pi\rho_w \left(\frac{D}{2}\right)^4 a = \frac{4}{3}\pi(\rho_s - \rho_w)g\left(\frac{D}{2}\right)^3 r_b - \frac{1}{2}\rho_w C_l \pi \left(\frac{D}{2}\right)^2 u^2 r_b \tag{2.10}$$

- D: Diameter of the coral head (m)
- r_b: radius of the coral bottom (m)
- O1: the point at which the coral will tip over

(a) Spherical (b) Hemispherical

Figure 2.2 The idealized shape of the coral [6]

Simplying π, ρ_w, $\left(\frac{D}{2}\right)^3$ we have:

$$\Leftrightarrow \frac{1}{2}C_d|u|u - \frac{51}{24}\left(\frac{D}{2}\right)a = \frac{4}{3}\pi\frac{(\rho_s-\rho_w)}{\rho_w}gr_b - \frac{1}{2}C_l\left(\frac{2}{D}\right)r_b u^2 \quad (2.11)$$

Here, the ratio between the area of the coral base and the largest cross-sectional area is called the [6]:

$$\delta = \frac{2r_b}{D} \approx \exp(-1.083D^{0.9}) \quad (2.12)$$

Replacing (2.12) into (2.11), we have:

$$\Leftrightarrow \frac{1}{2}C_d|u|u - \frac{51}{24}\left(\frac{D}{2}\right)a = \frac{4}{3}\pi\frac{(\rho_s-\rho_w)}{\rho_w}g\frac{\delta D}{2} - \frac{1}{2}C_l\delta u^2 \quad (2.13a)$$

Besides, the velocity and acceleration of water particles are represented as follows:

$$u = \frac{\pi H}{T_p}\frac{\cosh k(z+h)}{\sinh kh}\cos(kx - \omega t) = U\cos(kx - \omega t) \quad (2.13b)$$

$$a = \frac{2\pi^2 H}{T_p^2}\frac{\cosh k(z+h)}{\sinh kh}\sin(kx - \omega t) = \frac{2\pi}{T_p}Usin(kx - \omega t \qquad (2.13c)$$

With *U* the velocity of the surrounding flow,

$$U = \frac{\pi H}{T_p}\frac{\cosh k(z+h)}{\sinh kh} \qquad (2.13d)$$

We replace (2.13b) and (2.13c) into (2.13a), we have:

$$\begin{aligned} \Leftrightarrow\ & \frac{1}{2}C_d|U\cos(kx-\omega t)|U\cos(kx-\omega t) \\ & -\frac{51}{24}\left(\frac{D}{2}\right)\left(\frac{2\pi}{T_p}U\sin(kx-\omega t)\right) \\ & +\frac{1}{2}C_l\delta(U\cos(kx-\omega t))^2 - \frac{2}{3}\pi\frac{(\rho_s-\rho_w)}{\rho_w}g\delta D = 0 \end{aligned} \qquad (2.14)$$

Assuming the center of the coral head is located at the plane x = 0:

$$\begin{aligned} \Leftrightarrow\ & \frac{1}{2}U^2C_d|\cos(-\omega t)|\cos(-\omega t) + \frac{1}{2}U^2C_l\delta(\cos(-\omega t))^2 \\ & +\frac{51}{24}\left(\frac{D}{2}\right)\left(\frac{2\pi}{T_p}U\sin(-\omega t)\right) - \frac{2}{3}\frac{(\rho_s-\rho_w)}{\rho_w}g\delta D = 0 \end{aligned} \qquad (2.15)$$

Applying cos(-x) = cos(x) và sin(-x) = - sin(x) into (2.15):

$$\begin{aligned} \Leftrightarrow\ & \frac{1}{2}U^2\left(C_d|\cos(\omega t)|\cos(\omega t) + \delta C_l\cos^2(\omega t)\right) \\ & -\frac{51}{24}\left(\frac{D\pi}{T_p}U\sin(\omega t)\right) - \frac{2}{3}\frac{(\rho_s-\rho_w)}{\rho_w}g\delta D = 0 \end{aligned} \qquad (2.16)$$

Replace the velocity of the surrounding current with the following equation: (2.16a), we have:

$$\Leftrightarrow \frac{1}{2}\left(\frac{\pi H}{T_p}\frac{\cosh(k(z+h))}{\sinh(kh)}\right)^2 \left(C_d|\cos(\omega t)|\cos(\omega t)+\delta C_l\cos^2(\omega t)\right) - \frac{51}{24}\left(\frac{D\pi}{T_p}\left(\frac{\pi H}{T_p}\frac{\cosh(k(z+h))}{\sinh(kh)}\right)\sin(\omega t)\right) - \frac{2}{3}\frac{(\rho_s-\rho_w)}{\rho_w}g\delta D = 0 \quad (2.17)$$

When the velocity of the surrounding current U is approximated at the center of the sphere, (z+h) equals the distance from the center to the seabed plane, and for the spherical case, that distance is equal to the radius of the sphere $\left(\frac{D}{2}\right)$ so we have:

$$\Leftrightarrow \frac{1}{2}\left(\frac{\pi H}{T_p}\frac{\cosh\left(k\frac{D}{2}\right)}{\sinh(kh)}\right)^2 \left(C_d|\cos(\omega t)|\cos(\omega t)+\ \delta C_l\cos^2(\omega t)\right) - \frac{51}{24}\left(\frac{D\pi H}{T_p}\left(\frac{\pi}{T_p}\frac{\cosh\left(k\frac{D}{2}\right)}{\sinh(kh)}\right)\sin(\omega t)\right) - \frac{2}{3}\frac{(\rho_s-\rho_w)}{\rho_w}g\delta D = 0 \quad (2.18)$$

Let $U_1 = \frac{\pi}{T_p}\frac{\cosh\left(k\frac{D}{2}\right)}{\sinh(kh)}$, we have the second-order differential equation with respect to H as follows:

$$\Leftrightarrow \frac{1}{2}U_1^2[C_d|\cos(\omega t)|\cos(\omega t)+C_l\delta\cos^2(\omega t)]H^2 - \left[\frac{51}{24}\pi\frac{DU_1}{T_p}\sin(\omega t)\right]H - \frac{2}{3}\pi\frac{(\rho_s-\rho_w)}{\rho_w}g\delta D = 0 \quad (2.19)$$

Where:

δ: the ratio of the coral bottom to its largest cross-sectional area

H: wave height threshold (m)

h: depth from the water surface to the coral bottom (m)

The solution of the second-order equation (2.19) for H is the result of calculating the wave height threshold for a spherical coral.

II.3.2 Hemispherical coral (*Diploastrea heliopora*):

Similarly to the analysis done for the hemisphere shape (Figure 2.2b), the inertial forces, drag forces, lift forces, and gravity forces for the hemispherical model can be expressed as follows [6]:

$$\boldsymbol{F_i} = \pi\rho_w \left(\frac{D}{2}\right)^3 a\, \boldsymbol{i_x} \tag{2.20}$$

$$\boldsymbol{F_d} = \frac{1}{4}\rho_w C_d \pi \left(\frac{D}{2}\right)^2 |u|u\, \boldsymbol{i_x} \tag{2.21}$$

$$\boldsymbol{F_l} = \frac{1}{4}\rho_w C_l \pi \left(\frac{D}{2}\right)^2 u^2\, \boldsymbol{i_z} \tag{2.22}$$

$$G = \frac{2}{3}\pi(\rho_s - \rho_w) g \left(\frac{D}{2}\right)^3 \tag{2.23}$$

The velocity u and acceleration a are now applied at the center of mass of the research area. For the hemispherical case, where the distance to the seafloor is approximately $\frac{2D}{3\pi}$, the equilibrium equation is as follows [6]:

$$F_x(t)\frac{2D}{3\pi} \geq F_v(t)\frac{D}{2} \tag{2.24}$$

Similar to the spherical model, we also replace the components of forces into the equilibrium equation as follows:

$$(F_d + F_i)\frac{2D}{3\pi} = (G - F_l)\frac{D}{2} \tag{2.25}$$

Simplify by canceling out D on both sides and proceed with distributing both sides of the equation (2.25):

$$\begin{aligned} \Leftrightarrow\ & \frac{1}{4}\rho_w C_d \pi \left(\frac{D}{2}\right)^2 |u|u\frac{2}{3\pi} + \pi\rho_w \left(\frac{D}{2}\right)^3 a\frac{2}{3\pi} \\ & = \frac{1}{3}\pi(\rho_s - \rho_w)g\left(\frac{D}{2}\right)^3 - \frac{1}{8}\rho_w C_l \pi \left(\frac{D}{2}\right)^2 u^2 \end{aligned} \tag{2.26}$$

Simplify π, ρ_w, $\left(\frac{D}{2}\right)^2$ on both sides (2.26), we have:

$$\begin{aligned} \Leftrightarrow\ & \frac{1}{4}C_d|u|u\frac{2}{3\pi} + \frac{1}{8}C_l u^2 + \left(\frac{D}{3\pi}\right)a - \frac{1}{3}\frac{(\rho_s - \rho_w)}{\rho_w}g\left(\frac{D}{2}\right) \\ & = 0 \end{aligned} \tag{2.27}$$

Replace the equation of water particle (2.13b) and (2.13c) into (2.27), we have:

$$\begin{aligned} \Leftrightarrow\ & \frac{1}{6\pi}C_d|U\cos(kx - \omega t)|U\cos(kx - \omega t) \\ & + \frac{1}{8}C_l(U\cos(kx - \omega t))^2 \\ & + \left(\frac{D}{3\pi}\right)\left(\frac{2\pi}{T_p}U\sin(kx - \omega t)\right) - \frac{1}{3}\frac{(\rho_s - \rho_w)}{\rho_w}g\left(\frac{D}{2}\right) \\ & = 0 \end{aligned} \tag{2.28}$$

Assuming the center of the coral head is located at the plane x = 0:

$$\Leftrightarrow \frac{1}{6\pi}U^2 C_d|\cos(-\omega t)|\cos(-\omega t) + \frac{1}{8}U^2 C_l(\cos(-\omega t))^2 + \left(\frac{D}{3\pi}\right)\left(\frac{2\pi}{T_p}U\sin(-\omega t)\right) - \frac{1}{3}\frac{(\rho_s - \rho_w)}{\rho_w}g\left(\frac{D}{2}\right) = 0 \quad (2.29)$$

Apply cos(-x) = cos(x) and sin(-x) = - sin(x) into equation (2.29):

$$\Leftrightarrow U^2\left(\frac{1}{6\pi}C_d|\cos(\omega t)|\cos(\omega t) + \frac{1}{8}C_l\cos^2(\omega t)\right) - \left(\frac{D}{3\pi}\right)\left(\frac{2\pi}{T_p}U\sin(\omega t)\right) - \frac{1}{3}\frac{(\rho_s - \rho_w)}{\rho_w}g\left(\frac{D}{2}\right) = 0 \quad (2.30)$$

We substitute the velocity of the surrounding water at the coral head (2.13d) into (2.30), have:

$$\Leftrightarrow \left(\frac{\pi H}{T_p}\frac{\cosh(k(z+h))}{\sinh(kh)}\right)^2\left(\frac{1}{6\pi}C_d|\cos(\omega t)|\cos(\omega t) + \frac{1}{8}C_l\cos^2(\omega t)\right) - \left(\frac{D}{3}\right)\left(\frac{2}{T_p}\left(\frac{\pi H}{T_p}\frac{\cosh(k(z+h))}{\sinh(kh)}\right)\sin(\omega t)\right) - \frac{1}{3}\frac{(\rho_s - \rho_w)}{\rho_w}g\left(\frac{D}{2}\right) = 0 \quad (2.31)$$

Similarly to the spherical case, we take (z+h) as the distance from the center to the seabed plane, and in the case of the hemisphere, this distance is equal to $\left(\frac{2D}{3\pi}\right)$:

$$\Leftrightarrow \left(\frac{\pi H}{T_p}\frac{\cosh\left(k\frac{2D}{3\pi}\right)}{\sinh(kh)}\right)^2\left(\frac{1}{6\pi}C_d|\cos(\omega t)|\cos(\omega t)+\frac{1}{8}C_l\cos^2(\omega t)\right) - \left(\frac{D}{3}\right)\left(\frac{2H}{T_p}\left(\frac{\pi}{T_p}\frac{\cosh\left(k\frac{2D}{3\pi}\right)}{\sinh(kh)}\right)\sin(\omega t)\right) - \frac{1}{3}\frac{(\rho_s-\rho_w)}{\rho_w}g\left(\frac{D}{2}\right) = 0 \quad (2.32)$$

Similarly, let $U_1 = \frac{\pi}{T_p}\frac{\cosh\left(k\frac{2D}{3\pi}\right)}{\sinh(kh)}$, we have:

$$\Leftrightarrow U_1^2\left(\frac{1}{6\pi}C_d|\cos(\omega t)|\cos(\omega t)+\frac{1}{8}C_l\cos^2(\omega t)\right) - \left(\frac{2}{3}\frac{DU_1}{T_p}\sin(\omega t)\right)H - \frac{1}{3}\frac{(\rho_s-\rho_w)}{\rho_w}g\left(\frac{D}{2}\right) = 0 \quad (2.33)$$

After the transformation, we have a second-degree equation for H as follows:

$$\Leftrightarrow {U_1}^2\left(\frac{1}{3\pi}C_d|\cos(\omega t)|\cos(\omega t)+\frac{1}{4}C_l\cos^2(\omega t)\right)H^2 - \left(\frac{1}{3}\frac{DU_1}{T_p}\sin(\omega t)\right)H - \frac{1}{3}\frac{(\rho_s-\rho_w)}{\rho_w}gD = 0 \quad (2.34)$$

The solution of the second-degree equation (2.34) is the calculated threshold wave height for a hemisphere-shaped coral.

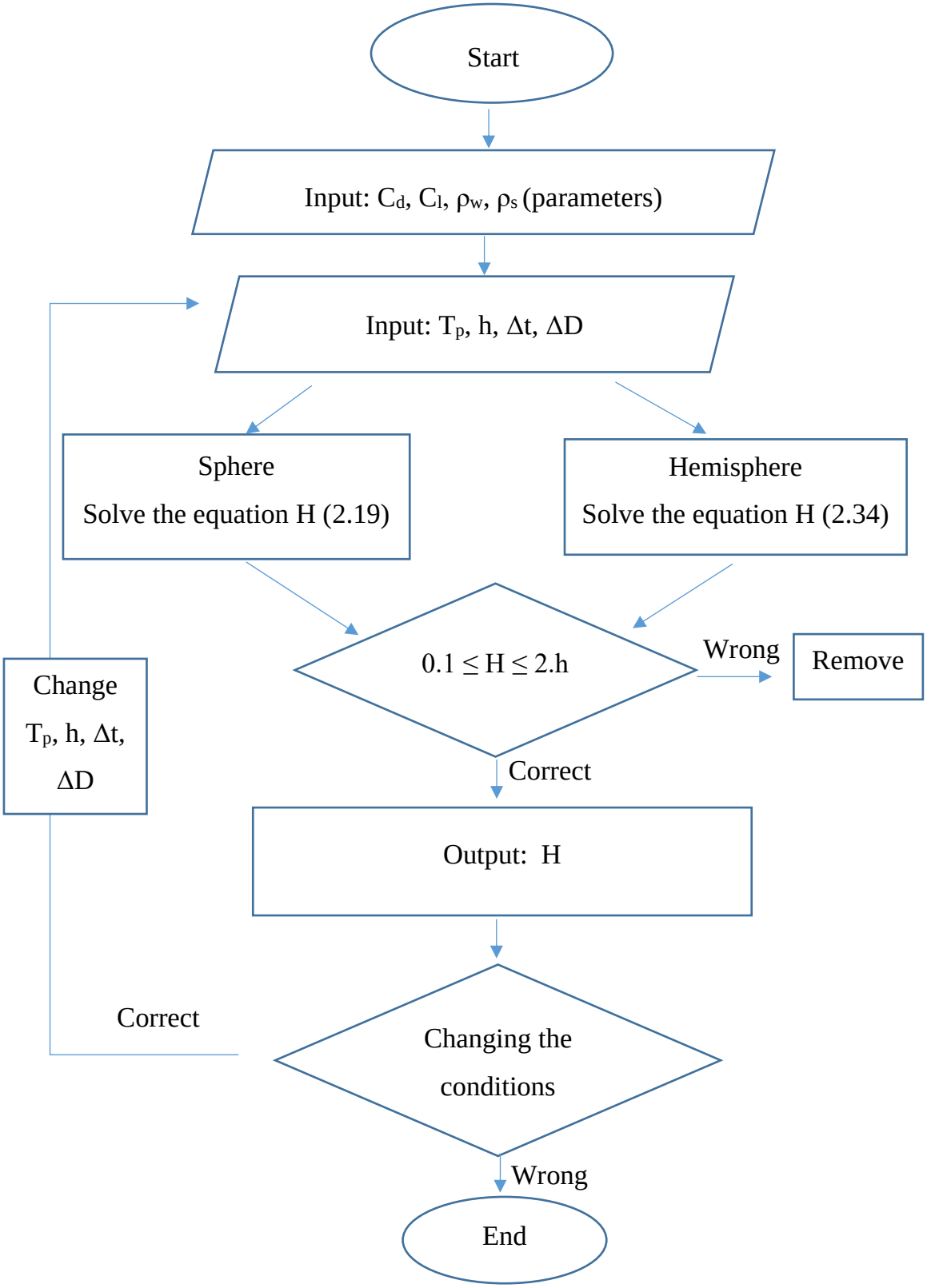

Figure 2.3 Block diagram of the calculation for the threshold wave height

CHAPTER III: RESULTS

III.1 CALCULATED MODEL

From Figure 2.3 we have the main input parameters for the problem as follows:

- Depth h (m)
- Peak wave period T_p (s)
- Time step Δt (s)
- Coral diameter increment ΔD (m) with D changing from 0 – 2.5 m.
- Drag coefficient C_d: dependent on the flow regime through the sphere and determined by the Reynolds number.

To determine the C_d coefficient, we rely on the experimental data presented in the chart by Newman, J. N. (1977) [8]. The Reynolds number (Re) is calculated using the formula:

$$Re = \frac{uD}{\upsilon} \tag{3.1}$$

Under the assumption of circular orbital motion for water particles (deep-water waves), the velocity is calculated as follows, according to Holthuijsen Leo H. (2007) [5]:

$$u = \omega a = \frac{2\pi}{T_p}\frac{H}{2} = \frac{\pi H}{T_p} \tag{3.2}$$

The C_d coefficient can be calculated based on the correlation with the Re coefficient as shown in Figure 3.1. In this calculation, if the wave period $T_p \approx 8$s, wave height $H \approx 2$m and the spherical diameter D = 2m then we have $\boldsymbol{Re} \approx 1.5 \cdot 10^6$. According to the experimental chart, $C_d \approx 0.45$. This result is consistent with the calculation

based on the experimental formula by Newman, 1977, for the drag coefficient $C_d \approx 0.45$.

- The experimental lift coefficient C_l is obtained by $C_l \approx 0.15$ [6].

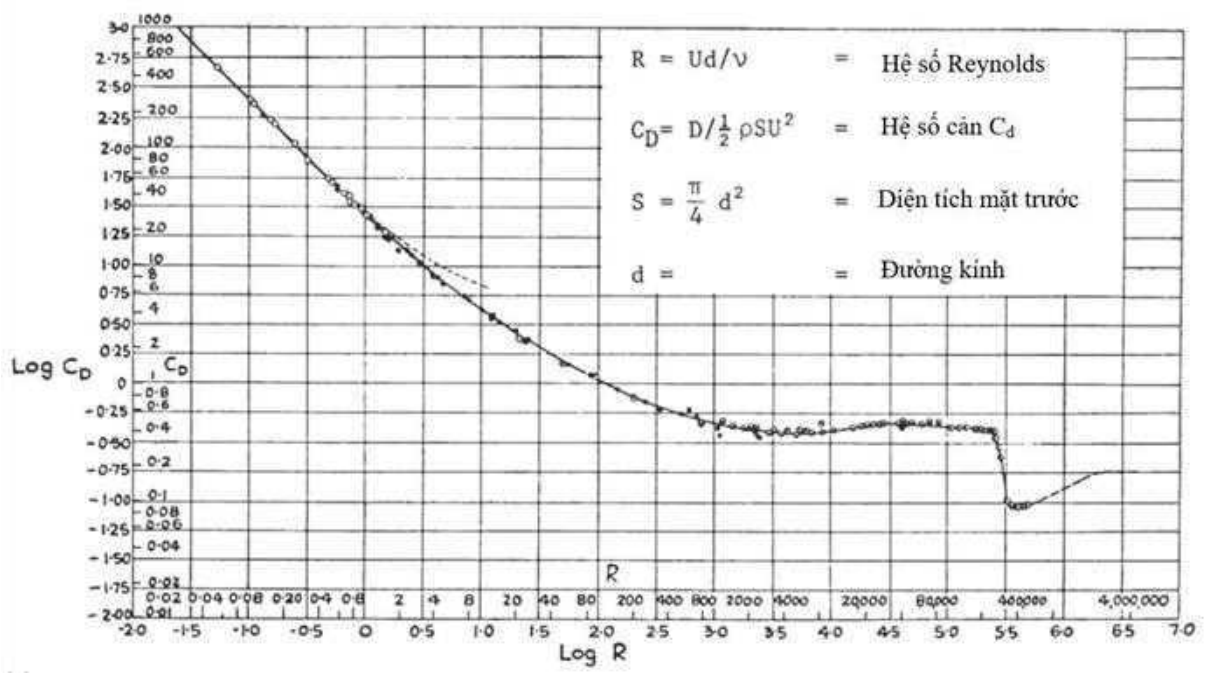

Figure 3.1 The experimental chart illustrates the correlation between the Reynolds number (Re) and the drag coefficient C_d [8]

- The density of coral skeleton (ρ_s) for spherical coral (e.g., *Porites*) is 1450 kg/m^3 [6]
- The density of coral skeleton (ρ_s) for hemispherical coral (e.g., *Diploastrea heliopora*) is 1250 kg/m^3 [2].
- Seawater density ρ_w = 1025 kg/m^3.

III.2 RESULTS OF SPHERICAL CORAL

III.2.1 Short-period storm waves

The input conditions for the spherical coral case under consideration during a storm with a short wave period are as follows:

- Depth h is considered at 3 m, 6 m, 9 m, 12 m.
- Wave period T = 7 s
- ΔD = 0.1 m
- The diameter D will be examined from 0 – 2.5 m

Table 3.1 Solving a quadratic equation and the results of the solutions in various cases

Condition	**Solutions**
a = 0 and b = 0	$x_1 = x_2 = 0$
a = 0	$x_1 = x_2 = -c/b$
a # 0 and $\Delta < 0$ (no solution case)	$x_1 = x_2 = 0$
a # 0 and $\Delta = 0$ (case with only one solution)	$x_1 = x_2 = \frac{-b}{2a}$
a # 0 and $\Delta > 0$ (case with two distinct solutions)	$x_1 = \frac{-b+\sqrt{\Delta}}{2a}$ $x_2 = \frac{-b-\sqrt{\Delta}}{2a}$

- $C_d = 0.45$; $C_l = 0.15$; $\rho_s = 1450$ kg/m^3; $\rho_w = 1025$ kg/m^3.
- In this model, to simplify the problem and avoid complicating the exponential function, instead of using the approximate formula $\delta \approx \exp(-1.083D^{0.9})$ (equation 2.12). We use the formula $\delta = \frac{2r_b}{D}$, where the relationship between the radius of the coral base rb and the diameter of the largest cross-section D is assumed to be $r_b = \frac{D}{3}$.

Figures 3.2, 3.3 and 3.4 depict the calculated wave height thresholds as a function of diameter at different depths for varying time intervals, namely $\Delta t = 0.1$s , $\Delta t = 0.5$s and $\Delta t = 1.0$s.

The result from Figure 3.2 indicate that the wave height threshold is nearly independent of the coral diameter. Although the threshold increases with depth, there

is no clear trend with respect to diameter D. Specifically, the threshold increases from D = 0 to 0.5 m but then exhibits no significant increase. With greater depth, the wave height threshold also increases: at h = 3 m, it's approximately 3 m; at h = 9 m, it's around 8 m, and at h = 12 m, it rises to nearly 10 m.

In the case of Δt = 0.5 s, the wave height threshold exhibits an unusual increase and decrease pattern with both diameter D and depth h. When Δt = 1.0 s, although the threshold follows a similar trend with depth, there is a sudden increase and decrease in values within the diameter range of D = 0 – 0.7 m. This demonstrates that as Δt increases, the wave height threshold H increases with D, but there is no stability in the relationship.

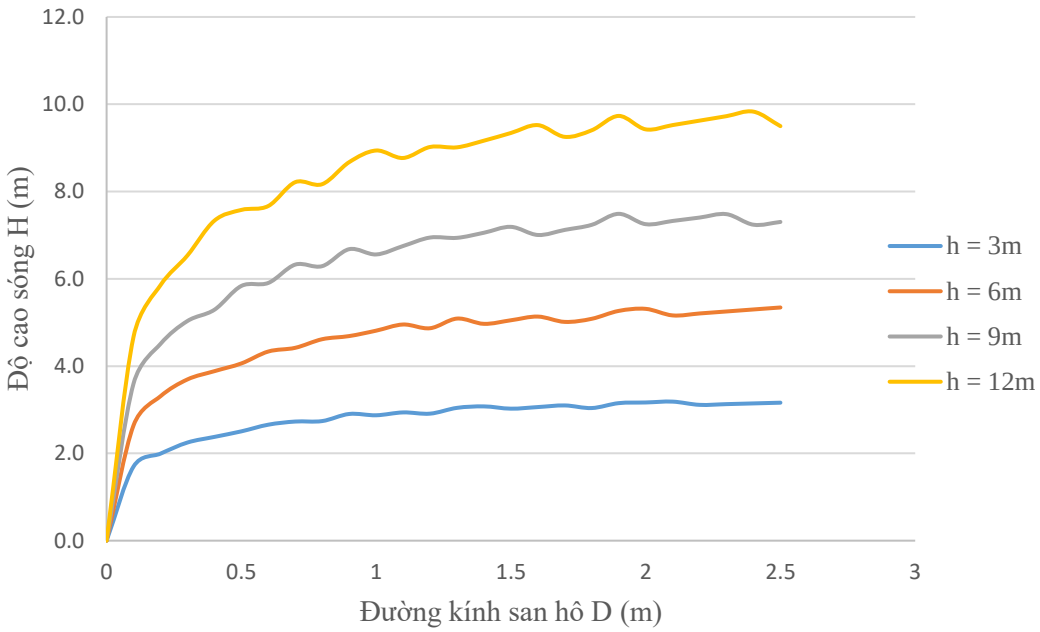

Figure 3.2 The wave height threshold results (H) for spherical coral under short-wave storm conditions with Δt = 0.1s.

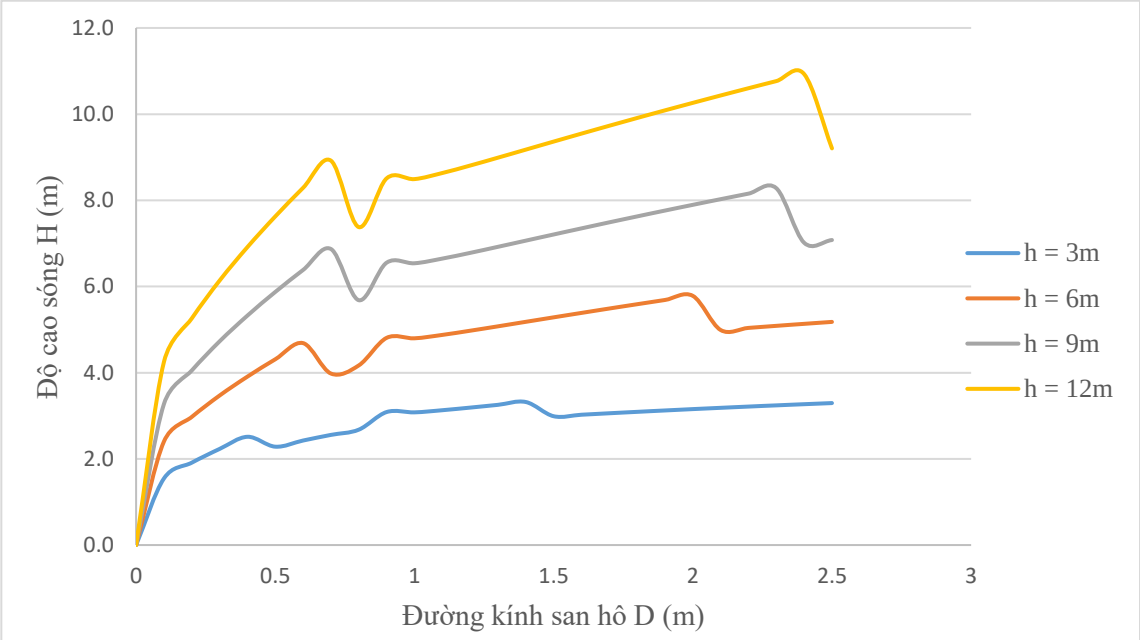

Figure 3.3 The wave height threshold results (H) for spherical coral under short-wave storm conditions with $\Delta t = 0.5s$

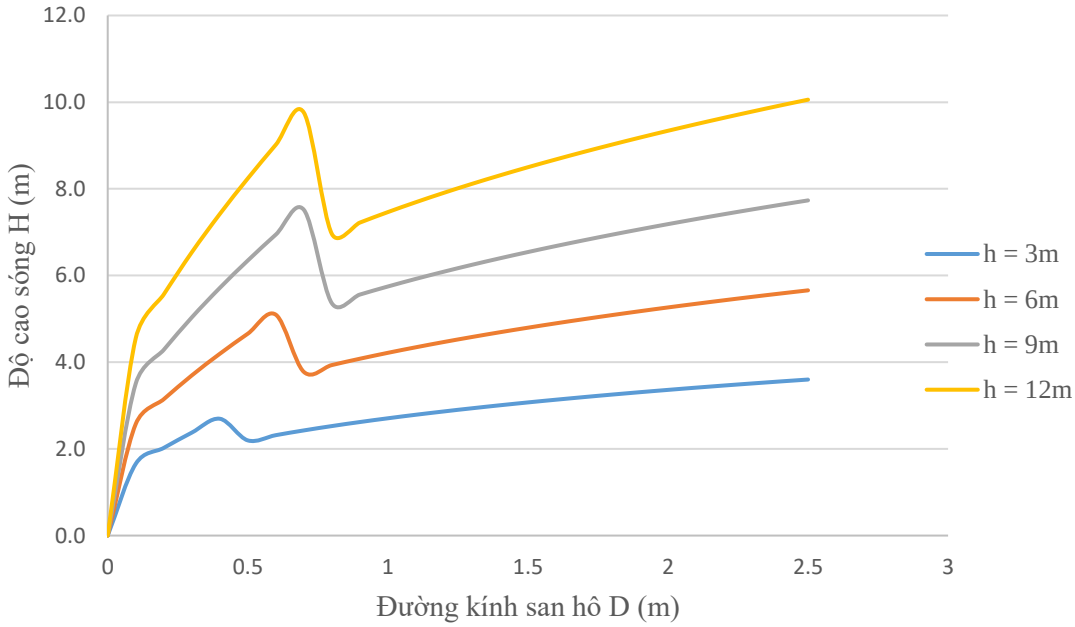

Figure 3.4 The wave height threshold results (H) for spherical coral under short-wave storm conditions with $\Delta t = 1.0s$

The results show that when selecting $\Delta t = 0.5$ s and $\Delta t = 1$ s, the phenomenon of missing solutions occurs. Therefore, for short-wave storms, choosing $\Delta t = 0.1$ s is the most appropriate option. These results also indicate that the wave height threshold is nearly independent of the coral diameter. This conclusion aligns with the findings of Massel và Done (1993) [6].

III.2.2 Long-period storm wave

For the case of long-wave storms, the input conditions are similar to Part III.1.1, except for the changes in wave period T and time step Δt.

- $T = 12$ s
- $\Delta t = 0.2$ s. Similar to Part III.1.1, when dealing with a long wave period T = 12s, we cannot choose $\Delta t = 0.1$ s because such a small Δt relative to the T_p period can lead to numerical instability. Therefore, in this case, the study presents results for the most suitable time step, which is $\Delta t = 0.2$ s.

Figure 3.5 illustrates the wave height threshold H as a function of coral diameter D. In the case of long-wave storms with T = 12s, the wave height threshold exhibits a more pronounced dependence on diameter compared to short-wave storms. The threshold increases with the coral's diameter. Larger corals are more resistant to toppling, so the required wave height threshold for overturning them needs to be higher. When the depth h is small, such as 3 m or 6 m, the threshold value may exceed the depth value. However, when the depth h is higher, like 9 m and 12 m, the threshold value approximates the depth value. This indicates that as the depth h increases, the wave height threshold H also increases. Additionally, the dependence of the wave height threshold H on the diameter becomes more evident.

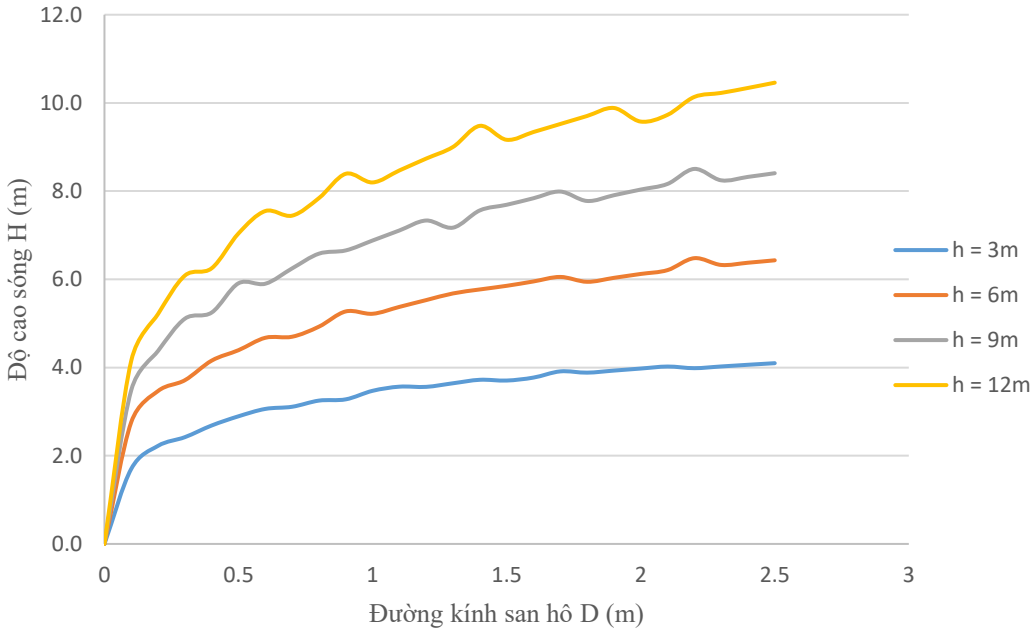

Figure 3.5 The wave height threshold results (H) for spherical coral under long-wave storm conditions

III.3 CALCULATED RESULT OF THE HEMISPHERICAL CORAL

The input conditions for the hemisphere coral model in the short wave period storm are considered similarly to the hemisphere model in section III.1.1, with a time step of $\Delta t = 0.1$ s.

Figure 3.6 depicts the variation of wave height threshold with the coral diameter. The results clearly show a significant dependence of the wave height threshold on the coral size. When the depth h = 3 m, the highest threshold is approximately 5 m, and when the depth h = 6 m, the highest threshold is approximately 8 m. The maximum wave height threshold values almost exceed the depth values.

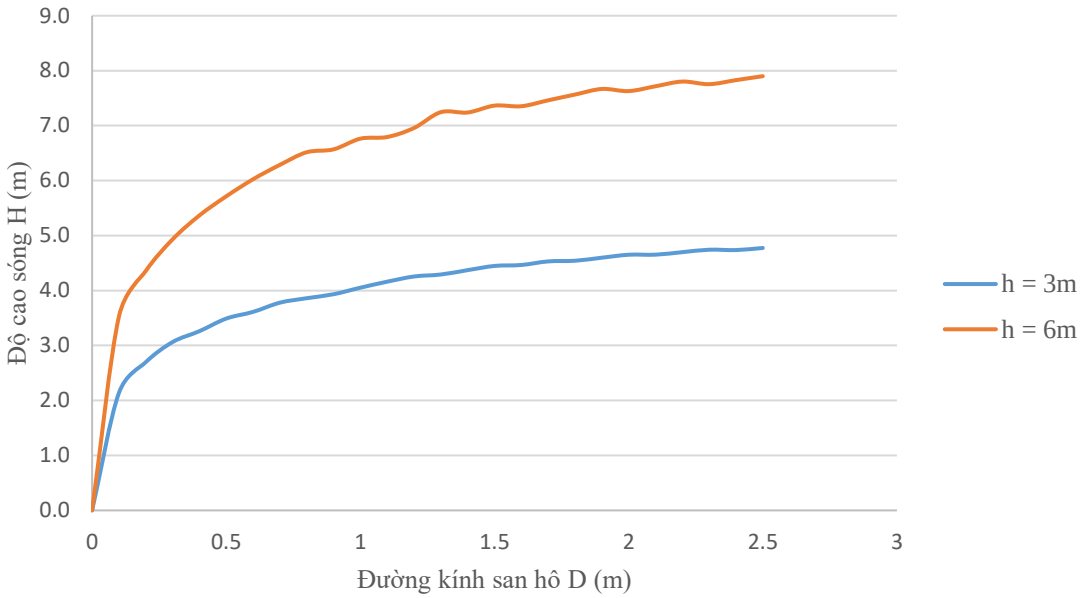

Figure 3.6 The wave height threshold for the hemispherical coral model in a short - period storm.

Comparing with the wave height threshold of the hemisphere coral case, the hemisphere's wave height threshold is significantly higher. The main reason is that the hemisphere coral has a lower center of gravity, which results in better stability compared to the hemisphere coral. In this calculation, only two depths, 3 m and 6 m, are considered because such wave heights are rarely encountered in reality since high waves are almost always breaking in shallow waters. However, this model does not account for wave breaking. When the depth is greater than 6 m, the wave height threshold seems much higher than any realistic wave, so such cases are disregarded.

CHAPTER IV: APPLYING CALCULATION MODEL OF THE WAVE HEIGHT THRESHOLD IN VAN PHONG – BEN GOI BAY AREA

In this chapter, the model will be applied to a specific area and time frame. The selected research area is Van Phong – Ben Goi bay, located in the northern part of Khanh Hoa province, Vietnam. The chosen storms are Typhoon Mirinae (November 2009) and Typhoon Damrey (April 2017), both of which made landfall in Khanh Hoa. After applying the model, the project provides empirical formulas to calculate the actual wave heights for comparison with the calculated wave height thresholds.

IV.1 OVERVIEW OF VAN PHONG - BEN GOI BAY (KHANH HOA PROVINCE)

Figure 4.1 The landscape of a corner of Van Phong Bay [13]

IV.1.1 Natural Conditions

Van Phong - Ben Goi bay is located in the northern part of Khanh Hoa province, with a total area of 46,100 hectares, including 5,050 hectares of islands and 51,050 hectares of water surface. Areas with a depth of less than 10 meters cover 17,000 hectares, and areas with a depth of 10 to 40 meters cover 35,000 hectares. Specifically, Ben Goi Bay at the top is relatively enclosed, while Van Phong Bay has better interaction with the open sea [1].

IV.1.2 Distribution and Morphology of Coral Reefs

Studies on the structure of coral reefs in this region have revealed that coral reefs here can be categorized into three structural groups [1]:

- *Open reefs*: distributed at depths ranging from 10 to 15 meters, with a width of 30 to 80 meters, dominated by branching formations.
- *Closed reef*: found at depths of 6 to 8 meters, with widths ranging from 100 to 150 meters, dominated by block or fragment formations.
- *Semi-closed reef*: located at depths of 8 to 10 meters, with widths of 70 to 100 meters, exhibiting the highest species diversity.

Coral reefs in Van Phong Bay - Ben Goi have a wide distribution, including coral belts along the southern shoreline of the bay, such as Ninh Phuoc, Ninh Tinh, the southern and southeastern parts of Hon Lon, around islands like Hon Ong, Hon Den, Hon My Giang, and small islands within the Ben Goi basin. They are also found along the Hon Gom Peninsula (Khai Luong) and in some independent reef formations like Trao Reef and Man Reef…[1].

IV.1.3 Biodiversity

Studies on coral reefs have identified 215 species of hard corals belonging to 52 genera and 14 families, with the Faviidae family having the highest number (23 species), followed by *Acroporidae* (21 species) and *Poritidae* (11 species). The dominant genera mainly include *Acropora, Porites, Goniopora, Montipora*, and *Favia*. Coral cover varies from 10% to 38.7% for hard corals and from 0.3% to 14.9% for soft corals, with an average of 22.5% for hard corals and 4.5% for soft corals [1].

IV.1.4 Current situation and threats

According to the statistic of Vo Si Tuan (2006), the majority of coral reefs are not in good condition. The average coral cover value on 9 study reefs ranges from 10% to 38.7%. Monitoring data from fixed reef sites between 2003 and 2005 indicate an increasing trend in coral mortality in areas such as Hon Den, Bai Tre, and the southern part of Hon My Giang. Most of the coral reefs in the Cum Meo and Ran Tuong areas have already died, except for some block-shaped coral formations and surviving soft corals [1]. Threats to these reefs include overexploitation, destructive practices (such as blast fishing or the use of harmful chemicals), outbreaks of crown-of-thorns starfish, sedimentation and siltation, pollution, and other potential threats [1].

IV.2 CALCULATION OF WAVE IN TYPHOONS

IV.2.1 Typhoon information:

- ***Typhoon Mirinae (2009)***

known as Storm No. 11 in Vietnam according to the Central Meteorological and Hydrological Forecasting Center, made landfall in Vietnam on November 2, 2009 [18]. Figure 4.2 is a map depicting the path of the typhoon.

Mirinae brought heavy rainfall to the central region of the Philippines after occurring as a Category 2 typhoon (on the Saffir-Simpson scale), equivalent to Category 12-13 on the tropical storm scale in Vietnam, with wind speeds of 85 knots (~157.7 km/h). Mirinae weakened into a tropical storm as it moved into the South China Sea but quickly regained strength, becoming a tropical storm again just before hitting Vietnam on Monday, November 2, 2009, in the coastal province south of Phu Yen [18].

Figure 4.2 Track of typhoon Mirinae [11]

- ***Typhoon Damrey (2017)***

Typhoon Damrey (November 4, 2017) was the strongest storm to hit Vietnam since 2001 and originated from a tropical low-pressure system in the Philippines on October 31, 2017 (Figure 4.3). It emerged in the South China Sea a few days later, developing into a dangerous Category 2 typhoon. It was named Typhoon No. 23 of the 2017 Pacific Typhoon season and Typhoon No. 12 in the South China Sea. On the early morning of November 4, 2017, Typhoon Damrey made landfall in Vietnam, directly hitting Khanh Hoa Province with wind speeds of up to 135 km/h. Typhoon Damrey was classified as Category 13 on the Vietnamese tropical storm scale (equivalent to

Category 2 on the Saffir-Simpson scale). The typhoon affected a total of fifteen provinces in Central Vietnam. Over the course of two days (November 4 and 5), heavy rainfall averaged 500-700mm [10]. The total rainfall decreased as Damrey moved westward and gradually dissipated over Cambodia. [17].

Figure 4.3 The track of typhoon Damrey [12]

IV.2.2 Input parameters for scenarios.

Since the surveyed area primarily consists of spherical-shaped coral reefs, scenarios here are only applicable to the *Porites* coral model with a spherical shape. To apply these scenarios to the model, we also require the following input parameters:

- *Depth h*: In the Van Phong - Ben Goi bay, considering the coral reef morphologies introduced in section (IV.1.2), the closed reef area, where many *Porites* individual coral formations are found and is the focus of this study, is the most suitable region for model application. The depth distribution in this area is approximately 6 - 8 meters, so the scenarios will be applied for two depths: h = 6 meters and h = 8 meters.
- *Wave peak period* T_p: The steps to obtain the wave period T_p as an input parameter will be detailed in section (IV.3.1)

- *Coefficients*: drag coefficient C_d, lift coefficient C_l, skeleton density ρ_s, sea water density ρ_w.
- Time steps Δt and diameter division ΔD.

IV.2.3 Calculation of average wave height at the surface and wave period from the typhoon wind speed.

a) Theory:

Based on the typhoon wind speed, the significant wave height H_s and wave period T_p at a specific location can be calculated using the JOHNSWAP formula as follows [7]:

$$\frac{gH_s}{U^2} = 1.6.10^{-3}\left(\frac{gX}{U^2}\right)^{0.5} \quad (4.1)$$

$$\frac{gT_p}{U} = 0.286\left(\frac{gX}{U^2}\right)^{0.33} \quad (4.2)$$

Where:

U: Wind speed (m/s)

X: fetch (m)

g: gravitational acceleration (9.81 m/s^2)

Then, the probability distribution formulas for wave height are applied [7]:

$$\bar{H} = \sqrt{2\pi}\sigma_\zeta \quad (4.3)$$

$$H_s = 4\sigma_\zeta \quad (4.4)$$

To find the relationship between significant wave height (Hs) and average wave height $\bar{H}$:

$$H_s = 1.6\bar{H} \quad (4.5)$$

b) Applying the calculation of average wave height at the surface and wave period for Typhoon Mirinae (2009):

According to Figure 4.4, the star marks the area under consideration, which is the Van Phong - Ben Goi bay with a wind speed of U = 23 m/s. By choosing a fetch distance X = 200 km and substituting it into equation (4.2), the wave period $T_p \approx 10$s. Substituting this value into equations (4.1) and (4.5), the average wave height at the surface $\bar{H}$ is calculated to be 5.25 meters.

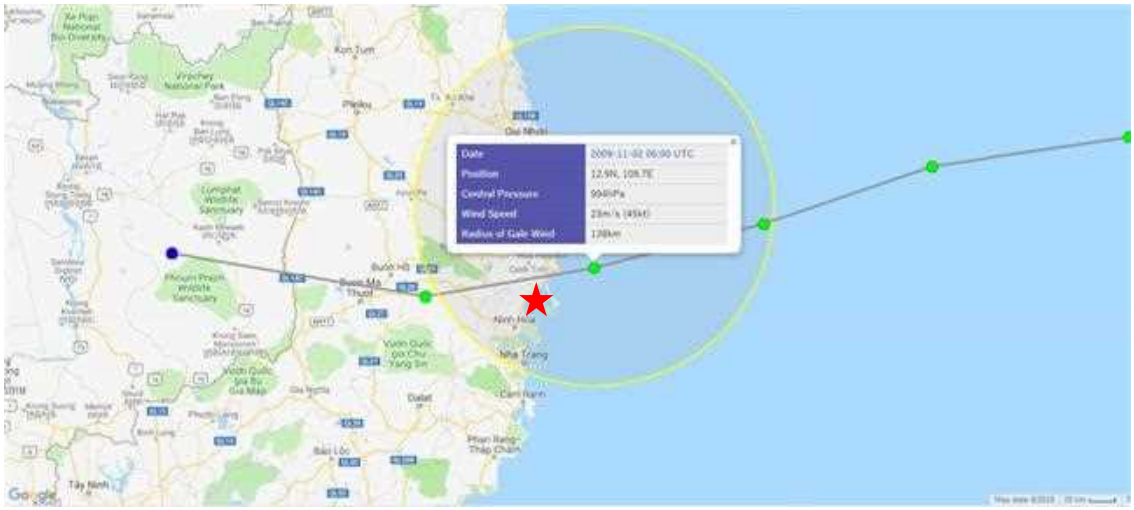

Figure 4.4 The position of Typhoon Mirinae used in the model [11]

c) Applying the Calculation of Average Wave Height at the Surface and Wave Period for Typhoon Damrey (2017):

Similarly, according to Figure 4.5, with a fetch distance X = 200 km, but with a wind speed U of 35 m/s, substituting these values into equations (4.2) and (4.1), (4.5) yields the results for the wave period of Typhoon Damrey as $T_p \approx 11.6$ s and the average wave height at the surface $\bar{H}$ = 8.0 m

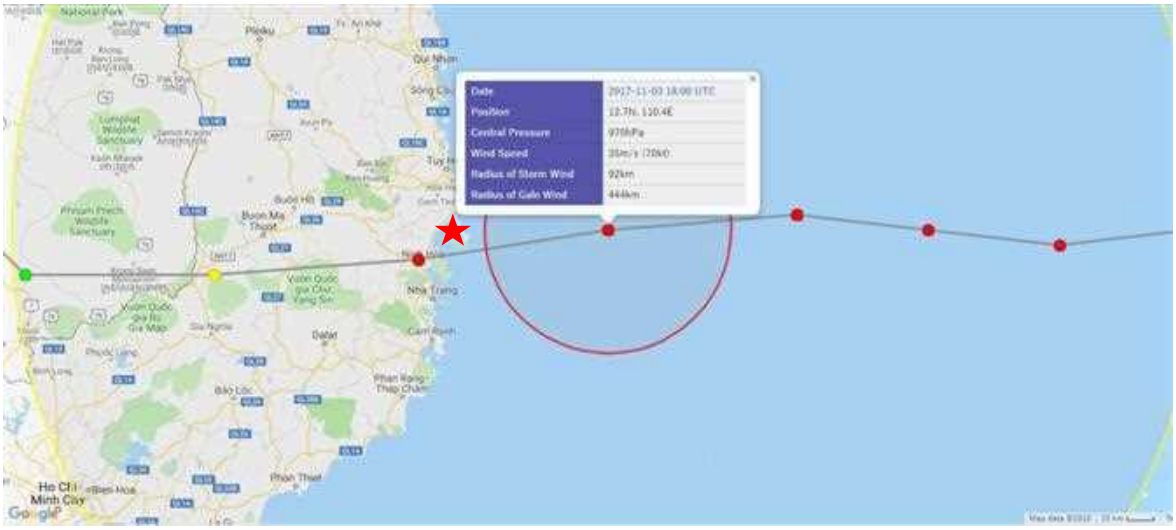

Figure 4.5 The position of Typhoon Damrey used in the model [12]

IV.2.3 Calculating wave height attenuation with depth

In order to make a more comprehensive comparison and observation, the wave height at the bottom H_r is calculated from the data of the typhoon to compare it with the threshold wave height (H) results of the problem. The wave height H_r is calculated using the UNESCO formula for depth attenuation, following these calculation steps.

- Step 1: Calculate the average wave height $\overline{H}$ at the surface (z = 0) from the significant wave height H_s using formula (4.5).
- Step 2: Calculate the pressure (caused by the waves) at the bottom (z = h) using the formula for the pressure amplitude caused by waves in deep water [5].

$$p_{wave} = \rho_w g a e^{kz} = \rho_w g \frac{\overline{H}}{2} e^{kz} \quad (4.6)$$

Where:

p_{wave}: Pressure at the considered depth

a: wave amplitude (m)

$\bar{H}$: average wave height (m)

ρ_w: water density (kg/m^3)

g: gravitational acceleration (m/s^2)

z: vertical position (m), here we choose z = h = const

k: wave number

Note: The pressure in formula (4.6) is in units of N/m^2 so it needs to be converted to dbar for application in formula (4.8). Therefore, the pressure calculation formula (4.6) will be transformed into:

$$p_{wave} = \rho_w g \frac{\bar{H}}{2} e^{kz}.10^{-4} \quad (4.7)$$

- Step 3: Obtain the pressure at the bottom at a specific depth, substitute it into formula (4.8) to calculate the wave height H_r at the bottom (z = h).

$$H_r = H = \frac{C_1.p + C_2.p^2 + C_3.p^3 + C_4.p^4}{g(\theta) + \frac{1}{2}\gamma'.p} \quad (4.8)$$

Trong đó:

- H: Converted wave height (m)
- p: Pressure recorded by the wave measuring device (dbar)
- $C_1 = 9.72659$
- $C_2 = -2.2512.10^{-7}$
- $C_3 = 2.279.10^{-10}$
- $C_4 = -1.82.10^{-15}$
- $\gamma = 2.184.10^{-6}$
- $g(\theta) = 9.780318\ [1 + 0.0052788.\sin^2(\theta) + 0.0000236.\sin^4(\theta)]$

- θ: Latitude of the calculation area (for Van Phong – Ben Goi bay is North 12.6660^o)

Applying the calculation method to the research area, the table below presents the converted wave heights at the seafloor for the reef areas in Van Phong – Ben Goi bay with depths of 6 m and 8 m.

IV.2.4 The threshold wave heights at Van Phong – Ben Goi bay

a) General initial conditions for Van Phong – Ben Goi bay:

- h = 6 m and 8 m
- ΔD = 0.1 m and diameter D is calculated from 0 – 2.5 m.
- $C_d \approx 0.45$
- $C_l \approx 0.15$
- $\rho_s = 1450$ kg/m^3
- $\rho_w = 1025$ kg/m^3

b) Typhoon Mirinae:

- Wave period $T_p \approx 10$ s.
- $\Delta t = 0.1$ s

c) Typhoon Damrey:

- Wave period $T_p \approx 11.6$ s
- $\Delta t = 0.2$s

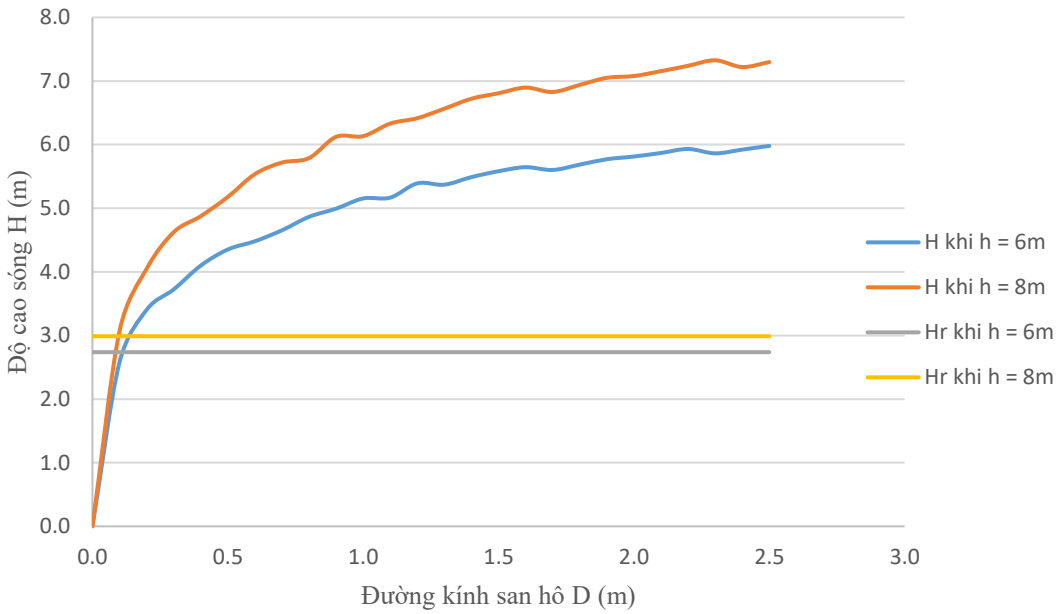

Figure 4.6 The wave height threshold H and converted wave height H_r in Van Phong – Ben Goi bay during typhoon Mirinae (2009)

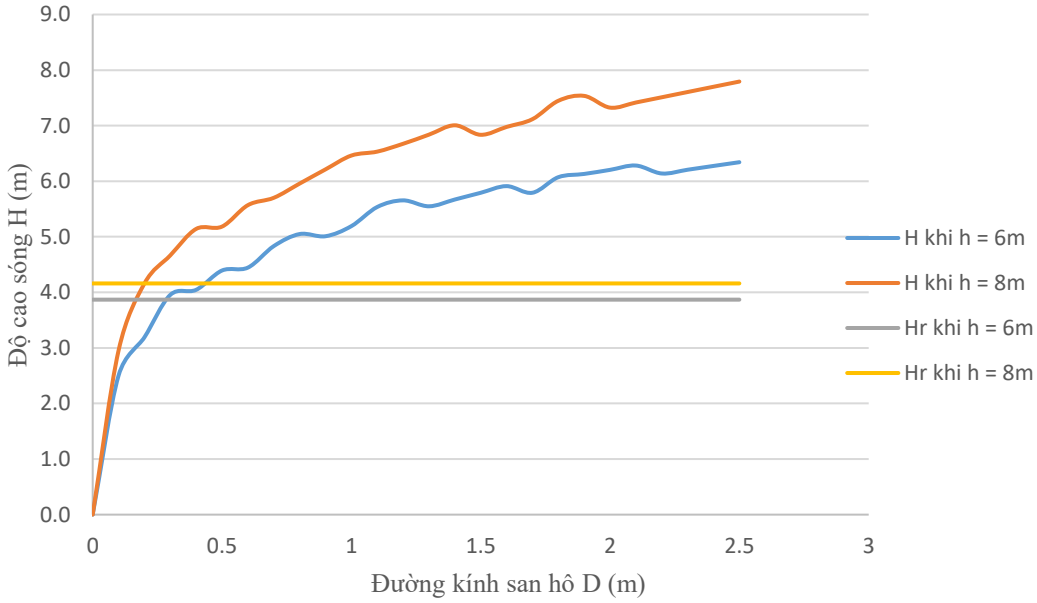

Figure 4.7 The wave height threshold H and converted wave height H_r in Van Phong – Ben Goi bay during typhoon Damrey (2017)

Through the two results (Figure 4.6 and Figure 4.7), it can be observed that the wave height threshold increases significantly with coral reef diameter, as seen in the results for long-period hurricanes. In the case of Typhoon Mirinae (2009), with lower storm intensity compared to Typhoon Damrey (2017), the wave height threshold is lower. Specifically, at a depth of 6 meters, during Typhoon Damrey, the wave height threshold exceeds 6 meters, whereas during Typhoon Mirinae, it is approximately 6 meters, and similarly with different depths, as the depth increases, the threshold also increases.

When using the results in Table 4.1 and comparing them with the two charts of wave height threshold in Figure 4.6 and Figure 4.7, it can be concluded that the calculated wave height at the bottom (Hr) is insufficient to cause significant mechanical impacts on corals, except for immature coral individuals. Therefore, theoretically, waves generated by storms cannot exert significant mechanical effects on corals. If there are any effects, they are only for corals weakly attached to the substrate, as in the case considered in the model.

This result is consistent with some previous studies on the impact of storms on spherical corals:

- In comparison with a specific case, Typhoon Pamela (1976), which passed through and swept the island of Guam, was mentioned in a statistical study of the impact of typhoon on *Porites* coral reefs by Mireille L. Harmelin-Vivien (1994). Typhoon Pamela (1976) is considered one of the largest typhoons in the history of Guam, with maximum wind speeds reaching up to 240 km/h, and its course lasted for 12 days (from May 14, 1976, to June 1, 1976). However, according to the statistical table of the impact of Typhoon Pamela on *Porites* corals distributed at depths from 0 to 20 meters, the impact was very low, affecting mainly only branch-shaped coral species [3].

- Similarly, Hurricane Hugo (1989), which passed through Saint Croix Island in the Caribbean Sea with maximum wind speeds of 260 km/h, had a prolonged path from September 10, 1989, to September 25, 1989. Statistics on the impact of this hurricane on coral reefs distributed at depths from 0 to 12 meters showed that only 8% of the *Porites Astreoides* coral species were damaged by the storm. [3].

From this, it can be seen that for coral species with branching structures, the percentage of damage caused by waves from hurricanes is very low. If there is damage to coral reefs due to waves from storms, it is mainly to the branching coral species. Alternatively, the damage may not be directly caused by wave-related factors but could be due to indirect factors such as large waves stirring up sediment on the seabed, leading to increased sediment concentration. Additionally, the rainfall from the storm could rapidly reduce salinity, which can also be harmful to coral life.

Table 4.1 Result of wave height H_r in each case are as follows

Typhoon	Wind speed U (m/s)	Storm wave period T (s)	Surface wave height $\overline{H}$ (m)	Depth h (m)	Wave height H_r at bottom (z = h) (m)	The range of wave height thresholds H (m)
Mirinae (2009)	23	10	3.28	6	2.737	0 – 6
				8	2.988	0 – 7.3
Damrey (2017)	35	11.6	5.0	6	3.869	0 – 6.5
				8	4.160	0 – 8.0

CONCLUSION

The model for assessing the impact of wave height thresholds on coral individuals is based on the hydrodynamic equations developed by Massel and Done (1993). The model applies to idealized spherical and hemispherical coral shapes with varying diameters at specified depths and wave periods during specific storms. The results show:

Sperical coral:

- Short wave period storm (T_p = 7s): The wave height threshold is almost independent of coral size.
- Long wave period storm (T_p = 12 s): The wave height threshold depends on coral size, with larger corals having higher wave height thresholds.

Hemispherical coral:

- The results indicate that the wave height threshold strongly depends on coral size during short wave period storms (T_p = 7 s)

The model was applied to the Van Phong Bay area for two storms, Mirinae (2009) and Damrey (2017). Actual wave heights at the seabed were calculated using experimental formulas to determine the real wave heights generated by the storms. The results show that the actual wave heights during the storms are still lower than the calculated wave height thresholds predicted by the model. Wave heights generated by the storms have less impact on coral blocks with sizes D > 0.5 m. The calculated results are consistent with reality and previous research.

However, the model still has some limitations as it can only be applied to idealized spherical or hemispherical shapes, while corals come in various forms such as branches, fragments, and flats. The model does not account for wave breaking due to bottom friction.

Nevertheless, this study represents an initial step in developing computational models and researching the hydrodynamic effects on coral reef ecosystems in the future..

REFERENCE

Vietnamese

[1] Võ Sĩ Tuấn, (2006), *Hệ sinh thái rạn san hô biển Vệt Nam*, Nhà xuất bản khoa học và kĩ thuật.

English

[2] Done, T., D. Potts, (1992), Influences of habitat and natural disturbances on contributions of massive Porites corals to reef communities, *Marine Biology*, 114, 479-493.

[3] Harmelin-Vivien, M. L., (1994), The effects of storms and cyclones on coral reefs: a review, *Journal of Coastal Research*, 12, 211-231.

[4] Harris, D. L., A. Rovere, E. Casella, H. Power, R. Canavesio, A. Collin, A. Pomeroy, J. M. Webster, V. Parravicini, (2018), Coral reef structural complexity provides important coastal protection from waves under rising sea levels, *Science Advances*, 4, 1-7.

[5] Holthuijsen, L. H., (2007), *Waves in oceanic and coastal waters*, Cambridge university press.

[6] Massel, S., T. Done, (1993), Effects of cyclone waves on massive coral assemblages on the Great Barrier Reef: meteorology, hydrodynamics and demography, *Coral Reefs*, 12, 153-166.

[7] Massel, S. R., (1996), *Ocean surface waves: their physics and prediction*, World scientific.

[8] Newman, J. N., (1977), *Marine hydrodynamics*, Massachusetts Institute of Technology, Cambridge, Mass.

Reference

[9] Salles, T., J. Pall, J. M. Webster, B. Dechnik, (2018), Exploring coral reef responses to millennial-scale climatic forcings: insights from the 1-D numerical tool pyReef-Core v1. 0, *Geoscientific Model Development*, 11, 2093-2110.

[10] The World Bank assessment team, (2018), *2017 Vietnam Post-Typhoon Damrey Rapid Damage and Needs Assessment*, The World Bank.

Tài liệu internet

[11] http://agora.ex.nii.ac.jp/digital-typhoon/summary/wnp/g/200921.html.en: đường đi cơn bão Mirinae (2009)

[12] http://agora.ex.nii.ac.jp/digital-typhoon/summary/wnp/g/201723.html.en: đường đi cơn bão Damrey (2017)

[13] https://bacvanphongkhanhhoa.com.vn/vinh-van-phong/vinh-van-phong-vi-tri-dia-ly-lich-su-hinh-thanh-va-du-an-quy-hoach-trieu-do/: cảnh quan vịnh Vân Phong.

[14] https://wwf.panda.org/our_work/oceans/coasts/coral_reefs/: thông tin khái quát về san hô.

[15]http://www.coralsoftheworld.org/species_factsheets/species_factsheet_images/porites-solida/#: hình ảnh san hô *Porites solida.*

[16] https://www.coris.noaa.gov/about/what_are/: thông tin khái quát về san hô

[17] https://www.nasa.gov/feature/goddard/2017/damrey-nw-pacific-ocean: thông tin về cơn bão Damrey (2017).

[18]https://www.nasa.gov/mission_pages/hurricanes/archives/2009/h2009_Mirinae.html: thông tin về cơn bão Mirinae

[19] https://www.sealifebase.ca/summary/Diploastrea-heliopora.html: hình ảnh san hô *Diploastrea heliopora.*

[20]http://www.wildsingapore.com/wildfacts/cnidaria/coralhard/faviidae/diploastrea.htm: thông tin về san hô *Diploastrea heliopora.*

UNIVERSITY OF SCIENCE,
VIETNAM NATIONAL UNIVERSITY HO CHI MINH CITY
Physics & Engineering Physics Faculty
Department of Oceanology, Meteorology and Hydrology

SOCIALIST REPUBLIC OF VIETNAM
Independence – Freedom – Happiness
--o0o---

GRADUATION THESIS COURSE REVIEWS

Student: Nguyen Thi To Van

Title: **The calculated modeling of wave height threshold affecting on the coral bottom**

Field of Oceanology, major: Oceanology

Reviewer: (Full name, Academic title, Degree) Asso. Prof., PhD. Vo Luong Hong Phuoc

Working agency: University of Science, VNU-HCM

Role:

☒ Supervisor ☐ Reviewer

Comments and evaluation of graduation thesis:

1. **Scientific significance**:

Coral reefs are important marine ecosystems that support high biodiversity. They provide food, income, and storm protection for millions of people. However, coral reefs are under threat from climate change factors like ocean warming, acidification, and extreme weather. One of the threats to coral reefs is damage from large waves during storms or cyclone events. Waves can physically break and dislodge coral structures. Understanding the wave energy thresholds that cause damage can help better predict and manage these impacts.

Accurate modeling of these coral damage wave height thresholds can help create early warning systems for reef managers. Warnings can be issued before a cyclone so preparations and protection measures can be taken proactively.

Conclusions, studying the modeling of damaging wave heights on coral reefs provides knowledge to help forecast, minimize and mitigate wave impacts. This is important for protecting these fragile ecosystems under climate change pressures.

2. **Content**:

2.1: Find the wave height threshold equation via Modeling and Applying the model

2.2: Buiding up the modeling via Mathematical equations by FORTRAN program

2.3: Author's attitude

- Work hard, and responsible her work
- Be honest and ethical, and open-minded to consider different ideas and viewpoints. Look for opportunities to learn and grow.

- Show determination - Write the program yourself and refer to reference documents

=> Good student!!

3. **Form**:

Good enough and in stadard

4. **Conclusion:**

The thesis meets the requirements of a university graduation thesis

We respectfully request the thesis grading committee to approve the thesis with points: 10/10

City. Ho Chi Minh, July 12th 2015

REVIEWERS

Vo Luong Hong Phuoc

UNIVERSITY OF SCIENCE,
VIETNAM NATIONAL UNIVERSITY HO CHI MINH CITY
Physics & Engineering Physics Faculty
Department of Oceanology, Meteorology and Hydrology

SOCIALIST REPUBLIC OF VIETNAM
Independence – Freedom – Happiness
--o0o---

GRADUATION THESIS COURSE REVIEWS

Student: Nguyen Thi To Van

Title: **The calculated modeling of wave height threshold affecting on the coral bottom**

Field of Oceanology, major: Oceanology

Reviewer: (Full name, Academic title, Degree) MSc. Le Nguyen Hoa Tien

Working agency: University of Science, VNU-HCM.

Role:

☐ Supervisor ☒ Reviewer

Comments and evaluation of graduation thesis:

1. **Scientific significance**:

When it comes to coral issues, we often think of research related to biological, ecological or environmental processes. and rarely think of those related to similar dynamic processes. or physical processes for corals. However, this topic has explored the impact of the surrounding environment on corals from the perspective of dynamic processes. This is a very new issue, has great scientific significance and needs more research investment.

Specifically, the project develops a program to calculate the wave height threshold for coral reefs that create ideal spherical and hemispherical reefs in the case of different long and short-wave periods, as well as the impact of the stream to erosion around the coral head. In addition, the model was also applied to real conditions for the Van Phong - Ben Goi bay area (Khanh Hoa) during two storms Mirinae (2009) and Damrey (2017).

Content:

The thesis content includes 4 chapters:

Chapter 1: overview of corals as well as characteristics of the type of coral that the topic is considering and studies on the effects of dynamics on corals.

Chapter 2: Theory and solution of mathematical equations on the model to calculate the threshold of wave height affecting coral reefs, which considers the impact of dynamic processes through analysis of force components impact on corals.

Chapter 3: Calculation process and results for each case: spherical coral, hemispherical coral and erosion around the coral head

Chapter 4: Applying model results to reality in the Van Phong - Ben Goi Bay area.

2. Form:

The format of the thesis is beautiful and complies with regulations

The thesis has a reasonable layout

Images and tables are clear, beautiful, and full of information

Very few spelling errors, however, the image order captions are incorrect

Add the calculation program to the appendix.

3. Conclusion:

The thesis meets the requirements of a university graduation thesis.

We respectfully request the thesis grading committee to approve the thesis with points: 9.75/10

Ho Chi Minh City, July 12th 2015

REVIEWERS

Le Nguyen Hoa Tien

HIGH THRESHOLD CALCULATION MODEL WAVES IMPACT ON CORAL FEET

SCIENTIFIC CONFERENCE XII

Nguyen Thi To Van, Vo Luong Hong Phuoc

Department of Oceanography, Meteorology and Hydrology

University of Natural Sciences, Vietnam National University-HCM

GENERAL

• The damage to coral reefs after storms is huge, of which the **mechanical impact** caused by storm waves is not least. • The model is mainly based on hydrodynamic formulas to calculate **the threshold wave height** that can overturn simple spherical or hemispherical coral individuals.

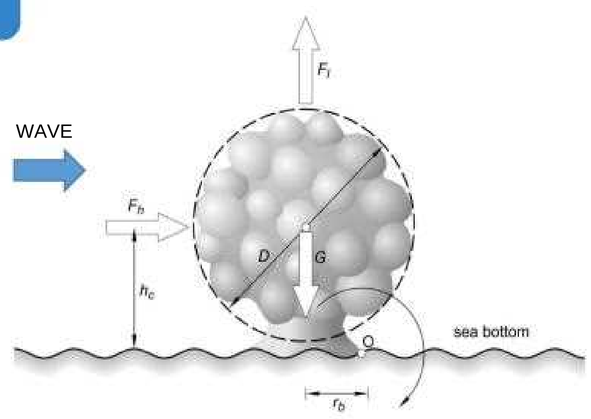

COMPUTATIONAL MODEL

Calculate the *H* wave height threshold affecting corals

Globular

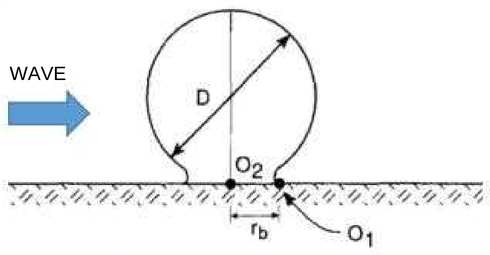

$$\frac{}{2}\ {}^{2}_{1}\left[\ |\cos(\ )|\cos(+\cos 2\qquad(\ )\right]^{2}$$

$$\left[\frac{51}{24}\ \frac{}{}\ \text{sine}(\ )\right]\quad\frac{2}{3}\ \frac{(\qquad)}{\qquad}\qquad=0 \qquad \text{(first)}$$

Hemispherical shape

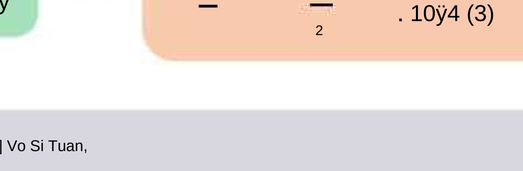

$$\left(\frac{}{3}\quad|\cos(\ )|\,1\cos+4\quad-\quad\cos2(\ )\right)^{2}$$

$$\left(\frac{}{3}\ \frac{}{}\ \text{sine}(\ )\right)\quad\frac{}{3}\ \frac{(\qquad)}{\qquad}\qquad=0 \qquad (2)$$

Porites coral block (Great Barrier Reefs)

Coral Diploastrea heliopora

Based on formulas (1) and (2) for spherical and hemispherical corals, respectively, the model calculates the *H* wave height threshold based on the drag and lift coefficients *(Cd* and *Cl),* wave periods in storms. *Tp* (represents the impact force of the wave) and coral diameter *D* (represents the supporting force of the coral).

Calculate the actual wave height *Hr* during storms

Surface wave height Hÿ → Use the pressure drop formula with depth to calculate the pressure at the bottom:

$$=\ \frac{}{2}\ .\ 10ÿ4\ (3)$$

→ Calculate the wave height Hr at depth h (UNESCO 1983):

$$=\ \frac{1.+2.\quad 2+\ {}_{3.}\quad 3+\ {}_{4.}\quad {}^{4}}{(\ )+\frac{1}{2}\ \frac{}{}\ ÿ\ .} \qquad (4)$$

RESULT

Below are the results of the *H* wave height threshold that can cause mechanical impact to topple spherical and hemispherical corals at depths of 3m and 6m respectively in a storm with a short wave period (Tp = 7s). Compared to the case of spherical corals, hemispherical corals have a much higher wave height threshold. The main reason is because hemispherical corals have a lower center of gravity, so balance is better than spherical corals.

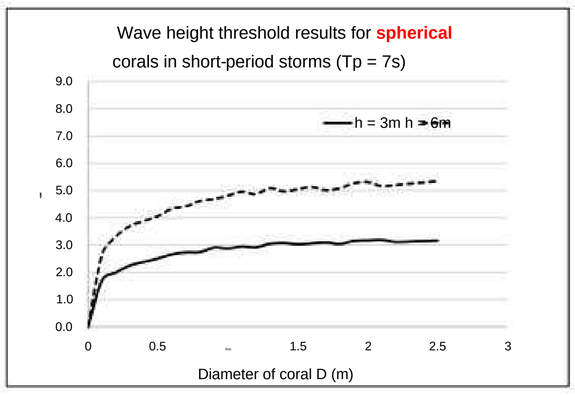

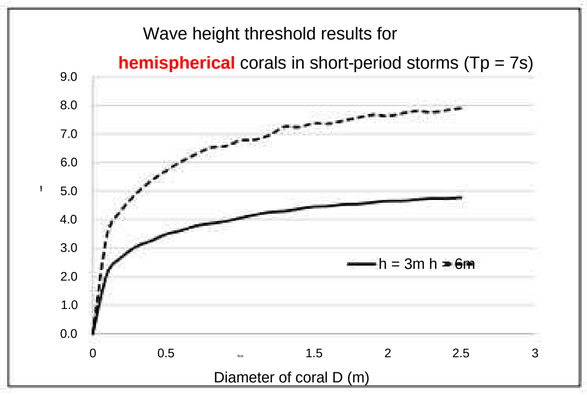

APPLY MODEL

(VAN PHONG - BEN GOI BAY AREA) To evaluate the effectiveness of the calculation model, we apply the model in the Van Phong - Ben Goi bay area (Khanh Hoa) with two actual storms, Mirinae (2009) and Damrey (2017). We compare the results obtained from the model with the damages recorded in the past to evaluate the quality of the model.

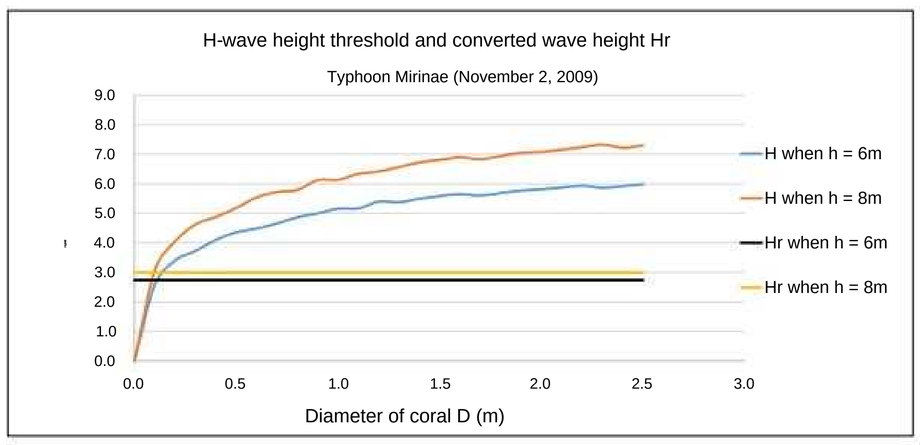

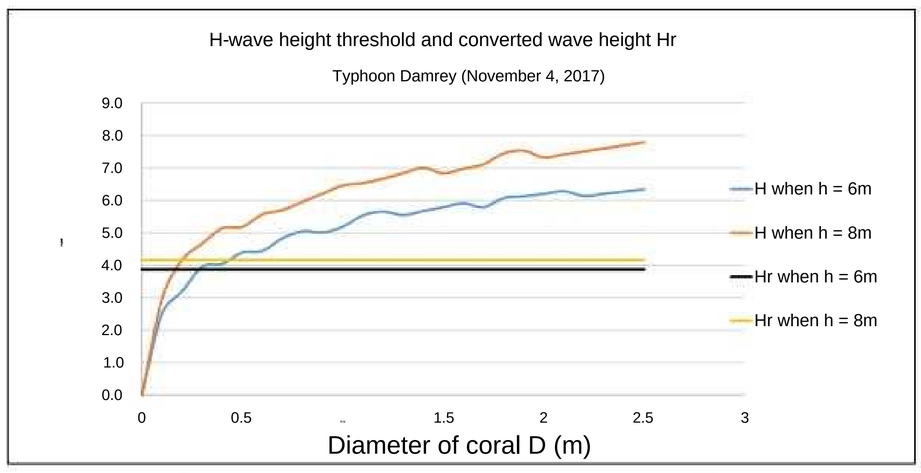

CONCLUDE

ÿBuild a model to calculate the wave height threshold to consider the impact of waves caused by storms on coral individuals (spherical and hemispherical): ÿIn the case of

spherical corals: wave height threshold is almost does not depend on the size of corals in short-wave period storms (Tp = 7 s) ÿIn the case of hemispherical corals:

wave height threshold depends strongly on coral size in short-wave period storms (Tp = 7 s) ÿThe results when applying the model at Van Phong - Ben

Goi bay during two storms Mirinae (2009) and Damrey (2017) also show that the wave height threshold depends on coral size.

ÿ Thereby, it shows that storm waves do not seriously affect spherical coral masses except for small, immature coral individuals.

REFERENCES [1] Vo Si Tuan, (2006), *Coral reef ecosystem of the Vietnam Sea,* Science and Technology Publishing House.

[2] Done, T., D. Potts, (1992), Influences of habitat and natural disturbances on contributions of massive Porites corals to reef communities, *Marine Biology,* 114, 479-493.

[3] Harmelin-Vivien, ML, (1994), The effects of storms and cyclones on coral reefs: a review, *Journal of Coastal Research,* 12, 211-231.

[4] Harris, DL, A. Rovere, E. Casella, H. Power, R. Canavesio, A. Collin, A. Pomeroy, JM Webster, V. Parravicini, (2018), Coral reef structural complexity provides important coastal protection from waves under rising sea levels, *Science Advances,* 4, 1-7.

[5] Holthuijsen, LH, (2007), *Waves in oceanic and coastal waters,* Cambridge university press.

[6] Massel, S., T. Done, (1993), Effects of cyclone waves on massive coral assemblages on the Great Barrier Reef: meteorology, hydrodynamics and demography, *Coral Reefs,* 12, 153-166.

[7] Massel, SR, (1996), *Ocean surface waves: their physics and prediction,* World scientific.

[8] Newman, J.N., (1977), *Marine hydrodynamics,* Massachusetts Institute of Technology, Cambridge, Mass.

[9] Salles, T., J. Pall, J.M. Webster, B. Dechnik, (2018), Exploring coral reef responses to millennial-scale climatic forcings: insights from the 1-D numerical tool pyReef-Core v1. 0, *Geoscientific Model Development,* 11, 2093-2110.

[10] The World Bank assessment team, (2018), *2017 Vietnam Post-Typhoon Damrey Rapid Damage and Needs Assessment,* The World Bank.

MÔ HÌNH TÍNH TOÁN NGƯỠNG ĐỘ CAO SÓNG TÁC ĐỘNG ĐẾN CHÂN SAN HÔ

HỘI NGHỊ KHOA HỌC LẦN THỨ XII

Nguyễn Thị Tố Vân, Võ Lương Hồng Phước
Bộ môn Hải dương, Khí tượng và Thủy văn
Trường ĐH Khoa học Tự nhiên, ĐHQG-HCM

Oceanology Meteorology Hydrology
University of Science - Ho Chi Minh City

KHÁI QUÁT

- Những thiệt hại của các bãi san hô sau những cơn bão là rất lớn, trong đó **tác động cơ học** do sóng bão gây ra là không ít.
- Mô hình chủ yếu được vận dụng vào các công thức thủy động lực nhằm tính toán **ngưỡng độ cao sóng** có thể tác động lật đổ những cá thể san hô hình cầu hoặc bán cầu đơn giản.

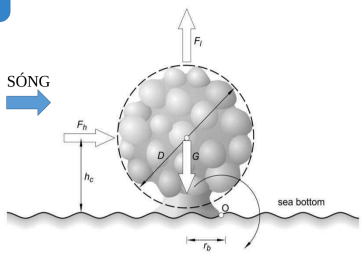

MÔ HÌNH TÍNH TOÁN

Tính toán ngưỡng độ cao sóng *H* tác động đến san hô

Hình cầu

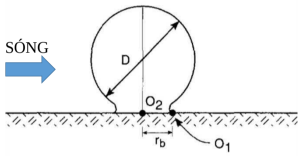

$$\frac{1}{2}U_1^2[C_d|\cos(\omega t)|\cos(\omega t)+C_l\delta\cos^2(\omega t)]H^2 - \left[\frac{51}{24}\pi\frac{DU_1}{T_p}\sin(\omega t)\right]H - \frac{2}{3}\pi\frac{(\rho_s-\rho_w)}{\rho_w}g\delta D = 0 \quad (1)$$

Khối san hô Porites (Great Barrier Reefs)

Hình bán cầu

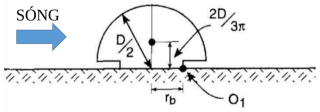

$$U_1^2\left(\frac{1}{3\pi}C_d|\cos(\omega t)|\cos(\omega t)+\frac{1}{4}C_l\cos^2(\omega t)\right)H^2 - \left(\frac{1}{3}\frac{DU_1}{T_p}\sin(\omega t)\right)H - \frac{1}{3}\frac{(\rho_s-\rho_w)}{\rho_w}gD = 0 \quad (2)$$

San hô Diploastrea heliopora

Dựa vào công thức (1) và (2) để tính được chiều cao ngưỡng độ cao sóng H tác động cắt chân và nâng (C_d và C_l), chu kỳ sóng tương ứng T_p (đại diện cho tác động của) và đường kính thân sao D đại diện cho tác động của hô)

Tính toán độ cao sóng thực H_r trong các cơn bão

Độ cao sóng bề mặt $\bar{H}$ → Sử dụng công thức suy giảm áp suất theo độ sâu tính áp suất tại đáy:

$$p = \rho_w g\frac{\bar{H}}{2}e^{kz}.10^{-4} \quad (3)$$

→ Tính độ cao sóng H_r tại độ sâu h (UNESCO 1983):

$$H_r = \frac{C_1.p+C_2.p^2+C_3.p^3+C_4.p^4}{g(\theta)+\frac{1}{2}\gamma'.p} \quad (4)$$

KẾT QUẢ

Bước đầu về quá trình ngưỡng độ cao H có thể gây động học đổ hình cầu và bán cầu ở các độ sâu được 3m và 6m (ứng một cơn bão có sóng ngắn = 7s) So sánh hình cầu và bán cầu cho thấy nhận chính do sao hình bán cầu có ngưỡng độ cao cắt hẳn. Nguyên nhân chính do sao hình bán cầu tăng bằng cắt nên tác động lật tăng bằng cắt hình cầu.

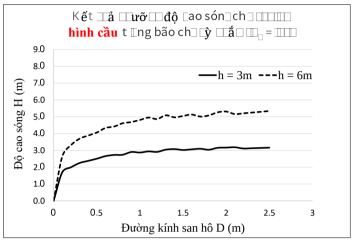

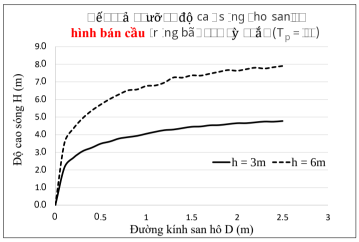

ÁP DỤNG MÔ HÌNH

(VÙNG VỊNH VÂN PHONG – BẾN GỎI)

Để xét độ tin cậy của mô hình tính toán, chúng tôi áp dụng mô hình cho vùng vịnh Vân Phong – Bến Gỏi (tỉnh Khánh Hòa) với hai cơn bão lịch sử Mirinae (2009) và Damrey (2017). Chúng tôi đánh giá kết quả thu được từ mô hình cùng những số liệu đã được ghi nhận trong quá khứ nhằm đánh giá độ tin cậy của mô hình.

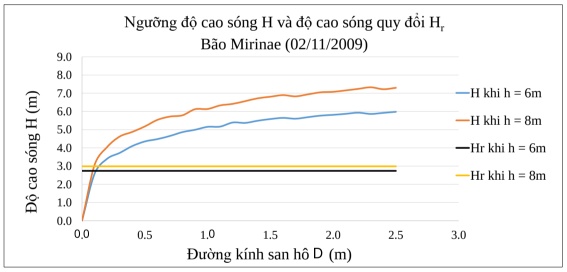

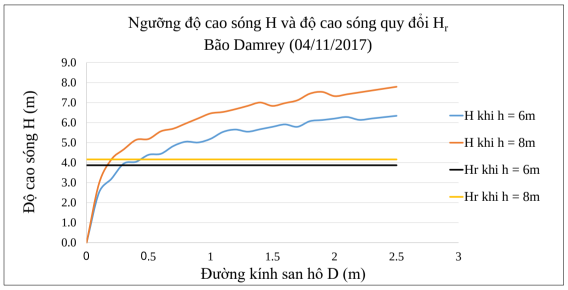

KẾT LUẬN

- Kết quả mô hình tính ngưỡng độ cao sóng tác động lật đổ do cắt chân và nâng hô trong bão:
  - Trường hợp san hô hình cầu: ngưỡng độ cao sóng hầu như không phụ thuộc vào kích thước san hô hô trong bão chu kỳ sóng ngắn (Tp = 7 s)
  - Trường hợp san hô hình bán cầu: ngưỡng độ cao sóng phụ thuộc mạnh vào kích thước san hô trong bão chu kỳ sóng ngắn (Tp = 7 s)
- Kết quả tính toán mô hình áp dụng cho Phong – Bến Gỏi (Mirinae 2009) và (Damrey 2017) cũng cho kết quả ngưỡng độ cao sóng tác động lật đổ trong cắt chân hô.
  - Qua đó, cho thấy do không ảnh hưởng đến độ cao sóng hô và đến hô hô trong bão chu kỳ sóng ngắn.

TÀI LIỆU THAM KHẢO

[1] Võ Sĩ Tuấn, (2006), *Hệ sinh thái rạn san hô biển Việt Nam*, Nhà xuất bản khoa học và kĩ thuật.

[2] Done, T., D. Potts, (1992), Influences of habitat and natural disturbances on contributions of massive Porites corals to reef communities, *Marine Biology*, 114, 479-493.

[3] Harmelin-Vivien, M. L., (1994), The effects of storms and cyclones on coral reefs: a review, *Journal of Coastal Research*, 12, 211-231.

[4] Harris, D. L., A. Rovere, E. Casella, H. Power, R. Canavesio, A. Collin, A. Pomeroy, J. M. Webster, V. Parravicini, (2018), Coral reef structural complexity provides important coastal protection from waves under rising sea levels, *Science Advances*, 4, 1-7.

[5] Holthuijsen, L. H., (2007), *Waves in oceanic and coastal waters*, Cambridge university press.

[6] Massel, S., T. Done, (1993), Effects of cyclone waves on massive coral assemblages on the Great Barrier Reef: meteorology, hydrodynamics and demography, *Coral Reefs*, 12, 153-166.

[7] Massel, S. R., (1996), *Ocean surface waves: their physics and prediction*, World scientific.

[8] Newman, J. N., (1977), *Marine hydrodynamics*, Massachusetts Institute of Technology, Cambridge, Mass.

[9] Salles, T., J. Pall, J. M. Webster, B. Dechnik, (2018), Exploring coral reef responses to millennial-scale climatic forcings: insights from the 1-D numerical tool pyReef-Core v1. 0, *Geoscientific Model Development*, 11, 2093-2110.

[10] The World Bank assessment team, (2018), *2017 Vietnam Post-Typhoon Damrey Rapid Damage and Needs Assessment*, The World Bank.

NATIONAL UNIVERSITY – HO CHI MINH CITY

UNIVERSITY OF SCIENCE

FACULTY PHYSICS AND ENGINEERING PHYSICS

Graduation Thesis

CALCULATION OF GREENHOUSE GASES EMISSIONS (CO_2, CH_4) AT THE SURFACE OF TRI AN AND DAU TIENG RESERVOIRS IN THE RAINY AND DRY SEASONS

Supervisor: Dr. BUI Thi Ngoc Oanh

Student: DO Hoang Minh Cuong

HCMC, 07/2021

CALCULATION OF GREENHOUSE GASES EMISSIONS (CO_2, CH_4) AT THE SURFACE OF TRI AN AND DAU TIENG RESERVOIRS IN THE RAINY AND DRY SEASONS

Abstract

Reservoirs is one of the sources of greenhouse gas emissions to the atmosphere. To measure these fluxes of greenhouse gases (methane and carbon dioxide), the study was carried out in *situ* within 24 hours with chamber measurements at the surface of Tri An and Dau Tieng reservoirs in the rainy and dry seasons. At Dau Tieng reservoir, the average CH_4 emission rate in the dry season is 35.87 ppm/m^2/hr and in the rainy season is 13.2 ppm/m^2/hr. The average CO_2 emission rate in the dry and rainy seasons is 2418.83 ppm/m^2/hr and 10129.1 ppm/m^2/hr, respectively, and both emission rates of gas are correlated with biochemical factors in the water (dissolved oxygen, temperature and pH). At Tri An reservoir, the average CH_4 emission rate in the dry season is 18.21 ppm/m^2/hr, and in the rainy season is 7.82 ppm/m^2/hr and no correlation with biochemical factors in the water. The average CO_2 absorption rate in the dry is 1131.84 ppm/m^2/hr, and in the rainy season is 3835.15 ppm/m^2/hr and is correlated with dissolved oxygen and temperature.

Table of Contents

Preamble

Increasing concentration of greenhouse gases (GHG) (such as CO2, CH4) in the atmosphere is one of the main causes of climate change. GHG are emitted from both natural and anthropogenic sources. Natural sources of GHG emissions originated from volcanic activity, plants and animals, soil, and surface waters in oceans, rivers, lakes or streams. Vietnam has a dense network of rivers and relatively large hydroelectricity resources, so our country has many irrigation and hydroelectric reservoir systems. Besides, there are still several households living there, so human activities can affect GHG emissions in irrigation and hydropower reservoirs. Therefore, the topic "*Calculation of greenhouse gas emissions (CO_2, CH_4) at the surface of Tri An and Dau Tieng Lake in the rainy and dry seasons*" was proposed to understand the factors affecting the process of greenhouse gas emission or absorption at the surface of Tri An and Dau Tieng reservoirs and comment on their changes over time and seasonally.

Due to the limitation of means of transportation and cost, the study surveyed a representative location in each of Tri An and Dau Tieng lakes within a period of 24 hours in each season. Because of the short survey period, there are a number of factors that do not show a clear influence on the emission or absorption of greenhouse gases at the lake's surface.

Chapter 1: Research Overview on Methane Emission in the rice field

1.1 Introduction to methane

There are two primary sources of GHG emissions in the atmosphere: natural and anthropogenic sources, of which the main causes are human activities.

Natural sources: Activities occurring in nature are also sources of GHG emissions, such as volcanic activity; forest fires cause GHG emissions in the atmosphere when burned. It will produce much CO2 directly into the atmosphere **Error! Reference source not found.**.

Anthropogenic sources: This is the main cause of GHG emissions in the atmosphere. The activities of burning fields, exploiting forests, burning fossil fuels, ... these activities contribute significantly to the emission of GHG into the atmosphere **Error! Reference source not found.**.

Scientists have found vast reservoirs of CO_2 and CH_4 under the seafloor. The ocean also absorbs a third of CO_2 emissions in the atmosphere and 90% of excess heat, making it the largest CO_2 reservoir on the Earth. The CO_2 and CH_4 gases under the seabed are prevented from escaping into the oceans and atmosphere by the caps of frozen (CO_2 and CH_4 gases are compressed at high pressure and low temperature), called hydrate. Warming seawater could lead to the melting of these hydrates, releasing vast amounts of carbon dioxide into the atmosphere, with dire consequences for climate change**Error! Reference source not found.**. In addition, CH_4 in the ocean can also be emitted from areas with shallow depths; CH_4 gas accumulates from within the sediment layer and then escapes at the surface of the sea floor. In addition, the GHG emissions from the lake to the atmosphere are mainly caused by the accumulation of CO_2 and CH_4 under the sediment, biochemical activities and human activities. In which the GHG emissions due to the accumulation process below the sediment dominate, the reason that the dead organisms sink to the bottom of the lake, from which the decomposition of organisms produces CO_2 and CH_4 gases. These gases gradually accumulate in the sediment. When these gases are oversaturated, they will escape from the sediment at the bottom to the surface and out to the atmosphere. CH_4 in the soil is produced by methanogenic microorganisms under anaerobic conditions and consumed by heterotrophic organisms, which use O_2 and CH_4 for their metabolism under aerobic conditions **Error! Reference source not found.**.

The equation for generating CH4 gas in nature:

$CO_2 + 4H_2 \rightarrow CH_4 + 2H_2O$

$CH_3COOH \rightarrow CH_4 + CO_2$

Oxidation of CH_4 to CO_2 in nature:

$CH_4 + 2O_2 \rightarrow CO_2 + H_2O$

I.2 CO_2 and CH_4 in surface water

In irrigation and hydropower reservoir systems, the supply of CH_4 can be divided into two types: natural sources and artificial sources. Natural CH_4 sources are formed under anaerobic environments such as wetlands, freshwater lakes, rivers, and streams and released in thermogenic areas such as in volcanic and bedrock hydrates. In addition, the decomposition of organic matter includes the wastes of organisms living in the aquatic environment in that area, and the carcasses of organisms that sink to the bottom; then they are decomposed in the aerobic environment. Organic matter accumulates inside the sediment at the bottom. Man-made sources include domestic, agricultural and industrial wastes discharged by humans and accumulated at the bottom. The supply of CO_2 in the water is also divided into two sources, natural sources and anthropogenic sources. Natural sources is the respiratory activity of organisms living in the aquatic environment; Man-made sources are caused by human waste discharged into water sources **Error! Reference source not found.**.

Studies show a close relationship between CO_2 and CH_4; these two gases can be converted to each other. CO_2 is one of the critical molecules in the formation of CH_4, the conversion of CO_2 to CH_4 is called methanogenesis by heterotrophic microorganisms called methanogens; these microorganism's CH4 gas is generated in the absence of oxygen; this is the final step in the biomass decomposition process, in addition, CH_4 gas is also formed through the decomposition of organic matter. However, only 40% of the CH_4 gas produced from CH_4 production escapes to the atmosphere because most of it is oxidised to CH_4 in aerobic and anaerobic environments **Error! Reference source not found.**. Before being released into the atmosphere from the surface of the water, it was partially oxidised by converting CH_4 into CO_2 into energy by some heterotrophic organisms called methanotrophs under both deficient environmental conditions, gas and anaerobic **Error! Reference source not found.**,**Error! Reference source not found.**.

CH_4 can escape from the aquatic environment into the atmosphere through two processes: diffusion (ebullition) and bubbling (bubbling). CH_4 emissions from below the sediment to the water column are promoted by CH_4 production, which depends on organic matter supply and temperature, and CO_2 exchange at the water surface and atmosphere interface to CH_4 formation. When the concentration of CH_4 formed in the sediment reaches a certain level, it will combine to create air bubbles inside the sediment at the bottom, then due to external factors or because it has accumulated enough gas. Then this bubble will escape and emit CH_4 into the water, but CH_4 emissions from the sediment going to the water's surface and then out into the atmosphere can be oxidised to CO_2, remaining in the

form of bubbles. Gaseous oxidation of CH4 gas may not be affected because its rate of upward transport is faster than the diffusion rate **Error! Reference source not found.**.

I.3 Factors affecting gas emissions

- Algae
- Nutrients
- Depth
- Ambient temperature
- Meteorological factors
- Mining activities
- Dissolved oxygen (DO) concentration

Chapter 2. Research Area and Methodology

2.1. Research Area Dầu Tiếng Lake

Dầu Tiếng Lake was started in 1981 và completed in 1985 in the upstream Sài Gòn River with a basin stretching from 11º12' to 12º North latitude and from 106º10' to 106º30' East longitude. Dầu Tiếng Lake is one of the largest reservoirs in Vietnam, with a water surface area of 270 km^2, and a capacity of 1,58 billion m^3 of water [1].

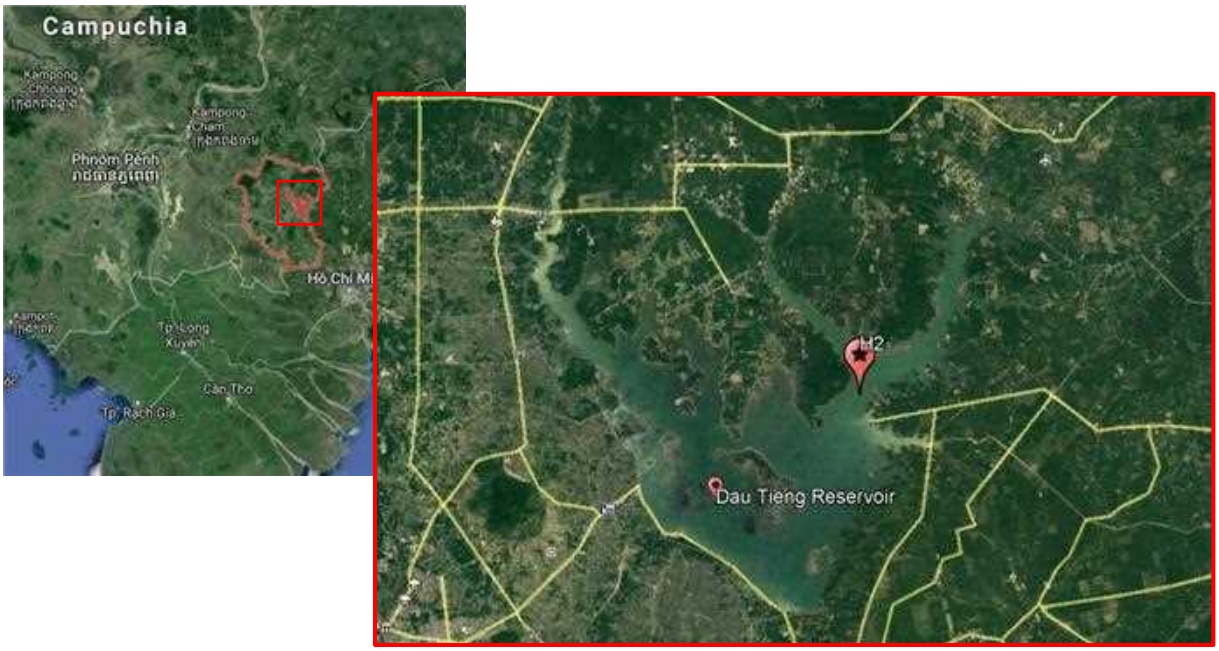

Figure 1.1. Location of Dau Tieng Lake and monitoring position (Source Google Earth)

Dau Tieng Lake is located in the tropical monsoon area. The climate in this area is divided into two distinct seasons: The rainy season starts from June to November, and the prevailing wind is the southwest wind with an average speed of 1.6 - 2.1 m/s, causing heavy rain from June to August. The dry season is from December to April next year, with the prevailing wind during this time being the northeast wind with an average speed of 1.8 - 2.2 m/s. The average rainfall in the rainy season in Dau Tieng Lakearea is 1,940 mm, accounting for about 85-90% of the annual rainfall. In the dry season, the rain only accounts for 10-15% of the yearly rainfall [2].

Dau Tieng Irrigation Reservoir receives water from the Saigon River, Vam Co Dong River, and streams, including Nuoc Duc and Krai flows from Cambodia that form on the Tha La River. Therefore, the hydrological regime of the area is highly dependent on the rainfall regime [2].

Table 2.1. Total number of indicators in the water of Dau Tieng Lake (2005) [3]

No.	Parameters	Values	QCVN 08-MT:2015/BTNMT column A1
01	pH	6.16	6 – 8.5
02	BOD_5 (mgO_2/l)	0.92	4
03	COD (mgO_2/l)	4.19	10
04	DO (mgO_2/l)	7	≥ 6
05	Ammonia (mg/l)	0.07	0.3
06	Nitrate (mg/l)	0.19	2
07	Nitrite (mg/l)	0.004	0.05

In general, the water quality of Dau Tieng Irrigation Reservoir is relatively good when compared with QCVN 08-MT:2015/BTNMT. Besides, sand mining activities in this area occur strongly, but most are unlicensed ships. Sand mining activities disturb the bottom sediments causing the release of large amounts of GHG into the aquatic environment and diffusion into the atmosphere. In addition, the daily activities of people on the boat and people living around the downstream area of the lake, citizen wastes water cause pollution of the lake. Besides, the raising of rafts and livestock in the downstream basin is also the cause of water pollution in the lake.

2.2. Methodology

Survey location

The ship is anchored at the location (Figure 1) to survey GHG emissions from the lake surface over time at the Dau Tieng reservoir. Data were collected in two seasons. In the rainy season, survey data was collected from October 22, 2020 to October 23, 2020. Dry season data was collected from March 28, 2021 to March 29, 2021.

Methodology

Data were collected from the survey trip at Dau Tieng Lake by Dr Le Xuan Thuyen, belongs to the National University-Category C project with the title: "*The Evolution of greenhouse gas emissions from lakes according to the Level of Eutrophication and climate change in the Southern Region*". During the survey, an Ultra-Portable Gas Analyzer (Los Gatos Research, manufactured in 2016, Figure 1.2 left) was used to measure CH_4 and CO_2 emissions and a 90FL-T device (TPS, manufactured in 2001) measuring biochemical indicators in water.

Figure 1.2. Left: Device picture of Ultra-Portable Gas Analyzer; Right: GHG emission measurement chamber

The gauges are set to be sampled every 3 hours for all indicators. Using equipment Elite-5 Ti (Lowrance, manufactured in 2016) to determine the coordinates and depth of the water column at the measurement location.

The concentration of GHG emissions from the lake surface is collected through a field measuring chamber (Figure 1.2 right) made of PVC material. The measuring chamber is attached to a float to float on the water's surface. Inside the measuring chamber, there are two holes to enter the air duct (one inlet to the gauge and one to discharge from the indicator). The chamber has a diameter of 29.14 cm and a height of 27 cm.

Calculation of gas emission rate

The data received during the survey shows the process of GHG emission when the data is positive and GHG absorption when the data is negative. The data measured here is the concentration of GHG emitted or absorbed at the surface and is primary data, which needs to be calculated to convert from emission or absorption data to emission or absorption rate. Besides, it is necessary to process noise filtering again for some data files with noise.

The rate of GHG emission of CO_2 and CH_4 is determined by the formula [5]:

$$F = \frac{V P_0}{R S(T_{0\,air} + 273.15)} \frac{dc}{dt}$$

Where:

F (ppm/m^2/hr): Emission rates

V (m^3): Volume of chamber

P_0 (kpa): Pressure in the water at the measuring position

R: Ideal gas constant (R=8.314 $Jmol^{-1}K^{-1}$)

S (m^2): Area of chamber

$T_{0\ air}$ (^oC): Air temperature

Chapter 3. Results and Discussion

III.1 Seasonal rate of greenhouse gas emissions

III.1.1 CH_4 emission rate

A survey of CH_4 GHG emissions over time at Dau Tieng Lake in the dry season on March 28 and March 29, 2021 (Figure 3.1) shows during this period CH4 from the lake is continuously emitted to the atmosphere with an average rate of 35.87 ppm/m2/hour within 24 hours in the dry season. The highest rate at 22:00 on March 28 with a value of 60.99 ppm/m^2/hour, and the lowest emission rate at 04:00 on March 29 with a value of 15.06 ppm/ m^2/hour. Based on Figure 3.1, it can be seen that the CH_4 emission rate in the dry season at Dau Tieng Lake is higher at night than during the day. During the survey of the CH_4 emission rate at Dau Tieng Lake during the rainy season from October 22 to 23, 2020, due to bad weather conditions, two measurements were skipped at 12:30 and 23:30 days 22 October.

The rate of CH_4 emissions in the rainy season at Dau Tieng Lake changes over time. From Figure 3.1, it can be seen that from October 22, 2020, to October 23, 2020, the lake continuously discharged CH_4 gas into the atmosphere with an average value of within 24 hours in the rainy season, 13.2 ppm/m^2/hour. The highest recorded rate was 18.43 ppm/m^2/h at 9:30 on October 23, and the lowest emission rate recorded during the survey trip was 6.78 ppm/m^2/hour at 4:30 on October 23. The rate of CH_4 emission in the rainy season tends to be high during the day and gradually decreases at night.

Through two seasons, the rainy season and the dry season, it can be seen that Dau Tieng Lake continuously emits CH_4 into the atmosphere from the surface, but there is a vast difference in the emission rate between the two seasons. In the dry season, the CH_4 emission rate (35.87 ppm/m^2/hour) is 2.7 times higher than in the rainy season (13.2 ppm/m^2/hour). The rate of CH_4 emission at the surface of Dau Tieng Lake in the dry season is higher at night than during the day. However, the night is lower than the day during the rainy season. The cause may be an influence of temperature and dissolved oxygen in the water.

III.1.2 CO_2 emission rates

The rate of CO_2 emission at the surface of Dau Tieng Lakein the dry season varies in time (Figure 3.2), with the average emission value in 24 hours from March 28, 2021, to March 29, 2021, being 2418.8 ppm/m^2/hour. Unlike CH_4, Dau Tieng Lake both absorbs CO_2 from the atmosphere and emits CO_2 from the lake's surface to the atmosphere. The lake absorbs CO_2 from the atmosphere from 13:00 to 20:00 on March 28, with the average absorption rate value during this period in the dry season being 1561.8 ppm/m^2/hour.

Meanwhile, the highest absorption rate at 19:00 on March 28, with a value of 1737.8 ppm/m^2/hour and the lowest absorption rate at 1249.2 ppm/m2/hour at 14:00 on the same day. Other times during the two days of March 28 and 29, Dau Tieng Lake emitted CO_2 into the atmosphere, at 1:00 on March 29, the CO_2 emission rate reached the maximum value of 8270.3 ppm/m^2/hour, and the emission rate reached the lowest value of 604 ppm/m^2/hour at 9:00 on March 29.

During the survey of the CO_2 emission rate at Dau Tieng Lake during the rainy season from October 22 to October 23, 2020, due to weather conditions, two measurements were skipped at 12:30 and 23:30 on the 22nd of October.

Figure 3.2 shows the rate of CO_2 absorption and emission of the Dau Tieng Lake overtime during the rainy season. During the rainy season, it was only recorded at one time that Dau Tieng Lake absorbed CO_2 at the surface at 18:00 on October 22 with an absorption rate of 2626.7 ppm/m^2/hr. Different times of the two survey days during the rainy season were recorded as the lake emitting CO_2 into the atmosphere with an average rate of 10129.1 ppm/m^2/hour within 24 hours in the rainy season. The highest recorded emission rate was 20234.3 ppm/m^2/hr at 4:30 p.m. on October 23 and the lowest at 15:30 on October 22 with a 297.2 ppm/m2/hr value.

When comparing the CO_2 emission and absorption of the Dau Tieng Lake in the dry and rainy seasons, we find that during the day, Dau Tieng Lake both absorbs and emits CO_2, while at night, only CO_2 is emitted.

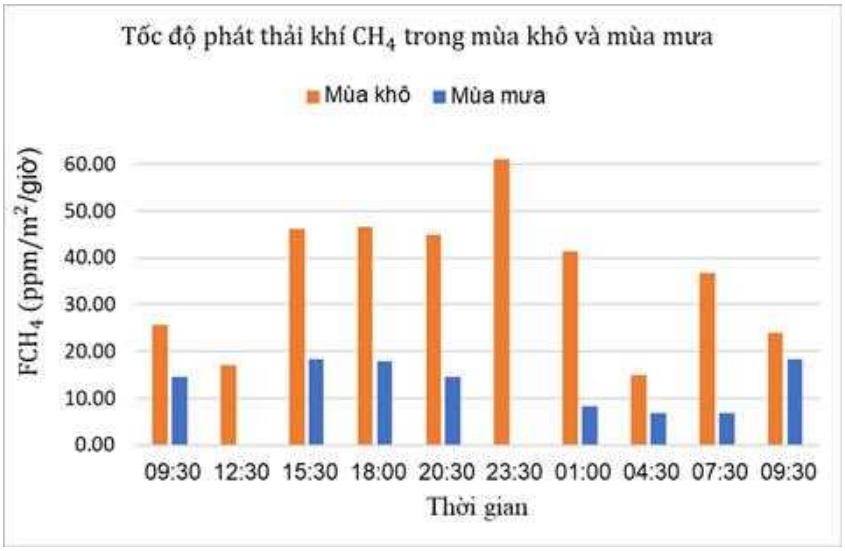

Figure 3.1: CH4 emission rate over time at the surface of Dau Tieng Lake in the dry season (March 28-29, 2021) and the rainy season (October 22-23, 2020).

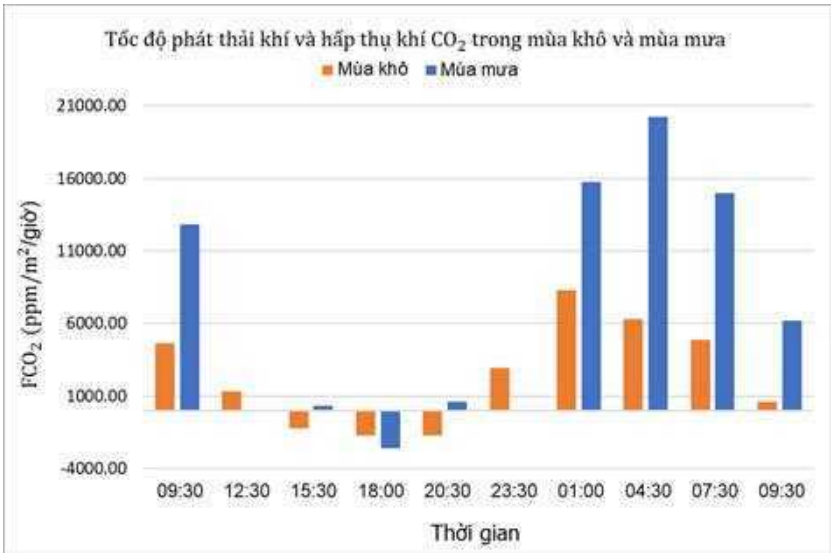

Figure 3.2: CO_2 emission rate over time at the surface of Dau Tieng Lake in the dry season (March 28-29, 2021) and the rainy season (October 22-23, 2020)

During the rainy season, the rate of CO_2 emissions (10129.1 ppm/m2/hr) was 2.8 times higher than in the dry rainy period (2418.83 ppm/m^2/hr), which is in contrast to the CH_4 emissions from the lake surface. Dau Tieng into the atmosphere. Besides, the absorption rate in the two seasons shows that the rainy season absorbs CO_2 (2626.7 ppm/m^2/hour) about 1.7 times more than the dry season (1561.78 ppm/m^2/hour). In both seasons, the rate of CO_2 emission is high between 1:00 and 7:30, which is due to the lack of solar radiation during this time, so there is no photosynthesis by plants.

III.2 Variation of CH_4 with other parameters

III.2.1 Variations of CH_4 with dissolved oxygen

The variations of CH_4 and DO emission rates in the dry and rainy seasons have the same oscillation phases. When DO increases, the change of CH_4 also increases and DO decreases, and the change of CH_4 also decreases.

Besides, it can be seen that the correlation between CH_4 and DO emission rates at the surface of Dau Tieng Lake with the correlation coefficient in the dry season and the rainy season is $R^2 = 0.6$ and $R^2 = 0.9$, respectively (Fig. 3.3). The rate of CH_4 gas emission in both seasons is directly proportional to DO, when the DO concentration increases, the gas emission rate at the lake surface increases.

III.2.2 Variations of CH_4 with dissolved oxygen

In the dry season, it can be seen that the CH_4 emission rate changes with the temperature having the same oscillation phase. When the temperature increases, the CH_4 emission also increases. In contrast to the dry season, during the rainy season, CH_4 changes with the same

temperature (from 9:30 to 20:30 on October 22); other periods show that the evolution of these two factors is opposite.

Figure 3.4a shows the correlation between the CH_4 emission rate and the temperature at the surface of the Dau Tieng Lake in the dry season with the correlation coefficient R^2 = 0.6. However, in the rainy season, there is no correlation between CH_4 emission rate and temperature, with a correlation coefficient of R^2 = 0.3 (Figure 3.4b). In addition, there is a difference in the ratio of the CH_4 emission rate to seasonal temperature. In the dry season, the rate of CH_4 emission is proportional to the temperature. When the temperature increases, the emission rate increases. In contrast, in the rainy season, the rate of CH_4 emission is inversely proportional to the temperature, when the temperature increases, the emission rate decreases.

III.2.3 Variation of CH_4 with pH

The evolution of the CH_4 gas emission rate and pH in the dry season and the rainy season have the same oscillation phase, when the pH increases, the CH_4 emission rate also increases, and the pH decreases, the CH_4 emission rate also decreases. Besides, it can be seen that the CH_4 emission rate is related to the pH in both seasons with the correlation coefficient in the dry season and the rainy season, respectively R^2 = 0.7 and R^2 = 0.9 (Fig. 3.10). The rate of CH_4 gas emission in both seasons is directly proportional to the pH, when the pH increases, the rate of gas emission at the lake surface increases.

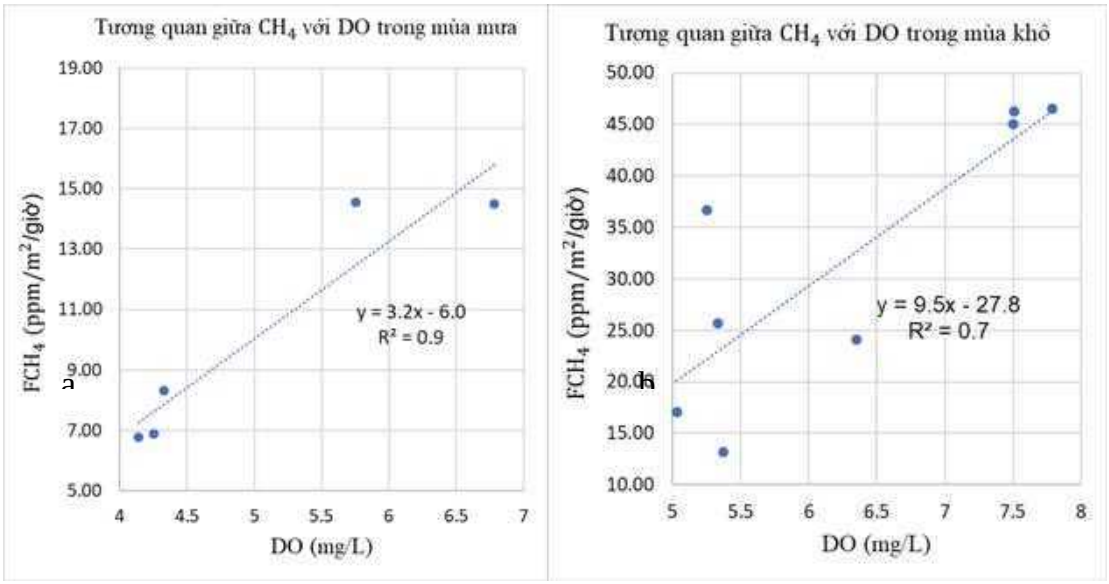

Figure 3.3: a) The relationship between CH_4 and DO emission rates in surface water in the dry season at Dau Tieng Lake(March 28-29, 2021). b) Relationship between CH_4 and DO emission rates in surface water during the rainy season at Dau Tieng Lake (October 22 - 23, 2020)

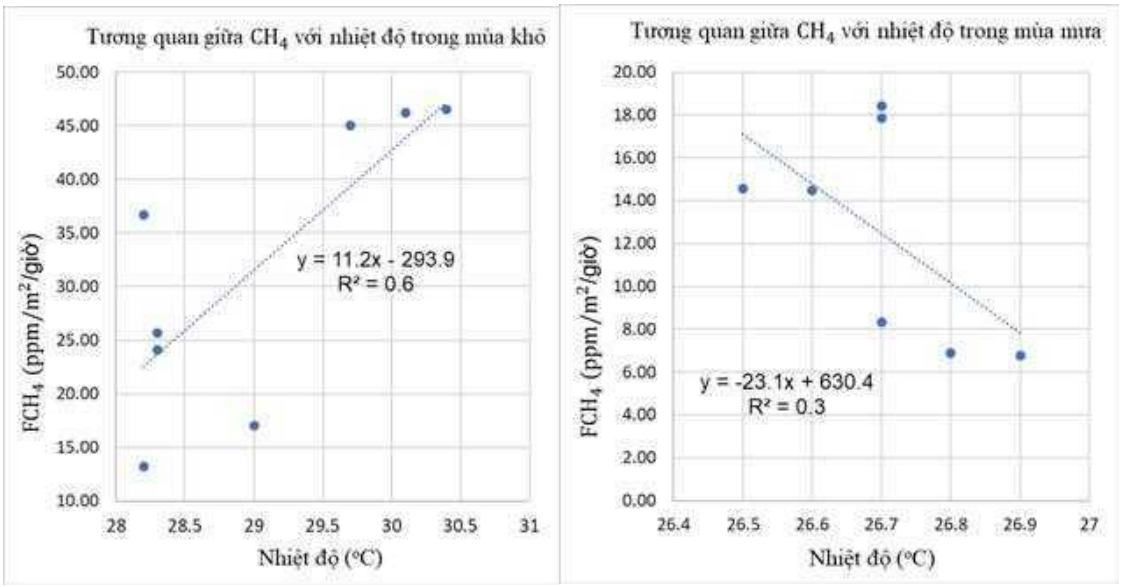

Figure 3.4: a) Relationship between CH_4 emission rate and surface water temperature in the dry season at Dau Tieng Lake (March 28-29, 2021). b) The relationship between CH_4 emission rate and surface water temperature during the rainy season at Dau Tieng Lake (October 22-23, 2020)

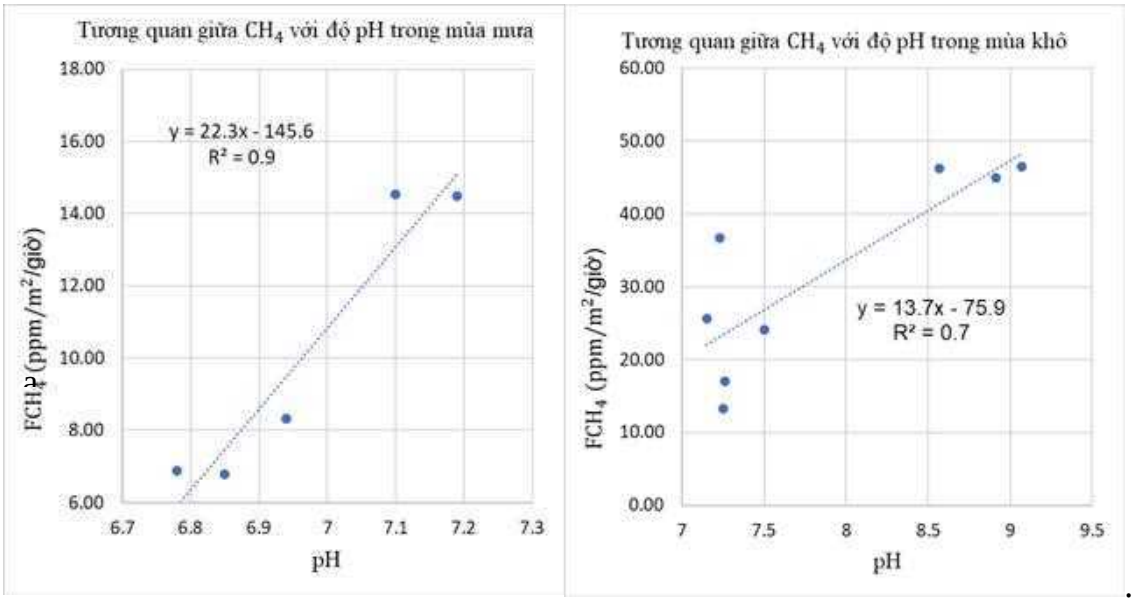

Figure 3.5: a) Relationship between CH_4 emission rate and pH in surface water in the dry season at Dau Tieng Lake (March 28-29, 2021). b) Relationship between CH_4 emission rate and pH in surface water during the rainy season at Dau Tieng Lake (October 22-23, 2020)

III.3.1 Variation of CO_2 with other parameters

III.3.1 Variation of CO_2 with dissolved oxygen

The variation of the CO_2 emission rate in the reverse phase fluctuates with DO in the dry and rainy seasons, when DO increases, the CO_2 emission rate decreases and DO decreases, the CO_2 emission rate increases. However, in the dry season, from 9:00 to 12:00 on March 28, it shows that the emission rate of CO_2 fluctuates in phase with DO during this period.

Figure 3.6 shows that the correlation between CO2 and DO emission rates at the surface of the Dau Tieng Lake with the correlation coefficient in the dry and rainy seasons is R^2 = 0.6 and R^2 = 0.8, respectively. The rate of CO_2 emission in both seasons is directly proportional to DO; when the DO concentration increases, the gas emission rate at the lake surface increases.

III.3.2 Variation of CO_2 with water surface temperature

The variation of the CO_2 emission rate with the temperature in the dry season shows that these two factors fluctuate in opposite phases. As the temperature increases, the CO_2 emission rate at the surface of Dau Tieng Lake decreases. However, in the rainy season, the opposite trend is observed; the variation of CO_2 emission rate with temperature shows that these two factors fluctuate in phase with each other; when the temperature increases, the CO_2 emission rate increases.

Figure 3.7 shows the relationship between the CO_2 emission rate and temperature at the surface of the Dau Tieng Lake, but there is a difference between the two seasons. In the dry season, the CO_2 emission rate is inversely proportional to the temperature with the correlation coefficient R^2 = 0.7; when the temperature increases, the CO_2 emission rate decreases. However, in the rainy season, on the contrary, the CO_2 emission rate is proportional to the temperature with the correlation coefficient R^2 = 0.6; when the temperature increases, the CO_2 emission rate also increases.

III.3.3 Variation of CO_2 with pH

The variation of CO_2 emission rate and pH in both seasons shows that these two factors fluctuate in opposite phases, when the pH increases, the rate of CO_2 emission at the surface of Dau Tieng Lake decreases. Figure 3.8 shows that the relationship between the CO2 emission rate and the pH at the surface of the Dau Tieng Lakewith the correlation coefficient in the dry and rainy seasons is R^2 = 0.7 and R^2 = 0.8, respectively. The rate of CO_2 emissions in both seasons is inversely proportional to the pH. As the pH in the water increases, the rate of CO_2 emissions decreases.

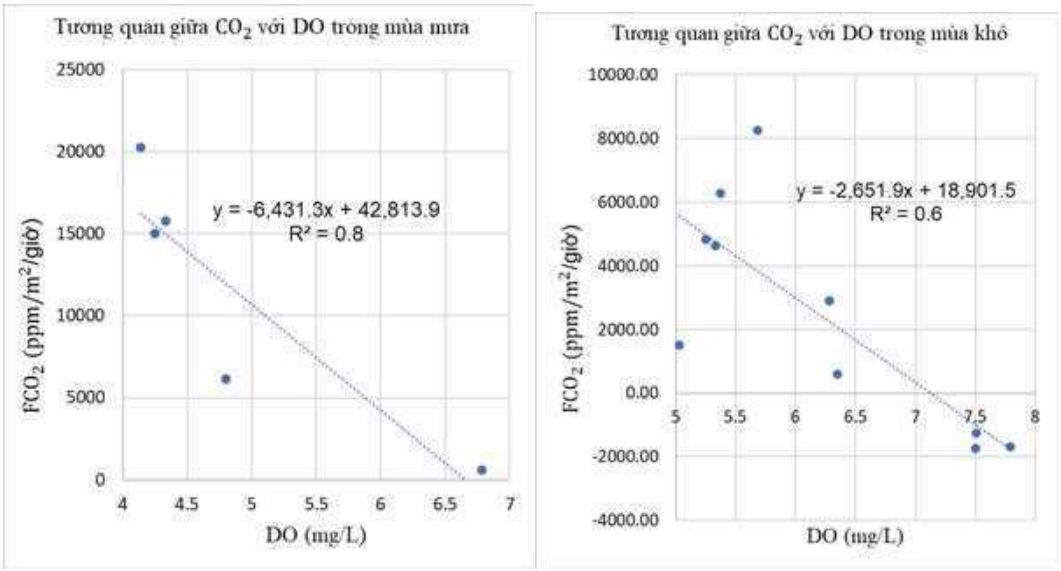

Figure 3.6: a) The relationship between CO_2 and DO emission rates in surface water in the dry season at Dau Tieng Lake(March 28-29, 2021). b) The relationship between CO_2 and DO emission rates in surface water during the rainy season at Dau Tieng *Lake* (October 22-23, 2020)

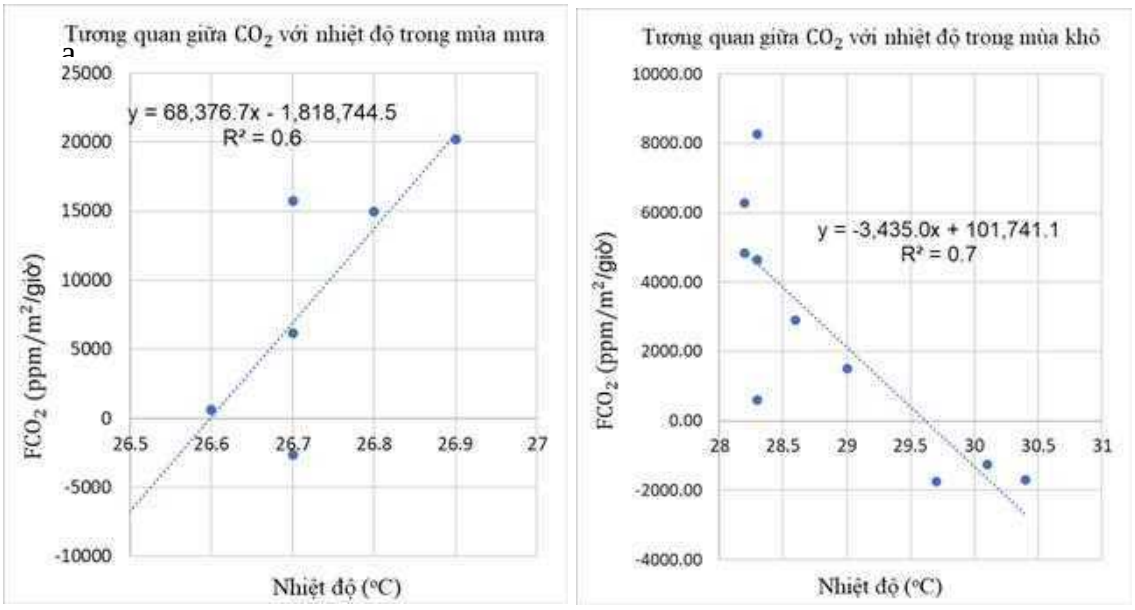

Figure 3.7: a) Relationship between CO_2 emission rate and surface water temperature in the dry season at Dau Tieng Lake (March 28-29, 2021). b) Relationship between CO_2 emission rate and surface water temperature during the rainy season at Dau Tieng Lake (October 22 - 23, 2020)

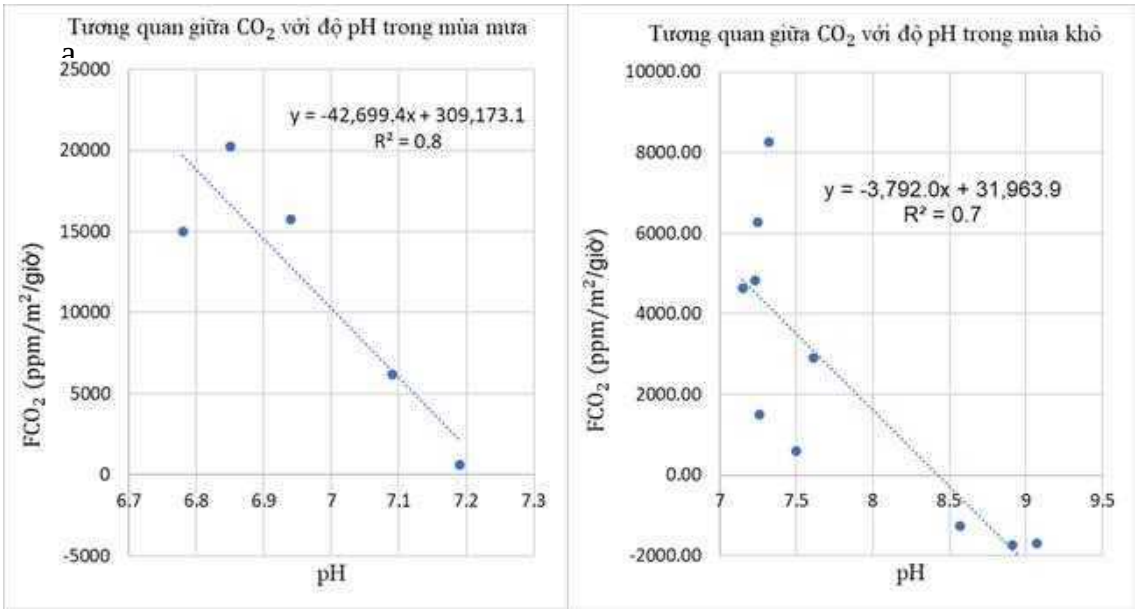

Figure 3.8: a) Relationship between CO_2 emission rate and pH in surface water in the dry season at Dau Tieng Lake (March 28 - 29, 2021). b) Relationship between CO_2 emission rate and pH in surface water during the rainy season at Dau Tieng Lake (October 22 - 23, 2020)

The survey at Dau Tieng Lake during the dry season (March 28-29, 2021) and the rainy season (October 22-23, 2020) showed that the CH_4 emission rate in the dry season was higher at night than during the day. But in the rainy season, on the contrary, the emission rate at night is lower than during the day. Besides, the CO_2 emission rate at the lake surface shows that in the rainy season, the CO_2 emission rate is higher than in the dry season, and in both seasons, the emission rate is high at night.

The survey at the Dau Tieng Lake in two seasons also showed that CH_4 and CO_2 emission rates are proportional and correlated with biochemical factors in the water. The rate of CH_4 emission at the surface of the Dau Tieng Lake in both seasons is directly proportional to DO and pH in the water, when these two biochemical factors increase, the rate of CH_4 emission at the lake surface increases. However, for the CO_2 emission rate, the opposite is true; the CO_2 emission rate at the lake surface is inversely proportional to the DO and the pH in the water at the surface; when these two biochemical factors increase, the rate increases. CO_2 emissions are reduced. The ratio of CH_4 and CO_2 emission rates to temperature differs between the two seasons. In the dry season, the rate of CH_4 emissions is directly proportional to the temperature, while in the rainy season, it is inversely proportional to the temperature. The CO_2 emission rate is opposite to CH_4, in the dry season, the CO_2 emission rate is inversely proportional to temperature, but in the rainy season, it is directly proportional to temperature.

Table 3.1: Correlation between CH_4 emission rate and biochemical factors at Dau Tieng Lake

Biochemical factors	CH_4		Correlation coefficients R^2	
	Dry season	Rainy season	Dry season	Rainy season
DO	Positive Correlation		0.7	0.9
pH	Negative Correlation		0.7	0.9
Temperature	Positive Correlation	No correlation	0.6	0.3

Table 3.2: Correlation between CO_2 emission rate and biochemical factors at Dau Tieng Lake

Biochemical factors	CO_2		Correlation coefficients R^2	
	Dry season	Rainy season	Dry season	Rainy season
DO	Negative Correlation		0.6	0.8
pH	Negative Correlation		0.7	0.6
Temperature	Negative Correlation	0.7	0.7	0.8

Chapter 4. Conclusions

Conclusions

Through the implementation of the graduation thesis, it helps to understand more about GHG and the consequences of increasing GHG concentration in the atmosphere. In addition, it helps to understand more about the natural and human-made factors affecting the GHG concentration in the lake and the GHG emissions from the surface of the irrigation and hydropower reservoirs.

When participating in two survey trips at Dau Tieng Lake and Tri An Lake during the dry season, Dr Le Xuan Thuyen belongs to the National University-Category C project with the title: "*The variation of greenhouse gas emissions from lakes according to the level of eutrophication and climate change in the southern region",* helping better to understand the process of greenhouse gas emissions from lakes. Sampling processes and method of measuring GHG emissions at the surface of freshwater lakes in the field by chamber measurement. Besides, it helps to understand the difficulties of scientists better when conducting surveys such as transportation, weather conditions and health.

The emission and absorption rates of CH_4 and CO_2 in Dau Tieng and Tri An reservoirs within 24 hours during the dry season and the rainy season are shown through the topic. The results show the difference in the rate of CH_4 and CO_2 emission or absorption in the two seasons and the difference between the two lakes.

For CH_4, in both lakes, it is shown that in both seasons, the Dau Tieng Lake and Tri An Lake emit CH_4 to the atmosphere from the surface, and the rate of emissions in the dry season is higher than in the rainy season. At the surface of the Dau Tieng Lake, the average CH_4 emission rate in the dry season is 35.87 ppm/m^2/hour and in the rainy season, it is 13.2 ppm/m^2/hour. At the surface of Tri An Lake, the average CH_4 emission rate in the dry and rainy seasons is 18.21 ppm/m^2/hour and 7.82 ppm/m^2/hour, respectively. The results show that Dau Tieng Lake emits more CH_4 gas into the atmosphere than Tri An Lake.

For CO_2, in Dau Tieng Lakeboth seasons emit CO_2 into the atmosphere with average emission rates in the dry and rainy seasons, respectively 1561.78 ppm/m^2/hr and 2626.7

ppm/m^2/hr, respectively. It can be seen that in the rainy season, the CO_2 emission rate is higher than in the dry season. In Tri An Lake, it is opposite to Dau Tieng Lake, which absorbs CO_2 from the atmosphere in both seasons, with an average absorption rate in the dry season of 1131.84 ppm/m^2/hr and 3835.15 ppm/m^2/hour in the rainy season. The results show that Tri An Lake absorbs more CO2 in the rainy season than in the dry season.

The study's results also show the relationship between CH_4 and CO_2 fluxes with biochemical factors in water (DO, temperature and pH) at Dau Tieng and Tri An lakes.

In the Dau Tieng reservoir, the CH4 emission rate in both seasons is positively correlated with DO and pH. However, CO_2 emission rates in both seasons were negatively correlated with DO and pH, in contrast to CH_4. Besides, the correlation between CH_4 and CO_2 emission rates with temperature has seasonal differences. For CH_4, in the dry season, the gas emission rate is positively correlated with temperature, but there is no correlation between these two factors in the rainy season. For CO_2, in the dry season, the CO_2 emission rate is negatively correlated with the temperature. Still, in the rainy season, on the contrary, these two factors have a positive correlation with each other.

At the surface of Tri An Lake, there is a difference between the CH_4 emission rate and the CO_2 absorption rate with seasonal biochemical factors. For CH_4 gas, in both seasons, there is no correlation between the CH_4 emission rate and biochemical factors (DO, temperature and pH). For CO_2, there was no correlation between CO_2 absorption rate and temperature in both seasons. During the dry season, the rate of CO_2 absorption was not correlated with DO; however, it was negatively correlated with pH. During the rainy season, the rate of CO_2 absorption is negatively correlated with DO; however, there is no correlation with the pH in the rainy season, which is the opposite in the dry season.

Request

Through the research, the topic proposes some recommendations as follows to get more accurate and more precise results on the factors affecting the process of GHG emissions at the surface of irrigation and hydropower reservoirs:

- Surveying the GHG emission rate at the lake surface over a more extended period, maybe three days, to accurately track the factors affecting the GHG emission rate.

- Increase the number of large surface stations to assess the influence of natural and anthropogenic factors on the rate of GHG emissions at the surface of the irrigation and hydropower reservoir systems.

- Measure more dynamic factors to consider the influence of active processes on the rate of GHG emissions. In addition, measure the concentration of nutrients in the water and the density of plankton and algae.

- Besides measuring at the surface, it is possible to measure the concentration of GHG in water in layers to monitor their diffusion and foaming.

References

1. Đoàn Thị Kim Chi (2016), *Nhận diện và đề xuất quản lý rủi ro liên vùng của hồ Dầu Tiếng đến thành phố Hồ Chí Minh,* Luận văn tốt nghiệp, Trường đại học Tài nguyên và Môi trường TPHCM.

2. Nguyễn Thanh Tuấn (2011), *Ứng dụng công nghệ GIS và mô hình SWAT đánh giá chất lượng nước lưu vực hồ Dầu Tiếng,* Luận văn tốt nghiệp, Trường Đại học Nông Lâm thành phố Hồ Chí Minh.

3. Quan trắc thành phần môi trường đất, nước, không khí trên địa bàn tỉnh Tây Ninh năm 2022, Trung tâm Quan trắc tài nguyên và môi trường tỉnh Tây Ninh.

4. Tô Thị Tuyết Giang (2016), *Nhận diện và đề xuất quản lý rủi ro liên vùng của hồ Trị An đến thành phố Hồ CHí Minh,* Luận văn tốt nghiệp, Trường đại học Tài nguyên và Môi trường TPHCM.

5. Xu. Liukang, Mcdermitt. Dayle, Hupp. Jason, Johnson. Mark, Madsen. Rod (2015), Capturing and processing soil GHG fluxes using the LI-8100A. EGU General Assembly.

UNIVERSITY OF SCIENCE,
VIETNAM NATIONAL UNIVERSITY HO CHI MINH CITY
Physics & Engineering Physics Faculty
Department of Oceanology, Meteorology and Hydrology

SOCIALIST REPUBLIC OF VIETNAM
Independence – Freedom – Happiness
--o0o---

GRADUATION THESIS COURSE REVIEWS

Student: **ĐỒ HOÀNG MINH CƯỜNG**

Title: **Calculating greenhouse gas emissions (CO2, CH4) at the surface of Tri An lake and Dau Tieng lake in the rainy and dry seasons**

Field of Oceanology, major: Oceanology - Meteorology - Hydrology

Reviewer: (Full name, Academic title, degree) Dr. Bùi Thị Ngọc Oanh

Working agency: University of Science, VNU-HCM

Role:

☒ Supervisor ☐ Reviewer

Comments and evaluation of graduation thesis:

1. **Scientific significance:**

The increase in greenhouse gases in the atmosphere is an issue of current concern to scientists, due to its impact on global warming. These gas emission sources come from artificial sources and natural sources such as ponds, lakes, rivers, oceans, and mangrove forests, including hydroelectric/irrigation lakes. Research on this gas emission in hydroelectric reservoirs in our country is still very limited, and many issues need attention. For example, the amount of material deposited in the lake, the lake ecosystem, water quality status, gas emissions from bottom sediments or lake water to the atmosphere, etc. Up to now, research on gas emissions Greenhouses from hydroelectric lakes is still limited in our country. Therefore, studying gas emissions at this interface is meaningful in determining the gas emission content in water reservoirs.

2. **Contents**:

The topic includes: Introduction, 4 chapters, a conclusion and references, lists of figures and tables

- Introduction: state the objectives, meaning of the topic, reasons for choosing, and limit the research area.
- Chapter 1: Overview of greenhouse gases: provides an overview of CO_2 and CH_4, influencing factors, impacts of greenhouse gas emissions
- Chapter 2: Research area and methods: students stated the research area (Dau Tieng Lake and Tri An Lake) and related research methods when carrying out the topic. In addition, students also actively

participated in two survey trips in the dry season (March 2021) with project leader Dr. Le Xuan Thuyen to learn how to operate measuring machines and survey and collect data.

- Chapter 3: Survey results of CH4 and CO2 emissions at Dau Tieng Lake. The results are that the CO2 and CH4 emission rates change over time, and the average gas emission rate changes in each season (dry season and rainy season). In addition, there are also results evaluating other biochemical indicators such as water temperature, pH, and DO, as well as the relationship of biochemical indicators with emission rate.
- Chapter 4: Survey results of CH_4 and CO2 emissions at Tri An Lake. Similar to Chapter 3, it applies to Tri An Lake.
- Chapter 5: Conclusion: students state the results achieved during the process of implementing the topic, and, at the same time, make recommendations to expand the research.

3. Form:

The topic includes 55 pages. The presentation format is clear, images are presented with captions. There are some minor errors in the article that need to be corrected.

3. Conclusion: Does the thesis meet the requirements of a university graduation thesis?

The thesis achieves the requirements of a university graduation thesis.

We respectfully request that the thesis grading committee approve the thesis with points: **9.75/10.0** (Nine seventy-five points)

Ho Chi Minh City, July 31st 2021

REVIEWERS

Bui Thi Ngoc Oanh

UNIVERSITY OF SCIENCE,
VIETNAM NATIONAL UNIVERSITY HO CHI MINH CITY
Physics & Engineering Physics Faculty
Department of Oceanology, Meteorology and Hydrology

SOCIALIST REPUBLIC OF VIETNAM
Independence – Freedom – Happiness
--o0o---

GRADUATION THESIS COURSE REVIEWS

Student: Do Hoang Minh Cuong

Title: **Calculating greenhouse gas emissions (CO2, CH4) at the surface of Tri An lake and Dau Tieng lake in the rainy and dry seasons**

Field of Oceanology, major: Oceanology - Meteorology - Hydrology

Reviewer: (Full name, Academic title, Degree) Dr. Le Xuan Thuyen

Working agency: University of Science, VNU-HCM.

Role:

☐ Supervisor ☒ Reviewer

Comments and evaluation of graduation thesis:

1. **Scientific significance**:

   This is a new research direction, but students have mastered the basic knowledge, as well as practice to explain the results.

2. **Content**:

   The contents are explained clearly and coherently in the chapters according to regulations to reach the final conclusion.

3. **Form**:

   The presentation format is good, clear, and meets general regulatory requirements.

4. **Conclusion:**

   The thesis meets the requirements of a university graduation thesis.

We respectfully request the thesis grading committee to approve the thesis with points: 9/10

City. Ho Chi Minh, July 31st 2021

REVIEWERS

Le Xuan Thuyen

VIET NAM NATIONAL UNIVERSITY HO CHI MINH CITY
UNIVERSITY OF SCIENCE
FACULTY OF PHYSICS AND ENGINEERING PHYSICS
DEPARTMENT OF OCEANOLOGY, METEOROLOGY AND HYDROLOGY

UNDERGRADUATE THESIS

Thesis title:

ANALYSIS OF THE EFFECTS OF SOIL SURFACE TEMPERATURE AND WATER LEVEL ON METHANE EMISSIONS IN THE RICE FIELD

Student: Võ Huỳnh Hương

Supervisor: Dr. Bùi Thị Ngọc Oanh

HO CHI MINH CITY – 2023

VIET NAM NATIONAL UNIVERSITY HO CHI MINH CITY
UNIVERSITY OF SCIENCE
FACULTY OF PHYSICS AND ENGINEERING PHYSICS
DEPARTMENT OF OCEANOLOGY, METEOROLOGY AND HYDROLOGY

UNDERGRADUATE THESIS

Thesis title:

ANALYSIS OF THE EFFECTS OF SOIL SURFACE TEMPERATURE AND WATER LEVEL ON METHANE EMISSIONS IN THE RICE FIELD

Code: 7440228

Specialization: Department of Oceanology, Metteorology and Hydrology

Student: **Võ Huỳnh Hương**

Supervisor: **Dr. Bùi Thị Ngọc Oanh**

TP HỒ CHÍ MINH – 2023

GUARANTEE

I hereby certify that my bachelor's thesis in the field of Oceanology, Metteorology and Hydrology, titled “Analysis of the effects of soil surface temperature and water level on methane emissions in the rice field” is a scientific work conducted under the guidance of Dr. Bui Thi Ngoc Oanh.

The research findings of this thesis are entirely truthful and accurate.

Student conducted

Võ Huỳnh Hương

ACKNOWLEDGEMENTS

I would like to express my deep gratitude to the esteemed faculty of the Department of Oceanology, Meteorological, and Hydrological Sciences, Faculty of Physics - Engineering Physics, University of Natural Sciences, Ho Chi Minh City National University, for imparting valuable knowledge and providing the best possible conditions for my education over the past four years. Additionally, I would like to thank the Greenhouse Gas and Climate Change Research Center, University of Natural Sciences for providing methane data and the Moc Hoa, Long An meteorological station for supplying meteorological data for my research.

I am incredibly grateful to Ms. Bui Thi Ngoc Oanh for her dedicated guidance and mentorship while I worked on my thesis.

On this occasion, I would also like to extend my heartfelt thanks to my family, friends, and the entire class 19HDH for their constant love and support throughout this journey.

Ho Chi Minh City, July 2023

Võ Huỳnh Hương

ABSTRACT

ANALYSIS OF THE EFFECTS OF SOIL SURFACE TEMPERATURE AND WATER LEVEL ON METHANE EMISSIONS IN THE RICE FIELD

Methane is a potent greenhouse gas generated under oxygen-deficient conditions. Climate change has caused increasingly severe consequences in recent years, negatively impacting humans and the natural environment. Globally, methane emissions from rice fields account for 50% of agricultural emissions, significantly contributing to atmospheric methane levels. This study conducted data analysis from the Center for Greenhouse Gases and Climate Change to provide practical analysis and assessment. The study aimed to evaluate the correlation between methane emissions and two factors: soil surface temperature and water level, during three crops from 01/07/2020 to 30/06/2021. The results revealed that methane emissions have a positive correlation with soil surface temperature during the 8-days period after seeding. The relationship between methane emissions and the water level was closely related, although the correlation between these two factors was not clearly determined.

TABLE OF CONTENTS

LIST OF FIGURES

LIST OF TABLES

PREFACE

Introduction

In today's world, society is experiencing continuous development, accompanied by an increasing demand for food and agricultural products. However, the processes of urbanization and population growth are gradually diminishing agricultural land availability. Concurrently, climate change, natural disasters, and environmental degradation pose new challenges to food production. This situation presents a concerning issue: the demand for food and agricultural products is rising while the supply is limited. To address these challenges, it is imperative to develop sustainable agriculture practices while safeguarding and restoring the environment.

Significance of the Topic

Greenhouse gases play a significant role in climate change. Climate change has diverse and alarming consequences such as extreme weather events, droughts, floods, disease outbreaks, rising sea levels, all of which have adverse effects on the environment, human beings, and the economy. In the realm of agriculture, rice paddies contribute up to 50% of methane emissions into the atmosphere, thereby contributing to global warming. Methane (CH_4) is a potent greenhouse gas, more than 25 times stronger than CO_2 when present in the atmosphere. CH_4 is emitted into the atmosphere from various sources, including soil, water, vegetation, fertilizers, and notably, it is produced during flooded rice cultivation.

Recognizing the paramount importance of the issues outlined above, I have chosen to undertake the research project titled "***Analysis of the effects of soil surface temperature and water level on methane emissions in the rice field***". This thesis emphasizes the analysis and evaluation of the relation between methane emissions and soil temperature and water levels. The research project is based on methane data from the Greenhouse Gas and Climate Change Research Center and meteorological data from the Moc Hoa, Long An meteorological station.

Research Objectives

The research encompasses various factors, including air temperature, humidity, soil temperature, rainfall, water levels, and methane emission rates.

Research Area and Scope

The study is conducted in the rice fields of the Lang Sen Wetland Reserve, Long An Province, which is characterized by submerged land.

The research content in the thesis includes:

– Preface

– Chapter I: Research Overview

– Chapter II: Research Area and Methodology

– Chapter III: Results and Evaluation, Comments

– Conclusion

CHAPTER 1: RESEARCH OVERVIEW

1.1 Methane (CH_4) Emissions and the Impact of Methane on Climate Change

Methane (CH_4) is a hydrocarbon and a significant component of natural gas. Methane is also a greenhouse gas (GHG), and its presence in the atmosphere affects the Earth's temperature and climate system. The global average temperature has increased by 1.1°C, with methane contributing to 0.3°C of this increase. Methane is emitted from both natural and human activities [1]. Approximately 40% of methane emissions come from natural sources, while up to 60% result from anthropogenic sources. The primary sources of methane production include anaerobic decomposition in wetlands (marshes, ponds, seabed methane hydrates), livestock waste, coal mining, oil production, agricultural activities, wastewater treatment, and some industrial processes. Methane is flammable in the air and is used as a fuel for combustion and lighting in households and the energy sector [2].

Methane is a potent greenhouse gas, with a global warming potential 25 times greater than carbon dioxide (CO_2) when considered over 100 years [1]. According to the World Meteorological Organization (WMO), the global average concentration of methane in the atmosphere was 260% of pre-industrial levels as of 2019 [3]. The global average CH_4 concentration measured at monitoring stations reached a new high of 1869 ± 2 ppb in 2018, an increase of 10 ppb compared to the previous year. This increase in 2018 exceeded the 7 ppb observed during 2016–2017 and the average annual increase over the past decade. The average yearly increase in CH_4 concentrations has decreased from around 12 ppb per year in the late 1980s to nearly zero from 1999 to 2006. Methane levels in the atmosphere have risen since 2007, reaching 259% of pre-industrial levels (approximately 722 ppb) due to increased emissions from anthropogenic sources [4], especially from wetland areas in tropical regions [3].

According to the Intergovernmental Panel on Climate Change (IPCC), methane significantly impacts climate change. Methane contributes to air pollution

as it is a significant precursor of tropospheric ozone, a potent greenhouse gas and hazardous air pollutants [5]. Increased atmospheric methane emissions have resulted in serious consequences, the most notable being the greenhouse effect and global warming. This leads to adverse effects on ecosystems and humans [6]. Higher temperatures cause ice and snow melting in high-latitude regions, leading to rising sea levels. Climate extremes such as droughts, floods, and storms are intensified. Methane emissions affect both terrestrial and aquatic ecosystems. In terrestrial environments, methane affects the respiration of soil microorganisms and disrupts the ecological balance. In aquatic environments, methane emissions from lakes, ponds, and wetlands affect the development of freshwater and marine ecosystems [7].

Furthermore, methane negatively impacts the environment and harms human health. Methane exposure can lead to difficulty breathing, red eyes, and skin irritation. Additionally, methane is associated with cardiovascular and nervous system issues [6].

1.2 Methane in Agricultural Activities

1.2.1 Overview of Vietnam's Agricultural Sector

Agriculture plays a crucial role in Vietnam's economy. Developing agriculture is a core issue to ensure food security and social welfare. In the first three months of 2023, Vietnam achieved positive results in GDP, with an estimated growth of 3.32% compared to the same period in the previous year. The added value of agriculture in the first three months of 2023 increased by 2.43% compared to the same period last year, contributing 0.22% to the overall economic growth [8].

Rice production is necessary in the agricultural sector, as Vietnam has a long history of rice cultivation. However, in recent years, most rice-growing areas have been reduced due to inefficient land conversion or imbalanced water resource allocation towards more economically productive structures like vegetable and fruit cultivation aquaculture. High-quality rice cultivation models have been promoted, focusing on improving quality and economic efficiency. The proportion of fragrant

and high-quality rice has increased while rice production has decreased in quantity [8].

In the first three months of this year, regions focused on planting and caring for the winter-spring rice crop, the largest rice crop of the year. According to the General Statistics Office, in the first quarter of 2023, the Red River Delta region planted 47.4 thousand hectares, a decrease of 7.8 thousand hectares. The northern midlands and mountainous regions planted 220.6 thousand hectares, an increase of 1 thousand hectares. The North Central region reached 34.9 thousand hectares, a decrease of 2.3 thousand hectares. The winter-spring rice crop in South Vietnam reached 98.2% compared to the 2022 winter-spring crop. In particular, the Mekong Delta region planted 1478.7 thousand hectares, a 1.9% decrease from the previous year. The Mekong Delta is the largest rice granary in Vietnam, contributing over 90% of Vietnam's rice exports. It has affirmed Vietnam's position as a leading rice exporter globally, ensuring food security for the nation and creating jobs for 65% of the rural population in the region [8].

Although Vietnam's agriculture sector has significantly contributed to the national economy, it faces various challenges. Urbanization processes have led to a reduction in arable land. Issues include as diseases and the increasing use of pesticides, which have affected crop quality. With global climate change, extreme weather events have significantly impacted agriculture, particularly rice cultivation. Consequences of climate change, such as droughts, saline intrusion, and abnormal rainfall, have affected agricultural production, including rice, and increased greenhouse gas emissions [9].

In Vietnam, irrigated rice fields contain organic matter, leading to methane formation. Therefore, greenhouse gas emissions in rice fields deviate from global emissions patterns, with CH_4 accounting for 45% of emissions, compared to CO_2 at only 6%, due to imbalanced and improper fertilizer use, leading to N_2O emissions of up to 46% [10].

According to Vietnam's 2014 National Greenhouse Gas Inventory Technical Report, the agriculture sector accounted for 27.92% of greenhouse gas emissions. In

line with global efforts, Vietnam has set targets to reduce greenhouse gas emissions by 2030. The main goals outlined in Vietnam's Implementation Plan for the Paris Agreement on Climate Change for the period 2021-2030 include:

Firstly, the nationally self-financed contribution goal. By 2030, Vietnam aims to reduce its total greenhouse gas emissions by 8% compared to the usual development scenario. It includes reducing emissions intensity by 20% per unit of GDP compared to 2010 and increasing forest coverage to 45% [11].

Secondly, the contribution goals are consistent with international support. The 8% contribution mentioned above can be increased to 25% with international supporting through bi-lateral and multi-lateral cooperation and the mechanisms within the new global climate agreement, including a 30% reduction in emissions intensity per unit of GDP compared to 2010. To achieve this pathway, Vietnam must actively and substantively participate in global efforts and make a decisive transition towards low-emission greenhouse gas development [11]. At COP26 (December 2021), Prime Minister Pham Minh Chinh committed that Vietnam will strive to achieve net-zero emissions by 2050. Two related commitments closely linked to the agricultural sector are the commitment to participate in the "Global Methane Pledge" and the commitment to implement the "Glasgow Declaration on Forests and Land Use" [12]. At the United Nations Food Systems Summit, Vietnam aimed to become a transparent, responsible, and sustainable food producer and supplier to meet the food and nutrition needs of around 100 million people in Vietnam and for exports [12]. To fulfil the COP26 commitments, Vietnam needs to transform its food and agriculture systems towards being "green" with fewer greenhouse gas emissions and develop a sustainable agricultural sector. Investments are required to build and establish agricultural infrastructure, promote private sector involvement in agricultural investment, and apply science and technology. The active use of digital technologies in agricultural value chains and expanding public-private partnerships are essential [12]. However, the agricultural sector faces substantial impacts from climate change and contributes significantly to greenhouse gas emissions, accounting for 13.9% of the nation's total greenhouse gas emissions.

Greenhouse gas emissions in the agricultural sector include CO_2, CH_4, and N_2O emissions [12].

1.2.2 Methane Emissions in Flooded Rice Fields

Human-induced CH_4 emissions from agricultural land account for approximately 50% of total CH_4 emissions [13]. Rice fields are among the most important CH4 sources in the atmosphere. Rice is a primary food crop for about 50% of the world's population [Maclean, 2002]. IPCC (2006) estimates global CH_4 emissions from rice paddies range from 20 to 100 Tg/year. These CH_4 emission estimations are based on measurements from rice paddies in the United States, Spain, Italy, China, India, Australia, Japan, and Thailand [14].

Measurements of CH_4 emissions from rice fields at various locations around the world show significant temporal variations. Over time, the variations in CH4 emissions depend on various factors, including climate, soil and rice plant characteristics, agricultural practices, and water management. The factors influencing methane emissions vary widely in space and time [14].

In Vietnam, the Climate Change Department and expert groups from various ministries and agencies conducted an inventory of methane emissions. The main sectors included in the methane emissions inventory for 2020 were energy, waste, agriculture, and land use (AFOLU). The inventory results showed that the total methane emissions from these sectors were 98.3 million tons of CO_2 equivalent. Among these, AFOLU accounted for the highest share of CH_4 emissions at 57.75%, followed by waste at 26.84% and energy at 15.41% [15].

Due to its excellent system of water irrigation channels, the Mekong Delta region can now flood its fields for rice cultivation throughout all seasons, enabling nearly year-round rice production. It is a favourable environment for the phenomenon of methane emissions. Rice cultivation is the largest source of methane emissions when all sources of methane (CH4) emissions are considered. In the agriculture, forestry, and land use (AFOLU) sectors, methane emissions account for up to 40.44% of the total emissions in 2020 [15].

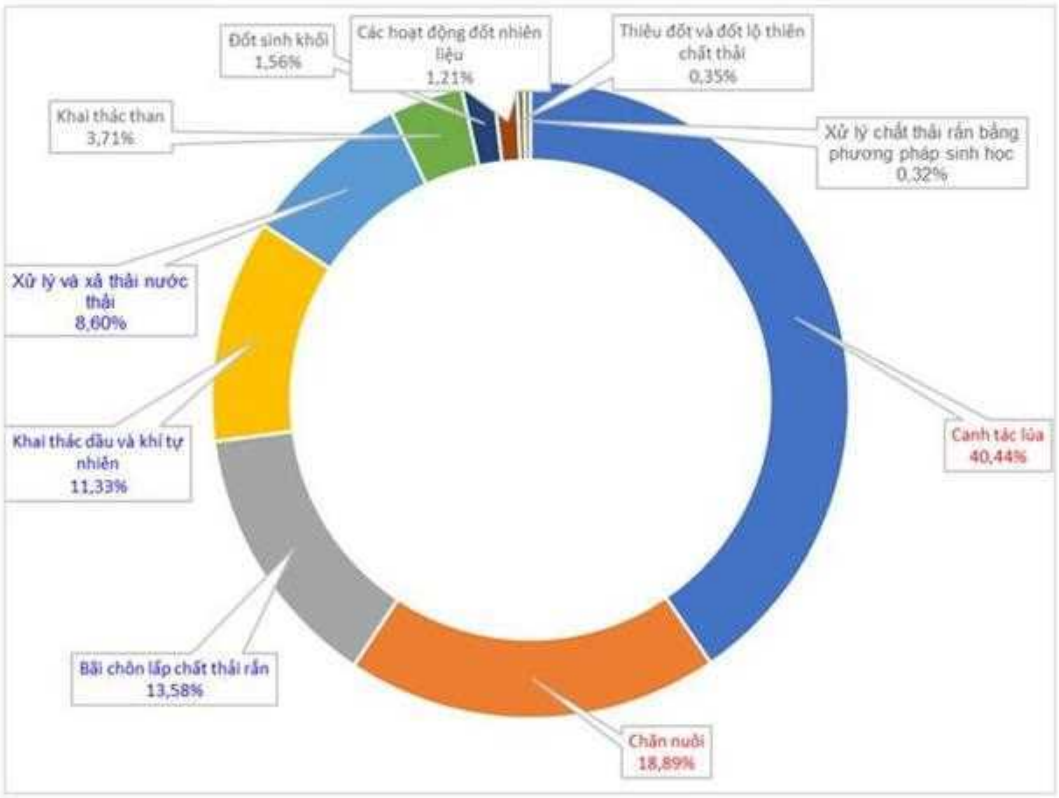

Figure 1.1: Methane Emission Intensity in 2020 by Sectors [14]

Given the conditions where submerged rice roots produce methane, the process of carbon decomposition in soil generates methane gas. Subsequently, methane is released into the environment through three main pathways. About 90% of methane emissions from rice fields are released into the atmosphere through gas transport mechanisms within the rice plants. Afterwards, methane continues to be emitted into the environment through the nodes and leaf blades. Around 9% of methane emissions occur through methane diffusion across the water surface layer of the rice field. Only 1% of methane emissions enter the atmosphere through gas bubbles within the surface water layer of the rice field [15].

1.2.3 Factors Influencing Methane Emissions in Rice Fields

Methane emissions in rice cultivation depend on various factors. Controlling temperature, irrigation practices, fertilizer application, and suitable cultivation techniques all play a part in reducing methane emissions.

a. Rice Variety and Rice Roots

Different rice varieties can significantly influence the amount of CH_4 emissions into the atmosphere. Other rice varieties have varying compositions and quantities of substances released from their roots, which substantially affect CH_4 emissions. Physiological characteristics of rice roots positively correlate with seed yield. However, factors like root length, root oxidation activity, total number of roots, and root surface area inversely correlate with total CH_4 emissions [16].

The root development process and substances produced by roots can enhance CH_4 production by providing organic matter for methanogenesis by methanogenic bacteria. These nutrients stimulate microbial activities, leading to increased CH_4 emissions. The initial growth stages of rice plants up to pre-harvest contribute to over 90% of the total emissions in one growing season. CH_4 emissions vary throughout the rice plant's growth cycle [16].

b. Growth Stage

The highest methane emission rates occur during the rice plant's growth stage, especially when the rice plant reaches maximum tillering and actively forms biomass. During the rice grain-filling stage, when fields need to remain continuously flooded, and when it is the rainy season, CH_4 emissions increase significantly. As the rice plant progresses through later stages, emissions gradually decrease. The rice plant has accumulated stable biomass, and water is drained to facilitate ripening and harvesting [17].

c. Field Management

Field management practices, such as fertilizer application, straw management after harvest, and cultivation activities, affect CH_4 production. According to the FAO, nutrient losses in the Mekong Delta reach nearly 70%. Rice plants only absorb around 30% of the applied fertilizer. Overuse and improper use of fertilizers are issues contributing to increased greenhouse gas emissions in rice production in the Mekong Delta while causing nutrient imbalances in the soil [10].

Straw management, especially for the summer and winter crop residues, poses significant challenges in the Mekong Delta. After harvesting during the winter crop season, fields dry out, and cleaning the fields using machines to remove crop residues is easy. However, areas flood after harvesting during the summer crop season, coinciding with the rainy season, making it challenging to clear fields or burn crop residues. Farmers are forced to bury straw in the soil, leading to considerable greenhouse gas emissions from straw decomposition [10].

d. Water Management in Rice Fields

Water levels in rice fields affect methane emissions into the atmosphere. When water levels are high, CH_4 is retained in the soil, resulting in lower methane emissions into the environment, but this is reduced when rice fields are dry or have low water levels. However, a continuously flooded rice field creates favourable conditions for the phenomenon of methanogenesis, which is conducive to more significant CH_4 emissions. Therefore, appropriate water management measures are essential. Additionally, good water management in rice cultivation helps conserve irrigation water and promotes healthy and stable rice plant growth [16]. Currently, in flooded rice cultivation, a practice known as intermittent wetting and drying is recommended by the International Rice Research Institute (IRRI). Implementing this method helps mitigate the methane environment, reduce greenhouse gas emissions and significantly conserve water during rice cultivation [18].

There are three main growth stages of rice plants: the growth stage (0-60 days after sowing), the reproductive stage (61-90 days after sowing), and the maturation stage (91-120 days after sowing) [19].

From 0-7 days after sowing, the water level in the field should be maintained at saturation or about 1 cm above the soil surface. During this period, the soil should only be moist enough for the rice roots to establish in the soil and for rice seedlings to grow.

From 7-25 days after sowing, keep the water level around 1-3 cm above the soil surface and maintain it continuously for about 20-25 days after sowing. During this time, water is an essential requirement for rice plant growth. Maintained water in the field helps create an anaerobic environment, limiting weed seedling growth and conserving soil moisture for rice seedling growth.

From 25-40 days after sowing, water is still needed, but too much water can limit tillering. During this time, maintain the water level in the field from the soil surface to no more than 15 cm below the soil surface. Water is pumped into the field when the water level drops below this level. The farther below the soil surface the water is (but not less than 15 cm below the soil surface), the better it helps rice roots penetrate deeper into the soil, prevents lodging, and facilitates harvesting.

From 40-45 days after sowing, pump water into the field to a depth of 1-3 cm, combined with fertilization. Water is essential for dissolving fertilizers (especially nitrogen) and preventing decomposition and evaporation.

From 45-60 days after sowing, maintain the water level at 2-3 cm, avoiding field drying, as this is the time when rice is prepared for grain filling, and adequate water is crucial. Insufficient water during this period can affect the quantity and quality of rice grains [20].

From 60-70 days after sowing, as rice starts to flower, continuously maintain the water level at 3-5 cm for about 10 days. It ensures easy pollination and prevents rice grains from sticking together or floating.

From 70 to 90 days after sowing, the rice is mature and robust in the milk-ripe stage. Therefore, the water level in the field should be maintained from the soil surface to no more than 15 cm below the soil surface during this period. This thin layer of water provides just enough moisture to the soil [20].

From 90-120 days after sowing (or about 10 days before harvesting), drain the water to accelerate ripening and ensure the field is dry, making it easier for harvesting [20].

e. Soil Properties

Soil properties (mechanical composition, organic matter content, pH, Eh) influence CH_4 emissions.

The emission of CH_4 gas from flooded rice fields depends significantly on soil properties. In rice fields, CH_4 production is strongly influenced by the composition and structure of the soil and the content of inorganic electron acceptors. Different types of soils have different periods, from soil submergence to the initiation of methane production [14].

According to Xiong's study, soils with a high sand fraction release more CH_4 than soils with a low sand fraction. K. R. Brye's research results indicate that clay soils emit up to 23% less CH_4 than sandy soils. A study in China by Huang, which investigated 18 different soil types, showed that CH_4 emissions were linearly related to the sand fraction in the soil [16].

Mechanical composition (clay-silt-sand ratio) and organic matter content play significant roles in CH_4 emissions. These two factors are interrelated. Soils with a lighter mechanical composition (higher sand content than silt) generally have lower total organic matter content than soils with a heavy mechanical composition (lower sand content and higher silt content). Clayey soils protect organic matter, making it less susceptible to decomposition. Therefore, CH_4 emissions depend on the soil's mechanical composition and the characteristics of the organic matter that releases CH_4 under anaerobic conditions. These two factors affect CH_4 emissions from flooded rice fields [16].

pH is one factor affecting the CH_4 production process, especially in flooded rice cultivation. The effective formation of CH_4 occurs in a narrow pH range around neutral (pH from 6.4 to 7.8). Flooding can alter the soil's pH, increasing it in acidic soils and decreasing it in alkaline soils [14].

The redox potential (Eh) is an essential factor in CH_4 production in the soil. Eh of the soil decreases after flooding. Patrick's research (1981) demonstrated that CH_4

production requires a soil redox potential condition below about -150 mV. The study of Yamane and Sato (1964) also showed that CH_4 production from flooded rice fields begins when the Eh decreases below -150 mV [14].

f. Soil Temperature

Soil temperature influences the production and release of CH_4. Temperature is a critical factor in determining the soil's biological processes. Yamane and Sato (1961) discovered that CH_4 formation peaks at 35°C in waterlogged peat soil, while the CH_4 formation rate is very low at temperatures below 20°C [17].

Research by Mohammed and colleagues (2020) shows that as soil temperature increases, methane emissions also increase. The conversion rate of organic matter into methane depends heavily on temperature. Higher soil temperatures create favourable conditions for methanogenic bacteria (CH_4 producers) to thrive and become more active. Consequently, elevated temperatures expedite the decomposition of organic matter, leading to increased CH_4 production. Furthermore, temperature is related to soil moisture, heat capacity, and thermal conductivity, with dry soils having lower values than wet soils [17].

In summary, Chapter 1 of this study provided an overview of the research topic. Firstly, Chapter 1 presented a general perspective on the impact of methane on climate change and emphasized the importance of reducing methane emissions into the atmosphere. The next issue discussed was methane emissions in agricultural activities, particularly rice production. It is a significant source of methane emissions into the atmosphere due to the anaerobic decomposition of organic matter. Additionally, Chapter 1 provided an overview of the methane production and emission processes in agriculture, highlighting the crucial role of soil temperature, water level, and other factors influencing methane emissions in rice fields. These two main aspects outlined in Chapter 1 form the basis for further research and a deeper understanding of methane emissions in rice fields.

CHAPTER 2: RESEARCH AREA AND METHODOLOGY

2.1 Overview of the Research Area

2.1.1 Geographic Location

Long An is situated in the Mekong Delta region, located at geographical coordinates 105°30'30" to 106°47'02" east longitude and 10°23'40" to 11°02'00" north latitude. The natural area of the entire province covers 449194.49 hectares, accounting for 1.35% of the country's total area and 11.06% of the Mekong Delta's area [21].

Long An's administrative boundaries are as follows: to the east and northeast, it borders Ho Chi Minh City and Tay Ninh Province; to the west and northwest, it shares borders with Cambodia and Dong Thap Province; and to the south and southwest, it is adjacent to Dong Thap Province and Tien Giang Province. Long An Province is subdivided into 15 administrative units, including districts such as Duc Hue, Duc Hoa, Ben Luc, Can Duoc, Can Giuoc, Thu Thua, Tan Tru, Chau Thanh, Thanh Hoa, Tan Thanh, Moc Hoa, Vinh Hung, Tan Hung, the town of Kien Tuong, and the city of Tan An, with 188 administrative units at the commune level comprising 161 communes, 12 wards, and 15 towns [22].

Long An is strategically located for economic and social development as a crucial link between Ho Chi Minh City's economy and the vital southern provinces in the Mekong Delta region. The province's trade connectivity with Ho Chi Minh City and the provinces of the Southeastern and Southwestern regions is facilitated by National Highways 1A, 50, N1, N2, the Ho Chi Minh City - Trung Luong Expressway, several provincial roads, and a waterway transportation system [22].

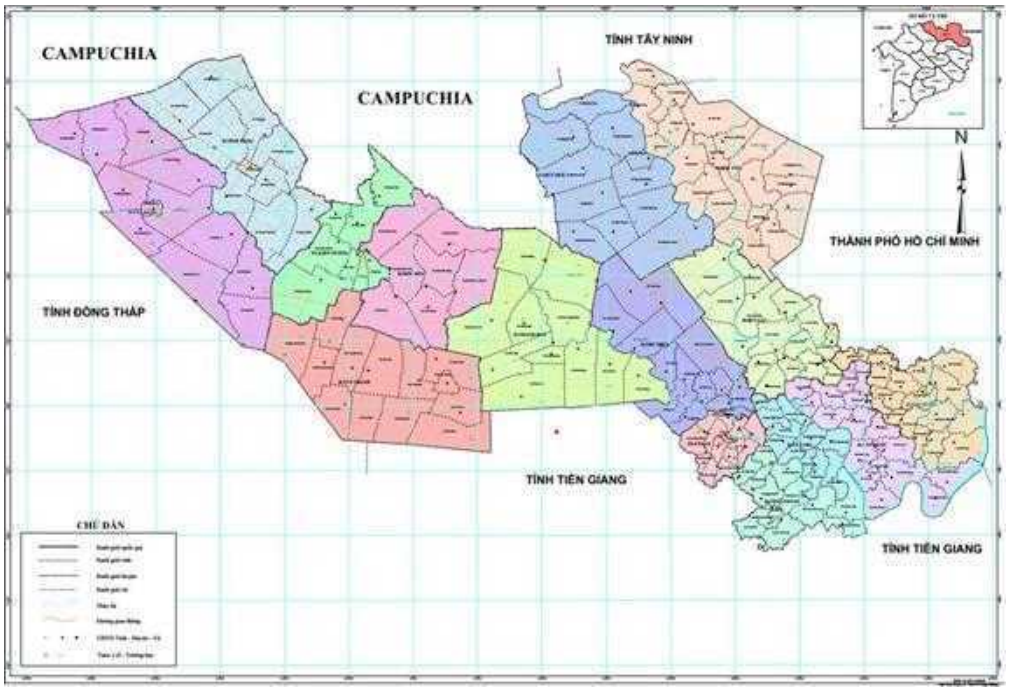

Figure 2.1: Administrative Map of Long An Province [21].

2.1.2 Natural Characteristics

2.1.2.1 Climate Conditions

Long An falls within the tropical monsoon climate zone and experiences high humidity. Due to its proximity to the Southeastern and Southwestern regions, it exhibits characteristics of the Mekong Delta region while retaining unique features of the Eastern part. Long An's climate is characterized by a tropical monsoon climate near the equator, resulting in abundant heat and humidity, prolonged sunshine, high temperatures, and a high annual cumulative temperature (the total average temperature of a season), with minimal temperature fluctuations between months, creating a temperate climate [21].

Monthly average temperatures range from 27.2°C to 27.7°C, with an annual average temperature of approximately 27°C - 28°C [2]. The temperature difference between the hottest and coldest months is about 6.5°C. The coldest months are typically December and January, while the hottest months are April and May. Air temperature directly affects the atmosphere's dispersion, dilution, and transformation of pollutants. Higher temperatures accelerate chemical reactions in

the atmosphere and reduce the residence time of substances in the atmosphere. Additionally, temperature influences the evaporation of organic solvents and odorous substances, making it a crucial factor affecting human health [22].

Annual rainfall varies from 966 mm to 1325 mm and decreases progressively from adjacent areas to Ho Chi Minh City towards the west and southwest. Intense rain can cause erosion on high hills and lead to flooding.

Air humidity depends on the amount of rainfall during the different seasons of the year. Average humidity at Long An's observation stations ranges from 72% to 93% [3]. Average daily sunlight duration ranges from 6.8 to 7.5 hours per day, with an annual average of 2500-2800 hours [1]. Average hourly shine of 182-246 hours of sunshine per month in Long An from 2015 to 2019 [3]. The total annual cumulative temperature ranges from 9700-10100°C. Temperature fluctuations between months vary from 2°C to 4°C [21].

The dry season typically spans from November to April, while the rainy season extends from May to October. The prevailing winds throughout the year are the Northeastern monsoon from October to April and the Southwestern monsoon from May to September [2]. The average wind speed is slightly higher during the rainy months than during the dry season, with minimal differences between months. The average wind speed throughout the year is 2.8 m/s, and the strongest winds, reaching speeds of 30-40 m/s, occur primarily during the rainy season, with west or southwest winds prevailing [22].

The dry season witnesses a significant decrease in rainfall, resulting in lower river flow, reduced groundwater levels, and increased seawater intrusion along the rivers. Rainfall patterns influence air quality as rain cleanses and washes away atmospheric dust and pollutants, reducing their concentrations. Furthermore, water dilutes and transports surface contaminants, significantly leached salts, and reduces soil pollution levels [22].

From a natural perspective, Long An is relatively homogenous in terms of elevation, with an average elevation of approximately 2-3 meters above sea level and minimal terrain height variations across the province. Consequently, there is slight variation in climate, weather, temperature, and rainfall across different locations within the region [23].

2.1.2.2 Topography and Terrain

Long An features relatively flat terrain with a gradual decline from the north-northeast to the south-southwest. The northern and northwestern parts of the province consist of low hills while a plain characterizes the central region, and the southern part represents the low-lying region of the Đồng Tháp Mười (Mekong Delta) with tracts of land covering nearly 66.4% of the province's total natural area. This low-lying area is prone to annual flooding. In some regions of Đức Hòa district, parts of Đức Huệ district, northern Vĩnh Hưng district, and Tân An city, there are pockets of well-drained soil with high bearing capacity, making foundation treatment less complex. However, most other areas in the province have weak soil foundations with low bearing capacity [22].

Long An's topography is divided by the Vàm Cỏ Đông and Vàm Cỏ Tây rivers, along with a network of small canals. The Vàm Cỏ Tây river stretches 186 km through the province, primarily fed by the Tiền River via the Hồng Ngự Canal, serving as a vital water source for agricultural production and household use. The confluence of the Vàm Cỏ Đông and Vàm Cỏ Tây rivers forms the Vàm Cỏ River, which is 35 km long and has an average width of 400 meters. It empties into the Soài Rạp River and flows into the East Sea. The Rạch Cát River (Cần Giuộc River) within Long An province is 32 km long, with minimal water flow during the dry season and poor water quality due to the inflow of wastewater from urban areas in Ho Chi Minh City, significantly affecting the livelihoods and production of the local population [22].

2.1.2.3 Water Resources and Hydrological Regime

Long An is an area with an extensive network of rivers, streams, and small canals linked to the Tiền River and the Vàm Cỏ river system, crucial waterways for agricultural production and domestic use. However, surface water resources in Long An are not abundant, and water quality is limited in various aspects. The groundwater reserves in Long An are generally assessed as not being plentiful, with uneven distribution and relatively poor quality. Most groundwater is distributed at depths ranging from 50 to 400 meters, spanning the Pliocene – Miocene layers [23].

Flooding occurs annually in northern districts within the Đồng Tháp Mười region of Long An, typically beginning in August or mid-August and lasting until the end of November. During this period, rainfall is concentrated, with the highest flow rates and intensities of the year, creating challenges for production and daily life. The upper reaches of the Mekong River primarily drive flooding. The depth and duration of floods also depend on local topography. Long An is far from the Tiền River, resulting in delayed floods that are not as deep but tend to recede slowly [24].

Saltwater intrusion: The primary source of saltwater intrusion into Long An's territory is from the East Sea through the Soài Rạp River. The degree of saltwater intrusion (scale and salinity) depends on various factors, including tides, wind direction, upstream water flow, water usage, rainfall, and prolonged sunlight [25].

Regarding tides, Long An is affected by the irregular semi-diurnal tidal regime of the East Sea through the Soài Rạp River. The southern districts along National Highway 1A are most affected, experiencing saltwater intrusion for about 4-6 months each year. Tides from the East Sea at the mouth of the Soài Rạp River have significant amplitudes ranging from 3.5-3.9 meters, penetrating deep into the interior during the dry season when there is minimal freshwater input to the Vàm Cỏ rivers. The maximum tidal amplitude ranges from 217-235 cm in Tân An and 60-85 cm in Mộc Hóa. Due to the high tidal amplitudes, the peak tides during the dry season significantly threaten saltwater intrusion into the southern region. However, during the rainy season, tides can be utilized for self-irrigation in the

areas along the Vàm Cỏ Đông and Vàm Cỏ Tây rivers, reducing production costs[25].

2.1.2.4 Soil Resources

Long An province is characterized by six main soil groups, the majority being alluvial soils mixed with various organic materials. These soils have a loose structure, poor physical and chemical properties, and are often saline and accumulate toxins [2].

Long An is particularly rich in saline soils, covering an area of 208,449 hectares, which accounts for 69.8% of the total area in the Mekong Delta region and constitutes 46.41% of the province's natural area. There are two low-lying saline areas in Bắc Đông and Bo Bo - Mỏ Vẹt. The saline water cycles occur twice a year during the early rainy season (from April to July) and the late rainy season (from November to January) [25].

Soil Temperature Measurement Standards

• Surface Soil Temperature Measurement

– Recording surface soil temperature values using standard thermometers.

– Recording minimum soil temperature values.

– Recording maximum soil temperature values.

• Deep Soil Temperature Measurement

– Measuring temperature values at various depths, including 5 cm, 10 cm, 15 cm, and 20 cm, along a depth scale.

– For digital soil temperature measurement devices, activate the device and read the displayed values at depths of 5 cm, 10 cm, 15 cm, and 20 cm [26].

2.1.3 Seasonal Information

Long An's climate is highly suitable for agricultural cultivation, especially rice cultivation. The Mekong Delta region, in general, and Long An in particular, have

three main rice crops: spring-winter, summer-autumn, and autumn-winter crops [27].

For this research project, three rice crops were studied with the following specific timeframes: the autumn-winter crop started from July 01, 2020, to September 30, 2020; the spring-winter crop began from November 01, 2020, to February 28, 2021; and the summer-autumn crop started from March 01, 2021, to June 30, 2021, based on the Gregorian calendar.

Currently, some areas in Long An province have shifted from low-yield rice cultivation to annual crops, mainly including watermelon, sesame, and peanuts, as well as long-term crops, primarily including jackfruit, oranges, and guavas. Most of these converted crops have provided high economic returns for farmers. However, the sustainability of this crop structure conversion is still lacking due to various factors, especially market prices and product outlets. Production organization has not followed local planning and direction and remains predominantly spontaneous [27].

2.2 Research Methods

The research methods used in this project include:

2.2.1 Literature Review Method

The literature review method involves gathering, evaluating, and summarizing existing documents related to a specific research topic. This method aims to synthesize, analyze, and consolidate information from sources such as books, articles, previous research, reports, and online materials. The literature review method helps researchers gain comprehensive and in-depth insights into a particular issue by synthesizing and analyzing existing documents, thus providing a profound understanding of the subject matter [11].

To implement this literature review method:

- Define the research objectives.

- Conduct searches for relevant sources related to the research topic through databases, libraries, journals, websites, and other document sources.

- Assess the reliability and select documents that are relevant to the research objectives.

- Summarize information from selected documents and analyze, compare, and draw conclusions or general trends.

- Write a literature review report, including the purpose, methodology, results, and findings.

2.2.2 Statistical Method

The statistical method is a research approach used in both natural and social sciences that involves collecting, analyzing, and interpreting numerical data and descriptions. This method is crucial in summarizing information, correlating data, calculating statistical parameters, and creating charts and graphs. The statistical method helps researchers understand data more deeply and draw evidence-based conclusions from numerical foundations [28].

The statistical method involves the following steps:

- Data Collection: Gathering numerical data from various sources, such as measurements, surveys, observations, experiments, or existing data.

- Data Preprocessing: Check and filter data to remove outliers or missing values.

- Data Analysis: Applying statistical methods and data analysis to understand relationships, calculate statistical parameters, and create charts and graphs.

- Interpretation of Results: Based on the analysis results, interpreting data to understand the significance and apply them to the research issue or defined objectives.

2.2.3 Data Information

In this thesis, the data under investigation were collected from the Greenhouse Gas and Climate Change Research Center and the Moc Hoa Meteorological Station in Long An. The collected and processed data encompass various factors, including temperature, humidity, rainfall, water level, soil temperature, and methane for 2020, 2021, and 2022.

Upon receiving the data, two processing stages were applied. The first stage involved data processing using Excel algorithms. In contrast, the second stage utilized the processed data from the first stage to create charts and make observations, assessments, and evaluations of the obtained results.

Specific data collected from the Moc Hoa Meteorological Station in Long An include (Table 1.1):

Continuous temperature and humidity data for three years, 2020, 2021, and 2022, measured 24 hours a day (with 24 data points per day).

Average hourly and daily water levels at the Moc Hoa Station, Vam Co Tay River. The Continuous water level data for three years of 2020, 2021, and 2022. Daily averages are equivalent to one data point per day, while hourly averages consist of 24 data points per day. Hourly water level data were measured every 30 minutes, resulting in 48 data points per day, covering the period from July 2020 to 2021.

The continuous rainfall data for three years (2020, 2021, and 2022) with measurements taken every 24 hours (with 24 data points per day).

Continuous surface soil temperature data for 2020, 2021, and 2022. These measurements were taken daily: 1:00 AM, 7:00 AM, 1:00 PM, and 7:00 PM. Additionally, soil temperature data were collected every 30 minutes, covering July 2020 to 2021.

Continuous methane data from July 2020 to 2021 was measured every 10 minutes but was later processed using EddyPro software to produce data points

every 30 minutes. Additionally, continuous data for water level and soil temperature were recorded. Continuous gas measurements were taken by the Greenhouse Gas and Climate Change Research Center station affiliated with the Faculty of Natural Sciences at the University.

Upon collecting data, a thorough examination was performed to ensure it was reliable and suitable for the research topic. Statistic calculations for necessary parameters relevant to the research content were performed. Following the data processing stage, the next step involved creating charts to analyze and evaluate the relevant factors. The types of charts utilized in this thesis include line charts, scatter plots, and bar charts. Methane fluctuation analysis charts are typically presented over time.

Table 1: Information from Data Collected at Moc Hoa Weather Station, Long An.

Meteorological Factors	**Continuous Data Time**	**Measurement Time**
Temperature	01/01/2020 - 31/12/2022	Hourly
Humidity	01/01/2020 - 31/12/2022	Hourly
Rainfall	01/01/2020 - 31/12/2021	Hourly
Water Level	01/01/2020 - 31/12/2022	Hourly
	01/07/2020 – 31/12/2021	1 data/day; 1 data each 30 minutes
Soil Temperature	01/01/2020 - 31/12/2022	4 data points (at 1h, 7h, 13h, 19h)/day
	01/07/2020 – 31/12/2021	1 data each 30 minutes
Metan	01/07/2020 – 31/12/2021	1 data each 30 minutes

After creating the charts, observations and evaluations were conducted on the general trends of the various factors over the years. The main objective of this study is to analyze and assess methane emissions concerning ground temperature and water level during three rice cropping seasons: the winter-spring season (01/07/2020-30/09/2020), the autumn-winter season (01/11/2020-28/02/2021), and the summer-autumn season (01/03/2021-30/06/2021).

2.2.4 Measurement Equipment Information

The LI-7700 instrument is crucial in measuring methane concentrations and monitoring methane emissions. Developed by LI-COR, this device utilizes the principle of air sampling and analysis to measure methane concentrations in the surrounding air [30]. The LI-7700 employs a system of pumps and valves to sample air from the environment, which is then converted into pure gas for analysis. This instrument uses near-infrared absorption spectroscopy (NIR) to determine methane concentrations. This principle relies on the absorption of light by methane at specific wavelengths within the NIR range [30]. The LI-7700 is specifically designed for eddy covariance flux measurements to assess methane emissions from the landscape. Under varying temperature and pressure conditions, the LI-7700 maintains accuracy and can perform 40 measurements per second [29]. The eddy covariance flux data is calculated as the sum of the total flux and the turbulent fluctuation term.

The LI-7700 is designed for straightforward and flexible operation in rice fields. The measurement data is automatically recorded and stored within the device, providing essential information on methane emissions and their temporal variations [29]. The LI-7700 instrument's methane measurements in rice fields are crucial in monitoring methane concentrations. The data collected on methane emissions can be analyzed and evaluated to better understand the scale and trends in methane emissions in agriculture, particularly in rice cultivation, better. It contributes to developing methane emission reduction measures and supports environmental management and protection efforts in the agricultural sector.

At the measurement station, the LI-700 instrument is tilted at an angle of approximately 30 degrees (Figure 2.1). Due to the concave design of the instrument's surface, placing it straight would cause rainwater to accumulate in the concave area, potentially leading to inaccurate measurements. In the context of Vietnam's commitment to producing clean rice and reducing greenhouse gas emissions, as stated by the Prime Minister at COP26, measuring methane emissions (CH4) in rice fields is crucial in providing effective mitigation solutions.

Figure 2.2: LI-7700 Device for Methane Emission Measurement in Rice Fields at Lang Sen Wetland Reserve, Long An.

Table 2: Basic Technical Specifications of the LI-7700 Device [29].

Resolution (RMS noise)	5 ppb @ 10 Hz and 2000 ppb CH_4
Measurement Range	0 to 25 ppm @ -25 °C, 0 to 40 ppm @ 25 °C
Data Communication	Ethernet (up to 40 Hz)
Detection Method	Wavelength Modulation Spectroscopy 2f detection
Operating Pressure Range	50 to 110 kPa
Output Bandwidth	up to 20 Hz

Operating Temperature Range	-25 to 50 °C
Power Requirements	10.5 to 30 VDC
Power Consumption	8 W nominal, 16 W during cleaning cycle
Sensor	14.33 cm dia (5.64 inches), 82.8 cm height (32.6 inches)
Optical Path	0.5 m physical path (1.65 ft), 30 m measurement path (98.4 ft)
Weight	5,2 kg

A Pt100 sensor is employed to measure soil temperature. Sensit manufactures this device and operates based on a resistance temperature detector (RTD) principle. Pt100 Sensit temperature sensors are commonly used in scientific research, agriculture, and land resource management. The Pt100 Sensit temperature sensor is designed to withstand harsh soil environments. It features a robust and waterproof protective casing, safeguarding the sensor from moisture and other environmental factors. This design ensures the stable operation of the sensor and the acquisition of accurate data over extended periods [30]. The sensor is positioned directly at the soil surface and is covered with a thin layer of soil on top.

Figure 2.3: Pt100 Soil Temperature Sensor [30].

Figure 2.4: LMP 307i Water Level Sensor [31].

The LMP307i water level measurement device is a high-pressure sensor manufactured by BD Sensors. This device is designed with a corrosion-resistant protective casing and performs effectively in various environments, including saltwater, freshwater, and chemical environments. The operation principle of the LMP307i relies on pressure changes to measure water level values. It employs a pressure sensor to convert the static pressure of the water level into an electrical signal. The LMP307i device collects accurate data and is widely used in numerous environmental applications [31]. This device is positioned approximately 20 cm below the surface of the field.

In Chapter 2, the research methodology, study area, and relevant data information were outlined to analyse and evaluate methane levels in the paddy fields.

CHAPTER 3: RESULTS AND EVALUATION, COMMENTS

3.1 Meteorological Data Analysis

3.1.1 Average Air Temperature for the Years 2020, 2021, and 2022 at the Moc Hoa Weather Station, Long An

The average monthly air temperatures from 2020 to 2022 at the Moc Hoa Weather Station, Long An, are depicted in Figure 3.1. The average monthly temperatures generally showed relatively modest fluctuations, ranging from 0.1 to 1.5 ^{o}C. The highest average temperatures typically occur in May, which marks the end of the dry season and the transition to the rainy season. Due to higher evaporation rates compared to precipitation during this period, the weather tends to be hot, resulting in elevated temperatures. Conversely, the lowest average temperatures were observed in December and January, coinciding with the Northeast monsoon. The Southern region, in general, and Long An, in particular, are influenced by cold air masses from the Siberian high-pressure system, leading to lower average temperatures than other months of the year.

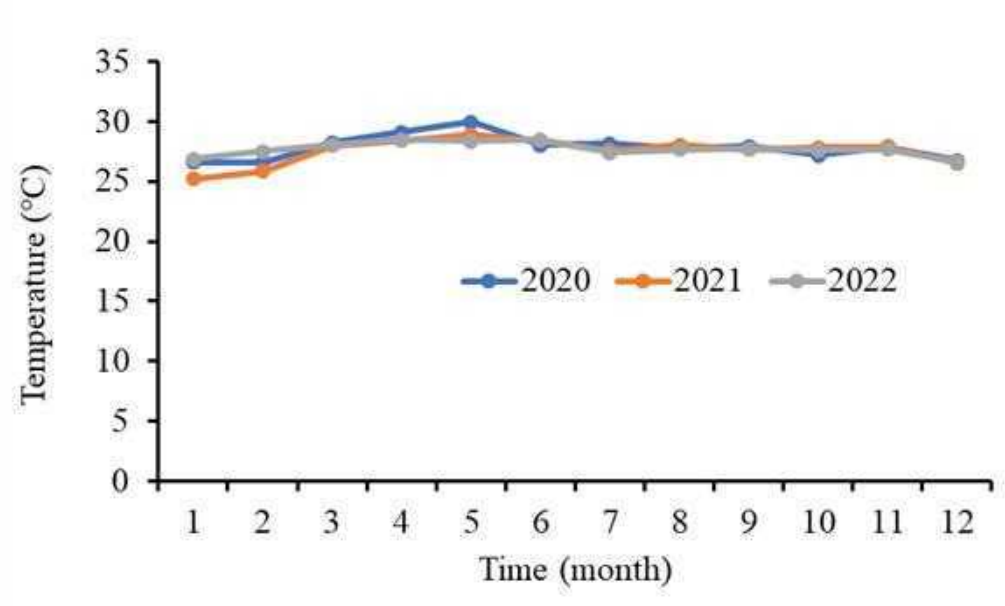

Figure 3.1: Average Air Temperature for the Years 2020-2022 at the Moc Hoa Weather Station, Long An.

3.1.2 Average Humidity for the Years 2020, 2021, and 2022 at the Moc Hoa Weather Station, Long An

The average monthly humidity levels from 2020 to 2022 at the Moc Hoa Weather Station, Long An, are illustrated in Figure 3.2. Generally, the month with the highest humidity is May, marking the beginning of the rainy season while still experiencing intense heat, resulting in greater evaporation and, consequently, higher humidity than other months of the year. The month with the lowest average humidity is December, which coincides with lower temperatures, leading to lower atmospheric moisture content.

In 2020, there is an exception, with June having the highest average humidity and March having the lowest. This anomaly can be attributed to the climatic variations that resulted in unusual heatwaves and elevated humidity during certain periods of that year.

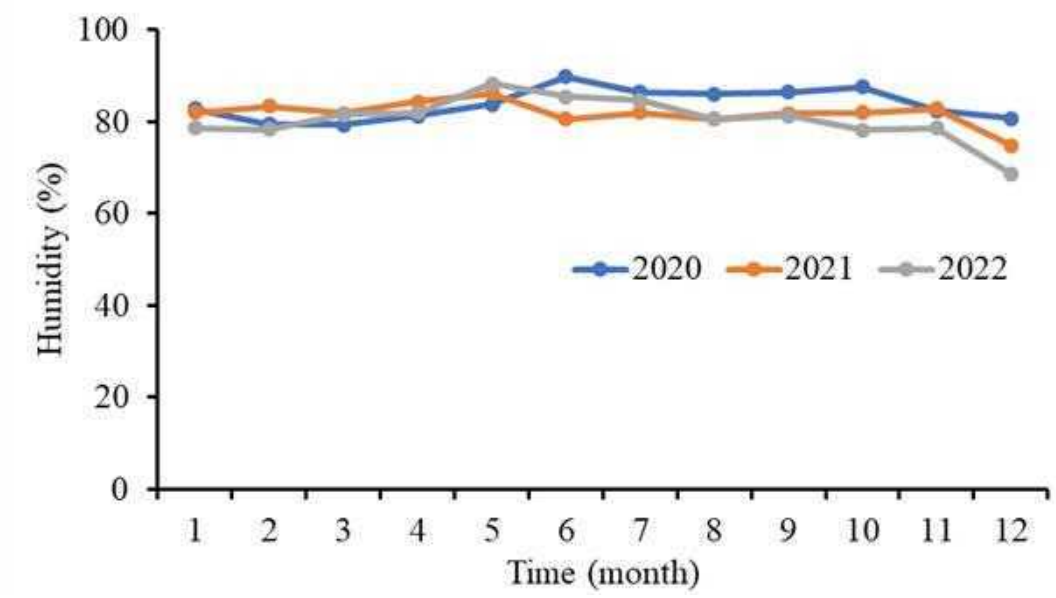

Figure 3.2: Average Humidity for the Years 2020-2022 at the Moc Hoa Weather Station, Long An.

3.1.3 Total Rainfall for the Years 2020, 2021, and 2022 at the Moc Hoa Weather Station, Long An

Figure 3.3 illustrates the total monthly rainfall for 2020 at the Moc Hoa Weather Station, Long An. Rainfall shows an increasing trend from April to early November, followed by a gradual decrease from mid-November to March. April and November mark the transitional months between the dry and rainy seasons. The month with the highest total rainfall is October, with a value of 551.8 mm. Conversely, March is the driest month, with minimal to no rain, recording a total rainfall value of 0 mm.

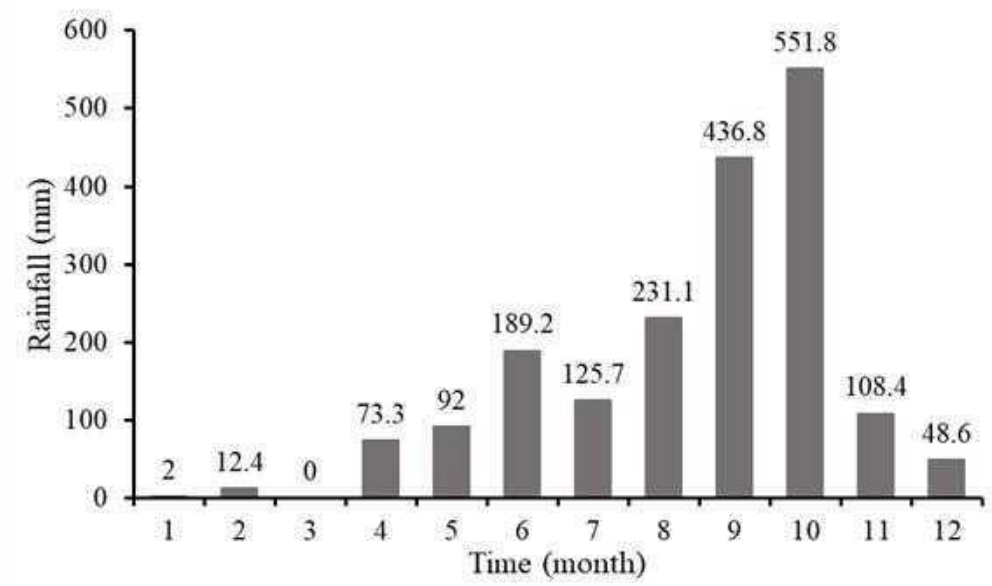

Figure 3.3: Total Monthly Precipitation for the Year 2020 at the Moc Hoa Weather Station, Long An.

Figure 3.4 illustrates the total monthly rainfall for 2021 at the Moc Hoa Weather Station, Long An. Rainfall shows an increasing trend from April to October, followed by a gradual decrease from November to March. Months with lower total rainfall are characterized by the absence of significant rainfall events exceeding 100 mm [32]. The month with the highest total rain is November, which is 245 mm. This increase in rainfall can be attributed to the influence of cold air masses, increased frequency of Northeast low-level winds, and the combination of upper-level easterly winds, resulting in heavy rainfall events. The three months with

no recorded rainfall are January, February, and March, each with a total monthly rainfall value of 0 mm.

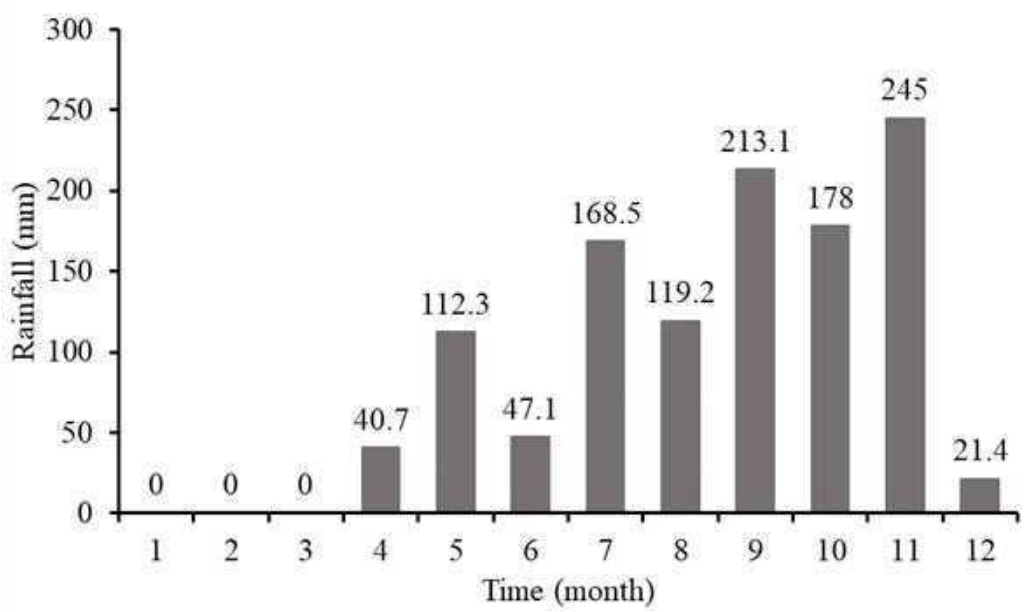

Figure 3.4: Total Monthly Precipitation for 2021 at the Moc Hoa Weather Station, Long An.

Figure 3.5 presents the total monthly rainfall for 2022 at the Moc Hoa Weather Station, Long An. Rainfall exhibits an increasing trend from February to May, followed by a decrease starting from June with irregular variations through December. The rainy season in 2022 extended later than the multi-year average. The immediate cause of this was the activity of the equatorial low-pressure belt, which was active between 4-7 degrees North, affecting the weather in the Southern region of Vietnam, resulting in sporadic rain and thunderstorms. On a larger scale, the influence of the La Niña phenomenon played a significant role. Statistics show that during La Niña years, the rainy season in Southern Vietnam tends to be longer than usual, and rainfall is also higher than the multi-year average [33]. The month with the highest total rainfall is May, with a value of 301.6 mm. January is the only month with no recorded rainfall, with a total monthly rainfall value of 0 mm.

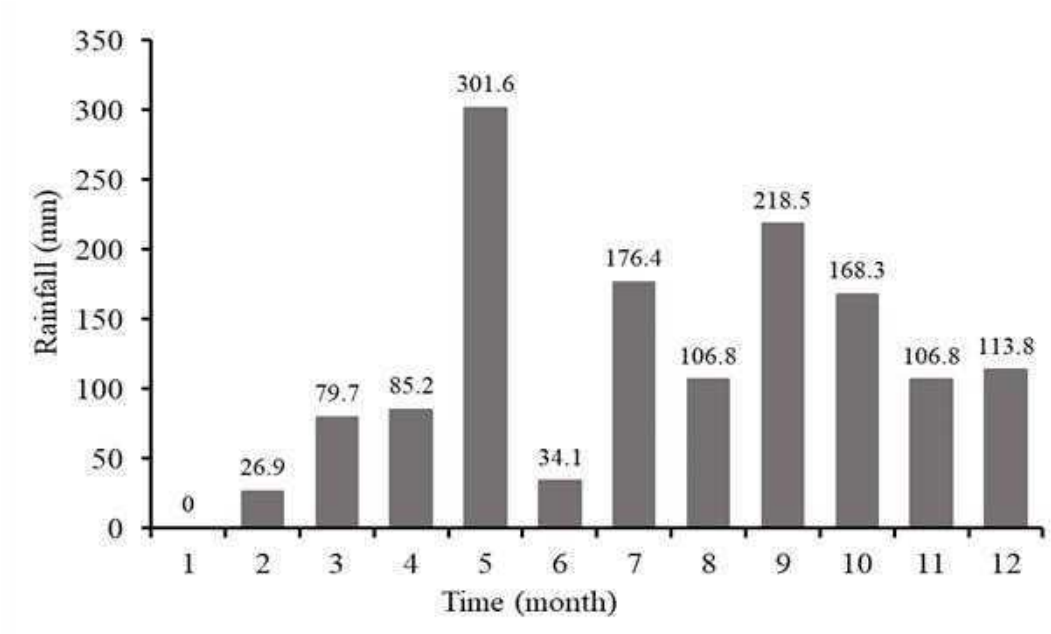

Figure 3.5: Total Monthly Precipitation for the Year 2022 at the Moc Hoa Weather Station, Long An.

3.1.4 Average Water Levels in 2020, 2021, and 2022 at the Moc Hoa Weather Station, Long An

Figure 3.6 illustrates the chart representing the average water levels in 2020 at the Moc Hoa Weather Station, Long An. The average water levels show an increasing trend from mid-May to nearly the end of October, followed by a gradual decrease. The highest average water level of the year was recorded on October 24, 2020, with a value of 0.142 meters. The lowest average water level of the year occurred on May 18, 2020, with a value of 0.06 meters.

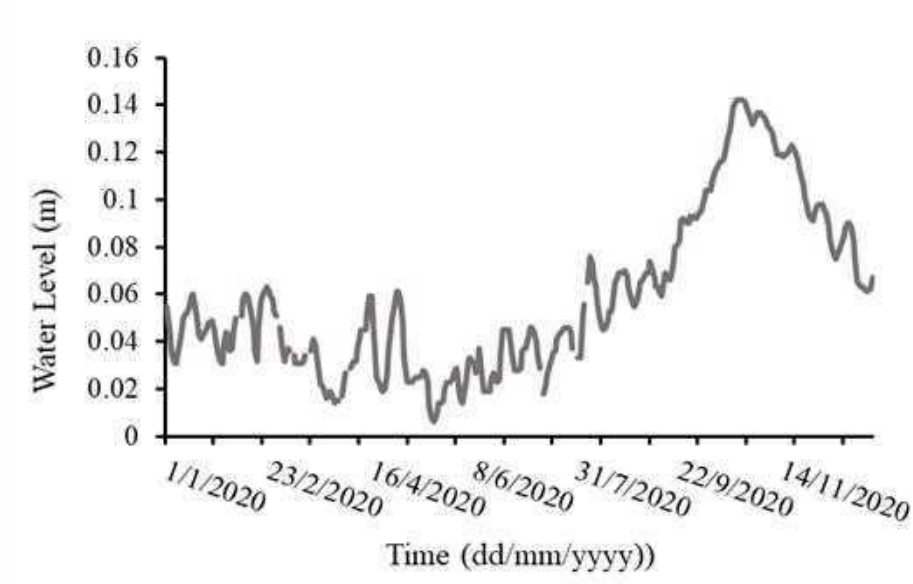

Figure 3.6: Average Water Levels for the Year 2020.

Figure 3.7 displays the chart representing the average water levels in 2021 at the Moc Hoa Weather Station, Long An. The average water levels increase from mid-May to mid-November, followed by a decrease until May. The highest average water level of the year was recorded on November 13, 2021, with a value of 0.129 meters. The lowest average water level of the year occurred on June 06, 2021, with a value of -0.03 meters.

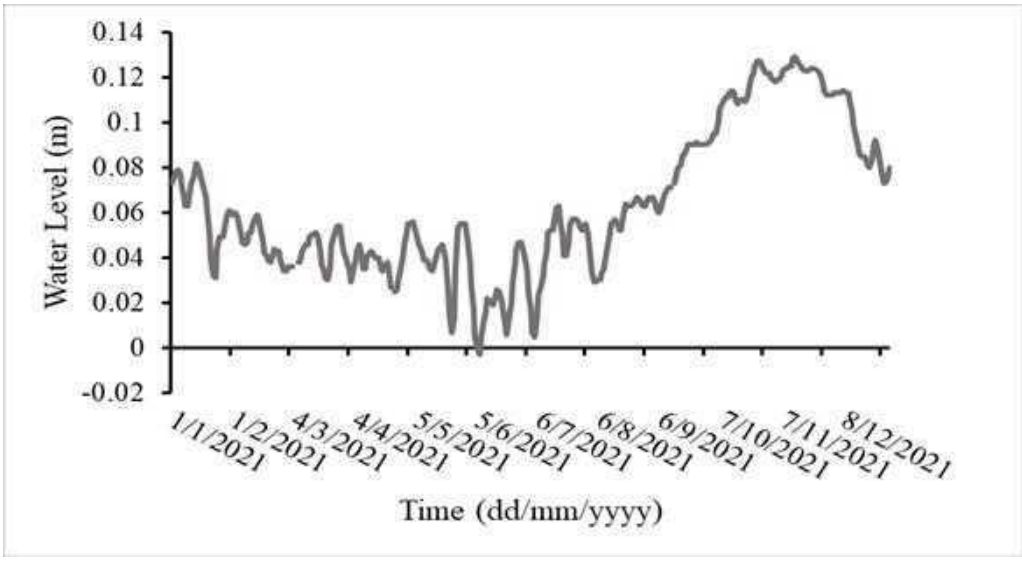

Figure 3.7: Average Water Levels for the Year 2021.

Figure 3.8 represents the chart depicting the average water levels in 2022 at the Moc Hoa Weather Station, Long An. The average water levels show an increasing trend from early July to the end of October, followed by a gradual decrease until May. The highest average water level of the year was recorded on October 30, 2022, with a value of 0.17 meters. The lowest average water level of the year occurred on June 06, 2021, with a value of -0.03 meters.

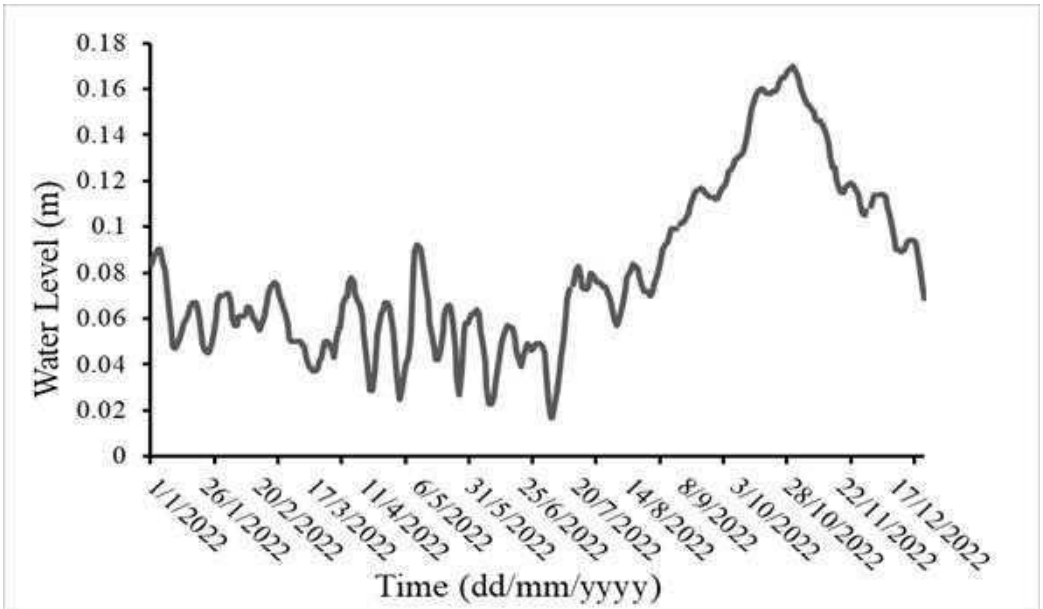

Figure 3.8: Average Water Levels for the Year 2022.

3.1.5 Average Surface Soil Temperature in 2020, 2021, and 2022

Figure 3.9 depicts the average surface soil temperature by month from 2020 to 2022. The chart illustrates the general trend of increasing average surface soil temperatures from January to around April, followed by a gradual decrease until December. Higher average surface soil temperatures typically occur in dry months when temperatures are high and there is little to no rainfall. During these months, the surface soil absorbs a significant amount of heat. The surface soil temperature tends to decrease from around April, which marks the onset of off-season rains, preparing for the rainy season. With the arrival of rain, the soil surface absorbs the rainwater, leading to a decrease in temperature.

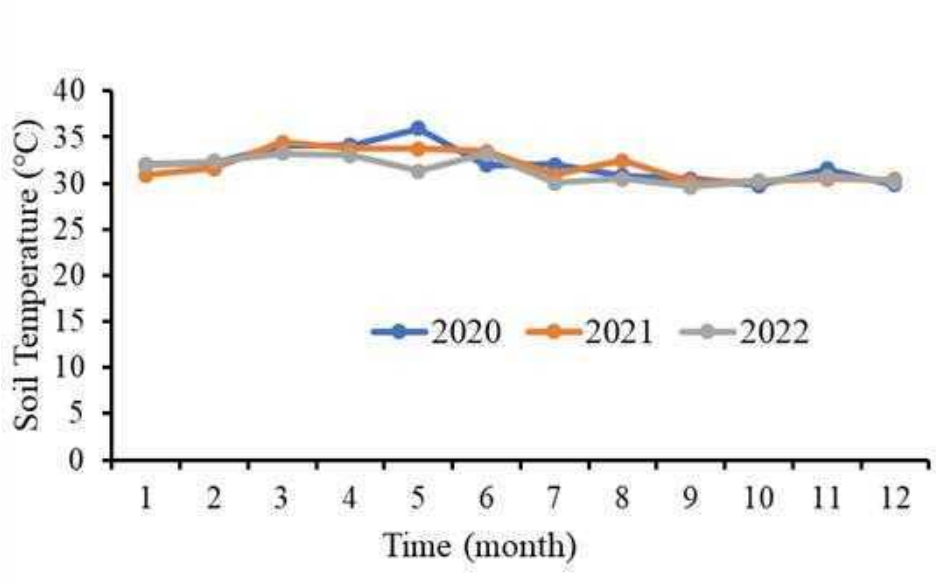

Figure 3.9: Average Soil Surface Temperature for the Years 2020-2021-2022 at the Moc Hoa Weather Station, Long An.

3.2 Correlation of Methane and Factors

3.2.1 Analysis of Methane Emission and Surface Soil Temperature

3.2.1.1 Analysis of Methane Emission and Surface Soil Temperature during the Winter Crop Season (01/07/2020-30/09/2020)

The variation in methane emissions and surface soil temperature during the winter crop season from 01/07/2020 to 30/09/2020 is presented in Figure 3.10. Based on the methane emission values in Figure 3.10, methane emissions exhibited relatively high frequencies in July 2020. The peak emission value during this period was 1.94 µmol/m^2/s recorded at 14:30 on 07/07/2020, with a surface soil temperature of 34.22°C. In August 2020, methane emission values were low, with some recorded values at 0 µmol/m2/s. In September 2020, the highest emission value of the winter crop season occurred at 5:00 on 06/09/2023, reaching 2.53 µmol/m2/s, with a surface soil temperature of 27.11°C.

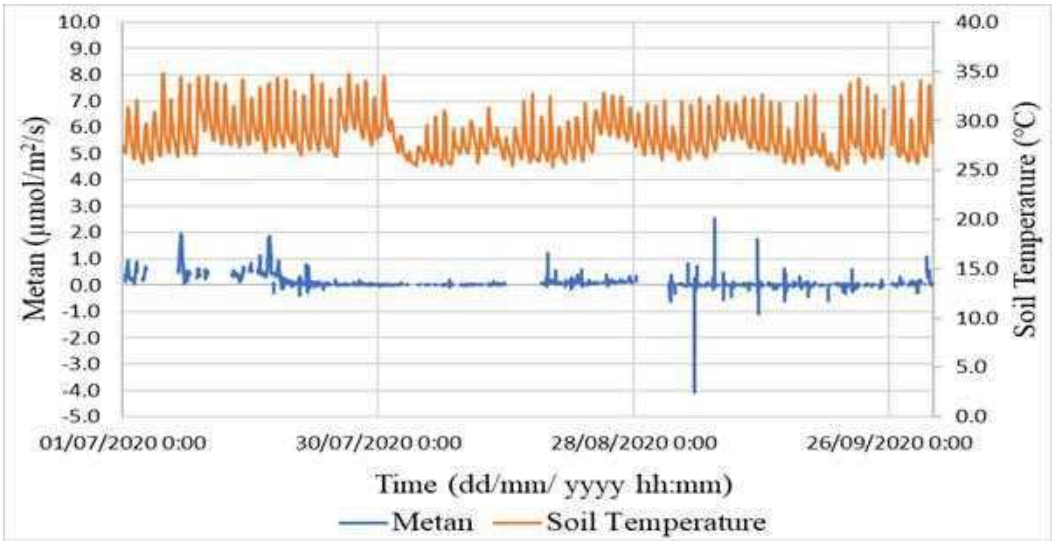

Figure 3.10: Methane Emission and Soil Surface Temperature Trends in the 2020 Winter Season from 01/07/2020 to 30/09/2020.

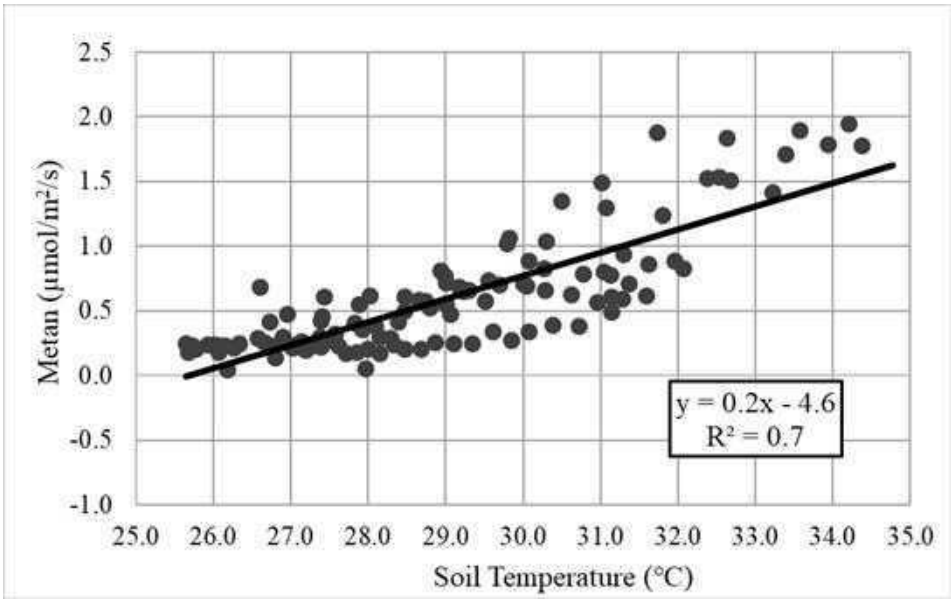

Figure 3.11: Correlation between Methane (CH4) and Soil Surface Temperature in the Initial 8 Days from 01/07/2020 to 07/07/2020.

Figure 3.11 illustrates the correlation between methane and surface soil temperature during the first 8 days after sowing, from 01/07/2020 to 07/07/2020. The correlation equation between methane and soil temperature is $y = 0.2x – 4.6$, with an R^2 value of 0.7. An R^2 value of 0.7 indicates a positive correlation between methane fluctuations and changes in soil temperature, suggesting a relatively strong

relationship between methane and soil temperature. As soil temperature increases, methane values tend to rise with a coefficient of 0.2.

3.2.1.2 Analysis of Methane Emission and Soil Surface Temperature During the Winter-Spring Crop Season (01/11/2020-28/02/2021)

The variation in methane emission and soil surface temperature during the winter-spring crop season from November 1, 2020, to February 28, 2021, is presented in Figure 3.12. Methane emissions were observed throughout the 2020 winter-spring crop season. Figure 3.12 indicates that there were two periods, at the beginning and end of the crop season, characterized by significant temperature fluctuations and high methane emissions. One month after transplanting, the peak methane emission occurred at 14:30 on July 7, 2020, with a value of 2.21 µmol/m²/s, and the soil surface temperature was 34.22°C. In December, methane emissions were concentrated in the late month, with lower emissions in the early and middle months of the season. The last two months of the 2020 winter-spring crop season saw dense methane emissions. The highest emission occurred at 7:30 on February 17, 2021, with a value of 4.23 µmol/m²/s, and the soil surface temperature was 23.19°C.

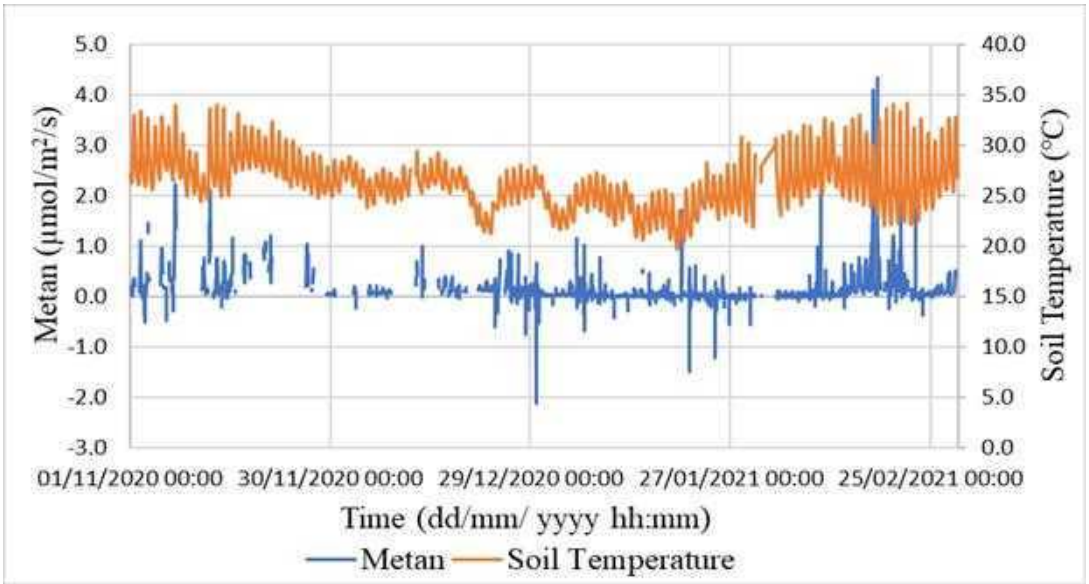

Figure 3.12: Methane Emission and Soil Surface Temperature Trends in the 2020-2021 Winter-Spring Season from 01/11/2020 to 28/02/2021.

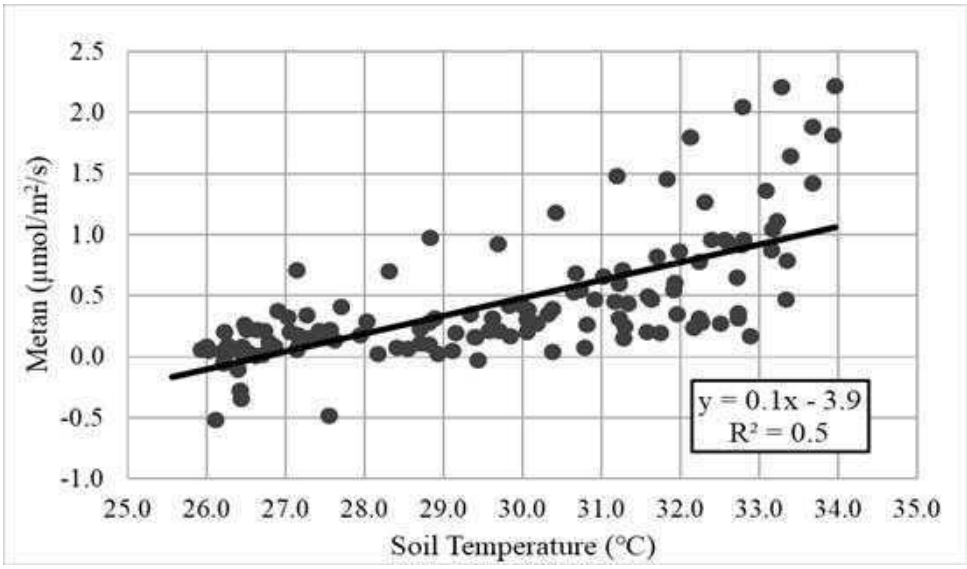

Figure 3.13: Correlation between Methane (CH4) and Soil Surface Temperature in the Initial 8 Days from 01/11/2020 to 07/11/2020.

Figure 3.13 presents the correlation between methane and soil surface temperature for the first 8 days after transplanting, from November 1, 2020, to November 7, 2020. The correlation equation between methane and soil surface temperature is $y = 0.1x – 3.9$, with an R^2 value of 0.5. The slope of the correlation line is 0.1, indicating that methane tends to increase with rising soil surface temperature. The R^2 value of 0.5 suggests a moderate positive correlation between methane and soil surface temperature.

3.2.1.3 Analysis of Methane Emission and Soil Surface Temperature During the Late Spring-Early Summer Crop Season (01/03/2021-30/06/2021)

The variation in methane gas emission and soil surface temperature during the late spring-early summer crop season from March 1, 2021, to June 30, 2021, is depicted in Figure 3.14. Based on the methane emission values shown in Figure 3.14, the methane emission rate is divided into three phases. Methane emissions were frequent from March 1, 2021, to April 20, 2021. The highest peak occurred at 6:00 on March 19, 2021, with a value of 11.93 µmol/m²/s and a soil surface temperature of 24.86°C. From April 21, 2021, to May 31, 2021, methane emission rates remained low, below 0.1 µmol/m²/s. In June, methane emissions were

relatively high, especially in the first half of the month. The highest peak in June was recorded at 15:00 on May 29, 2021, with a value of 6.07 µmol/m²/s and a soil surface temperature of 34.08°C.

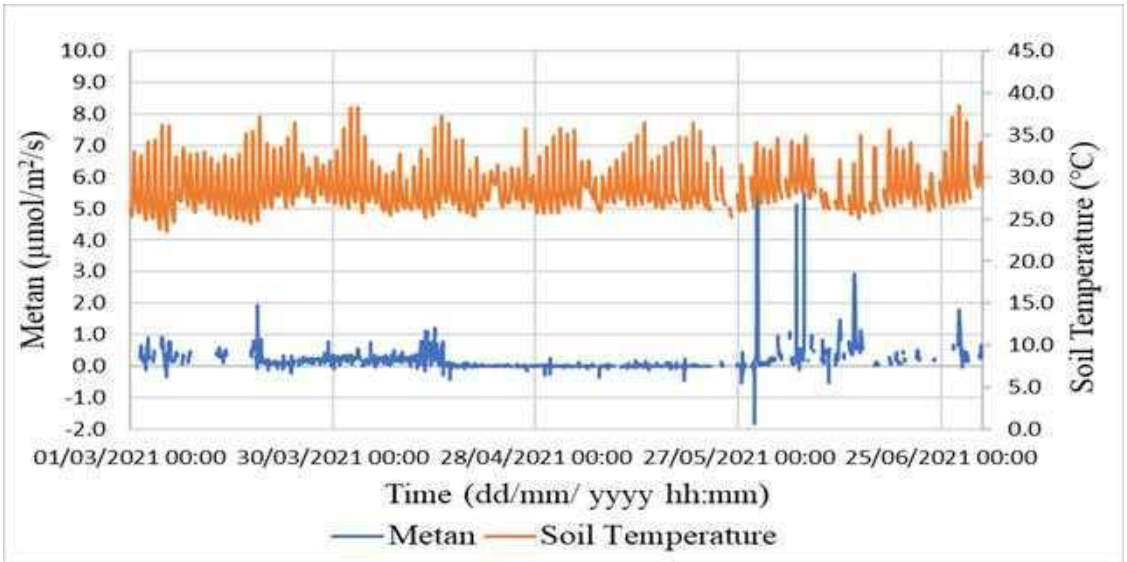

Figure 3.14: Methane Emission and Soil Surface Temperature Trends in the 2021 Summer-Fall Season from 01/03/2021 to 30/06/2021.

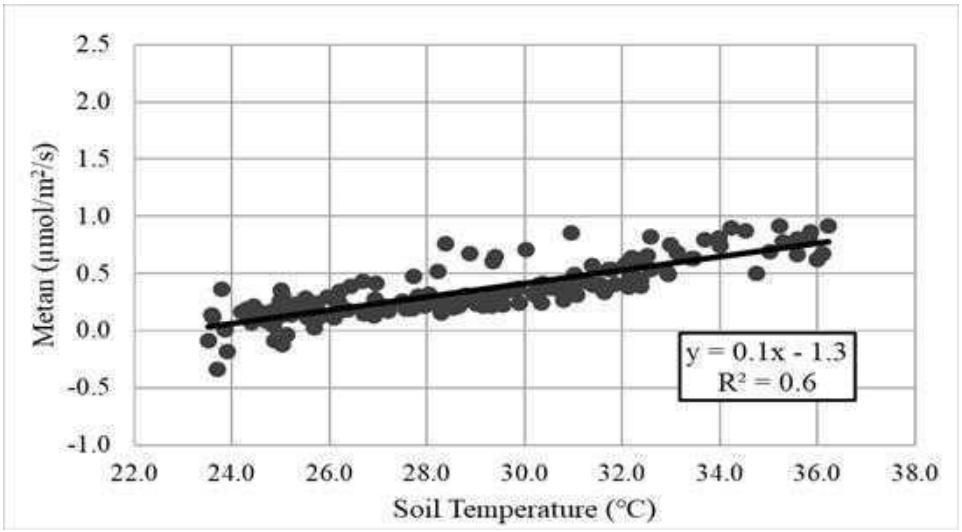

Figure 3.15: Correlation between Methane (CH4) and Soil Surface Temperature in the Initial 8 Days from 01/03/2021 to 07/03/2021.

Figure 3.15 illustrates the correlation between methane and soil surface temperature for the first 8 days after transplanting, from March 1, 2021, to March 7, 2021. The correlation equation between methane and soil surface temperature is y =

0.1x – 1.3, with an R^2 value of 0.6. The slope of the correlation line is 0.1, indicating that methane tends to increase with rising soil surface temperature. However, the variation in methane tends to be smaller than changes in soil surface temperature. The R^2 value of 0.6 indicates a relatively strong positive correlation between methane and soil surface temperature.

Overall, soil surface temperature exhibited high fluctuations for all three crop seasons from July 1, 2020, to June 30, 2021, with corresponding high methane emission rates. Most of the peaks in methane emissions occurred when soil surface temperature peaked. Based on the research across these three crop seasons, methane emissions showed a high correlation during the first 8 days after transplanting, while correlations in the remaining periods of all three crop seasons were lower (with R^2 values less than 0.5).

3.2.2 Methane Emission and Water Level Analysis

3.2.2.1 Methane Emission and Water Level Analysis During the Winter Crop Season (01/07/2020-30/09/2020)

The dynamics of methane emission and water levels during the winter crop season from July 1, 2020, to September 30, 2020, are presented in Figure 3.16. Water levels fluctuated between 0.61 m and 0.44 m in the first two days after transplanting. The peak methane emission occurred around 14:30 on July 7, 2020, with a value of 1.94 µmol/m²/s.

From 12:30 on July 16, 2020, to 15:30 on July 22, 2020, water levels significantly dropped from 0.59 m to 0.08 m. During this period, methane emissions were relatively high, with the highest peak at 16:00 on July 17, 2020, reaching a value of 1.84 µmol/m²/s. The water level at the time of high methane emission was 0.46 m.

Between days 21 to 45 after transplanting (July 22, 2020, to August 15, 2020), most methane emissions were very low, or at times, they were recorded as 0 µmol/m²/s. Based on the water level data (Figure 3.16), there was consistent water

in the fields during this period, with most water level values above 0.5 m and not falling below 0.3 m compared to the field surface.

From days 46 to 55 after transplanting (August 16, 2020, to August 24, 2020), water levels in the fields remained above 0.3 m. However, during this period, methane emissions increased, with the peak emission occurring at 1.21 µmol/m²/s on August 18, 2020, at 6:30, with a corresponding water level of 0.50 m.

When water levels in the fields dropped significantly for the second time (August 25, 2020, to September 1, 2020), indicating field drainage, methane emissions were observed. During the subsequent water pumping into the fields, there were two instances of relatively high methane emissions, with values of 2.53 µmol/m²/s at 5:00 on September 6, 2020, and 1.73 µmol/m²/s at 1:30 on September 11, 2020. The corresponding water levels were 0.54 m and 0.55 m, respectively. From September 17, 2020, until the end of the crop season, most methane emission values remained below 0.1 µmol/m²/s. During this period, water levels in the fields were above 0.3 m.

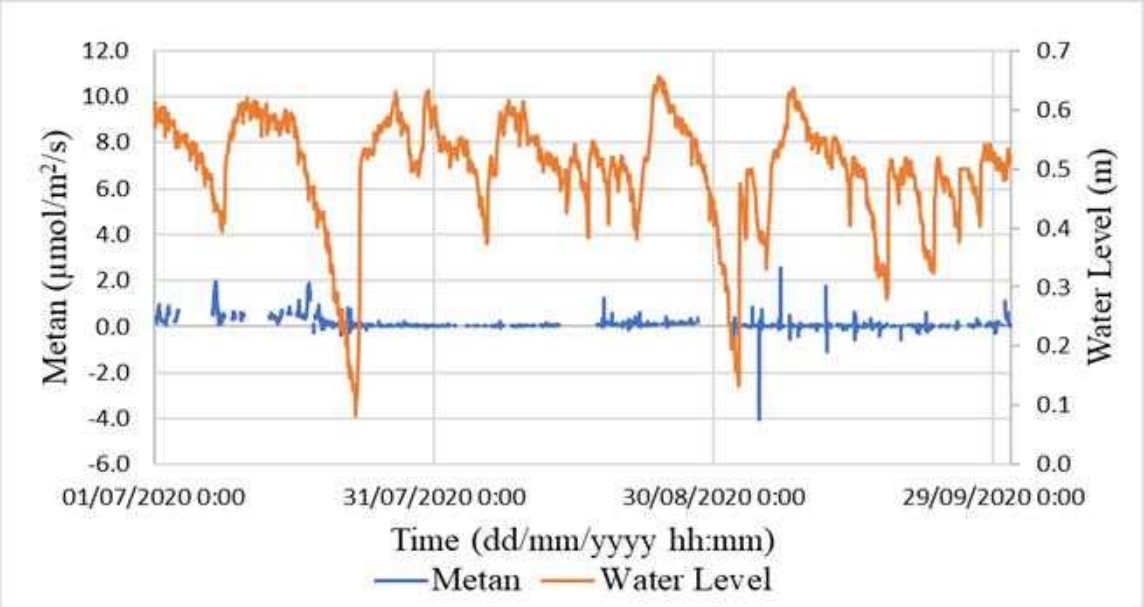

Figure 3.16: Methane Emission and Water Levels in the 2020 Winter Season from 01/07/2020 to 30/09/2020.

3.2.2.2 Methane Emission and Water Level Analysis During the Winter-Spring Crop Season (01/11/2020-28/02/2021)

Figure 3.17 illustrates the dynamics of methane emission and water levels during the winter-spring crop season from November 1, 2020, to February 28, 2021. In the first three weeks of the season (November 2, 2020, to November 21, 2020), methane emissions were relatively high, with most values exceeding 0.1 µmol/m²/s. During this period, water levels fluctuated between 0.33 m and 0.62 m, with a water level difference of 0.29 m due to water drainage. The two highest methane emission values during this time were recorded on November 7, 2020, at 14:30, with a value of 2.21 µmol/m²/s and a water level of 0.59 m. The second-highest methane emission value in the first three weeks was 2.10 µmol/m²/s at 15:00 on November 12, 2020, with a water level of 0.52 m.

Based on the methane emission values in Figure 3.17, approximately 22 to 50 days after transplanting (November 22, 2020, to December 20, 2020), methane emissions were low, and water levels in the fields were above 0.3 m compared to the field surface.

From approximately 51 to 80 days after transplanting (December 21, 2020, to January 19, 2021), methane emissions increased, with high emission peaks occurring as water levels in the fields decreased. The highest methane emission value during this period was 1.71 µmol/m²/s. This peak methane emission occurred at 22:00 on January 19, 2021, with a water level of 0.36 m.

Approximately 81 to 97 days after transplanting (January 20, 2021, to February 7, 2021), as water levels decreased significantly, the amount of methane retained in the soil after substantial emissions into the environment began to decline gradually. When water levels in the fields increased again, methane emissions were very low, with some instances of methane emissions measuring 0 µmol/m²/s. From February 8, 2021, until harvest, methane emissions increased once more as water levels in the fields decreased. The highest methane emission value recorded during this period was 4.23 µmol/m²/s at 07:30 on February 17, 2021, with a water level of 0.55 m.

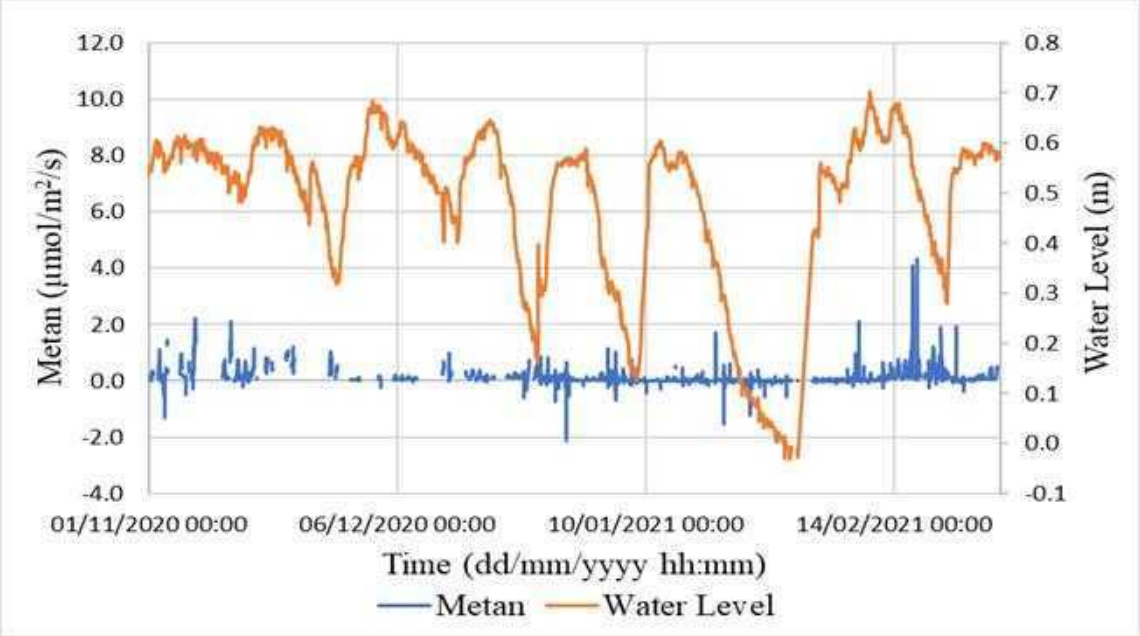

Figure 3.17: Methane emission and water levels in the 2020-2021 winter-spring season from 01/11/2020 to 28/02/2021.

3.2.2.3 Methane Emission and Water Level Analysis During the Summer-Autumn Crop Season (01/03/2021-30/06/2021)

Figure 3.18 presents the variations in methane emission and water levels during the summer-autumn crop season from March 1, 2021, to June 30, 2021. In the first two weeks of the cropping season (March 1, 2021, to April 13, 2021), most methane emission values were greater than 0.1 µmol/m²/s. During this period, water levels fluctuated between 0.27 m and 0.63 m, with the highest methane emission value recorded at 1.93 µmol/m²/s at 6:00 on March 19, 2021, with a water level of 0.39 m.

From 15 to 55 days after transplanting (March 15, 2021, to May 25, 2021), methane emissions into the environment were low, with values measured at the station consistently below 0.1 µmol/m²/s. During this time, water levels showed relatively large fluctuations, ranging from 0.03 m to 0.63 m, with a difference of approximately 0.59 m.

From approximately 55 days after transplanting to harvest (May 26, 2021, to June 30, 2021), methane emission values increased significantly. The highest

methane emission value recorded was 6.07 µmol/m²/s at 15:00 on May 29, 2021, with a water level of 0.55 m. Another notable methane emission value was 4.82 µmol/m²/s at 12:00 on June 03, 2021, with a water level of 0.57 m. Methane emission values of 5.48 µmol/m²/s and a water level of 0.62 m were recorded at 10:00 on June 05, 2021.

The methane emission and water level dynamics were analyzed across three rice cropping seasons: winter-spring, summer-autumn, and summer-season from July 1, 2020, to June 30, 2021. Across these three rice cropping seasons, there was a general trend of increasing methane emissions into the atmosphere coinciding with the onset of decreasing water levels or during drainage periods. There were typically six main drainage events in a single rice cropping season. Methane is generated through anaerobic decay, and when rice fields have high water levels, methane gas is retained in the soil, making it difficult to release into the environment.

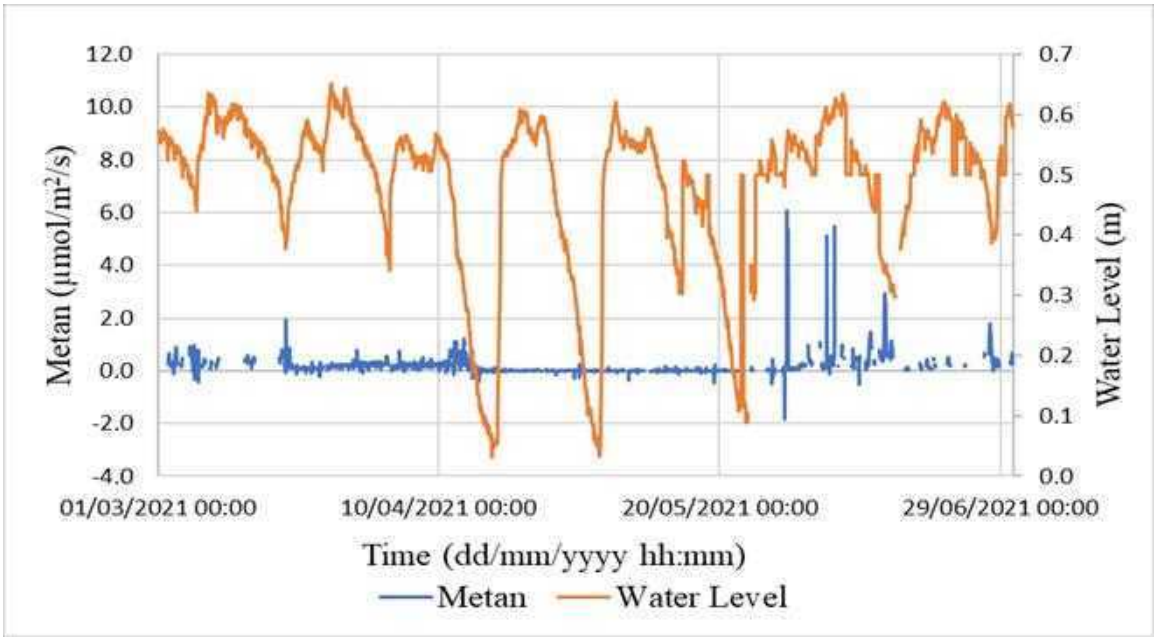

Figure 3.18: Methane Emission and Water Levels in the 2021 Summer-Fall Season from 01/03/2021 to 30/06/2021.

During the initial stage, from seeding to 10 days after seeding, elevated methane emissions into the atmosphere are primarily attributed to the accumulation of methane gas beneath the soil from previous rice crops. This buildup of methane is caused by the decomposition of rice straw from the last season's crop. The rice crop residues in the field decompose more rapidly, typically within 2-3 weeks after harvest. Approximately two weeks after seeding, methane emissions continue to be high. It is because rice plants begin to tiller during this stage, and the growth of branches and roots contributes to methane formation (as discussed in Chapter I - Section 1.2.3). As the rice crop matures and the water level is consistently maintained in the fields during the vegetative growth stage, this becomes an optimal environment for methane formation. After methane forms, it continues to be trapped in the soil by water. Therefore, when the rice plants reach the flowering stage and the water is drained, a period of continued high methane emissions is marked.

CONCLUSIONS

Through the completion of this thesis project, this research has provided a clear insight into the influence of soil temperature and water level on methane emissions in rice fields. The results of this study contribute to more effective research and management of methane emissions in the agricultural sector, particularly in flooded rice cultivation. Consequently, this contributes to environmental protection and reducing greenhouse gas emissions into the atmosphere, mitigating the impact of global climate change.

During the thesis research process, meteorological data (from 2021 to 2022) and greenhouse gas data (from 2020 to 2021) were collected, analyzed, and assessed. From this data, an analysis was conducted, focusing on the correlation between the variations of meteorological factors, particularly the analysis of methane emissions concerning soil temperature and water level.

Different growth stages of rice crops exhibited varying methane emissions. However, the highest emissions occurred during the rice tillering or field drying period, with lower emissions at other times. The research indicates that soil temperature significantly influences methane emissions in rice fields. The results show that methane emissions positively correlate with soil temperature and exhibit a direct relationship (with R-squared values ranging from 0.5 to 0.7) with soil temperature measured in the first 8 days after seeding.

Additionally, the water level in rice fields also has a substantial impact on methane emissions. Based on the research results from three rice cropping seasons spanning from July 1, 2020, to June 30, 2021, the summer-season crop in 2020 exhibited the highest methane emission rate among the three cropping seasons. Methane emissions peaked when the water level began to decrease, especially during the initial phase of the drainage period. The results consistently showed increased methane emissions after drainage in all three cropping seasons, although no correlation with water level was identified.

These findings show that managing soil temperature and water level in rice fields is crucial for reducing methane emissions. Maintaining appropriate water levels and controlling soil temperature can significantly minimise methane emissions in agriculture, particularly in rice production.

Recommendation: Methane emissions in rice fields depend on various factors. However, due to the limited timeframe of this thesis, the analysis focused only on two factors influencing methane emissions in rice fields: soil surface temperature and water level. Therefore, it is recommended to conduct further analysis and evaluation of other influencing factors, such as rice growth stages, Eh, DO, pH in the soil, organic compounds, and other relevant factors. Additionally, this thesis only covered three cropping seasons from July 2020 to June 2021; hence, further research is needed in different timeframes to provide a more comprehensive assessment of methane emissions in rice fields.

LIST OF REFERENCES

[1].Mausami Desai, Vincent Camobreco, "EPA (2023) Inventory of U.S. Greenhouse Gas Emissions and Sinks: 1990-2021," in *U.S. Environmental Protection Agency, EPA 430-R-23-002*, 2023

[2].Clare Nullis, "Carbon dioxide levels continue at record levels, despite COVID-19 lockdown," in *The World Meteorological Organization*, 23 November 2020.

[3]. A. i. t. o. scientists, "Global methane assessment released," in *World Meteorogical Oganization*, 7 May 2021.

[4]. World Meteorological Organization Atmospheric Environment Research Division, "The State of Greenhouse Gases in the Atmosphere," in *WMO GREENHOUSE GAS*, No. 15, 25 November 2019.

[5]. Tiy Chung, "Global Assessment: Urgent steps must be taken to reduce methane emissions this decade," in *Climate and Clean Air Coalition*, 06 May 2021.

[6]. D. Shindell, "Health and Food Security: Benefits from Climate Change Mitigation," in *NASA's Goddard Institute for Space Studies*, New York, No. 1 & 2 Vol. XLIX, June 2012.

[7]. https://www.un.org/en/climatechange/what-is-climate-change (Định nghĩa Biến đổi khí hậu). [Truy cập 15/02/2023].

[8]. Tổng cục thống kê, “Thách thức phát triển nông nghiệp những tháng đầu năm”, 11/04/2023. [Trực tuyến]. Địa chỉ: https://www.gso.gov.vn/du-lieu-va-so-lieu-thong-ke/2023/04/thach-thuc-phat-trien-nong-nghiep-nhung-thang-dau-nam/. [Truy cập 27/02/2023].

[9]. Tổng cục thống kê, “Thông cáo báo chí về tình hình kinh tế – xã hội quý I năm 2020”, 27/03/2020. [Trực tuyến]. Địa chỉ: https://www.gso.gov.vn/du-lieu-va-so-lieu-thong-ke/2020/03/thong-cao-bao-chi-ve-tinh-hinh-kinh-te-xa-hoi-quy-i-nam-2020/. [Truy cập 10/03/2023]

[10]. Nông nghiệp Việt Nam, “Sản xuất lúa ở Việt Nam phát thải khí nhà kính cao hơn nước khác”, 06/11/2022. [Trực tuyến]. Địa chỉ:

https://nongnghiep.vn/san-xuat-lua-o-viet-nam-phat-thai-khi-nha-kinh-cao-hon-nuoc-khac-d337169.html. [Truy cập 07/04/2023]

[11]. Bộ Tài nguyên và Môi trường, " Thực trạng phát thải khí nhà kính (KNK) ở Việt Nam", 19/05/2020. [Trực tuyến].

Địa chỉ: https://monre.gov.vn/Pages/thuc-trang-phat-thai-khi-nha-kinh-(knk)-o-viet-nam.aspx. [Truy cập 11/04/2023]

[12]. Tổng cục thống kê, "Thực hiện cam kết COP26 từ xây dựng một nền nông nghiệp phát triển bền vững", 03/08/2022.

[Trực tuyến]. Địa chỉ: https://www.gso.gov.vn/tin-tuc-khac/2022/08/thuc-hien-cam-ket-cop26-tu-xay-dung-mot-nen-nong-nghiep-phat-trien-ben-vung/. [Truy cập: 11/04/2023]

[13]. Minghua Zhou, Xiaoguo Wang, Yanqiang Wang, Bo Zhu, "A three-year experiment of annual methane and nitrous oxide emissions from the subtropical permanently flooded rice paddy fields of China: Emission factor, temperature sensitivity and fertilizer nitrogen effect", *Agricultural and Forest Meteorology*, pp. 299-307, 2018.

[14]. Agriculture IPCC Guidelines for National Green house Gas Inventories, "Methane Emissions from Rice Cultivation", *Flooded Rice Fileds*, vol. 250-255, p. chapter 4,1996.

[15]. Khánh Ly, "Canh tác lúa là nguồn phát thải khí mê tan lớn nhất", 25/03/2022, [Trực tuyến]. Địa chỉ: https://baotainguyenmoitruong.vn/canh-tac-lua-la-nguon-phat-thai-khi-me-tan-lon-nhat-338066.html. [Truy cập 25/04/2023]

[16]. Đồng Phú Hảo, Nguyễn Thanh Bình, Lê Hoàng Anh, "Phát thải khí metan (CH_4) trong sản xuất lúa nước tại Việt Nam: hiện trạng và giải pháp", Tạp chí khoa học ĐHQGHN: Khoa học Trái đất và Môi trường, Tập 39, Số 1, tr. 28-41, 2023

[17].Nguyễn Kim Thu, Trần Văn Dũng, Cao Văn Phụng, Hồ Nguyễn Hoàng Phúc, Huỳnh Ngọc Huy, "Nghiên cứu phát thải metan trên đất lúa trong mô hình thâm canh và luân canh", Tạp chí Khoa học Công nghệ Nông nghiệp Việt Nam, số 3, trang 88, 2018.

[18]. Cổng thông tin điện tử Bộ nông nghiệp và phát triển nông thôn, "Kỹ thuật tưới lúa "Ướt khô xen kẽ" của IRRI", 22/03/2011. [trực tuyến]. Địa chỉ https://www.mard.gov.vn/Pages/ky-thuat-tuoi-lua--uot-kho-xen-ke--cua-irri-7292.aspx. [Truy cập 02/05/2023].

[19]. Nguyễn Ngọc Đệ, Giáo trình cây lúa, Nhà xuất bản Đại học Quốc gia TP.Hồ Chí Minh, 2008.

[20]. Hà Lê, "Phương pháp canh tác lúa thân thiện môi trường và kỹ thuật canh tác lúa cải tiến SRI". [Trực tuyến]. Địa chỉ:
https://hoinongdan.thanhhoa.gov.vn/portal/Pages/2022-9-6/Phuong-phap-canh-tac-lua-than-thien-moi-truong-va-npfccr.aspx. [Truy cập 02/05/2023].

[21]. Sở văn hóa, thể thao và du lịch Long An, "Tài nguyên du lịch tự nhiên", 19/09/2022. [Trực tuyến]. Địa chỉ: https://www.longan.gov.vn/Pages/GioiThieuChiTiet.aspx?ID=71&CategoryId=Th%u01b0%u01a1ng+m%u1ea1i+-+Du+l%u1ecbch&InitialTabId=Ribbon.Read. [Truy cập: 06/03/2023].

[22]. Trung tâm Phát triển quỹ đất và dịch vụ tài nguyên, "Báo cáo hiện trạng môi trường tỉnh Long An giai đoạn 2016 - 2020," *Sở Tài nguyên và Môi trường tỉnh Long An*, năm 2020.

[23].Cổng thông tin điện tử tỉnh Long An "Tài nguyên nước mặn, nước ngầm", 28/11/2014. [Trực tuyến]. Địa chỉ:
https://www.longan.gov.vn/Pages/GioiThieuChiTiet.aspx?ID=26&InitialTabId=Ribbon.Read. [Truy cập 07/03/2023]

[24].Cổng thông tin điện tử tỉnh Long An, "Tình hình lũ lụt", 05/11/2008. [Trực tuyến]. Địa chỉ: https://www.longan.gov.vn/Pages/GioiThieuChiTiet.aspx?ID=11&CategoryId=%u0110i%u1ec1u+ki%u1ec7n+t%u1ef1+nhi%u00ean%2c+l%u1ecbch+s%u1eed&InitialTabId=Ribbon.Read&PageIndex=1. [Truy cập 07/03/2023].

[25]. Cổng thông tin điện tử tỉnh Long An, "Tình hình chua phèn", 05/11/2008. [Trực tuyến]. Địa chỉ: https://www.longan.gov.vn/Pages/GioiThieuChiTiet.aspx?ID=10&CategoryId

=%u0110i%u1ec1u+ki%u1ec7n+t%u1ef1+nhi%u00ean%2c+l%u1ecbch+s%u1eed&InitialTabId=Ribbon.Read&PageIndex=1. [Truy cập 09/03/2023].

[26]. Cổng thông tin điện tử tỉnh Cà Mau, "Quy định về kỳ quan trắc, trình tự quan trắc về quan trắc khí tượng", 24/11/2022. [Trực tuyến]. Địa chỉ: https://www.camau.gov.vn/wps/portal/?1dmy&page=trangchitiet&urile=wcm%3Apath%3A/camaulibrary/camauofsite/trangchu/tuytruyenphapluat/thongtinvequydinhphapluat/874dp2022. [Truy cập 07/05/2023].

[27]. Cổng thông tin điện tử tỉnh Long An, "Công bố kết quả thực hiện dự án Điều tra, đánh giá chất lượng đất, tiềm năng đất đai và dự án Điều tra, đánh giá thoái hóa đất kỳ đầu trên địa bàn tỉnh", 08/03/2023. [Trực tuyến]. Địa chỉ: https://www.longan.gov.vn/Lists/CongKhai/DispForm.aspx?ID=139&CategoryId=Qu%u1ea3n+l%u00fd+v%u00e0+s%u1eed+d%u1ee5ng+%u0111%u1ea5t&InitialTabId=Ribbon.Read. [Truy cập 18/04/2023].

[28]. Lê Văn Hảo, "*Phương pháp nghiên cứu khoa học*", Trường Đại học Nha Trang, 2015.

[29]. Thông tin máy đo phát thải metan. [Trực tuyến]. Địa chỉ: https://www.licor.com/env/products/eddy_covariance/LI-7700.html. [Truy cập 02/06/2023].

[30]. Thông tin máy đo nhiệt độ đất bề mặt. [Trực tuyến]. Địa chỉ: https://bff-tech.com/cam-bien-nhiet-do-pt100/#Uu_diem_cua_dong_cam_bien_Pt100_la_giLMP. [Truy cập 05/06/2023].

[31]. Thông tin máy đo mực nước liên tục. [Trực tuyến]. Địa chỉ: https://www.bdsensors.de/fileadmin/user_upload/Download/Datenblaetter_datasheets/DB_LMP307i_E.pdf. [Truy cập 05/06/2023].

[32]. "Mùa mưa 2021 tại miền Nam kéo dài, dự báo hạn mặn đến trễ ít khắc nghiệt", 21/11/2021. [Trực tuyến]. Địa chỉ: https://baolongan.vn/mua-mua-2021-tai-mien-nam-keo-dai-du-bao-han-man-den-tre-it-khac-nghiet-a125929.html. [Truy cập 28/05/2023].

[33]. Trần Hồng Thái, Đặc điểm khí tượng thủy văn Việt Nam năm 2022, Nhà xuất bản thanh niên Hà Nội, 2023.

UNIVERSITY OF SCIENCE,
VIETNAM NATIONAL UNIVERSITY HO CHI MINH CITY
Physics & Engineering Physics Faculty
Department of Oceanology, Meteorology and Hydrology

SOCIALIST REPUBLIC OF VIETNAM
Independence – Freedom – Happiness
--o0o---

GRADUATION THESIS COURSE REVIEWS

Student: Vo Huynh Huong

Title: **Analysis of the effects of soil surface temperature and water level on methane emissions in the rice field**

Field of Oceanology, major: Oceanology - Meteorology - Hydrology

Reviewer: (Full name, Academic title, Degree) Dr. Bui Thi Ngoc Oanh

Working agency: University of Science, VNU-HCM

Role:

☐ Supervisor ☒ Reviewer

Comments and evaluation of graduation thesis:

1. **Scientific significance**:

Methane is one of the greenhouse gases and its presence in the atmosphere affects temperature and climate. Of which, agriculture contributes nearly 40% of the total fields. Therefore, methane emissions in rice fields contribute significantly to climate change impacts. Some previous studies have shown that fields that are flooded or dry or alternately wet and dry will affect the rate of methane development in the field.

2. **Content**:

Introduction: pose the problem and state the problem, goal, and method to be chosen

Chapter 1: Research overview

Chapter 2: Research areas and methods were carried out

The research was conducted in Long An with meteorological data sets at Moc Hoa station and methane data of the Center for Greenhouse Gases and Climate Change.

Chapter 3: analysis results:

a. Part 1: Analyze meteorological data of Moc Hoa station for factors: rain, humidity, air temperature, soil temperature.

b. Part 2: Analyze the influence of soil temperature and water level on CH4 emission rate

c. Part 3: Draw conclusions for each factor.

Conclusion and recommendations: Summarize the problem and make recommendations.

3. **Form**:

Present images and tables clearly and beautifully, in accordance with presentation regulations.

4. **Conclusion:**

The thesis meets the requirements of a university graduation thesis.

We respectfully request the thesis grading committee to approve the thesis with points: 9.75/10

City. Ho Chi Minh, July 24th 2023

REVIEWERS

Bui Thi Ngoc Oanh

UNIVERSITY OF SCIENCE,
VIETNAM NATIONAL UNIVERSITY HO CHI MINH CITY
Physics & Engineering Physics Faculty
Department of Oceanology, Meteorology and Hydrology

SOCIALIST REPUBLIC OF VIETNAM
Independence – Freedom – Happiness
--o0o---

GRADUATION THESIS COURSE REVIEWS

Student: Vo Huynh Huong

Title: **Analysis of the effects of soil surface temperature and water level on methane emissions in the rice field**

Field of Oceanology, major: Oceanology - Meteorology - Hydrology

Reviewer: (Full name, Academic title, Degree) Asso.Prof., PhD. Dang Truong An

Working agency: University of Science, VNU-HCM

Role:

☐ Supervisor ☒ Reviewer

Comments and evaluation of graduation thesis:

1. **Scientific significance**:

Greenhouse gas emissions from agricultural production activities are receiving attention from humanity in the context of increasing population and the increasingly serious effects of climate change.

2. **Content**:

The research topic analyzing the influence of soil temperature and water level on methane emissions in rice fields is built with a structure of three chapters:

- Chapter 1: The author presents an overview of the research area which is a wetland in Lang Sen area, Long An province.
- Chapter 2: The author introduces an overview of the research area and research implementation approaches.
- Chapter 3: The author presents research results, evaluation and comments.

3. **Form**:

The thesis has a clear, clean presentation. Satisfy the requirements of a university graduation thesis.

4. **Conclusion: Does the thesis meet the requirements of a university graduation thesis?**

The thesis meets the requirements of a university graduation thesis.

We respectfully request the thesis grading committee to approve the thesis with points: 9.5/10

City. Ho Chi Minh, July 24th 2023

REVIEWERS

Dang Truong An

Vietnam National University-Ho Chi Minh City
University of Science
Faculty of Physics- Physics engineering
Department of Oceanography, Meteorology and Hydrology

Thesis

Topic:

DETERMINING CROP IRRIGATION WATER REQUIREMENTS FOR RICE IN THE PLAIN OF REEDS

Student: **NGUYEN THI CAM MI**
Supervisor: Dr. DANG TRUNG AN

HO CHI MINH, JULY/2018

LỜI CẢM ƠN

To complete this graduation thesis, I have received a lot of help, care, and dedicated guidance as well as encouragement from teachers, family, and friends.

I would like to express my sincere gratitude and deep appreciation to Dang Truong An, who has enthusiastically guided, supported, and imparted valuable knowledge and experience to me throughout the process of conducting this graduation thesis.

I sincerely thank the teachers of Department of Oceanography, Meteorology, and Hydrology, Faculty of Physics - Engineering Physics, University of Science for their dedicated teaching, which has provided me with valuable knowledge and skills. It has laid a solid foundation for me to successfully complete the graduation thesis and apply it in practice in the future.

I am very grateful to my family, especially my parents for always being by my side, encouraging and supporting me during this time.

And I would like to thank the entire Class 14HDH for accompanying me throughout the 4 years of university, with sincere and warm feelings, you have helped me overcome difficult times.

I sincerely thank everyone!

Finally, I would like to wish all the teachers good health and success in their research and teaching careers. I wish all families and friends good health, happiness, and success.

ABSTRACT

DETERMINING CROP IRRIGATION WATER REQUIREMENTS FOR RICE IN THE PLAIN OF REEDS

This study focuses on the AquaCrop model to calculate water requirements for different seasons in the Plain of Reeds. It also determines the reference crop evapotranspiration and crop evapotranspiration under standard conditions.

The findings indicate that the annual total reference crop evapotranspiration is estimated to be 1600 mm. The highest ETo value of 169.9 mm was observed in March in Cao Lanh and My Tho, while the lowest value of 123.0 mm was observed in November in Cao Lanh, Moc Hoa, and My Tho. Crop evapotranspiration under standard conditions peaked during the middle stage of the Fall-winter season in Moc Hoa, reaching 458.3 mm. Conversely, the lowest value of 20.0-21.0 mm was recorded during the Winter-spring season at all three stations.

CONTENTS

DANH MỤC HÌNH

DANH MỤC BẢNG

ABBREVIATIONS

B	Above-ground biomass production
CV	Climate variability
CC	Green canopy cover
CN	Curve Number
CR	Capillary rise
DP	Deep percolation
Dr	Root zone depletion
MD	Mekong Delta
PR	Plain of Reeds
E	Soil evaporation
ET	Evapotranspiration
ETc	Crop Evapotranspiration under the standard conditions
ETo	Reference evapotranspiration
FAO	The food and agriculture organization of the world
FC	Field Capacity
HI	Harvest Index
HI_0	Reference Harvest Index
Kc	Crop coefficient
Ksat	Saturated hydraulic conductivity
UN	United Nations
Rainf	Rainfall effective
PWP	Permanent wilting point
RO	Runoff

SAT	Volumetric water content at saturation
WP	Biomass water productivity
WP^*	Normalized biomass water productivity
WUE	Water use efficiency
Wr	Stored soil water
Y	Crop yield

INTRODUCTION

Reason for choosing research topic

Plain of Reeds (PR) is a floodplain area in the Mekong Delta (MD) with a natural area of about 697,000 hectares [23], spanning part of the land of 3 provinces: Tien Giang, Long An, and Dong Thap. It is a region with great potential in agricultural production. PR has about 350,000 hectares of cultivated land, with rice as the main crop, producing an annual output of over 3.0 million tons, contributing about 20% to the rice export output in the MD. In the context of climate change in recent years, PR has been affected, especially in terms of disadvantages for agricultural production in general and rice production in particular. In addition to extreme weather phenomena such as heatwaves, droughts, heavy rains, and floods, other unfavorable factors such as saltwater intrusion, alkalinity, water scarcity, etc. have directly affected and caused difficulties for production activities, as well as yield and output. Changes in rainfall patterns with increased rainfall in the rainy season but decreased in the dry season are the cause of more frequent and unpredictable floods and annual droughts, leading to increased saltwater intrusion [3]. Overall, the MD, including PR, is affected by saltwater intrusion, which leads to water shortages for crop production and increasingly threatens the livelihoods of farmers. Therefore, accurately estimating the water demand for crops is becoming more and more important (Surendran et al., 2014), especially in the research area heavily affected by climate change. Rainfall is one of the main factors affecting crops, but the rainfall is relatively low during the planting season, and in recent years, climate change has also caused changes in the distribution of rainfall (Poudel and Shaw, 2016). According to Aggarwal et al. (2016) and Surendran et al. (2014), the water demand for crops increases along with the rising temperature, thereby increasing the need for irrigation water. Global warming will significantly affect water resources and flow regimes, leading to water shortages during the rainy season and water stress for crops in the dry season, affecting evaporation and crop productivity. Therefore, improving water resource management and planning is necessary to ensure rational water use and distribution for crops and contribute to assessing future water needs

for agricultural production. In view of the above-mentioned issues, the research topic "Determining the irrigation water requirement for rice in the Plain of Reeds" was conducted by us.".

Objectives of the reserach

This research was conducted based on the application of the Aquacrop model developed by the Food and Agriculture Organization (FAO) to calculate crop yield, irrigation water sources, determine reference evapotranspiration, calculate suitable planting time to achieve high seasonal yield with low production costs. In this study, the Aquacrop model was used to simulate water balance and crop response to soil water and address irrigation conditions during climate change.

Research scope

In this research, the Aquacrop model is used to determine irrigation water needs in the PR.

In addition to the introduction and conclusion, the research includes three parts as follows:

Chapter I: Overview of the Plain of Reeds

Chapter II: Applying the Aquacrop model to determine irrigation needs

Chapter III: Analysis of calculation results

In a short time, with limited knowledge, shortcomings cannot be avoided. We look forward to receiving comments from teachers and readers.

CHAPTER I: OVERVIEW OF THE PLAIN OF REEDS

I.1. NATURAL CONDITIONS

I.1.1. Geographical position and terrain

Plain of Reeds is a low-lying, waterlogged area in the MD, with an area that stretches in the East-West direction. It borders Cambodia to the North, the Tien River to the Southwest, and the Vam Co Dong River to the North and Northeast. The natural area of PR covers approximately 697,000 hectares, accounting for 17.7% of the natural area of the MD, spanning three provinces: Long An, Tien Giang, and Dong Thap (Figure 1.1). According to data compiled from reports by the three provinces in the statistical yearbook of 2009, PR is specifically distributed among the provinces as follows:

Long An includes the districts of Vinh Hung, Tan Hung, Moc Hoa, Tan Thanh, Thanh Hoa, Duc Hue, Thu Thua, and Ben Luc, with an area of approximately 299,452 hectares, accounting for 47% of the PR. It can be seen that Long An occupies nearly half of the total area of the region.

PR has an area of approximately 239,000 hectares, accounting for 38% of this region, including the districts of Tam Nong, Thap Muoi, Tan Hong, Hong Ngu, and Thanh Binh, Cao Lanh.

Tien Giang is the province with the smallest area, with approximately 92,500 hectares, accounting for 15% of the region, including the districts of Cai Be, Cai Lay, Tan Phuoc, and a part of Chau Thanh district. The topography of the PR is relatively flat, sloping from the Northwest to the Southeast, with higher elevations at the border and along the banks of the Tien River, gradually decreasing towards the center of the PR, forming a wide, flood-prone depression that is filled with alluvium from the river and sea, creating a large area of alkaline soil. The entire region has a common elevation ranging from 1.0 to 2.0 meters, with the highest point being around 4.0 meters and the lowest point being 0.7 meters.

However, the areas of Hong Ngu and Tan Hong in Dong Thap province have a common elevation ranging from 2.5 to 4.0 meters [5].

Figure 1.1**:** Map of the Plain of Reeds

I.1.2. Natural condition

Like other areas in the MD, the Tien Giang Province is located in a tropical monsoon climate zone with distinct rainy and dry seasons. The dry season coincides with the Northeast monsoon period, lasting from December to April of the following year, characterized by dry, hot weather with little rainfall. The rainy season coincides with the Southwest monsoon period, lasting from May to November, characterized by hot, humid weather with abundant rainfall. The main land resources in the Tien Giang Province are agricultural land, followed by forestry land, with a small proportion of uncultivated land and residential land. There are three main soil groups: gray soil (14.4%), alluvial soil (25.8%), and saline soil (56.6%), with heavy saline soil accounting for 33.24% [10]. Among these soil groups, alluvial soil is the best type, rich in nutrients, suitable for growing various crops, especially fruit trees and short-term agricultural crops such as rice, beans, corn, potatoes, etc.

I.2. CLIMATE AND HYDROLOGICAL CHARACTERISTICS

I.2.1. Climate characteristics

I.2.1.1. Temperature

The average temperature of the PD ranges from 26-28^{o}C, with a temperature difference between dry months of 1-1.5^{o}C, and only about 0.3-0.5^{o}C during rainy months (Figure 1.2). The highest air temperature is in My Tho in the month of 30.2^{o}C, and the lowest temperature is 25.4^{o}C in Cao Lanh in January.

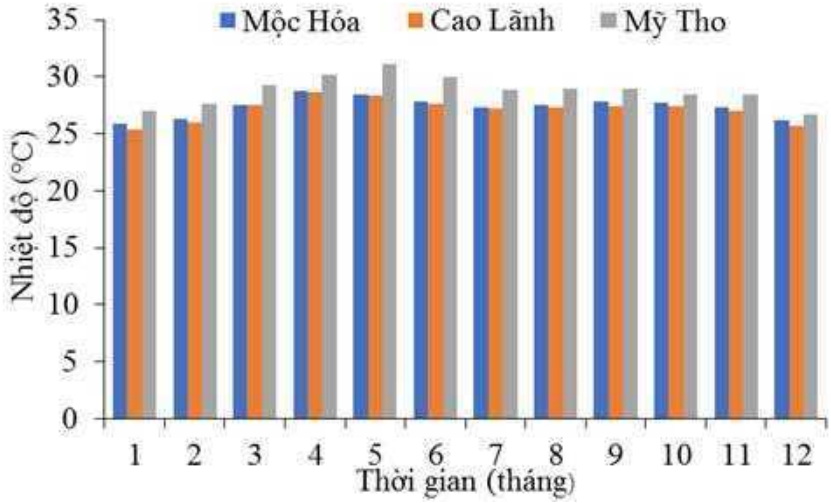

Figure 1.2: Map representing the average temperature by monthly average over many years in the PR.

I.2.1.2. Humidity

PR is a part of the MD with relatively flat terrain, so the humidity in the PR has common characteristics with the MD, with an average relative humidity of about 70-80% [14].

I.2.1.3. Rainfall

Annually, the rainy season lasts for 7 months from May to November, and the dry season lasts from December to April of the following year. The PR has an average rainfall of about 1450-1875 mm, with the highest rainfall of about 350 mm occurring in October and the lowest rainfall of about 150 mm occurring at the end of November (Figure 1.3).

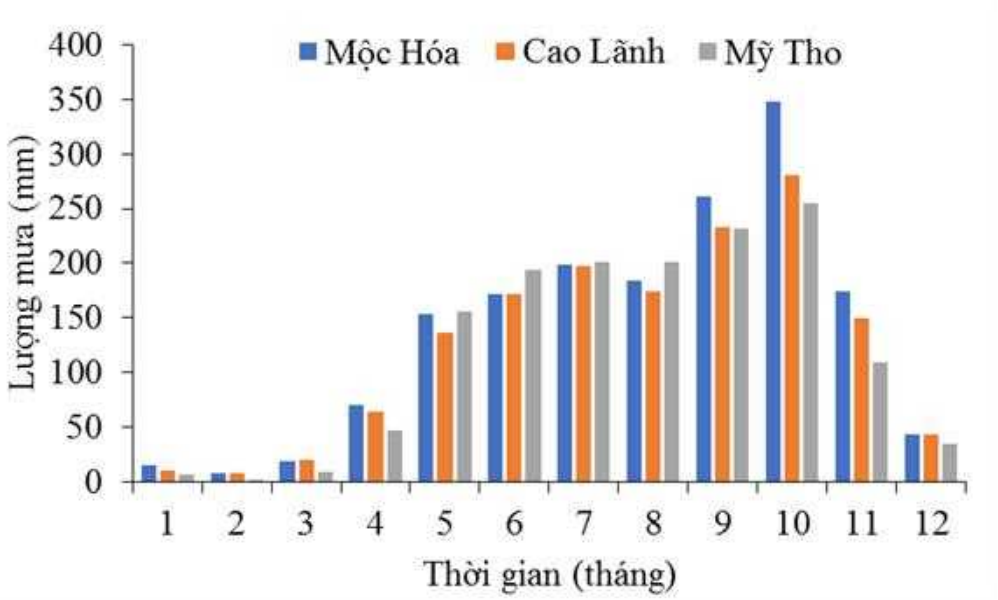

Figure 1.3: Graph showing average monthly rainfall and multi-year average in Dong Thap Muoi area in the period 1985-2015

I.2.1.4. Wind regime

The study area is affected by two main wind directions: the Southwest monsoon operates from May to November, blowing from the Gulf of Thailand, bringing a lot of moisture and causing rain, and the Northeast monsoon prevails from December to April of the following year, blowing from the mainland, making it dry and hot [5]. The average annual wind speed is about 2m/s in the plain, increasing to 3m/s along the coast, and the maximum wind speed can reach 20-30m/s [14].

I.2.2. Hydrological characteristics

The hydrological regime in the MD is directly influenced by the flow of the upper source, the East Sea tidal regime, a part of the Gulf of Thailand tidal regime, and the rainfall regime in the MD. Similar to the MD, the PR has characteristic hydrological features with annual flooding and a complex system of rivers, canals, and channels (Figure 1.4). The MD is considered a flood-prone area with a large annual flooded area due to its ability to receive high floods but poor flood drainage. It is surrounded by high natural embankments along the Vietnam-Cambodia border, natural dikes along the Tien River, and is blocked by the Vam Co Dong River. The causes of flooding in the MD are the Mekong River floodwaters, the East Sea tides, inland rainfall, topography,

geomorphology, river and canal networks, transportation routes, and other human impacts. The extent of flooding in the MD varies depending on space and time during the flood season. The flood level gradually decreases from northwest to southeast. The flood-prone border strip is about 100 km long. Dong Thap Muoi is also a place where floods from Cambodia flow into, with a flow rate of 8,000-10,000 m^3/s during major floods and not less than 3,000 m^3/s during minor floods. The floodwaters in the area are mainly drained into the Vam Co and My Tho rivers, but very slowly [7].

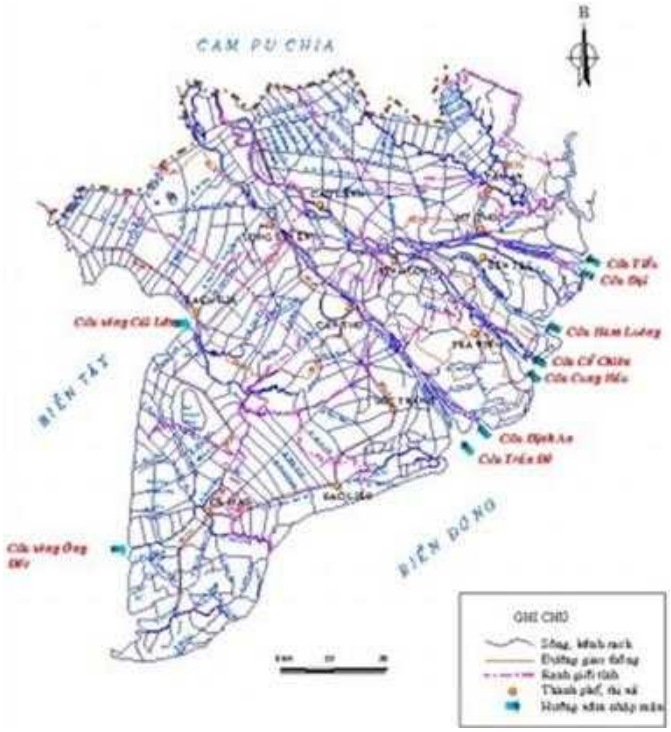

Figure 1.4: River network in the Mekong Delta [24]

I.3. ECONOMIC-SOCIAL CONDITIONS

The PR is a sparsely populated region with an average of over 2.0 hectares of cultivated land per household, which is much higher than in other areas of the country. Agriculture is the key economic sector, with rice being the main crop. The region also has many specialty fruits such as mangoes, longans, and pineapples. In addition, the research area can also grow various types of crops according to each specific region, such as day trees in Thanh Hoa and Moc Hoa districts (Long An province); melon and sweet potato in Tan Phuoc district (Tien Giang province); sesame in Duc Hue, Vinh Hung, Tan Hung, and Moc Hoa districts (Long An province), as well as Tan Hong and Hong Ngu districts (Dong Thap province).

However, the area and production of these crops are still relatively low compared to the potential of the land, water, and climate conditions here. Therefore, rice is still the main crop in this area because it has good tolerance to alkaline soil and is adaptable to the climate and terrain of the region.

The research area has the advantage of being a seasonal wetland ecosystem with diverse biological resources, creating favorable conditions for agricultural development. Furthermore, the area has a larger agricultural land area compared to other regions, but it is a saline land, so rice is the most suitable crop for the region because it has a high tolerance to salinity. Therefore, this area is considered a key rice production region with large rice fields spread throughout the region (Figure 1.5). Like other regions in the MD with low-lying and flat terrain, as well as the tropical monsoon climate, the research area has advantages in agricultural production, with a cultivated land area of about 350,000 hectares per year. The main crop is rice, with an annual production of over 3.0 million tons, contributing about 20% to the rice export output in the MD. In addition, the research area also produces other agricultural products such as sugarcane (850,650 tons), corn (28,624 tons), peanuts (20,438 tons), dragon fruit (97,469 tons), lime (95,880 tons), vegetables (169,000 tons), and various other diverse crops.

However, currently the PR rice plant is in a situation where the area and output are increasing, but the production efficiency is decreasing due to facing many major challenges such as extreme weather, climate change, rising sea levels, flooding, and saltwater intrusion. PR also has potential in the development of aquaculture and processing of aquatic products, bringing high economic value to the MD, with main models being farming on rice fields, cage or floating farming on rivers and canals during the flood season, with various types of fish such as snakehead, catfish, tilapia, ... Although small-scale, it brings economic efficiency, contributes to job creation and improves income for rural people. However, aquaculture here is limited to pond culture and still has limitations in terms of investment capital, low farming techniques, and unstable output, so it has not fully exploited the strengths of the region.

In addition, PR is also an area with great advantages in tourism exploitation and development, here owns Tram Chim National Park, Gao Giong ecotourism area, Go Thap historical and cultural relic area, Dong Sen-Thap Muoi tourist area, Xeo Quyt tourist area (Dong Thap); Tan Lap floating village ecotourism area, Lang Sen wetland conservation area (Long An), etc. Therefore, PR can invest and develop many types of tourism such as ecotourism, river and garden tourism, resort tourism as well as tourism to learn about the development period of the South and the old battlefields.

Figure 1.5: Rice field in Cao Lanh district, Dong Thap province.

CHAPTER II: APPLICATION OF AQUACROP MODEL TO DETERMINE IRRIGATION WATER REQUIREMENTS

II.1. INTRODUCING THE AQUACROP MODEL

II.1.1. General introduction

AquaCrop version 5.0 is a crop yield simulation model for multiple crop types, developed by FAO (see Figure 2.1). The AquaCrop model simulates the water balance and crop yield response to soil water content, and is particularly suitable for addressing conditions where water is the main limiting factor in crop production. The model's main feature is to calculate the achieved crop yield, compare it with the actual yield of a specific crop in a particular area, and identify constraints in seasonal production [17]. AquaCrop can be used as a planning tool and support in addressing agricultural issues, with the following practical applications: understanding crop responses to environmental changes, calculating crop yield, establishing irrigation schedules for production, studying the impact of climate change on production, etc..

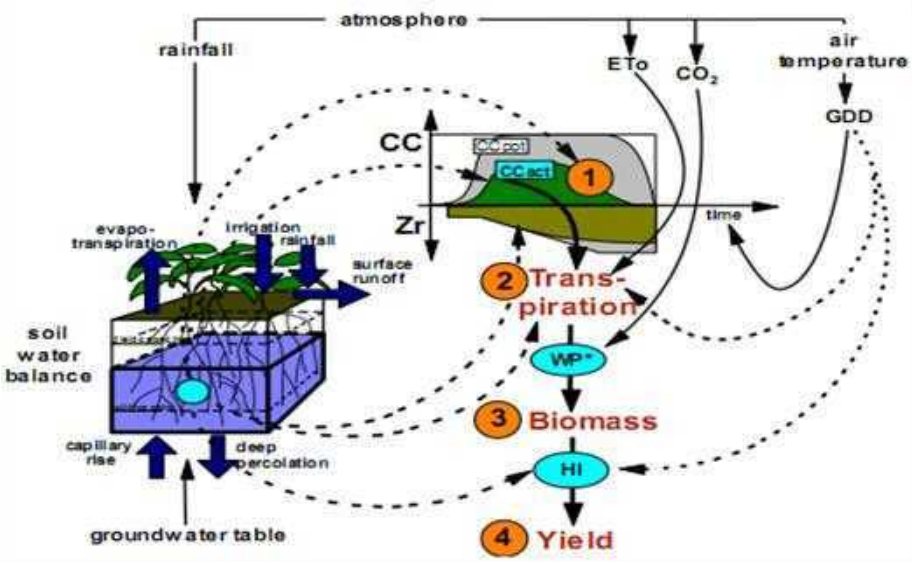

Figure 2.1: Interface of calculation steps in AquaCrop model [17]

II.1.2. The theoretical basis of the model and the computational modules

II.1.2.1. The structure of the model

The input data for the model includes natural conditions in the study area, which are the computational modules of the model including: climate module, cropping season module, field management module, irrigation management module, soil

data, and groundwater data. After simulating the model, the output data will include biomass and crop yield for specific environmental conditions, primarily the crop yield and irrigation water requirement of the crops (Figure 2.2).

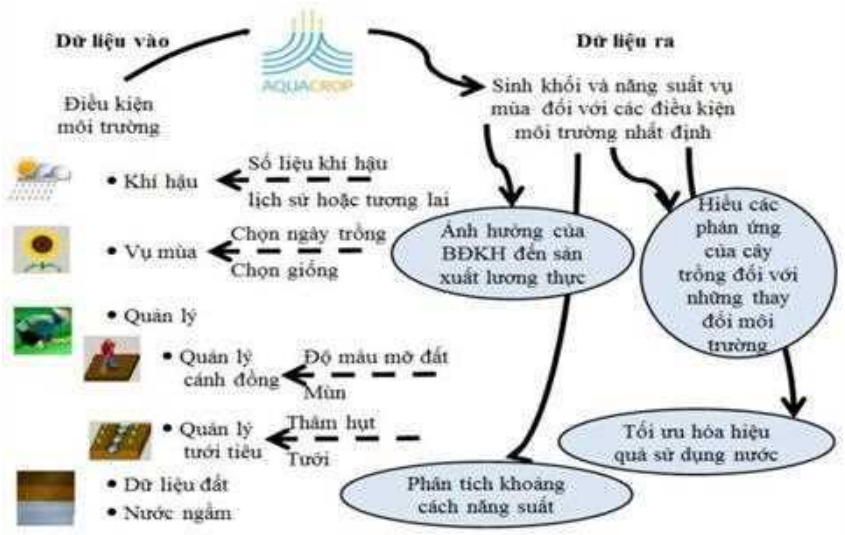

Figure 2.2: Practical applications of the AquaCrop model [17]

Table 2.1 Functions of the modules in the Aquacrop model [17]

Module	**Function**
Climate	Enter climate data. The data is updated directly through the file, including maximum and minimum air temperature, rainfall, and reference evapotranspiration ETo. ETo can be calculated by entering climate data. The Aquacrop model will create corresponding files containing climate data. Enter climate data. In climate data, there is a table or chart displaying climate characteristics, data is aggregated monthly and annually to evaluate climate conditions.
Crop	Update plant characteristic table: plant parameters are grouped in different table formats.
Management	Irrigation: choose the irrigation method according to the available conditions. Field: can adjust CN based on the characteristics of each type of soil. Consider factors that do not affect surface flow, soil (similar to previous version), and affect surface flow (new feature).

Soil	Update the values of SAT, FC, PWP, Ksat, CN, REW for each type of soil.
Simulation	Update the runtime, initial conditions, the model will give the result when running the model. Output the calculation result.

II.1.2.2. Theoretical basis of the model

1. Development of green canopy: in the AquaCrop model, leaf development is expressed through the canopy cover (CC) instead of leaf area index. CC is the proportion of the ground surface covered by the canopy, ranging from 0% at the sowing time (meaning 0% of the ground surface covered by the canopy) to a maximum value of 1 if full canopy cover is achieved (100% of the ground surface covered by the crop). By adjusting the soil water content daily, the AquaCrop model monitors the pressures that can occur in the root zone. Soil-water pressure can affect the leaves, leading to restrictions in canopy expansion and, more severely, premature canopy senescence.
2. Crop evapotranspiration: under good water conditions, crop evapotranspiration (ETc) is calculated by multiplying reference evapotranspiration (ETo) by the crop coefficient (Kc). The crop coefficient is proportional to the crop's growth process, so it will vary throughout the crop's life cycle. Water deficit not only affects the growth and development of the canopy but also causes stomatal closure, directly affecting the crop's evapotranspiration process.

$$ET_C = K_C * ET_O \quad (2.1)$$

3. Biomass on the ground: the amount of biomass on the ground (B) is proportional to the accumulated evaporation process of crops (ΣTr). The proportional factors are called water productivity biomass (WP). Due to the influence of climatic conditions, the standard water productivity biomass (WP*) has different values depending on the location, season, and carbon dioxide concentration (CO2).

$$B = WP.\sum Tr \quad (2.2)$$

II.1.2.3. Calculation modules and input data.

II.1.2.3.1. Climate module

Climate module requires temperature data (average, maximum or minimum in oC or oF), precipitation (mm), humidity (average, maximum or minimum in %), wind speed (m/s), sunshine hours, ETo (mm/day), CO2 concentration. Data can be entered on a daily or monthly basis [17]. Evaporation is an important factor that affects water use efficiency. The calculation of evaporation can be done using various methods, some of which require a lot of input parameters while others require less. Specifically, the following methods have been used:

The Penman-Monteith method requires information on maximum and minimum temperature, solar radiation, wind speed, and the orientation of the study area.

The Pan method requires wind speed, relative humidity, and daily evaporation.

The Priestley-Taylor method is used for areas with high humidity and low wind speed.

The Blaney-Criddle method requires monthly average temperature, minimum relative humidity, and daytime wind speed at a height of 2m. Methods that require more input parameters will provide better estimated results, such as the Penman-Monteith, Pan, and Blaney-Criddle methods. Among them, the Penman-Monteith method usually has a higher correlation coefficient than the other two methods. According to Allen et al. (1998), ETo is calculated as follows:

$$ETo = \frac{0.408\Delta(R_n - G) + \gamma \frac{900}{T + 273} u_2 (e_s - e_a)}{\Delta + \gamma(1 + 0.34u_2)} \quad (2.4)$$

ETo: reference evapotranspiration (mm/day) Rn: solar radiation on the crop surface (MJ/m^2/day) G: soil heat flux density (MJ/m^2/day) T: average daily temperature at a height of 2 meters from the ground (^{o}C) u_2: wind speed at a height of 2 meters from the ground (m/s) es: saturation vapor pressure (kPa) ea: actual vapor pressure (kPa) Δ: slope of the vapor pressure-temperature curve (kPa/^{o}C) γ: psychrometric constant (kPa/^{o}C)

- The ETo calculation tool has also been integrated into the AquaCrop model to calculate water evapotranspiration. ETo is calculated from climate data using the FAO Penman-Monteith equation (Allen et al., 1998). In this calculation program, daily, 10-day, and monthly climate data can be processed. The data used to calculate ETo [17]:
- Air temperature: the air temperature surrounding provides energy for crops and considers the influence of evaporation rate and temperature.
- Air humidity: the difference between saturated vapor pressure (es) and actual vapor pressure (ea) is called vapor pressure deficit or saturation deficit, which is an index that accurately determines the actual evaporation capacity of the air. es and ea cannot be directly evaluated, so they are often determined through the dew point temperature (Tdew) or relative humidity. In some cases where data is missing or data quality is problematic, ea can be calculated by assuming that Tdew is close to the minimum daily temperature (Tn).

II.1.2.3.2. Soil module

The water-holding characteristics of soil: The field capacity (FC) is essential when calculating groundwater balance. FC determines the amount of water retained by the root zone when the soil is fully saturated by rainfall or irrigation. The permanent wilting point (PWP) is reached when the soil is dry and plant roots can no longer extract water. The total available water (TAW) depends on the field capacity and the permanent wilting point. Knowing the upper and lower limits of water in the root zone determines the TAW for the growing season. Calculating groundwater balance: To monitor the water content in the root zone (Wr) and the corresponding water stress, the AquaCrop model balances water on a daily basis. The root zone is described as a reservoir (Figure 2.3), and changes in Wr are determined by tracking inflows and outflows of water. Water is added to the soil through rainfall (P) and irrigation (I). Some of the rainfall may be lost through surface runoff (RO). Water is also transported to the root zone by increasing

capillary rise (CR) from the groundwater. Processes such as soil evaporation (E), plant transpiration (Tr), and percolation losses (DP) will deplete water in the soil.:

$$W_{r,t+1} = W_{r,t} + (P - RO) + I + CR - E - Tr - DP \quad (2.7)$$

In which Wr,t and Wr,t+1 are the amount of water in the root zone at time t and t+1. Deep percolation (DP) occurs after heavy rain or excessive irrigation, when Wr exceeds the soil's holding capacity (i.e., the amount of water that can be retained in the root zone):

$W_{r,\,FC} = 1000\ \theta_{FC}\ Zr$:

$$DP = W_{r,FC} - W_r \quad (2.8)$$

The decrease in water content in the root zone (Dr) indicates the remaining amount of groundwater in the root zone, which can be said to be the amount of water deficit compared to the field capacity. The field capacity is chosen as the reference (Dr=0) to represent the remaining water content in the root zone after being fully saturated.:

$$Dr = W_{r,FC} - W_r \quad (2.9)$$

Movement of water in the soil Water drainage: The AquaCrop model uses the water drainage function to simulate the process of water infiltration through the soil layer, the infiltration of rainwater, and irrigation. The water drainage function requires water drainage characteristics τ, which is proportional to the saturated hydraulic conductivity (Ksat) of the soil layer, and τ represents the decrease in soil water content (Figure 2.4), which is a part of the total amount of water drained out [17]. Increase in capillary rise (CR) from groundwater: In the AquaCrop model, the potential CR is calculated by considering the soil layer and the saturated water conductivity (Ksat) of the soil layers, through which water moves upwards. To calculate the actual intensity of CR, the AquaCrop model considers the groundwater content below the root zone, as it determines the dynamic process [17].

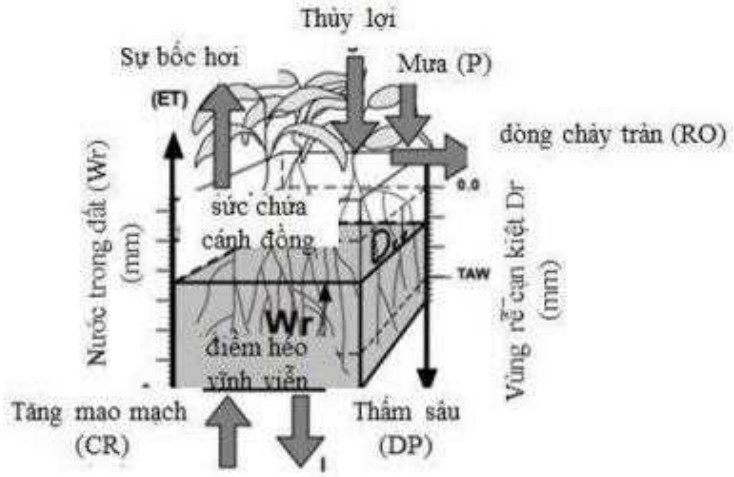

Figure 2.3: Reservoir in the root zone [17]

Surface flow (RO): The amount of water lost due to RO is determined by the curve number (CN). The CN value reflects the soil characteristics, which are determined by Ksat. During the simulation process, CN is adjusted according to the amount of water on the ground (see Figure 2.5). The CN value is adjusted according to slope and crop type. The AquaCrop model does not simulate surface flow when water is irrigated because irrigation is completely controlled by the farmer. In this case, irrigation is determined by the amount of irrigation water and the amount of water lost due to surface flow.

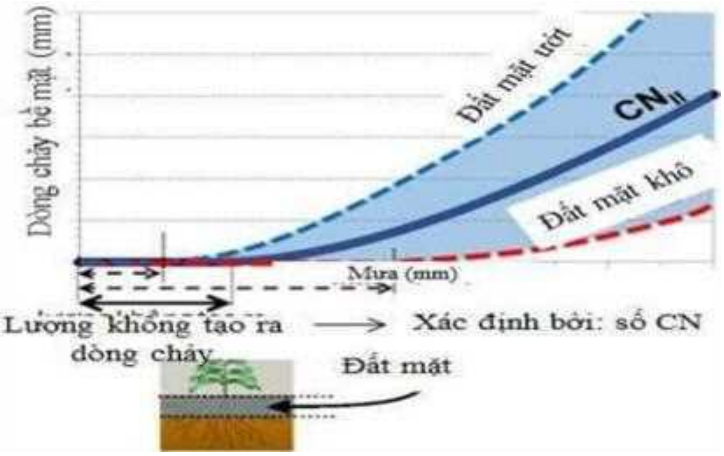

Figure 2.4: illustrates the relationship between surface runoff and rainfall amount for different soil moisture levels in the upper layer

II.1.2.3.3. Crop Module

Parameters affecting crops and management:

Planting method (seeding or direct sowing).

Vegetation density, characterized by initial leaf area index (CCo) and maximum leaf area index (CCx).

Time to reach maximum leaf area index (CCx).

Onset of leaf senescence.

Physiological maturity time.

Maximum root depth (Zx).

Root development rate (or time to reach Zx).

Development days: Root depth is simulated over time, and green cover development is simulated over time in the AquaCrop model. Growing degree days (GDD) are calculated by subtracting the base temperature (Tbase) from the average temperature (Tavg) [17].

$$0 \leq GDD = T_{avg} - T_{base} \tag{2.10}$$

The environment affects crop development and yield, simulated by the stress coefficient (Ks), with values ranging from 1 (no stress) to 0 (maximum stress). The relationship between the stress index and Ks is determined by three crop-specific parameters: upper threshold, lower threshold, and curve shape. At the upper threshold, no stress exists, and Ks=1. At the lower threshold, the impact of stress is maximum, and Ks=0. The shape of Ks between the thresholds can be linear or convex (Figure 2.6) [17].

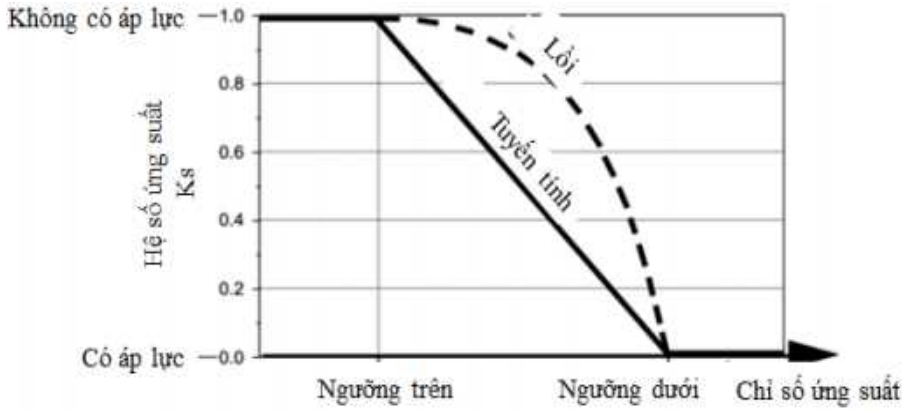

Figure 2.1: Stress coefficient (Ks) [17]

II.1.2.3.4. Management Module

In the management module, there are irrigation management and field management. Irrigation management: There are three forms of management, including determining irrigation water requirements, evaluating the current irrigation schedule, and creating a new irrigation schedule. The appropriate irrigation method needs to be determined to assess or create a suitable irrigation schedule [17].

Determining irrigation water requirements: The seasonal irrigation water requirement is calculated as the total amount of water added during that period. The irrigation water requirement is calculated by adding a small amount of water to the soil daily when the water content in the root zone falls below a specified threshold.

Irrigation schedule: It is necessary to determine the application timing, depth, and water quality. The performance of the schedule can be evaluated by checking the results in the simulation run, and the efficiency of the schedule is provided through biomass (B), crop yield (Y), and water use efficiency (WUE). WUE can be improved by adding or removing irrigation methods and adjusting the timing and amount of irrigation water.

However, under the current impact of climate change, water shortage can occur. When irrigation water is insufficient to meet the crop's demand, the yield will be reduced. To obtain an appropriate irrigation schedule from the simulation results, we can monitor the influence of water on crop growth and development.

Field management [17]: Curve number (CN): The AquaCrop model uses an indirect approach by following the effects of nutrient deficiency on leaf area development (CC) and biomass yield (WP*). For the initial season in the field with sufficient soil nutrients and small leaf area, the daily biomass yield corresponds to the daily crop yield. In Figure 2.7a, (1) slower leaf development means more time is needed to reach maximum leaf cover (CCx), (2) lower leaf cover (below CCx), (3) leaf cover undergoes continuous decline after CCx is reached in the middle of

the season. Nitrogen deficiency can also reduce WP*. As nutrients gradually deplete during crop growth, the effect of soil fertility on WP* is nonlinear throughout the season (Figure 2.7b).

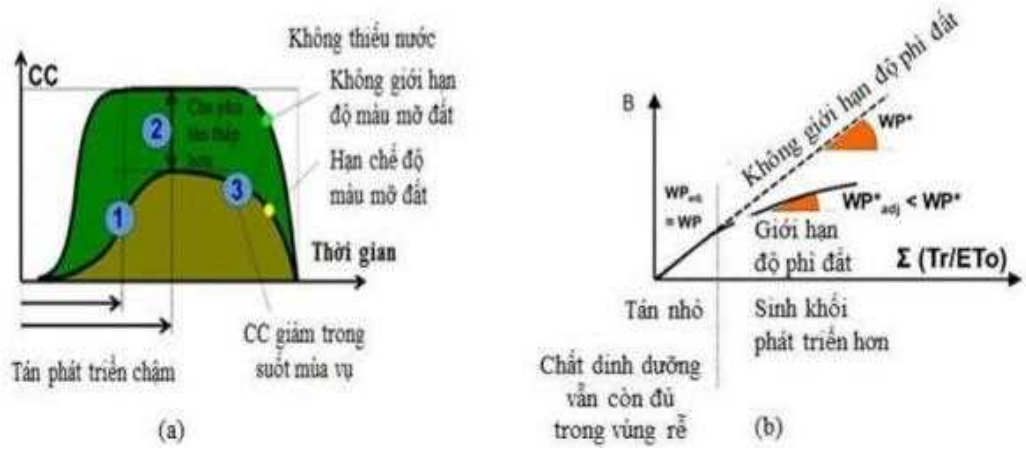

Figure 2.7: Influence of soil nutrient deficiency on leaf area development (a) and biomass yield (b) [17]

II.2. RELATED STUDIES

In recent years, climate change has had a significant impact on human life and production, with the agricultural sector being particularly affected. Climate change has caused droughts leading to water scarcity, decreased water quality, soil degradation, and reduced crop yields, resulting in increased production costs. In response to these challenges, numerous research works have been conducted.

II.2.1. International studies

The impact of climate change on agricultural production poses a threat to the socioeconomic development of nations. Agriculture is heavily dependent on climate conditions and water resources. Therefore, many studies have been conducted to minimize the disadvantages and effectively utilize weather factors for agricultural production.

Geneille and Wang (2016) conducted a study titled "Evaluation of FAO's AquaCrop Model in Simulating Growth and Yield of Maize under Water-Deficient Conditions in a Tropical Environment" [18]. In this study, the authors demonstrated that the AquaCrop model can accurately simulate crop yield and biomass under high precision. However, as the water deficit in irrigation increases, the model's performance decreases.

Consequently, it was concluded that the AquaCrop model is a valuable tool for developing effective irrigation water management strategies.

In 2014, Jin and colleagues applied the AquaCrop model to simulate wheat crop yield during the winter season in China. The study titled "Evaluation of AquaCrop Model for Simulating Winter Wheat Phenology, Biomass, and Grain Yield in the North China Plain" [22] was conducted in an area with an average annual rainfall of 650 mm and a 180-day long winter. The data used included climate data, soil characteristics, and crop data collected from field experiments. The authors affirmed that the AquaCrop model is stable and applicable to various crop types in different environmental conditions, and it can be used to improve irrigation management strategies to maximize crop yield.

Schultz and colleagues (2015) conducted a study titled "Optimizing Agricultural Water Productivity for Wheat in the Semi-Arid Region of Ethiopia" [21]. Field experiments were carried out at the Melkassa Research Farm in Ethiopia during both the rainy and dry seasons. The results confirmed that the AquaCrop model has advantages such as simplicity, low cost, and minimal data requirements. Crop yield depends on various factors, including soil fertility, fertilizer quantity and timing, and soil and water salinity.

A study on water use for crops under climate change conditions was conducted in Egypt in 2016. The study titled "Water Requirements for Major Crop Types" [20] by Samiha, Khaled, and Fouad projected water requirements until 2040 under climate change conditions. The authors noted that evapotranspiration (ET) will increase in all Egyptian provinces, emphasizing the need to adapt agricultural systems, supplement fertilizers, and improve irrigation practices.

Eggplant in Africa was used by Bwalya (2012) in the study titled "Application of AquaCrop Model for Irrigation Scheduling of Eggplant in Africa" [16]. The author emphasized that the AquaCrop model is an important tool for assessing the impact of water scarcity and optimizing water use in water-limited conditions to enhance

sustainability and profitability in farming. However, the author also noted that the model is not suitable for simulating severe water scarcity conditions.

II.2.2. Studies within the country

According to the assessment by the World Bank, Vietnam is among the countries most affected by climate change [15]. The Climate Change Report by the Ministry of Natural Resources and Environment indicated that the average temperature in the country increased by approximately 0.62°C during the period of 1958-2014, with a temperature increase of about 0.42°C during the period of 1985-2014 [2]. Vietnam relies heavily on manual agricultural production methods and is highly dependent on nature, particularly influenced by meteorological factors. Several studies on agriculture have been conducted in the Mekong Delta region. Calculation of the water storage required for irrigating corn during the dry season in Chau Phu district, An Giang province, was conducted by Nguyen Van Tuyen and colleagues (2015) [8]. The study determined the design parameters of water storage ponds using the water balance equation and the AquaCrop model. The authors observed that with an average rainfall of 0.24 m3/day, average evaporation from the pond surface of about 1.87 m3/day, and average deep percolation within the pond of about 4.12 m3/day, the irrigation requirement for corn was 8.30 m3/day.

In 2016, Nguyen Van Tuyen and colleagues [9] applied the AquaCrop model in a study on the irrigation water storage capacity for drought-tolerant crops during the dry season. The study aimed to develop a water-saving model that would enable crops to adapt to prolonged drought conditions and limited water resources, thus contributing to increased productivity and long-term sustainability in agricultural production. Nguyen Van Tuyen and Van Pham Dang Tri (2015) [4] conducted a study on the impact of climate conditions and variable irrigation on rice yield in Tra Noc ward, Can Tho city. The AquaCrop model was used in this study, with irrigation methods redesigned according to the actual irrigation needs in the research area. The study results showed that the AquaCrop model can be used to simulate the effects of climate conditions and different irrigation methods on crop yield.

Tat Anh Thu and colleagues (2013) [12] also carried out a research project using the AquaCrop model to simulate soybean yield under rainfed conditions. Through the study, the authors confirmed that the AquaCrop model accurately simulates crop development and water balance in the soil, enabling the prediction of crop yield. Additionally, the

authors noted that selecting appropriate sowing dates is an important factor in increasing soybean yield by utilizing rainfall water, thereby reducing irrigation costs..

II.3. INPUT DATA AND OPERATIONS WITH THE MODEL

II.3.1 Setting up input data

Climate data is inputted from a text document file with the extension .txt, which is stored in the Import folder within the AquaCrop main directory. After selecting the data, users need to choose the Import climate data command to save the data in the data folder according to each specific data type.

Crop data, irrigation data, field data, soil data, groundwater data, initial conditions, and simulation cycles are directly imported. The files are also stored in the data folder, similar to the climate file.

II.3.1.2. Setting up output data

After running the simulation, users select the command to save the results, which will be stored in the OUTP folder as a file in the AquaCrop model format. The calculation results can be viewed through the Excel program.

II.3.2. Input data

II.3.2.1. Meteorological data

In this study, the input meteorological data includes: solar radiation (hours/day), maximum daily temperature (°C), minimum daily temperature (°C), wind speed (m/s), average humidity (%), and rainfall (mm). These data were collected from Cao Lanh station (Dong Thap), Moc Hoa station (Long An), and My Tho station (Tien Giang).

II.3.2.2. Soil data

The soil characteristics data for the research area were based on soil analysis studies in the Mekong Delta region by Nguyen Bao Ve. These results indicated that the soil type in the research area is clay loam with a particle composition of 45.5% clay, 48.6% silt, and 5.9% sand [6]. The coefficients for this soil type (PWP, FC, SAT, and Ksat) are based on the reference coefficients from FAO included in the AquaCrop model (Appendix 1).

CHAPTER III. ANALYSIS OF CALCULATION RESULTS

III.1. CALCULATION RESULTS OF REFERENCE EVAPOTRANSPIRATION (ETo)

Evapotranspiration is an important factor related to the growth and development of crops, and changes in ETo have a significant impact on water management plans for crops. Therefore, considering the value of ETo is essential in agricultural production, especially under current climate change conditions.

According to the calculation results, the amount of reference evapotranspiration in the area is consistently higher than 120 mm. The total reference evapotranspiration in Cao Lanh reaches approximately 1683.1 mm, with a maximum ETo value of 169.9 mm in March and a minimum value of 123.0 mm in November. In Moc Hoa, the total reference evapotranspiration is around 1666.7 mm, with a maximum ETo value of 167.6 mm in March and a minimum value of 123.0 mm in November. The total reference evapotranspiration is about 1683.1 mm in My Tho, with a maximum value of 169.9 mm in March and a minimum value of 123.0 mm in November (Table 3.1). Generally, ETo reaches its maximum during the growing season of the summer-autumn crop and its minimum during the winter-spring crop. The process of water evapotranspiration is strong at the beginning of the summer-autumn season and gradually decreases towards the end, while rainfall increases. Conversely, during the winter-spring season, evapotranspiration occurs slowly at the beginning of the season, and ETo values gradually increase towards the end of the season, accompanied by less rainfall, leading to higher water demand compared to the summer-autumn crop.

Table 3.1: Temperature, effective rainfall, and reference crop evapotranspiration values.

Month	Cao Lanh			Moc Hoa			My Tho		
	temperature (°C)	LMHQ (mm)	ETo (mm)	temperature (°C)	LMHQ (mm)	ETo (mm)	temperature (°C)	LMHQ (mm)	ETo (mm)

1	26.6	11.1	130.8	26.0	14	127.9	26.6	9.0	130.8
2	27.7	5.2	139.4	27.3	6.2	142.2	27.7	1.1	139.4
3	29.4	27.3	169.9	28.5	26.2	167.6	29.4	10.6	169.9
4	30.2	59.0	159.0	29.3	59.6	165.2	30.2	43.2	159.0
5	29.8	95.7	143.68	28.9	92.0	151.6	29.8	126.1	143.68
6	29.4	127.0	154.9	28.3	138.3	138	29.4	153.6	154.9
7	28.9	152.1	141.1	27.7	135.5	130.5	28.9	150.0	141.1
8	28.9	147.6	136.8	27.7	147.9	139.4	28.9	157.1	136.8
9	28.8	187.0	142.3	28.0	176.5	130.3	28.8	172.4	142.3
10	28.5	194.0	128.9	27.9	244.8	127.2	28.5	168.0	128.9
11	28.0	102.0	123.0	28.8	129.5	123.0	28.0	88.7	123.0
12	26.6	46.2	123.9	26.3	30.6	123.9	26.6	33.7	123.9

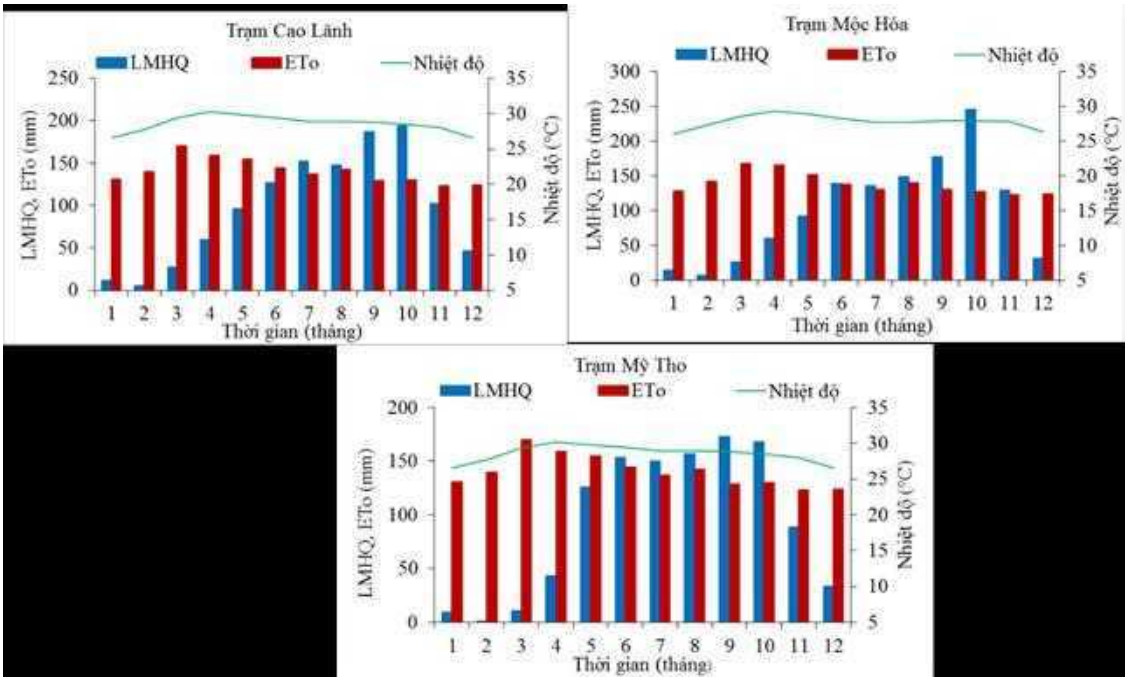

Figure 3.1: Chart depicting the relationship between temperature, effective rainfall, and reference crop evapotranspiration (ETo).

ETo and temperature are directly proportional, meaning that as temperature increases, ETo values also increase, and vice versa. On the other hand, ETo is inversely related to effective rainfall (Figure 3.1). Consequently, ETo tends to be higher during periods of high temperature and low rainfall, indicating a high-water demand for the crops.

The reference crop evapotranspiration values are lower during the early stage of the winter-spring season and higher towards the end of the season. In the autumn-winter season, there is a reverse trend with higher evapotranspiration at the beginning of the season and gradually decreasing towards the end. In the Winter season, there is relatively low variation throughout the season.

In general, the highest reference crop evapotranspiration (ETo) occurs during the winter-spring season, while the lowest values are observed during the autumn-winter season. The reference crop evapotranspiration is lower at the beginning of the winter-spring season and higher towards the end of the season. In the Autumn season, there is a reverse trend with higher evapotranspiration at the beginning of the season and gradually decreasing towards the end. In the Winter season, there is relatively low variation throughout the season.

III.2. ACTUAL CROP EVAPOTRANSPIRATION CALCULATION RESULTS

Below are the actual crop evapotranspiration values for each growth stage of the three rice cropping seasons in Cao Lanh, Moc Hoa, and My Tho.

Table 3.2: ETc values for each growth stage of rice plants in three cropping seasons

Stage	Cao Lanh			Moc Hoa			My Tho		
	Winter-spring	Summer-autumn	Autumn-winter	Winter-spring	Summer-autumn	Autumn-winter	Winter-spring	Summer-autumn	Autumn-winter
Prepare	21.0	27.8	24.2	21.0	29.2	23.6	21.0	27.8	24.2
Initial	22.0	57.9	50.6	22.0	65.8	81.8	22.0	57.9	50.6
Develop	128.2	159.4	133.1	204.8	260.8	407.9	128.2	159.4	133.1
Mild	179.2	177.5	154.4	199.9	186.5	458.3	179.2	177.5	154.4
End	166.6	139.5	129.4	179.9	145.7	243.2	166.6	139.5	129.4

The ETc values for all three rice seasons are highest during the middle stage because this stage has the highest Kc value, and they are lowest during the land preparation stage. In Cao Lanh and My Tho, the highest actual crop evapotranspiration (ETc) occurs during the Autumn season, while in Moc Hoa, it occurs during the winter-spring season (Figure 3.2).

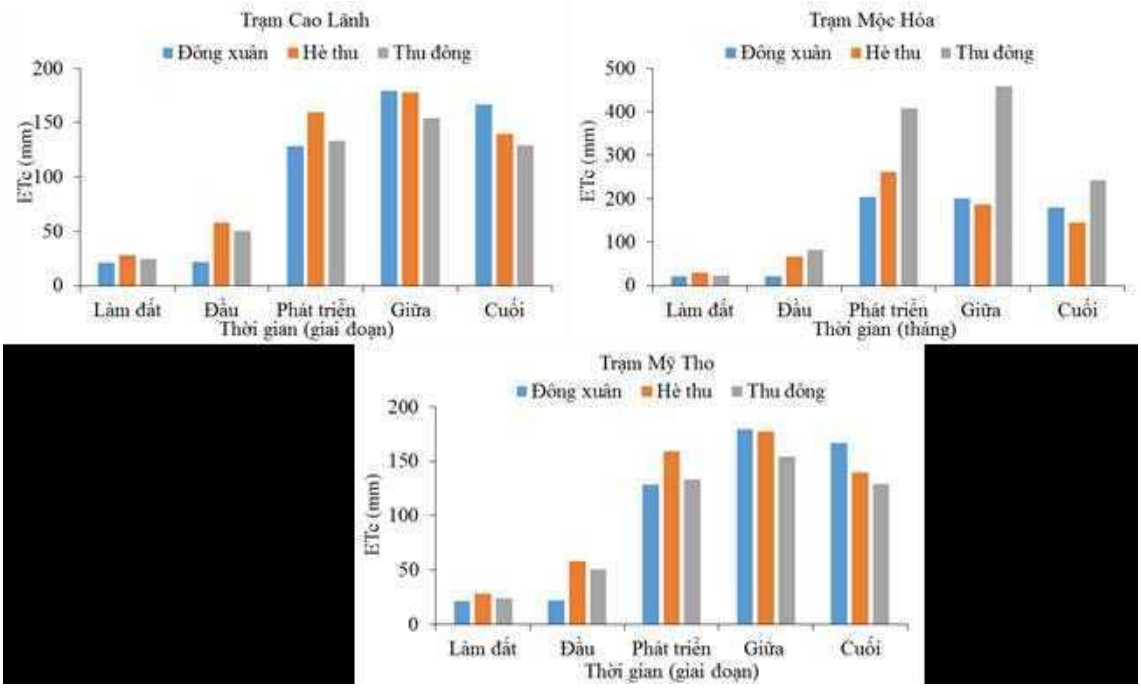

Figure 3.2: Chart depicting ETc (crop evapotranspiration) in three rice seasons

III.3. RAINFALL AND EFFECTIVE RAINFALL

According to FAO (1998), effective rainfall (LMHQ) is defined as a portion of rainfall that is efficiently utilized by crops, after accounting for surface runoff and calculated infiltration losses. It represents the final amount of rainfall used to determine irrigation water requirements [19].

The calculated results of LMHQ show significant monthly variations (Figure 3.3, 3.4, and 3.5). The LMHQ calculations reveal that the highest rainfall amount at the Cao Lanh station is 621.3 mm during the late stage of the Winter-Spring season, which is the rainy month, and the lowest amount is 7.2 mm during the middle stage of the Winter-Spring season. At the Moc Hoa station, the highest LMHQ occurs during the Winter season with 389.5 mm, and the lowest rainfall amount is 5.1 mm during the land preparation stage of the Winter-Spring season. During the middle stage of the Winter-Spring season, the LMHQ reaches its highest value of 282.5 mm and the lowest value of 2.7 mm during the Winter-Spring season. In general, LMHQ tends to have higher values during the Winter season and the middle stage of the Autumn season, mainly due to lower air temperatures and higher rainfall during these periods. The rainfall values in all three stations decrease from the end of the winter-spring season to the beginning of the autumn-winter season,

resulting in a decrease in LMHQ during the winter-spring season, possibly due to higher air temperatures.

Table 3.3 Values of LMHQ and rainfall by cropping stage at Cao Lanh station

Stage	LMHQ (mm)			Rainfall (mm)		
	Winter-spring	Summer-autumn	Autumn-winter	Winter-spring	Summer-autumn	Autumn-winter
Prepare	7.7	9.7	24.2	11.1	11.5	33.9
Initial	13.5	20.9	47.5	19.0	26.0	67.2
Develop	17.1	87.1	175.1	22.4	112.6	242.5
Mild	7.2	140.4	222.6	10.7	191.5	324.3
End	24.4	147.0	110.1	27.9	326.8	621.3

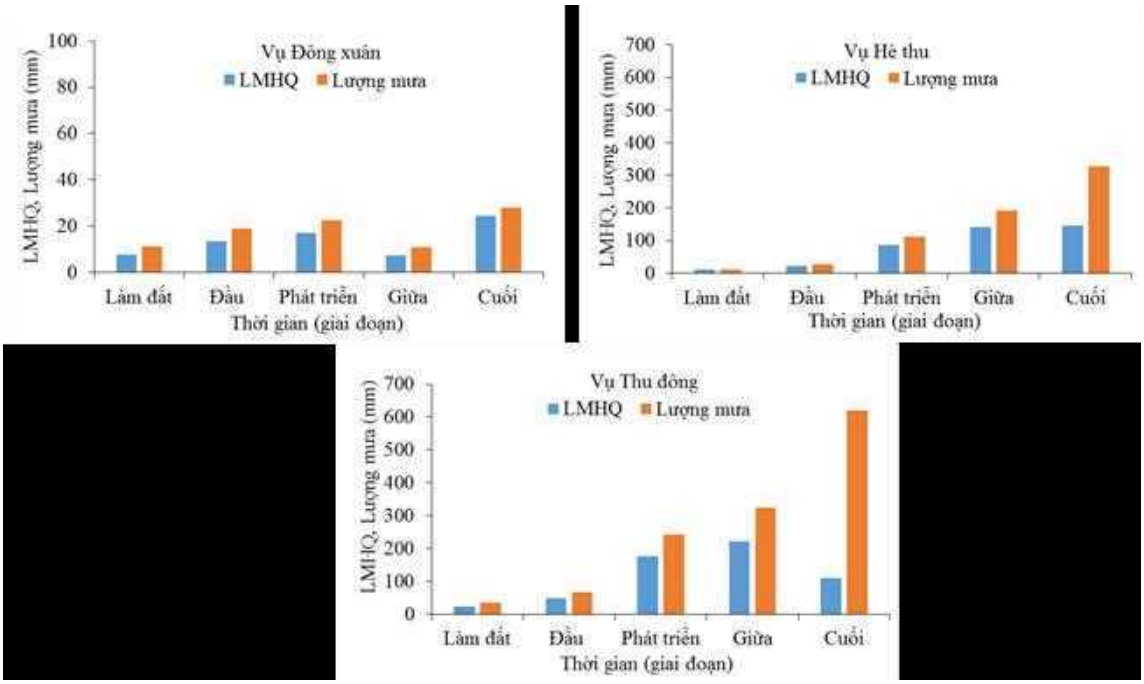

Figure 3.3: Chart depicting rainfall and effective rainfall by cropping season at Cao Lanh station

Table 3.1 Values of LMHQ and rainfall by cropping stage at the Moc Hoa station

Stage	LMHQ (mm)			Rainfall (mm)		
	Winter-spring	Summer-autumn	Autumn-winter	Winter-spring	Summer-autumn	Autumn-winter
Prepare	5.1	9.7	24.3	7.6	11.5	34.3
Initial	7.9	21.5	48.2	10.6	26.0	68.2
Develop	14.3	83.4	164.6	18.4	108.6	235.8
Mild	9.0	151.1	268.6	12.5	209.5	389.5
End	23.6	132.5	140.6	27.1	190.6	211.5

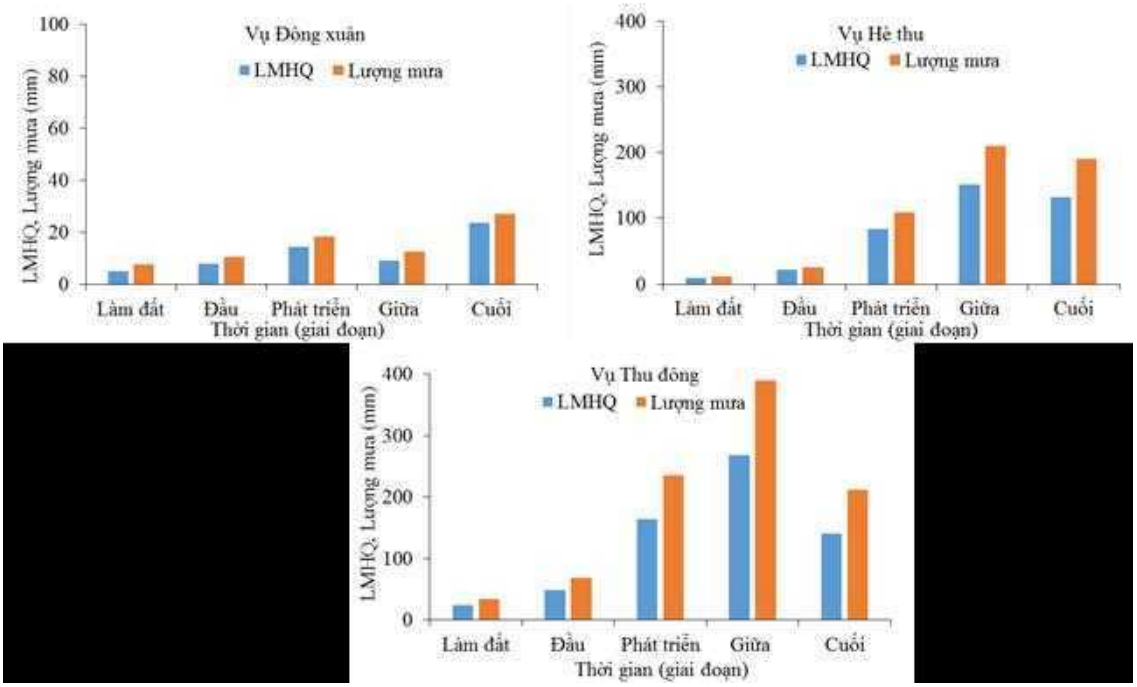

Figure 3.4: Chart depicting rainfall and effective rainfall by cropping season at Moc Haa station

Table 3.5: Values of LMHQ and rainfall by cropping stage at the Mỹ Tho station

Stage	LMHQ (mm)			Rainfall (mm)		
	Winter-spring	Summer-autumn	Autumn-winter	Winter-spring	Summer-autumn	Autumn-winter
Prepare	5.7	6.5	26.2	8.1	7.3	36.8
Initial	9.4	16.9	50.5	13.0	20.0	72.0
Develop	13.0	108.6	166.8	16.9	143.2	237.2
Mild	2.7	173.3	193.8	4.1	239.7	282.5
End	8.8	146.6	95.9	11.7	208.6	141.5

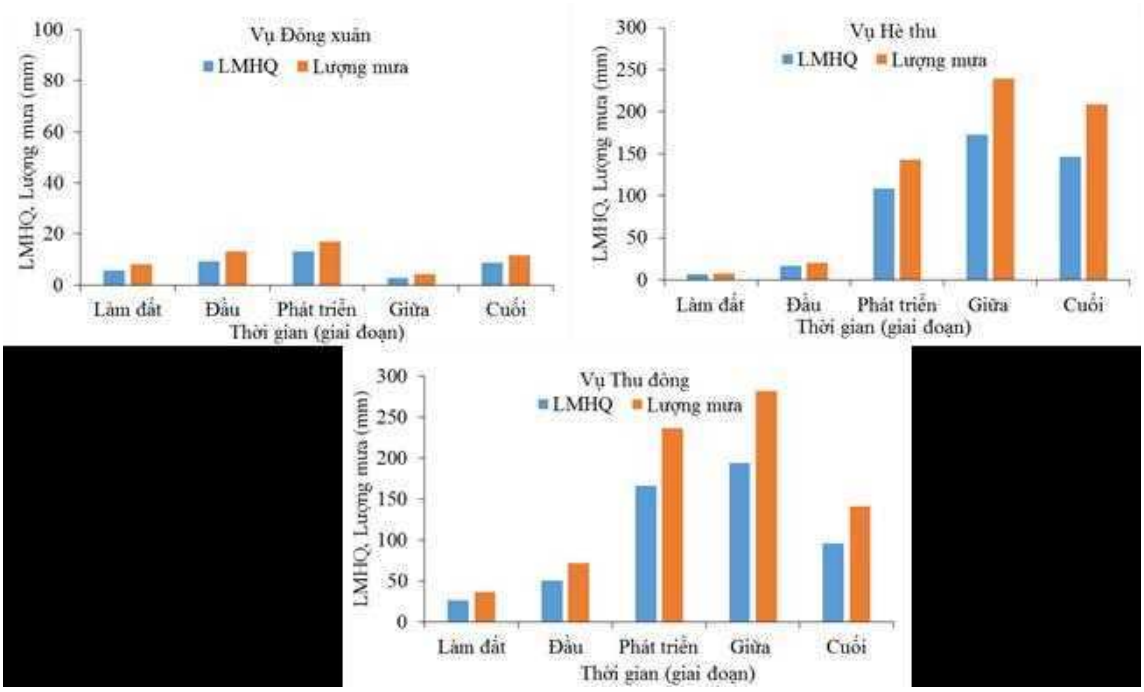

Figure 3.5: Chart depicting rainfall and effective rainfall by cropping season at the Mỹ Tho station

CONCLUSIONS

Through the process of conducting this research, we have drawn the following conclusions:

The reference crop evapotranspiration (ETo) in the Plain of Reeds is consistently higher than 120 mm, with a total reference crop evapotranspiration of approximately 1600 mm. The evapotranspiration process is strong at the beginning of the Autumn season and gradually decreases towards the end of the season, while rainfall increases. In contrast, during the winter-spring season, the evapotranspiration process is slow at the beginning of the season, and the ETo value gradually increases towards the end of the season. Therefore, it is necessary to consider the ETo value to limit water loss from rice plants and maintain an appropriate water level in the fields.

The actual crop evapotranspiration (ETc) of all three rice seasons reaches its highest value during the middle stage (which has the highest crop coefficient, Kc) and the lowest value during the land preparation stage. In general, the highest ETc value occurs during the development stage towards the end of the Autumn season, particularly for the Moc Hoa station, which has the highest ETc value during the Autumn season.

The actual evapotranspiration deficit (ETd) usually reaches its highest value during the Winter-Spring season and the middle stage of the Autumn season, mainly due to low air temperature and high rainfall during these periods. The rainfall in all three stations decreases from the end of the Winter-Spring season to the beginning of the autumn-winter season, leading to a decrease in ETd during the winter-spring season, possibly due to the higher air temperature.

References

[1]. Ministry of Agriculture and Rural Development, Cooperative Development in the Dong Thap Muoi Subregion: Electronic Information Portal.

[2]. Ministry of Natural Resources and Environment (2016), Climate Change Scenarios and Sea Level Rise for Vietnam, Resources and Environment Publishing House and Vietnam Map Publishing House.

[3]. Can Van Thu, Nguyen Thanh Son (2016), Hydrodynamic Simulation and Analysis of the Impact of Embankment Systems on Surface Flow Changes in the Dong Thap Muoi Region, Journal of National University, Hanoi, 32, page 257.

[4]. Hong Minh Hoang, Van Pham Dang Tri (2015), Influence of Climate Conditions and Irrigation Water Changes on Rice Yield in Tra Noc Ward, Can Tho City, Journal of Can Tho University, No. 39, 71-82.

[5]. Le Trong Quy (2011), Landscape Research and Evaluation for the Development of Agriculture, Forestry, and Tourism in the Dong Thap Muoi Area, Dong Thap Province, Environmental Department, Ho Chi Minh City University of Natural Sciences.

[6]. Nguyen Bao Ve (2003), Fixation of Potassium in Mekong Delta Paddy Soils, Soil Science Journal, No. 19, 16-24.

[7]. Nguyen Tan Dat (2007), Theoretical Basis and Practical Aspects for the Formation of Flood Control Plans along the Vietnam-Cambodia Border in Dong Thap Muoi, Southern Institute of Water Resources Planning, 70.

[8]. Nguyen Van Tuyen, Pham Van Toan, Nguyen Huu Chiem, Le Anh Tuan, Van Pham Dang Tri (2015), Calculation of Irrigation Water Storage for Maize in the Dry Season in Chau Phu District, An Giang Province, Journal of Can Tho University, Environment and Climate Change, 174-182.

[9]. Nguyen Van Tuyen, Hong Minh Hoang, Tran Thi Le Hang, Van Pham Dang Tri (2016), Study on Irrigation Water Storage Capacity for Drought-Tolerant Crops in the Dry Season using AquaCrop Model, Faculty of Environment and Natural Resources, Can Tho University.

[10]. Nguyen Viet Cuong, Tran Thi Hong Tham (2013), Research Results and Development of Rice Varieties Adapted to Difficult Conditions in Dong Thap Muoi - Orientation and Proposed Solutions, Dong Thap Muoi Rural Research and Development Center.

[11]. Nguyen Viet Cuong (2013), Crop Diversification on Paddy Soils in the Dong Thap Muoi Region - A New Direction of Interest, Southern Institute of Science and Technology.

[12]. Tat Anh Thu, Nguyen Minh Hoang An, Nguyen Van Qui (2013), Using the AquaCrop Model to Simulate Soybean Yield under Rainfed Conditions, Agricultural Science Journal.

[13]. Vietnam Standards on Irrigation Works for Water Supply and Drainage of Food Crops and Food Plants (TCVN 8641:2011).

[14]. Institute of Meteorology, Hydrology and Environment (2010), Project on Climate Change Impacts on Water Resources and Adaptation Measures, Hanoi.

[15]. Vuong Tuan Huy (2013), Application of AquaCrop Model in Simulating Rice Yield under Changing Climate Factors in the North of National Highway 1A, Bac Lieu Province. Journal of Can Tho University, 13, page 4.

[16]. Angela, B., (2012), *Validation of the AquaCrop model for irrigated African Eggplant (Solanum Macrocarpon) at the Unza field station*, Master degree, The University of Zambia.

[17]. Food and Agriculture Organization of the United Nations (2016), *AquaCrop training handbooks.*

[18]. Geneille, G., Yu-Min, W., (2016), Assessment of FAO AquaCrop Model for Simulating Maize Growth and Productivity under Deficit in Tropical Environment, *Flagship Journals*, 8, pp.557.

[19]. Lee, S.K., Dang, T.A., (2017), *Water requirement for rice crops in the context of changing climate: A case study in the Long Xuyen Quadrangle, Vietnam*,

[20]. Samiha, O., Khaled, A.E. and Fouad, K., (2016), *Water Requirements for Major Crops for different agro-climatic zones of Balochistan*, The World Conservation Union.

[21]. Schultz, E., (2015), Agricultural Water Productivity Optimization for Irrigated Teff (Eragrostic Tef) in Water Scarce Semi-Arid Region of Ethiopia, *CRC Press/Balkema-The Netherlands.*

[22]. Xiu-liang, J., Hai-kuan, F., Xin-kai, Z., Zhen-hai, L., Sen-nan, S., Xiao-yu, S., Gui-jun, Y., Xin-gang, X. and Wen-shan, G., (2014), Assessment of the AquaCrop Model for Use in Simulation of Irrigated Winter Wheat Canopy Cover, Biomass, and Granin Yeild in the North China Plain, *Plos One*, pp.9.

Oceanology Meteorology Hydrology
University of Science - Ho Chi Minh City

TRƯỜNG ĐẠI HỌC KHOA HỌC TỰ NHIÊN
KHOA VẬT LÝ - VẬT LÝ KỸ THUẬT
BỘ MÔN HẢI DƯƠNG, KHÍ TƯỢNG VÀ THỦY VĂN

BẢNG ĐIỂM CHẤM SEMINAR TỐT NGHIỆP K2014

NGÀY BẢO VỆ: 07/07/2017 **ĐỊA ĐIỂM: E402**

STT	MSSV	Họ tên sinh viên	Điểm của Cán bộ hướng dẫn	Điểm của Cán bộ phản biện	Ghi chú		Điểm TB	Điểm làm tròn	Điểm chữ
					Thời gian báo cáo	Tài liệu tham khảo			
1	1421253	Phạm Thu Thảo Nguyên	9.5	9.5	09'03	3	9.5	9.5	
2	1421338	Nguyễn Thị Hồng Thắm	9.5	9.5	07'53	3	9.5	9.5	
3	1421238	Nguyễn Thị Cẩm Mi	10.0	8.5	06'45	1	9.25	9.5	
4	1421332	Nguyễn Thị Xuân Thắm	10.0	9.75	07'20		9.875	10	
5	1421230	Lê Thị Pha Mi	9.5	9.5	09'42	3	9.5	9.5	
6	1321139	Phạm Minh Triết	9.0	9.0	07'31	1	9.0	9.0	
7	1421334	Kiều Hữu Toàn Thắng	9.0	9.5	08'24		9.25	9.5	
8	1421015	Nguyễn Thị Thanh Dừng	9.5	9.25	06'57		9.375	9.5	
9	1421185	Phạm Quang Huy	9.75	9.5	08'17		9.625	9.5	
10	1421410	Nguyễn Thị Xuân	9.5	9.5	07'08	1	9.5	9.5	
11	1421199	Nguyễn Văn Khánh	9.0	8.25	07'15	3	8.75	9.0	
12	1321084	Tôn Thất Phu Nguyên	8.0	8.0	09'40	1	8.0	8.0	
13	1421247	Trần Cẩm Nghi	9.5	9.5	07'15	3	9.5	9.5	
14	1421348	Trịnh Thị Thu Thủy	9.5	9.25	08'04	2	9.375	9.5	
15	1421083	Hoàng Hoài Thương	9.0	9.0	06'11		9.0	9.0	

TP.HCM, ngày 07 tháng 07 năm 2018

Vietnam National University- Ho Chi Minh City

University of Science, Ho Chi Minh City, Vietnam

Faculty of Physics and Engineering Physics

Department of Oceanography, Meteorology and Hydrology

Graduate Seminar

Topic:

UNDERSTANDING THE RELATIONSHIP BETWEEN CHLORCHILOX CONCENTRATION WITH TEMPERATURE, TURBIDITY, AND DISSOLVED OXYGEN CONCENTRATION IN WATER

Student Name: PHAM VAN PHUNG

Instructor: Assoc. Prof. Dr. VO LUONG HONG PHUC

To complete this graduation seminar, first of all I would like to extend my sincere thanks to all the professors in the Department of Oceanography, Meteorology and Hydrology at the University of Natural Sciences.

Especially, I would like to send my deepest gratitude to Professor Vo Luong Hong Phuoc, who has patiently guided and assisted me in completing this graduation seminar.

I sincerely thank the Department of Oceanography, Meteorology and Hydrology for creating favorable conditions and providing real data for me to optimize this graduation paper.

Finally, I thank my parents who have always been by my side and encouraged me throughout my academic journey, allowing me to succeed as I have today.

I sincerely thank you all!

ABSTRACT

Scientists usually study the algae and the phytoplankton via the chlorophyll concentration. In this study, by using the direct measurement by Multi-Exciter (JFE, Japan), the Chlorophyll concentration were collected in depth and in frequency during 24 hours from 11/1/2020 to 12/1/2020. The survey area is at Cho Lach hydrological station (Ben Tre). The Blackman Tukey method is used to analyze the spectrum of chlorophyll in depth and in nine different wavelength. From then, the distributions of the Diatom, Algae and Cyanobacteria according to the frequency are calculated. The results show that the distribution of chlorophyll concentration profile of small wavelengths is higher than that of higher wavelengths. The concentration of harmful algae (Cyanobacteria) is less than that of beneficial algae (Diatom and Algae). This shows that the water quality in the study site is good enough for environment.

CONTENTS

LIST OF FIGURES

LIST OF TABLES

CHAPTER I: THEORETICAL BASIS OF CHLOROPHYLL

I.1 Concept of chlorophyll:

Chlorophyll is a color pigment found in plants, algae, and phytoplankton [1]. This molecule is used in photosynthesis, as a photoreceptor. Photoreceptors absorb light energy, and chlorophyll specifically absorbs energy from sunlight. Chlorophyll gives plants and algae their green color because it reflects the green wavelengths found in sunlight, while absorbing all other colors (Figure 1.1).

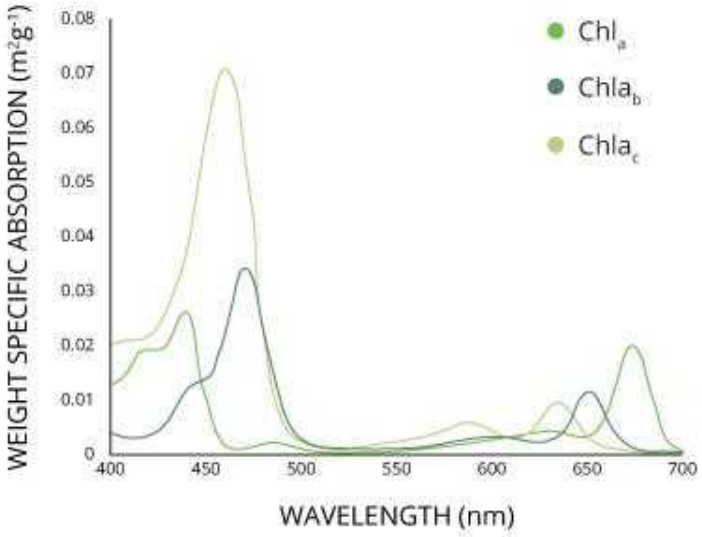

Figure 1.1 Some types of chlorophyll

Different forms of chlorophyll absorb slightly different wavelengths for more efficient photosynthesis [1].

However, chlorophyll is not really a single molecule. Six different chlorophylls have been identified. The different forms (A, B, C, D, E and F) reflect slightly different bands of green wavelengths. Chlorophyll A is the basic molecule that carries out photosynthesis. That means chlorophyll A is found in every photosynthetic organism, from terrestrial plants to algae and cyanobacteria. Additional forms of chlorophyll are accessory pigments, which are related to different groups of plants and algae and play a role in their taxonomic confusion. These other chlorophylls still absorb sunlight, and thus aid in photosynthesis.

As accessory pigments, they transfer any energy they absorb to primary chlorophyll A instead of being directly involved in the process.

Chlorophyll B is mainly found in terrestrial plants, aquatic plants, and green algae. In most of these organisms, the ratio between chlorophyll A and chlorophyll B is 3: 1. Due to the presence of this molecule, some organizations will group green algae into the Plant Kingdom. Chlorophyll C is present in red, brown, and dicotyledonous algae. This led to their classification under Kingdom Chromista. Chlorophyll D is an accessory pigment found in some red algae, while chlorophyll E is rarely found in yellow green algae. Chlorophyll F has recently been detected in several cyanobacteria near Australia. Each of these sub-pigments will strongly absorb different wavelengths, so their presence makes photosynthesis more efficient.

I.2 Some other pigments:

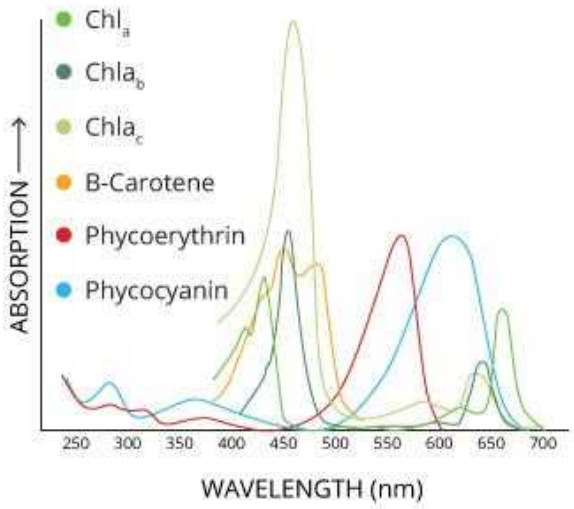

Figure 1.2 Some important pigments

Each pigment absorbs and reflects different wavelengths, but they all act as auxiliary pigments for chlorophyll A during photosynthesis (Figure 1.2)[1].

Chlorophyll is not the only photosynthetic pigment found in algae and phytoplankton. There are also carotenoids and phycobilins (biliproteins). These extra pigments are responsible for the colors of other organisms, such as yellow, red, blue, and brown. Like chlorophyll B, C, D, E, and F, these molecules improve their ability to absorb light energy,

but they are not a major part of photosynthesis. Carotenoids can be found in most phytoplankton and reflect yellow, orange and/or red light. There are two phycobilins found in phytoplankton: phycoerythrin and phycocyanin. Phycocyanin reflects blue light and is what gives the common name of cyanobacteria - blue-green algae. Phycoerythrin, which reflects red light, can be found in red algae and cyanobacteria.

Some algae will appear green despite the presence of these secondary pigments. Just like in plants, chlorophyll in algae has a relatively stronger absorption capacity than other molecules. As a dominant feature, the more strongly reflected green wavelengths can mask other, less reflective colors. In green algae, chlorophyll is also found in higher concentrations than accessory pigments. When the secondary pigments are more concentrated (such as red algae, brown algae, and cyanobacteria), other colors can be seen.

I.3 Concept of algae

Algae are aquatic, plant-like organisms [1]. They include a wide range of simple structures, from single-celled phytoplankton floating in water, to large marine algae (macroalgae) attached to the ocean floor. Algae can be found residing in oceans, lakes, rivers, ponds and even in snow, anywhere on Earth.

The difference between seaweed and submerged plants is in their structure. Macroalgae are simpler and attach themselves to the seabed with a stopper instead of real roots. Aquatic plants, whether floating, submerged, or floating (starting in the water and growing out) have specialized parts such as roots, stems, and leaves. Most plants also have vascular structures (xylem and phloem), which carry nutrients throughout the plant. While algae contain chlorophyll (just like plants), they do not have these specialized structures.

Algae are sometimes considered protists, while other times they are classified as vegetative or chromists. Phytoplankton is made up of unicellular algae and cyanobacteria.

Since algae can be unicellular, filamentous (chained) or vegetative, they are often difficult to classify. Most organizations group algae by their primary color (green, red, or brown), although this creates more problems than it solves. Different species of algae are very distinct from each other, not only in terms of pigment but also in cell structure,

complexity, and environment of choice. Thus, the taxonomy of algae is still under debate, with several taxonomic organizations belonging to different kingdoms, including Plantae, Protozoa and Chromista. While the overall gender classification is not always agreed upon, the species, genus, family, class, and phylum of each alga species. To further complicate this nomenclature, unicellular algae are often classified as phytoplankton widely.

I.4 The concept of phytoplankton

Phytoplankton are microorganisms that drift in water [1]. They are unicellular, but they can sometimes grow into colonies large enough to be seen with the human eye. Phytoplankton are photosynthetic, which means they can use sunlight to convert carbon dioxide and water into energy. While they resemble plants in this capacity, phytoplankton are not plants. The term "monocyte" is a misnomer and should not be used. Instead, phytoplankton can be divided into two classes, algae and cyanobacteria. These two layers share the same photosynthetic capacity but have different material compositions. Regardless of their classification, all phytoplankton contain at least one form of chlorophyll (chlorophyll A) and are therefore able to carry out photosynthesis for energy.

Phytoplankton, both algae and cyanobacteria, can be found in fresh or salt water. When they need light to photosynthesize, phytoplankton in any environment will emerge near the surface of the water, where sunlight hits. Most freshwater phytoplankton are made up of green algae and cyanobacteria, also known as blue-green algae. Marine phytoplankton is mainly composed of microalgae called diatoms and diatoms, although other algae and cyanobacteria may be present. The flagellates have some autonomous movements due to their "tails" (whips), but the diatoms are influenced by ocean currents.

Figure 1.3 Some common types of algae

Phytoplankton has many different structures, but all except cyanobacteria are algae. Collage adapted from drawings and microphotographs by Sally Bensusen, NASA's EOS Project Science Office

I.6 Some algae under consideration:

Diatoms (Diatoms):

Diatoms are a major group of algae, especially microalgae, found in the world's oceans, waterways and soils [2]. Living diatoms make up a significant portion of the Earth's biomass: they produce about 20 to 50% of the oxygen produced on the planet each year, receiving more than 6.7 billion tons of silicon per year from regions water where they live, and make up nearly half of the organic matter found in the oceans. The shells of dead diatoms can be as deep as half a mile (800 m) on the ocean floor, and the entire Amazon basin is fed annually by 27 million tons of diatomaceous earth dust transported by transatlantic winds from sub-Saharan Africa. Africa, many of which date from the Bodélé Depression, which was once made up of a system of freshwater lakes.

• Diatoms are unicellular: they appear as solitary cells or as colonies, which can be ribbon, fan, zigzag or star shaped. Individual cells range in size from 2 to 200 micrometers. Under conditions of adequate nutrients and sunlight, a living diatom population doubles approximately every 24 hours by repeated clonal fission; the maximum lifespan of individual cells is about six days. Diatoms have two distinct shapes: a few (central diatoms) are radially symmetrical, while most (fine diatoms) are bilaterally symmetrical.

• Diatoms are used to monitor past and present environmental conditions and are commonly used in water quality studies. Diatomaceous earth (diatomite) is a collection of diatomaceous earth shells found in the earth's crust. They are soft, silica-containing sedimentary rocks that are easily pulverized and typically have a grain size of 10 to 200 μm. Diatomaceous earth is used for a variety of purposes including water purification, as a mild abrasive, in cat litter and as an explosive stabilizer.

Figure 1.4 Diatoms have cell walls composed of transparent, milky silica. The diatom cell walls are decorated with intricate and striking patterns of silica [3].

The most common and beneficial diatoms:

- Diatoms convert energy from the sun into sugar [3]: Diatoms have light-absorbing molecules (chlorophyll a and c) that capture energy from the sun and convert it into chemical energy through photosynthesis process.

Figure 1.5 Diatoms turn energy from the sun into sugar

-Diatoms create 50% of the air we breathe: Through carbon fixation, diatoms remove carbon dioxide (CO2) from the atmosphere. CO2 is converted to organic carbon in the form of sugars and oxygen (O2) is released. We breathe in the oxygen released by the diatoms.

Diatoms that feed oceans, lakes and rivers: Diatoms produce these energy-rich magnetic acids that feed the entire food web, from zooplankton to aquatic insects, fish to whales.

Figure 1.6 Diatoms produce 50% of the air we breathe [?]

Green Algae:

• Green algae are a large group of algae, from which Embryophyta (or higher plants) arose[4]. As such, they form a paraphyletic group, although the group that includes both the green algae and the subfamily Embryonic plants are monophyletic (and are commonly known as the kingdom Plantae). Green algae include unicellular flagellates and flagellate colonies (usually but not always with 2 flagella per cell), as well as other forms of cocci and filamentous bacteria, and macroalgae. tissue. In the order Charales (most closely related to multicellular plants), there is a complete differentiation of tissues. There are about 6,000 species of green algae. Many species live their whole lives as unicellular, while others form colonies, coenobiums or long filaments or highly differentiated macroscopic algae.

• There are several groups of organisms that rely on green algae for their photosynthesis. Chloroplasts in euglenoidea and complex green algae (Chlorarachnea) are obtained from phagocytosis of green algae, and in the latter and retained group (nucleus morphology).

Green algae have also been found to live symbiotically in the hairy worm Paramecium, and in Hydra viridis as well as in some flatworms (Platyhelminthes). Several species of green algae, especially the genera Trebouxia and Pseudotrebouxia (class Trebouxiophyceae), can be found in symbiosis with lichen fungi. In general, fungi in lichens cannot live independently, while algae in nature usually do not live with fungi. The green algae of the genus Trentepohlia live as parasites on the bark of some tree species.

Figure 1.7 Shape of green algae in aquatic environment.

Cyanobacteria or Blue-green Algae (Cyannobacteria):

• Despite the ability to photosynthesize for energy, blue-green algae are a type of bacteria[1]. This means that they are single-celled, prokaryotic (simple) organisms. Prokaryotes mean cyanobacteria that do not have a nucleus or membrane-bound organelles inside their cell walls.

• Cyanobacteria are the only bacteria that contain chlorophyll A, a chemical required for oxygen-producing photosynthesis (the same process used by plants and algae). This process uses carbon dioxide, water, and sunlight to produce oxygen and glucose (sugar) for energy. Chlorophyll A is used to capture energy from sunlight to help with this process. Other bacteria can be considered photosynthetic organisms, but they follow a different

process known as microbial photosynthesis, or hypoxic photosynthesis. This process uses bacterial chlorophyll instead of chlorophyll A. These bacterial cells use carbon dioxide and hydrogen sulfide (instead of water) to produce sugar. Bacteria cannot use oxygen during photosynthesis and thus produce energy in an anaerobic (oxygen-free) manner. Cyanobacteria and other phytoplankton photosynthesize as plants, and produce the same sugar and oxygen for use in cellular respiration.

Figure 1.8 In 2011, Lake Erie experienced its worst blue-green algae bloom in decades (Image source: MERIS/NASA; handled by NOAA/NOS/NCCOS)

• In addition to chlorophyll A, blue-green algae contain the pigments phycoerythrin and phycocyanin, which give bacteria their blue color (hence the name blue-green algae). Although they do not have a nucleus, these microorganisms contain an inner sac called a vacuole that helps them float near the surface of the water.

CHAPTER II: METHOD OF ANALYZING THE RELATIONSHIP BETWEEN CHLOROPHYLL CONCENTRATION WITH TEMPERATURE, TURBIDITY AND DISSOLVED OXYGEN CONCENTRATION IN WATER

This study uses direct measurement method to obtain data of concentration, turbidity, temperature, depth and chlorophyll content in water environment. Chlorophyll data is collected from multi-meter exciter. Multi-exciter device uses the property of absorption and reflection of wavelengths in the spectral range to determine phytoplankton present in water. This device measures in situ, rapid continuous measurement, especially phytoplankton groups can be classified by wavelengths. The multi-exciter uses nine wavelengths in the visible spectrum: 375, 400, 420, 435, 470, 505, 525, 570, and 590 nm.

II.1 Introduction of the meter

The Multi-Exciter is a multi-excitation fluorescence meter for automatic algal layer detection. It is equipped with a chlorophyll fluorescence probe with 9-wavelength excitation LED for fluorescence spectroscopy, turbidity and temperature meter and depth sensor. The taxonomic compositions and chlorophyll-a concentrations of each class were estimated automatically by analytical software with a library of spectrums of different parts. The aim was to measure the biomass and composition of phytoplankton. This is essential for monitoring water quality and ecosystem health. Chlorophyll concentration was used as an indicator of biomass.

Measuring the biomass and composition of phytoplankton is necessary to monitor water quality and ecosystem health. Chlorophyll concentration was used as an indicator of biomass. During the 1960s, in vivo sulfur measurements for chlorophyll-a concentration estimates were introduced into oceanographic communities [1]. This methodology has been valuable in improving understanding of the spatial and temporal distribution of phytoplankton biomass. However, currently in vivo sulfur measurements are not sufficient to obtain information on phytoplankton components. This is one reason why manual microscopy is widely used. Phytoplankton composition analysis has become increasingly important with the outbreak of harmful algal blooms (HABs) over the past few decades.

HABs are produced by specific phytoplankton species, and spatial and temporal amplitudes change rapidly. Therefore, to monitor phytoplankton compositions, community oceanography requires autonomous technologies to identify phytoplankton species and types. Phytoplankton groups have different pigment compositions. Thus, the group can be identified by its composition [2]. However, it is not possible to quantify the pigment composition in water directly. The optical properties of phytoplankton change due to the pigment composition. Therefore, the compositions can be estimated from the optical characteristics. By optically measuring the properties of phytoplankton, the phytoplankton group is indirectly determined. The optical properties are significantly dependent on the pigment composition; the absorption and excitation spectra of phytoplankton exist. Measurement of phytoplankton absorption spectroscopy in this area is quite challenging because of its very low absorbance and interference with other properties (i.e. absorption and scattering of CDOM: Dissolved Color Organic Matter., muscle and suspended particles). Compared with the absorption spectrum, the excitation spectrum can be easily measured. All phytoplankton, including cyanobacteria, have emission fluorescence of around 680 nm. This emission characteristic in the aquatic environment is unique. The excitation spectrum of phytoplankton can be obtained with a high S/N ratio. Therefore, excitation spectroscopy is suitable for optical extraction of phytoplankton properties. Previous scientific papers have suggested that we can classify phytoplankton groups using spectroscopy [3, 4]. We have developed an in situ multi-excitation fluorescence meter, the Multi-Exciter, that measures the excitation spectroscopy of phytoplankton. The Multi-Exciter measures nine wavelengths of the excitation spectrum. Multi-Exciter both quantifies total phytoplankton biomass (chlorophyll-a) and estimates phytoplankton composition using excitation spectroscopy. To enhance its utility, a fluorometer has been developed to be highly sensitive and to reduce the effect of interference reflected from particles suspended in water. Through these calculations phytoplankton groups are identified and quantified.

II.2 Optical design and technology

The Multi-Exciter features nine wavelength LEDs to illuminate a sample of water. The central wavelengths of the nine LEDs are 375, 400, 420, 435, 470, 505, 525, 570 and 590 nm, respectively.

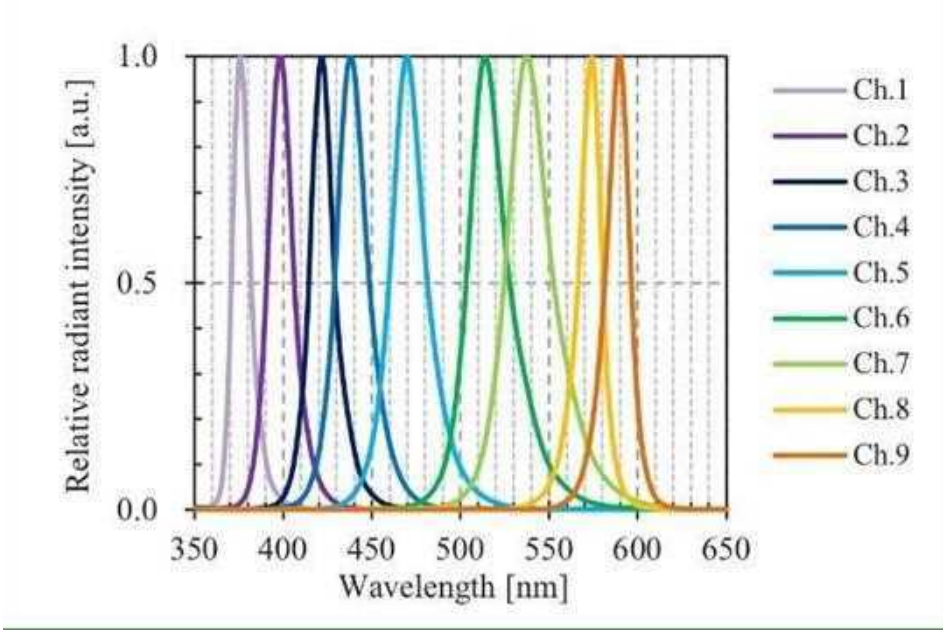

Figure 2.1 Spectral characteristics of LEDs.

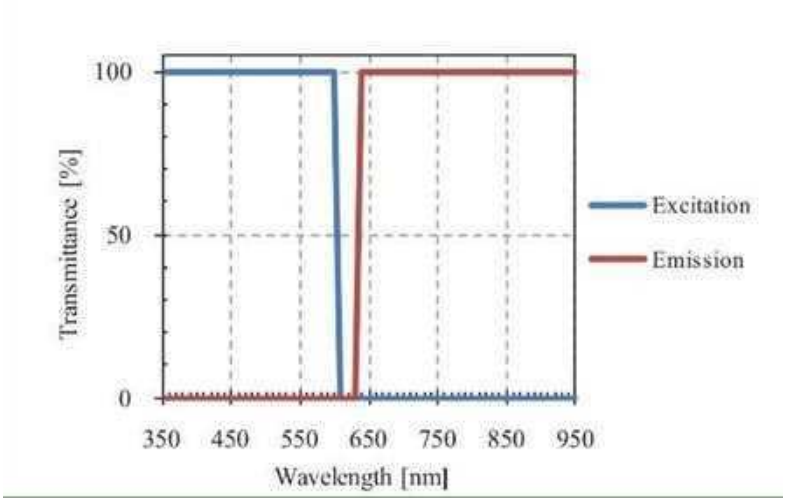

Figure 2.2 Diagram of the optical filter characteristics used in multi-size Exciters.

The excitation wavelengths of the LEDs were chosen by considering the maximum absorption of photosynthetic pigments, which occurs at wavelengths shorter than 600 nm.

The Multi-Exciter detects fluorescence signals from 630 nm to about 1000 nm, as phytoplankton typically emit red fluorescence that is distinguishable near 680 nm. Multi-Exciter's detector is a Si photodiode. Optical filters are used for excitation LEDs and photodiode detectors to intercept stray light generated through light scattering.

Multi-Exciter has temperature, depth and turbidity sensors. In addition, the instrument has a mechanical wiper to prevent biological fouling on the optical window. As a result, the device provides stable and accurate optical data during deployment time.

Figure 2.3 External appearance of multi-size Exciters.

CHAPTER III: ANALYSIS OF THE RELATIONSHIP BETWEEN CHLOROPHYLL WITH TEMPERATURE, TURBIDITY AND DISSOLVED OXYGEN CONCENTRATION IN TIEN RIVER, BEN TRE.

III.1 Introduction

This topic aims to understand the relationship between chlorophyll with temperature, turbidity and concentration depth of factors of chlorophyll concentration, temperature, turbidity and dissolved oxygen concentration on Tien river in Ben Tre province. Based on depth monitoring data of factors such as chlorophyll concentration, temperature temperature, turbidity, and dissolved oxygen concentration for 24 hours from 8:00 a.m. on January 11, 2020 to 8:00 a.m. on January 12, 2020. Data on chlorophyll, temperature, turbidity and dissolved oxygen concentrations were collected. by multi exciter (JFE, Japan) This device is set to measure every 60 minutes, 9000 samples are measured once and each sample is 0.1s apart.

III.2 Research scope

The surveyed study area at Tien River is located at geographical coordinates 10.279580 N–106.123410 E, in Ben Tre city of Ben Tre province, Vietnam (Figure 3.1). Ben Tre city is located in the sub-equatorial monsoon tropical climate, but it is outside the influence of the tropical monsoon, so the temperature is high, little variation during the year, the average annual temperature is from 26°C. – 27°C. The waters of Ben Tre belong to the area of irregular semi-diurnal tides. Most days there are 2 times of high water, 2 times of low water. Daily amplitude of tidal period

The storm surge is usually 1.5 to 2 times greater than the low tide period. The data of temperature factors, chlorophyll concentration, turbidity and dissolved oxygen concentration were obtained in this study area. , including 24 data series corresponding to 24 hours in two days 11/1/2020 and 12/1/2020

Figure 3.1: Study area (photo taken from google earth) (a) and hydrological station at Ben Tre in the southern region (b)

III.3 Some data processing methods

3.3.1 Setting the problem:

To analyze the data for 24 hours from 8:00am on January 11, 2020 to 8:00am on January 12, 2020, we must first preprocess some of the following data:

- Select data according to measurement depth, filter noise of measured values
- Methods of spectrum analysis
- Formula to calculate total spectrum and spectrum of algal elements:

• Formula to calculate total spectrum:

Specific Spectra=a_1*diatom+a_2*Green algae*a_3*Cyanbacteria

• Formula for calculating spectrum of algae elements:

3.3.2 Select data for 24 hours from 8:00am on January 11, 2020 to 8:00am on January 12, 2020:

Selective value changes according to depth:

-From the initial data recorded by the Multi exciter machine, we proceed to remove the data from 8:00 am and earlier, only taking the data from 8:00 am on January 11, 2020 to 8:00 am on January 12, 2020 and at the same time removing data with a depth of less than 0. Nearly equal values within a range are averaged.

-The data that has been filtered for noise is divided into 2 processes of dropping the machine down and pulling it up. The processing results show that the data of the drop-down process is more stable than that of the pull-up process.

Considering the opp data luc at 8 am on January 11, 2020, we have the results of the drop-down and pull-up chart.

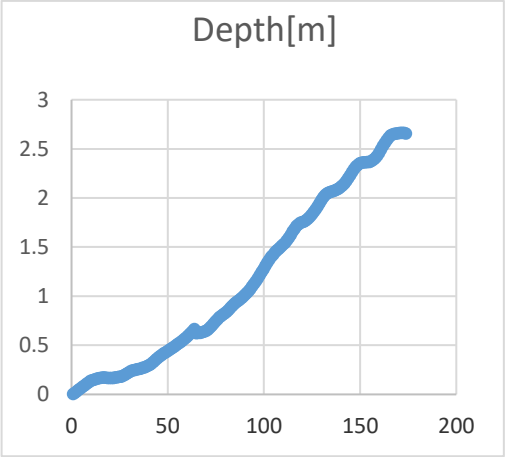

Figure 3.2: Drop-up Process

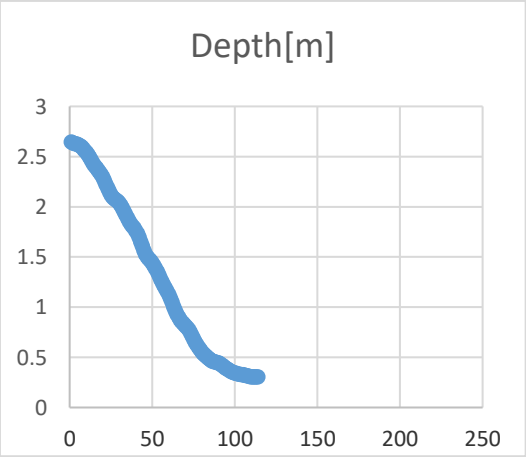

Figure 3.3: Pull-Up Process

Explanation: Dropping the device will be more stable because when we drop it, we will slowly drop it to measure the data, and when we pull it up, it will no longer measure, so we pull it up quickly, leading to instability.

3.3.3 Calculation of spectrum over time

B3.1 Tukey Blackman Spectral Method

Tukey Blackman's Theoretical Basis

Subtract a mean from the digital data {ζn}, remove and filter the trend (if necessary)

Calculation of the autocorrelation function

$$K(r\Delta t) = \frac{1}{N-r}\sum_{n=1}^{N-r} \zeta n\ \zeta n + r \quad r=0,1,2,\ldots,m, \ (1)$$

where r is called the delay number and m is the maximum delay < N. The choice of the value of m provides an optimal estimate for the autocorrelation function.

Prevent spectral leakage by using a window for auto-correlation. Such a window will activate the autocorrelation function to eliminate discontinuities at the end of the K function. There are many such windows in use. A typical window is Hanning.

$$Uhr = \frac{1}{2}(1 + \cos\frac{\pi r}{m}) \qquad (2)$$

The modified autocorrelation function becomes:

$$Kz(r\Delta t) = K(r\Delta t)\ Uhr \qquad (3)$$

Calculation steps => Write in fortran (see appendix)

Apply calculation

Input data: Consider opp data at 8:00 am on January 11, 2020 by time and by depth, including 9 wavelength data files: 375,400,420,435,470,505,525,570,590 nm.

From the data file we proceed to run in 31s from 8:00 to 8:00:31 including a total of 9 spectrums corresponding to 9 wavelengths respectively.

Outphut data: Calculation results by depth:

Bước sóng	375(nm)	400(nm)	420(nm)	435(nm)	470(nm)	505(nm)	570(nm)	590(nm)

Chlorophyll	1.573197 - 5.389925E-01 1.182077E-01 - 5.109473E-02 2.762989E-02 - 1.731285E-02 1.141351E-02 - 8.163861E-03 5.897953E-03 - 4.466563E-03 3.396752E-03 - 2.674563E-03 2.049270E-03 - 1.659538E-03 1.283351E-03 - 1.035861E-03 8.259104E-04 - 6.920566E-04 5.391521E-04 - 4.596904E-04 3.866677E-04 - 3.584472E-04 3.123833E-04 - 3.182325E-04	1.124276 - 3.873288E-01 8.475699E-02 - 3.690939E-02 1.989004E-02 - 1.264617E-02 8.260442E-03 - 5.945795E-03 4.245724E-03 - 3.262999E-03 2.421560E-03 - 1.952507E-03 1.456786E-03 - 1.189702E-03 9.228140E-04 - 7.658208E-04 5.784846E-04 - 5.023189E-04 3.845005E-04 - 3.398802E-04 2.651408E-04 - 2.563010E-04 2.213056E-04	1.138305 - 3.851027E-01 8.133619E-02 - 3.482818E-02 1.879052E-02 - 1.199991E-02 7.929196E-03 - 5.589440E-03 3.973905E-03 - 3.053442E-03 2.245826E-03 - 1.781294E-03 1.323194E-03 - 1.050486E-03 8.036256E-04 - 6.627630E-04 4.834466E-04 - 4.230934E-04 3.144231E-04 - 2.785528E-04 2.047602E-04 - 1.983291E-04 1.672861E-04	1.166019 - 3.997337E-01 8.783071E-02 - 3.769512E-02 2.068544E-02 - 1.297553E-02 8.675257E-03 - 6.288527E-03 4.654302E-03 - 3.478224E-03 2.616971E-03 - 2.038185E-03 1.557126E-03 - 1.274611E-03 1.001943E-03 - 7.671454E-04 6.152126E-04 - 5.159227E-04 4.357319E-04 - 3.595151E-04 2.997664E-04 - 2.686385E-04 2.450759E-04	3.889167E-01 - 1.335789E-01 2.921714E-02 - 1.256237E-02 6.854990E-03 - 4.355604E-03 2.976200E-03 - 2.146898E-03 1.556714E-03 - 1.149380E-03 8.587479E-04 - 6.810207E-04 5.241659E-04 - 4.304619E-04 3.351987E-04 - 2.665937E-04 2.103199E-04 - 1.705260E-04 1.335408E-04 - 1.135735E-04 9.502931E-05 - 8.723888E-05 7.923613E-05	1.023146E-01 - 2.615447E-02 3.070890E-03 - 1.322906E-03 6.333771E-04 - 3.331904E-04 2.705437E-04 - 8.133778E-05 3.056943E-05 - 2.765584E-05 4.218288E-05 - 3.896785E-06 1.273270E-05 - 6.395118E-05 2.508872E-05 - 2.543876E-05 3.801359E-05 - 3.386782E-05 2.920445E-05 - 2.711582E-05 3.391203E-05 - 3.139586E-05 2.980808E-05	7.991589E-01 - 2.119289E-01 2.714908E-02 - 1.243387E-02 9.042120E-03 - 5.364237E-03 3.720801E-03 - 2.376153E-03 2.131514E-03 - 1.340270E-03 1.352591E-03 - 9.781693E-04 7.587874E-04 - 4.668248E-04 4.032765E-04 - 2.042912E-04 1.790186E-04 - 2.934048E-05 3.514313E-05 - 2.914222E-05 4.229134E-05 - 6.959908E-05 8.670252E-05	1.736160E-01 - 5.103497E-02 8.590436E-03 - 3.851911E-03 2.318792E-03 - 1.373281E-03 9.343505E-04 - 5.554793E-04 3.747104E-04 - 2.893306E-04 2.281802E-04 - 1.751447E-04 1.202303E-04 - 6.691380E-05 5.974238E-05 - 4.052509E-05 1.822542E-05 - 3.582865E-06 1.171903E-05 - 1.106836E-05 1.078631E-06 - 1.938832E-06 2.004273E-06

	3.090516E-04 -3.359334E-04 3.527927E-04 -4.056237E-04 4.488345E-04 -5.222882E-04 5.870139E-04 -6.786757E-04 7.609490E-04 -8.750256E-04 9.846794E-04	-2.349186E-04 2.150072E-04 -2.469862E-04 2.501864E-04 -2.945217E-04 3.170408E-04 -3.813063E-04 4.152706E-04 -4.915810E-04 5.413601E-04 -6.337170E-04 7.006474E-04	-1.900589E-04 1.738805E-04 -2.091071E-04 2.091031E-04 -2.504149E-04 2.707938E-04 -3.363381E-04 3.733450E-04 -4.497867E-04 4.994943E-04 -5.899104E-04 6.548415E-04	-2.459219E-04 2.394132E-04 -2.557660E-04 2.761801E-04 -3.120962E-04 3.439377E-04 -3.971830E-04 4.445618E-04 -5.078317E-04 5.706187E-04 -6.526472E-04 7.340332E-04	-8.366047E-05 7.974521E-05 -8.762018E-05 9.182901E-05 -1.058046E-04 1.140278E-04 -1.331501E-04 1.467326E-04 -1.693160E-04 1.893987E-04 -2.187271E-04 2.430995E-04	2.678418E-05 -2.427175E-05 2.240356E-05 -2.017840E-05 1.785551E-05 -1.357163E-05 8.584118E-06 -5.922796E-06 -3.130069E-07 5.705857E-06 -1.269535E-05 1.751976E-05	6.867494E-05 -5.874964E-05 6.034251E-05 -4.055992E-05 1.841464E-05 2.376405E-05 -7.727463E-05 1.010316E-04 -1.295270E-04 1.849825E-04 -2.222181E-04 2.660021E-04	-1.051339E-06 1.694640E-06 -6.377267E-06 5.568646E-06 -1.106727E-05 1.479756E-05 -2.518960E-05 3.085111E-05 -4.065849E-05 4.722831E-05 -6.013337E-05 6.888783E-05

Table 3.1: Chlorophyll results by depth of 9 wavelengths

Result chart:

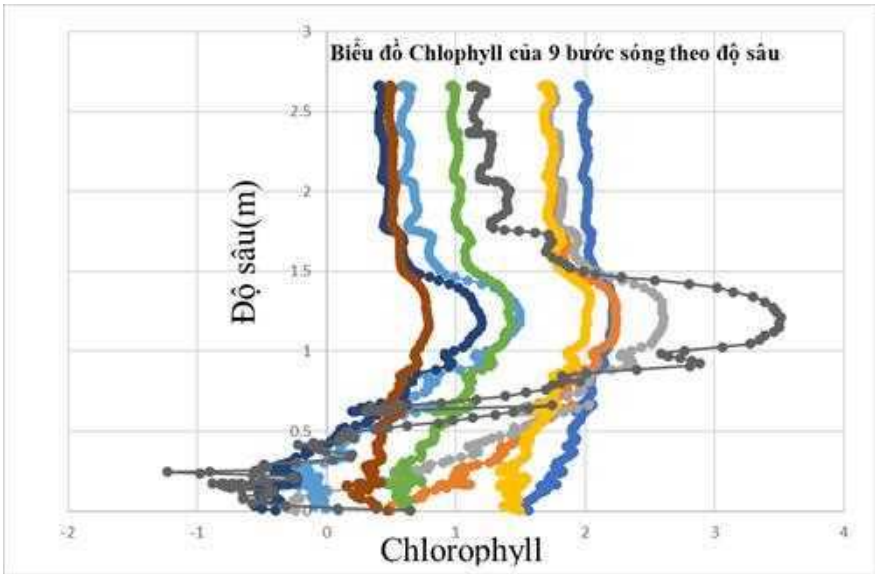

Figure 3.4 Chlorophyll plot of 9 wavelengths against depth.

3.3.4 Calculating 3 algal factors by frequency with correction factor from the machine.

Formulas for calculating spectrum by frequency:

Diatom=$0.8266\times S(\omega_1)+0.8537\times S(\omega_2)+1.1048\times S(\omega_3)+1.4103\times S(\omega_4)+1.1273\times S(\omega_5)+0.194\times S(\omega_6)+0.571\times S(\omega_7)+0.2531\times S(\omega_8)+ 0.0912\times S(\omega_9)$

Alga=$4.0861\times S(\omega_1)+4.1835\times S(\omega_2)+5.5058\times S(\omega_3)+6.3875\times S(\omega_4)+3.8234\times S(\omega_5)+0.5662\times S(\omega_6)+1.1348\times S(\omega_7)+0.6654\times S(\omega_8)+ 0.345\times S(\omega_9)$

Cyanobacteria=$0.1985\times S(\omega_1)+0.1327\times S(\omega_2)+0.1255\times S(\omega_3)+0.117\times S(\omega_4)+0.0479\times S(\omega_5)+0.0294\times S(\omega_6)+0.1656\times S(\omega_7)+0.6086\times S(\omega_8)+ 0.3445\times S(\omega_9)$

The results of the spectrum by frequency for 3 algae elements:

	Diatom	Alga	Cyanobacteria
Chlorophyll	6.106410	27.515670	1.386235
	-1.760087	-8.744761	-3.436262E-01
	6.482435E-01	2.424612	1.409171E-01
	1.940443E-02	-4.512516E-01	2.543169E-02
	2.908160E-01	8.441013E-01	7.486158E-02
	9.104863E-02	1.291340E-02	3.261693E-02
	1.761007E-01	4.612726E-01	4.702474E-02
	8.766986E-02	9.456667E-02	2.852412E-02
	1.719616E-01	3.994397E-01	4.783202E-02
	1.662969E-01	2.868038E-01	4.991100E-02
	1.951063E-01	4.205130E-01	5.551980E-02
	1.404209E-01	2.532119E-01	4.161240E-02
	9.646290E-02	2.112714E-01	2.730989E-02
	8.313330E-02	1.494020E-01	2.473944E-02
	1.468090E-01	3.040505E-01	4.211102E-02
	1.544919E-01	2.971992E-01	4.524071E-02
	1.450340E-01	2.958595E-01	4.173195E-02
	1.517955E-01	2.952273E-01	4.440396E-02
	1.845928E-01	3.719366E-01	5.322867E-02
	1.931097E-01	3.794332E-01	5.626551E-02
	1.999927E-01	4.009573E-01	5.777895E-02
	1.895265E-01	3.734096E-01	5.518869E-02
	1.917530E-01	3.839396E-01	5.540090E-02
	2.261658E-01	4.464906E-01	6.580005E-02
	2.402882E-01	4.803827E-01	6.949405E-02
	1.975480E-01	3.894351E-01	5.750416E-02
	1.959265E-01	3.926850E-01	5.661242E-02
	2.058573E-01	4.052846E-01	5.992811E-02
	2.088322E-01	4.192297E-01	6.034281E-02
	1.888547E-01	3.703407E-01	5.500561E-02
	1.927858E-01	3.886898E-01	5.565987E-02
	1.882928E-01	3.677256E-01	5.489363E-02
	2.139835E-01	4.325118E-01	6.176243E-02
	1.955608E-01	3.802550E-01	5.705381E-02
	1.822448E-01	3.715813E-01	5.248708E-02
Tần số	8.971429E-01	8.971429E-01	8.971429E-01
	1.794286	1.794286	1.794286
	2.691429	2.691429	2.691429
	3.588572	3.588572	3.588572
	4.485714	4.485714	4.485714
	5.382857	5.382857	5.382857
	6.280000	6.280000	6.280000
	7.177143	7.177143	7.177143
	8.074286	8.074286	8.074286
	8.971429	8.971429	8.971429

	9.868571	9.868571	9.868571
	10.765710	10.765710	10.765710
	11.662860	11.662860	11.662860
	12.560000	12.560000	12.560000
	13.457140	13.457140	13.457140
	14.354290	14.354290	14.354290
	15.251430	15.251430	15.251430
	16.148570	16.148570	16.148570
	17.045720	17.045720	17.045720
	17.942860	17.942860	17.942860
	18.840000	18.840000	18.840000
	19.737140	19.737140	19.737140
	20.634290	20.634290	20.634290
	21.531430	21.531430	21.531430
	22.428570	22.428570	22.428570
	23.325710	23.325710	23.325710
	24.222860	24.222860	24.222860
	25.120000	25.120000	25.120000
	26.017140	26.017140	26.017140
	26.914290	26.914290	26.914290
	27.811430	27.811430	27.811430
	28.708570	28.708570	28.708570
	29.605710	29.605710	29.605710
	30.502860	30.502860	30.502860
	31.400000	31.400000	31.400000

Diatom:

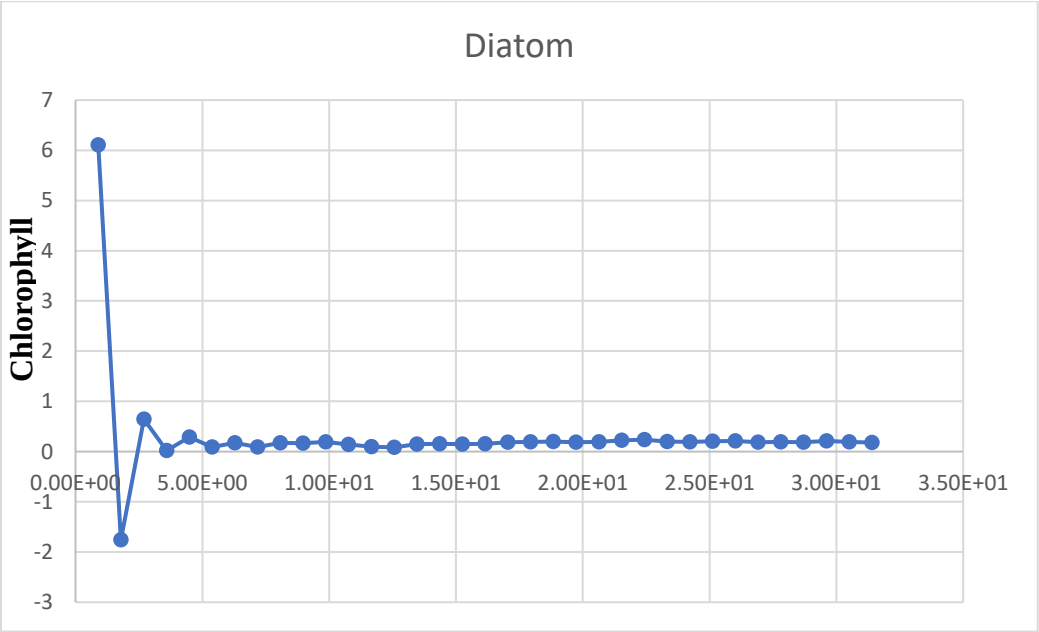

Alga:

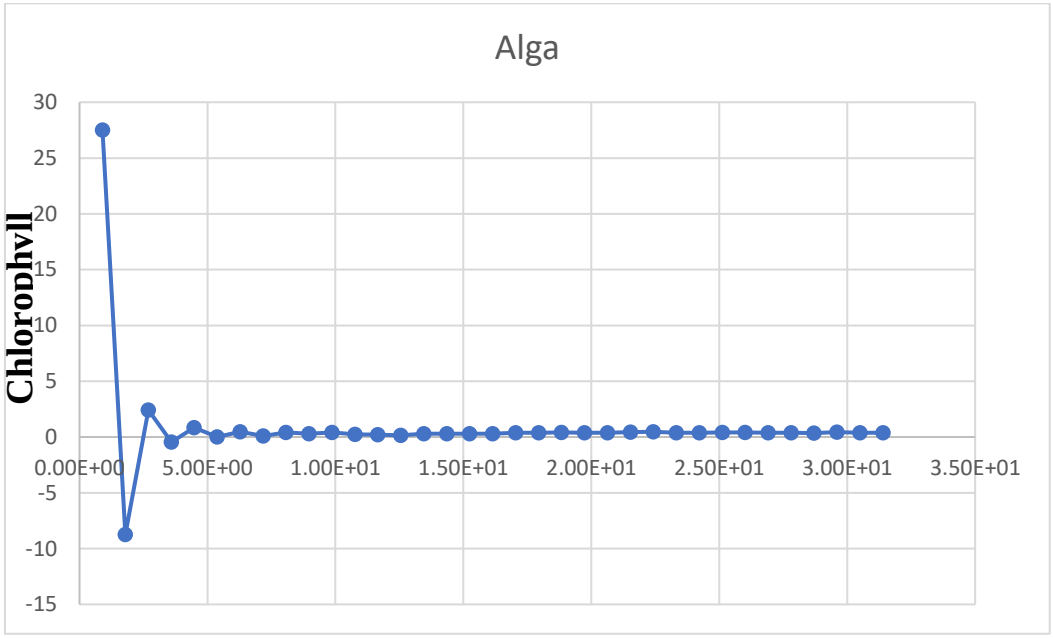
Alga
Chlorophyll
30
25
20
15
10
5
0
-5
-10
-15
0.00E+00
5.00E+00
1.00E+01
1.50E+01
2.00E+01
2.50E+01
3.00E+01
3.50E+01
Frequency

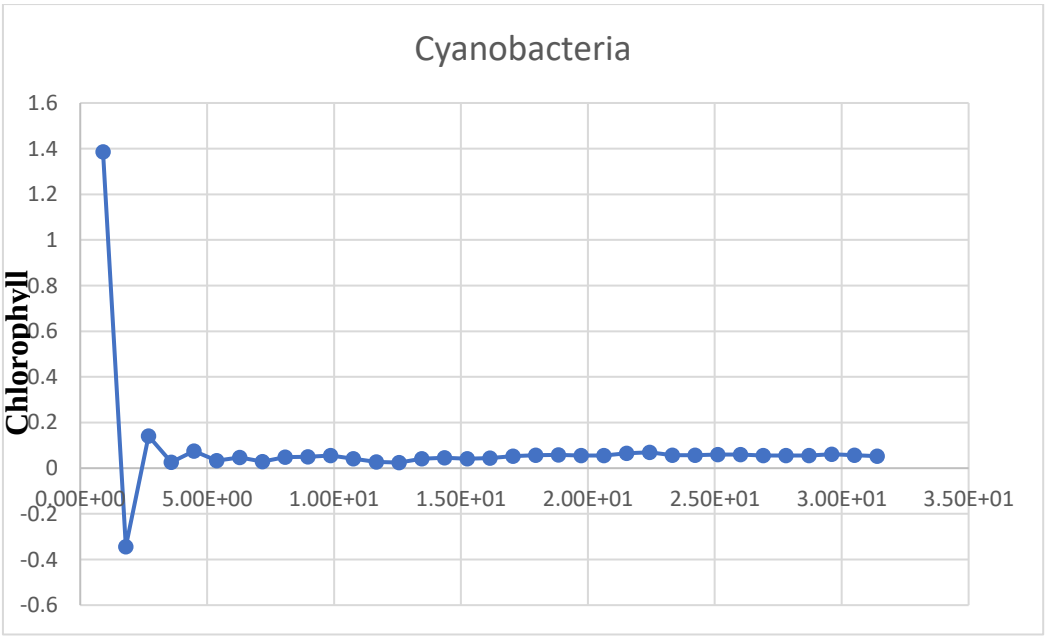
Cyanobacteria
Chlorophyll
1.6
1.4
1.2
1
0.8
0.6
0.4
0.2
0
-0.2
-0.4
-0.6
0.00E+00
5.00E+00
1.00E+01
1.50E+01
2.00E+01
2.50E+01
3.00E+01
3.50E+01
Frequency

Chlorophyll diagram of three algae:

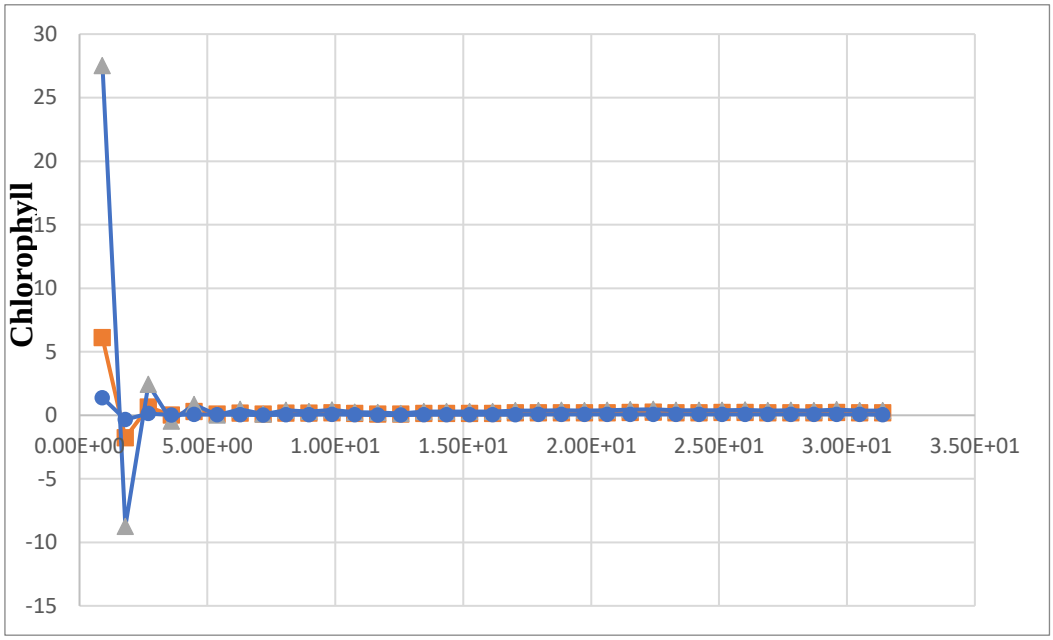

CONCLUSIONS

Chlorophyll analysis results by depth

Based on the chlorophyll graph of 9 wavelengths with depth, we see that the shape of 9 wavelengths is almost unchanged or has little or no significant change.

-From a depth of 0-1m Chlorophyll is disturbed in almost all 9 wavelengths

-From a depth of 1-1.5m Chlorophyll has a strong disturbance in all 9 wavelengths, especially Chlorophyll has a large change in 2 groups of wavelengths from 375nm-435nm and wavelengths from 470nm-590nm, with a specific wavelength of 570nm. more than the remaining 9 wavelengths.

-From a depth of 1.5m-2.7m ChlorophyII of 9 wavelengths is almost vertical

Frequency analysis results of Chlorophyll for 3 algal factors

- Diatom: Based on the chlorophyll chart according to the frequency of 3 algal factors, we can see that the shape of 3 algal elements is almost unchanged or has little insignificant change.

- Green algae (green alga) has the largest number, followed by diatoms (diatoms), cyanobacteria or blue-green algae (cyanbacteria) with the smallest number. Green algae and diatoms are both beneficial algae as sources. Food that is eaten by zooplankton.Diatoms feed the oceans, rivers and lakes and produce 50% of the air. Green algae give water a beautiful green color and provide a rich source of nutrients for all. aquatic microorganisms. Cyanobacteria are harmful algae because it has BGA-deadly hydrogen peroxide on its cell walls. The only peroxide listed by the EPA is a pesticide. After applying the peroxide, it will kill all other bacteria in the tank so there will be a horde of bugs being released which often leads to worse blooms weeks later.

Conclusion: The environment under consideration is a good environment.

REFERENCES

IN VIETNAMESE

[1]. Nguyen Chi Thoi, Doan Nhu Hai, Nguyen Thi Mai Anh, Ho Van The, Tran Thi Le Van, Phan Tan Luam, Nguyen Ngoc Lam (2015), The influence of tides on the phytoplankton community structure at the Nha Trang marine environmental monitoring station, *Collection of Marine Research,* 21(2), 188-200.

IN ENGLISH

[2]. André Fr. Bucci, Áurea Maria Ciotti, Ricardo C. G. Pollery, Renan de Carvalho1, Heitor.de Albuquerque1 and Leonardo Tomida Spalletti Simões (2012), Temporal Variablity of chlorophyll-a in the Sao Vicente Estuary, *Brazilian Journal of Oceanography*, 60(4), 485-499

[3]. Binding , Greenberg, McCullough, Watson a , Page (2018), An analysis of satellite-derived chlorophyll and algal bloom indices on Lake Winnipeg, *Journal of Great Lakes Research,* 44(3), 436-446.

[4]. Demarcq, Barlow and Shillington (2003), Climatology and Variability of Sea Surface Temperature and Surface Chlorophyll in the Benguela and Agulhas Ecosystems As Observed by Satellite Imagery, *African Journal of Marine Science*,25(1), 363-372

[5]. Đoàn Như Hải, Nguyễn Ngọc Lam, Julia Grossea, Deniz Bombar and Maren Vossa (2010), The Mekong River plume fuels nitrogen fixation and determines phytoplankton species distribution in the South China Sea during low- and high-discharge season, *the American Society of Limnology and Oceanography*, 55(4), 1668-1680.

[6]. Hubert Loisel , Vincent Vantrepotte, Sylvain Ouillon, Dat Dinh Ngoc , Marine Herrmann , Viet Tran, Xavier Mériaux , David Dessailly , Cedric Jamet , Thomas Duhaut , Huan Huu Nguyen , Thao Van Nguyen (2016), Assessment and

analysis of the chlorophyll-aconcentration variability over the Vietnamese coastal waters from the MERIS ocean color sensor, *Remote Sensing of Environment* 190, 217–232

[7]. JFE(2020), In Situ Multi-Excitation Chlorophyll Fluorometer for Phytoplankton Measurements, *Data processing and advanced instruments for river and coastal observations*,2, 59-67.

[8]. Kornkanok Kunlasak, Chanagun Chitmanat, Niwooti Whangchai, Jongkon Promya, Louis Lebel (2013), Relationships of Dissolved Oxygen with Chlorophyll-a and Phytoplankton Composition in Tilapia Ponds, *International Journal of Geosciences*, 4, 46-53.

[9]. Lars Hakanson and Jenny M. Eklund (2010), Relationships Between Chlorophyll, Salinity, Phosphorus, and Nitrogen in Lakes and Marine Areas, *Journal of Coastal Research*, 26(3), 494-498.

[10]. Mehmet Tahir Kavak and Sabri Karadogan (2011), The relationship between sea surface temperature and chlorophyll concentration of phytoplanktons in the Black Sea using remote sensing techniques, *Journal of environment biology*, 33(2), 493-498.

[11]. Nguyễn Tác An and Hoàng Trung Du (2001), Studies on Phytoplankton Pigments: Chlorophyll, Total Carotenoids and Degradation Products in Vietnamese Waters, *Proceedings of the Fourth Technical Seminar on Marine Fishery Resources Survey in the South China Sea, Area IV: Vietnamese Waters*, 233-250

[12]. Roegner, Charles Seaton and Baptista (2010), Climatic and Tidal Forcing of Hydrography and Chlorophyll Concentrations in the Columbia River Estuary, *Estuaries and Coasts*, 34(2), 281-29.

FROM INTERNET.

[13]. https://www.fondriest.com/environmental-measurements/parameters/water-quality/algae-phytoplankton-chlorophyll/#algae5

[14]. https://en.wikipedia.org/wiki/Diatom

[15]. https://diatoms.org/what-are-diatoms

[16]. https://vi.wikipedia.org/wiki/T%E1%BA%A3o_l%E1%BB%A5c

APPENDIX

CHANGES IN CHLORCHURHOLPHOLIA, TEMPERATURE, TURBIDITY AND DISSOLVED OXYGEN CONCENTRATION WITH DEPTH DURING JANUARY 11, 2020 AND JANUARY 12, 2020 IN BEN TRE

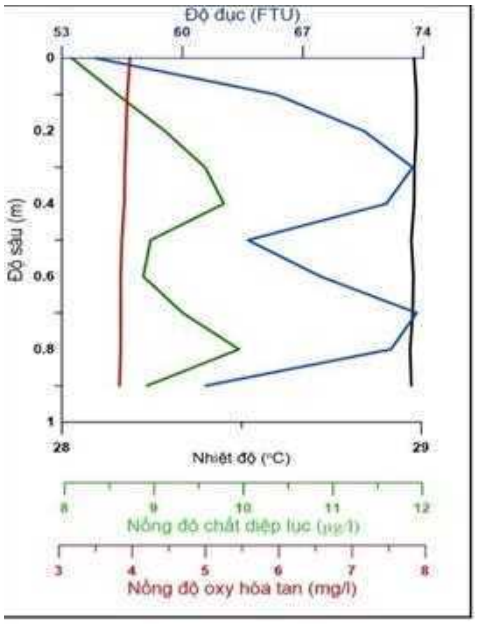

PL1: Vào lúc 10 giờ ngày 11/1/2020

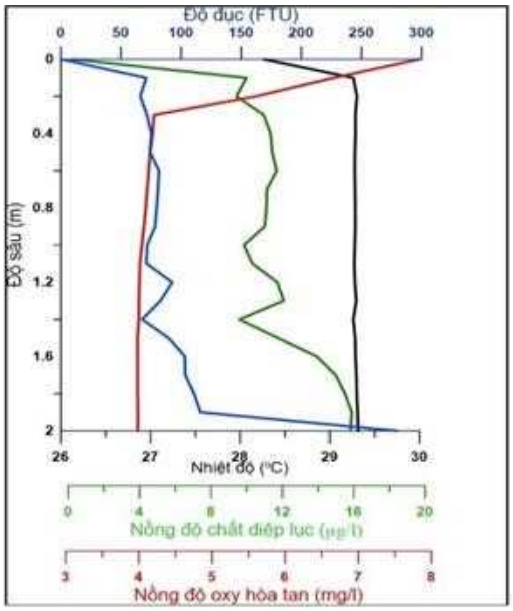

PL2: Vào lúc 11 giờ ngày 11/1/2020

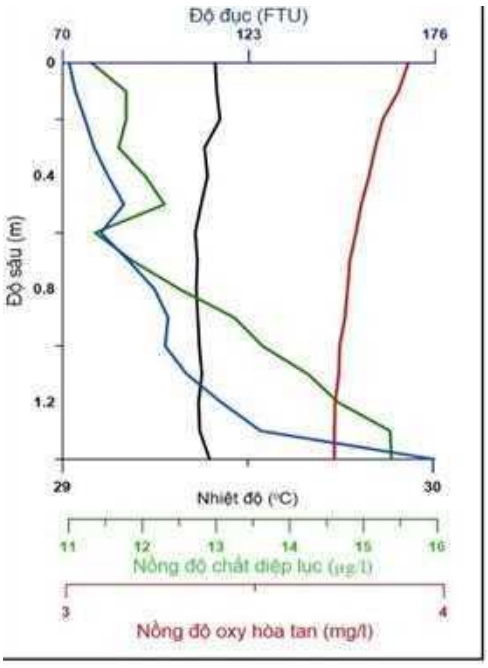

PL3: Vào lúc 13 giờ ngày 11/1/2020

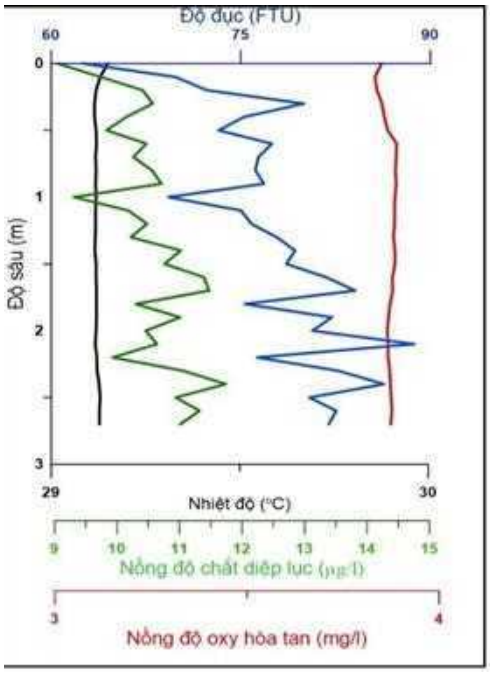

PL4: Vào lúc 14 giờ ngày 11/1/2020

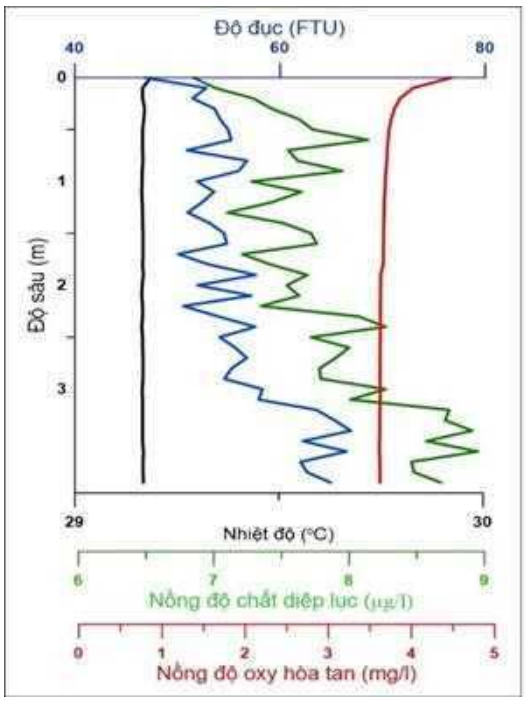

PL5: Vào lúc 15 giờ ngày 11/1/2020

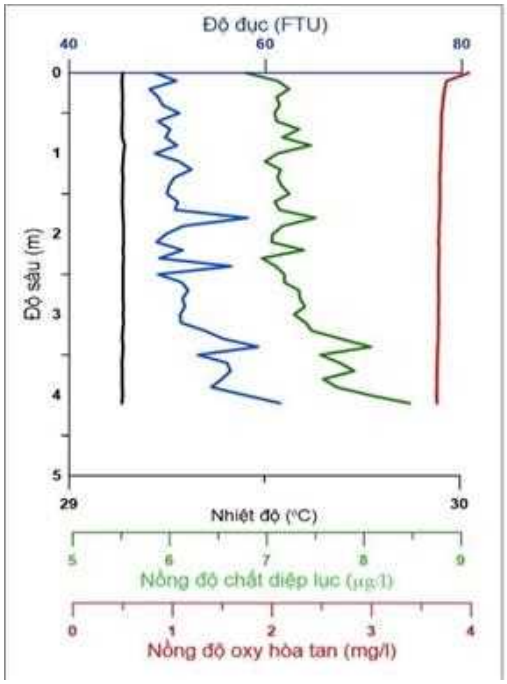

PL6: Vào lúc 16 giờ ngày 11/1/2020

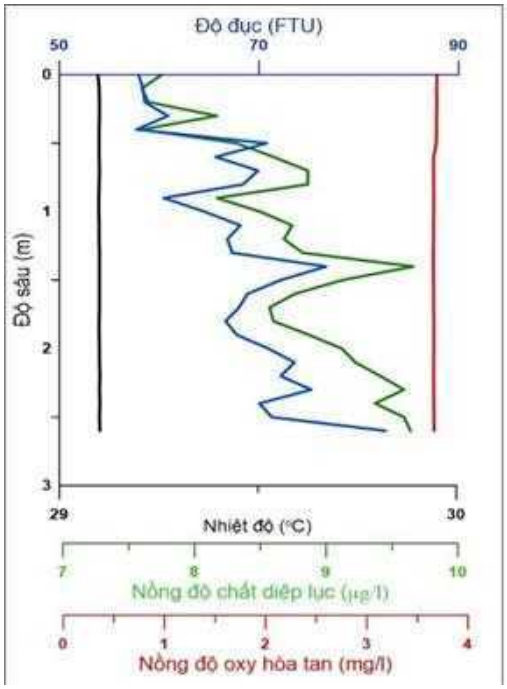

PL7: Vào lúc 17 giờ ngày 11/1/2020

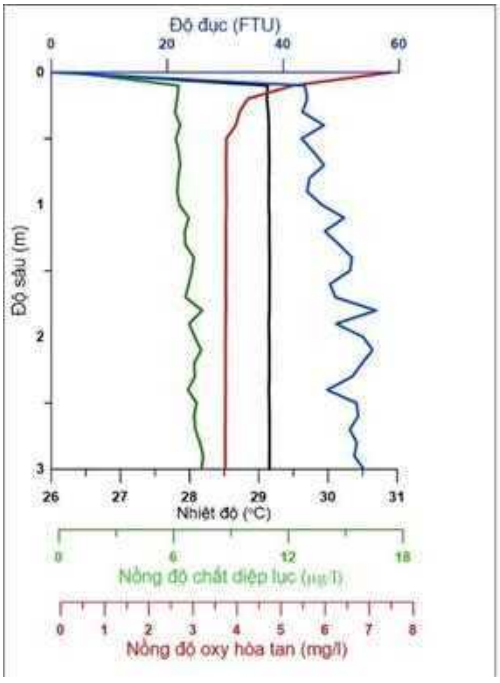

PL8: Vào lúc 18 giờ ngày 11/1/2020

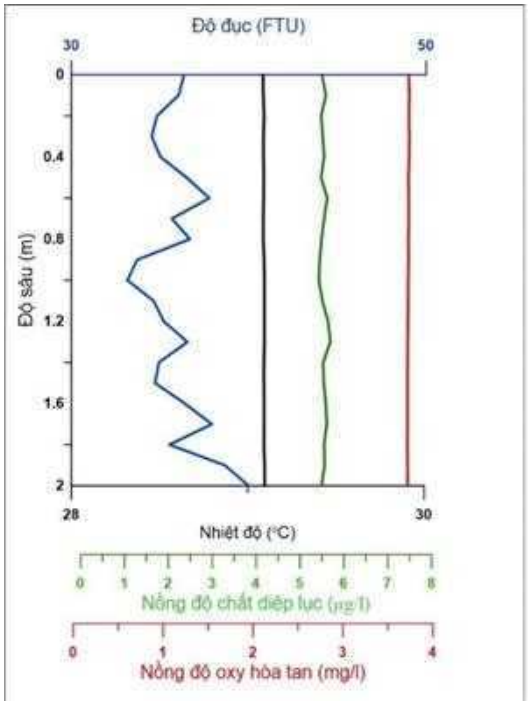

PL9: Vào lúc 20 giờ ngày 11/1/2020

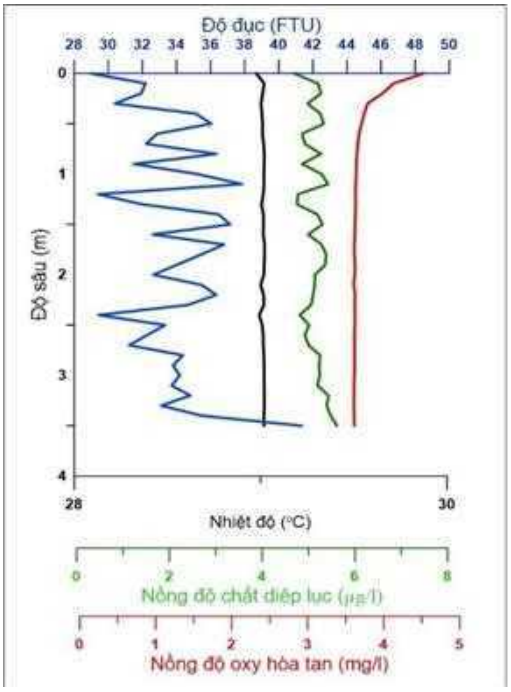

PL10: Vào lúc 21 giờ ngày 11/1/2020

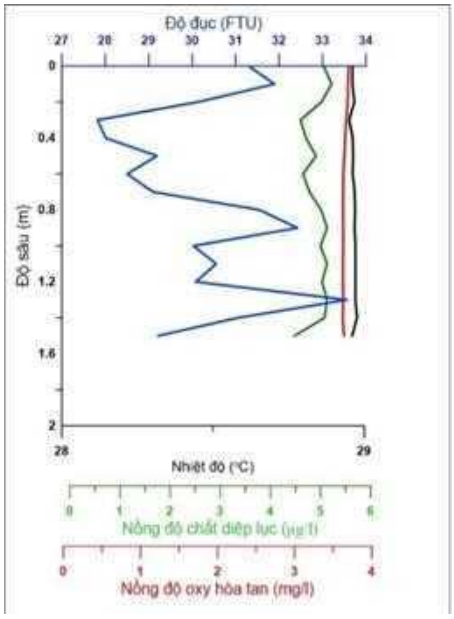

PL11: Vào lúc 22 giờ ngày 11/1/2020

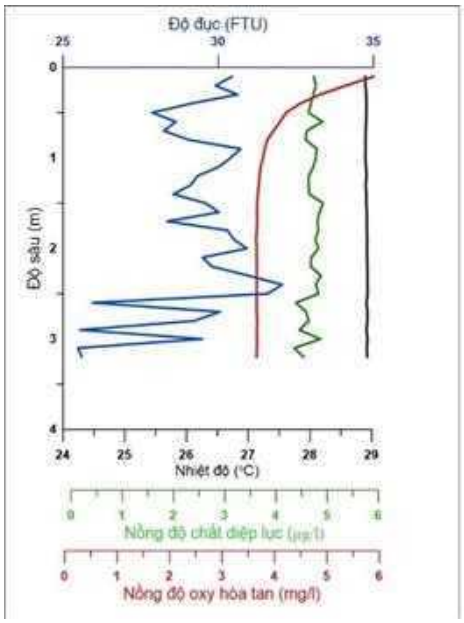

PL12: Vào lúc 23 giờ ngày 11/1/2020

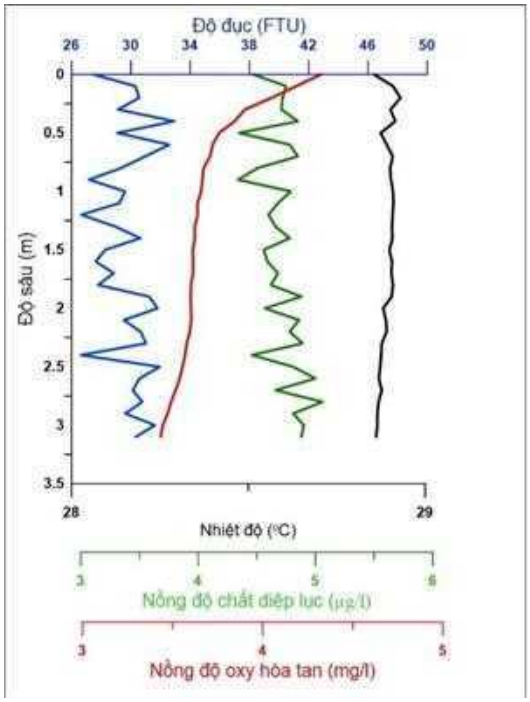

PL13: Vào lúc 00 giờ ngày 12/1/2020

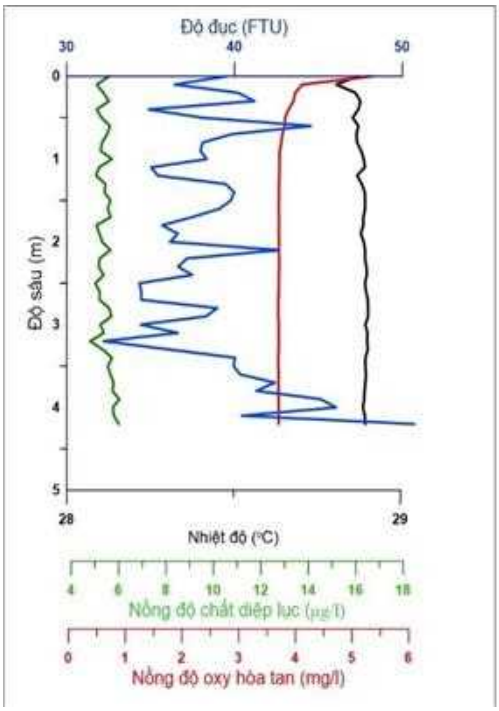

PL14: Vào lúc 2 giờ ngày 12/1/2020

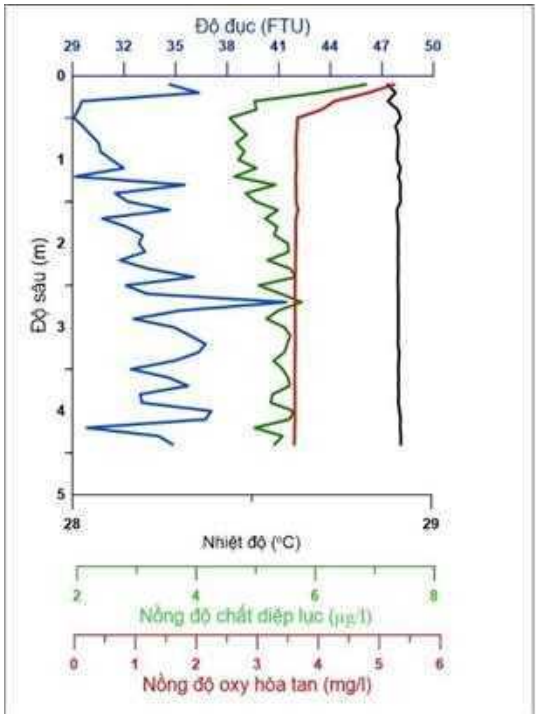

PL15: Vào lúc 3 giờ ngày 12/1/2020

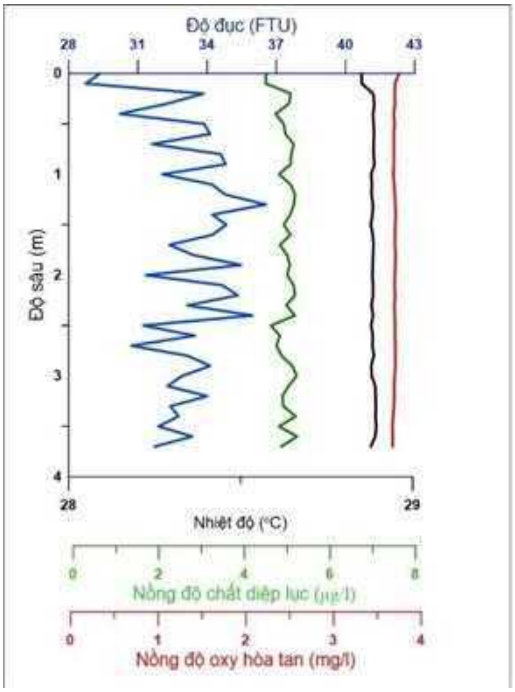

PL16: Vào lúc 4 giờ ngày 12/1/2020

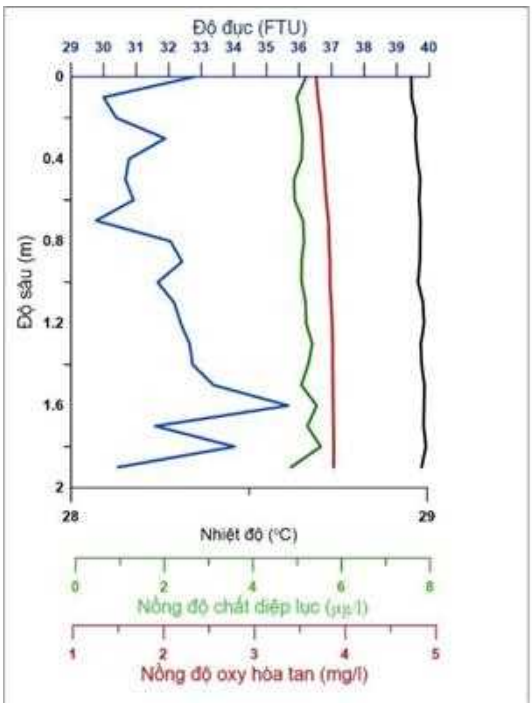

PL17: Vào lúc 5 giờ ngày 12/1/2020

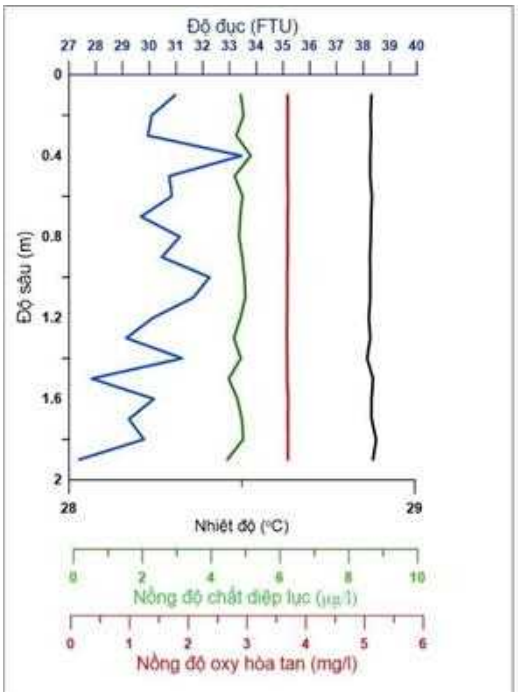

PL18: Vào lúc 6 giờ ngày 12/1/2020

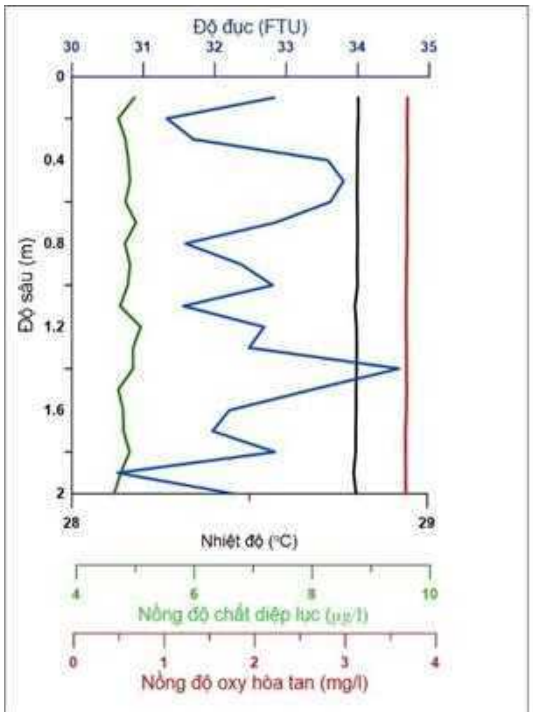

PL19: Vào lúc 7 giờ ngày 12/1/2020

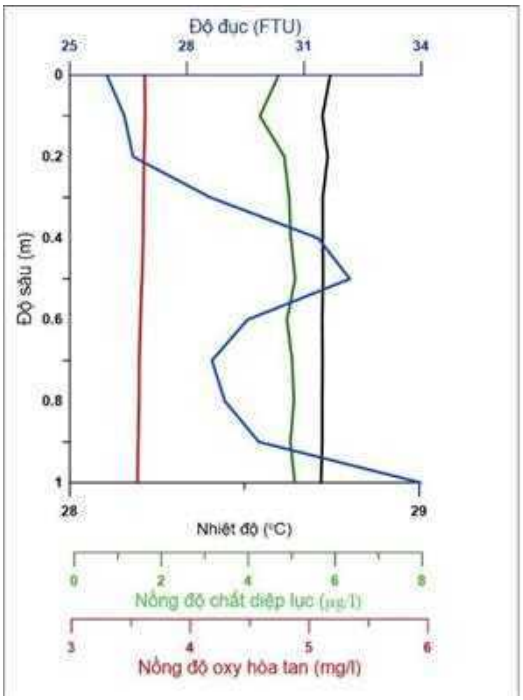

PL20: Vào lúc 8 giờ ngày 12/1/2020

UNIVERSITY OF SCIENCE,
VIETNAM NATIONAL UNIVERSITY HO CHI MINH CITY
Physics & Engineering Physics Faculty
Department of Oceanology, Meteorology and Hydrology

SOCIALIST REPUBLIC OF VIETNAM
Independence – Freedom – Happiness
--o0o---

GRADUATION THESIS COURSE REVIEWS

Student: Pham Van Phung

Title: **STUDYING THE CHLOROPHYLL CONCETRATION AT HYDROLOGICAL STATION IN CHO LACH (BEN TRE) BY USING THE MULTI-EXCITER**

Field of Oceanology, major: Meteorology

Reviewer: (Full name, Academic title, Degree) Asso. Prof., PhD. Vo Luong Hong Phuoc

Working agency: University of Science, VNU-HCM.

Role:

☒ Supervisor ☐ Reviewer

Comments and evaluation of graduation thesis:

1. **Scientific significance**:

Chlorophyll is an important element in the photosynthesis of algae and also represents phytoplankton. Chlorophyll concentration is of great importance in maintaining aquatic habitats as well as the existence of microorganisms living here.

2. **Content**:

Author contributions:

1. The author analyzed measurement data.
2. Write a program (Blackman Tukey method) to analyze the spectrum of Chlorophyll according to depth and nine different wavelengths.
3. Write a program to calculate the distribution of Diatoms, Algae, and Cyanobacteria by frequency.

The results show that the distribution of Chlorophyll concentration according to depth of small wavelengths is higher than the distribution of Chlorophyll concentration according to depth of larger wavelengths. The amount of harmful algae (Cyanobacteria) is less than the amount of beneficial algae (Diatom and Algae). This shows that the environment under consideration is an unpolluted environment.

Student's working attitude:

- In the beginning: The author worked very well and was commendable. They carefully searched for documents and performed calculations.
- After that time: The author avoided contacting the supervisor.
- Not proactive in work.
- Struggled to write and communicate effectively.

3. **Form**:

Qualified

4. **Conclusion:**

Seminar meets the requirements of a university graduation seminar.

We respectfully request the thesis grading committee to approve the thesis with points: 8

City. Ho Chi Minh, July 31st 2021

SUPERVISOR

Vo Luong Hong Phuoc

UNIVERSITY OF SCIENCE,
VIETNAM NATIONAL UNIVERSITY HO CHI MINH CITY
Physics & Engineering Physics Faculty
Department of Oceanology, Meteorology and Hydrology

SOCIALIST REPUBLIC OF VIETNAM
Independence – Freedom – Happiness
--o0o---

GRADUATION THESIS COURSE REVIEWS

Student: Pham Van Phung

Title: **STUDYING THE CHLOROPHYLL CONCETRATION AT HYDROLOGICAL STATION IN CHO LACH (BEN TRE) BY USING THE MULTI-EXCITER**

Field of Oceanology, major: Meteorology

Reviewer: (Full name, Academic title, Degree) MSc. Le Nguyen Hoa Tien

Working agency: University of Science, VNU-HCM

Role:

☐ Supervisor ☒ Reviewer

Comments and evaluation of graduation thesis:

1. **Scientific significance**:

This is a new and scientifically significant topic. The author tries very hard to convey the research content, but the theoretical writing is sometimes difficult to understand. This may come from the author's reference to English documents. I personally applaud this author's spirit, because this field is quite difficult and completely different from the major the author is studying. I think there's a lot of specialized terminology and the author certainly has to invest a lot in reading and understanding the documents.

2. **Content**:

The seminar content includes 3 chapters

Chapter I: Theoretical basis of chlorophyll

Chapter II: Method of analyzing chlorophyll concentration using Multi-Exciter device

Chapter III: Analysis of chlorophyll concentration spectrum according to frequency and spectrum of algae types

Regarding the content, I think the amount of work is quite a lot compared to a graduation seminar. The author researched a new measuring device (really new to me), and wrote a calculation program to be able to process data from this new measuring device.

3. **Form**:

Seminar includes 37 pages. The format meets the Department's presentation regulations, however the seminar also has some minor errors such as line spacing, white space, and spelling.

4. Conclusion: Does the thesis meet the requirements of a university graduation thesis?

Seminar meets the requirements of a university graduation seminar.

We respectfully request the thesis grading committee to approve the thesis with points:9.75/10

City. Ho Chi Minh, July 31st 2021

REVIEWERS

Le Nguyen Hoa Tien

HỘI NGHỊ KHOA HỌC LẦN XIII - NĂM 2022

Oceanology Meteorology Hydrology

University of Science - Ho Chi Minh City

STUDYING THE CHLOROPHYLL CONCETRATION AT HYDROLOGICAL STATION IN CHO LACH (BEN TRE) BY USING THE MULTI-EXCITER

Pham Van Phung[1], Vo Luong Hong Phuoc[1*]

[1] University of Science, Vietnam National University - Ho Chi Minh city

**vlhphuoc@hcmus.edu.vn*

I. INTRODUCTION

Scientists usually study the algae and the phytoplankton via the chlorophyll concentration.

In this study, by using the direct measurement by Multi-Exciter (JFE, Japan) (*Fig.1*), the Chlorophyll concentration were collected in depth and in frequency during 24 hours from 11/1/2020 to 12/1/2020. The survey area is at Cho Lach hydrological station (Ben Tre) (*Fig.2)*.

Fig. 2 Cho Lach hydrological station (Ben Tre)

II. METHODOLOGY

The Blackman Tukey method is used to analyze the spectrum of chlorophyll in depth and in nine different wavelength. From then, the distributions of the Diatom, Algae and Cyanobacteria according to the frequency are calculated.

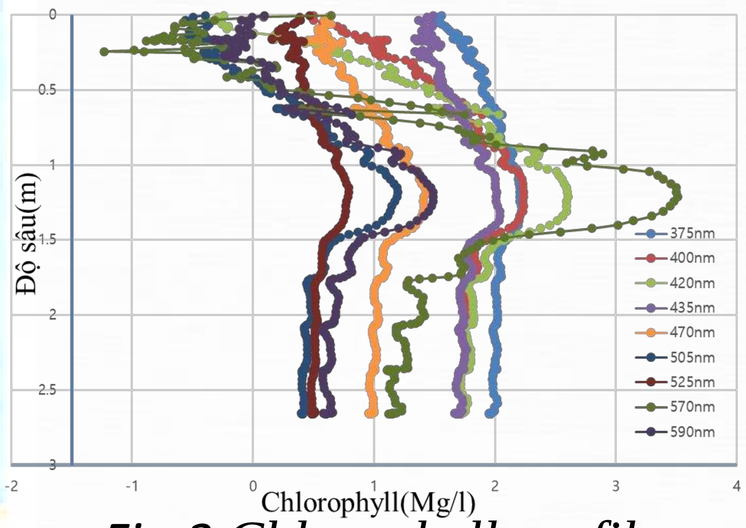

Fig.3 Chlorophyll profiles in nine wavelenghs

Fig.2 Multi-Exciter (JFE, Japan)

III. RESULTS AND CONCLUSIONS

The results show that the distribution of chlorophyll concentration profile of small wavelengths is higher than that of higher wavelengths (*Fig. 3*). The concentration of harmful algae (Cyanobacteria) is less than that of beneficial algae (Diatom and Algae). This shows that the water quality in the study site is good enough for environment.

VIETNAM NATIONAL UNVERSITY HO CHI MINH CITY
UNIVERSITY OF SCIENCE
FACULTY OF PHYSICS AND ENGINEERING PHYSICS
DEPARTMENT OF OCEANOLOGY, METEOROLOGY AND HYDROLOGY

ABSTRACTS OF GRADUATION THESIS AND GRADUATION SEMINAR (YEAR 2018)

Bachelor of Science in Oceanology

TABLE OF CONTENTS

ABSTRACTS OF GRADUATION THESIS

ABSTRACTS OF GRADUATION SEMINAR

ABSTRACTS OF GRADUATION THESIS

ANALYSIS METEOROLOGICAL DROUGHT TRENDS IN THE LONG XUYEN QUADRANGLE FOR THE PERIOD 1984-2015

Nguyen Thi Nhu Ngoc

Abstract

The study of meteorological drought trend in Long Xuyen Quadrangle in the period 1984-2015 was conducted by the meaning of evaluation drought indices: standardized precipitation index (SPI) and reconnaissance drought index (RDI) with time scales of 3, 6, 9 and 12 months.

The results show that meteorological drought in the Long Xuyen Quadrangle were complicated during the study period, occurring at three levels: drought, moderate and severe. Drought occurs in the dry season and even occurs during the rainy season. From the comparison between SPI and RDI_stwe find that the SPI has a good correlation with RDI_st. This papers reviews exciting strategy and measure for disaster preparedness and mitigation in Long Xuyen Quadrangle.

CALCULATION OF CASSAVA YIELD IN SON HOA DISTRICT, PHU YEN PROVINCE USING AQUACROP MODEL

Nguyen Ngoc Huyen

Abstract

Climate change is already affecting agricultural production, threatening the country's economic-social development. Agriculture is heavily dependent on water resources and climatic conditions. The application of the AquaCrop model was developed by the Food and Agriculture Organization (FAO) to determine cassava yield based on irrigation water from rain through reference evapotranspiration, evapotranspiration and determine water requirement. According to the results of the simulation of potential evapotranspiration, the scenario of displacing the current planting day at 22 days earlier is considered most suitable for the cassava cultivator in the province.

INITIAL STUDIES ON LOCOMOTION OF MARINE ANIMALS

Do Thi Ngoc Anh

Abstract

When moving in the sea environment, if the marine animals would like to fight against the drag of the environment, they need to have the appropriate swimming strategy. Each species of marine animals has its own specific way to minimize the energy for moving. The basic elements related to the locomotion of marine animals such as the buoyancy, Reynolds number, tail beat frequency, calculate the coefficient of the mechanics and the kinetic energy of some marine animal species have been calculated in the thesis. The results prove that when the marine animals move will create the vortex in the behind. The best swimming strategy for fish species in reality is “schooling”. When using this strategy, the vortex from moving will be used for the neighbor fish. By using the schooling scenarios in diamond shapes with many different cases (the ideal case and the damping vortex case), the results show that a large amount of energy for fish moving will be saved, probably up to 70%.

AREALIZATION OF THE PRESENT CONDITION OF EXPLOITING RESOURCES AT LONG HOA PARISH AND CAN THANH TOWN

Pham Minh Quan

Abstract

Partition of status quo of exploiting resources is to review, analyse and evaluate the exploitation activities in Long Hoa and Can Thanh towns. In order of partition the status of the coastal resource exploitation, the status quo of the resource and the exploitation status of the coastal area has been analyzed and evaluated as basis for zoning. At the same time, contradictions may occur in the exploitation of coastal resources due to overlapping management and exploitation interests are also concerned. By method of synthesis, analysis of documents combined with field survey and mapping method, the current status of coastal resource exploitation in Long Hoa and Can Thanh township has been zoned. Zoning of coastal resource exploitation is one of important steps that will serve as a basis for function partition of coastal zone, support to planning and management for coastal socio-economic development.

INTIAL BUILDING A PROGRAM TO CALCULATE WAVE PARAMETERS BASED ON NAVIER-STOKES EQUATION

Doan Thi Thu Cuc

Abstract

The aim of this study is to build a program to calculate wave parameters in deep water based on Navier-Stokes equation (tide and marine structures are not mentioned). The numerical method for solving Navier-Stokes is based on study of Chorin (1968). Stokes 5th order wave theory is applied for intial conditions and boundary conditions.

CLIMATE CHANGE AND A NUMBER OF TAY NINH CLIMATE CHANGES IN TREND THE CLIMATE CHANGE (FROM 2005 TO 2016)

Huynh Thi Chau Phi

Abstract

The content of this thesis topic is the presentation of climate change and climate change in Tay Ninh in the years 2005-2016. Regarding climate change, the concepts, causes such as causes as natural causes and human causes, climate change have caused bad impacts on water resources, human being,… all over the country, global climate change situation, in Vietnam. On climate change in Tay Ninh, state the climatic conditions and characteristics of Tay Ninh climate and finally talk about the trend of some climatic factors Tay Ninh is temperature, precipitation, moisture and evaporation in 2005 to 2016. It shows some changes in Tay Ninh climate, there are unstable changes, but not significant.

USING OF REMOTE SENSING AND GIS TO SURVEY THE VEGETATION COVER VARIATION AT CU LAO DUNG'S MANGROVE FORESTS OF SOC TRANG PROVINCE

Nguyen Thi Duyen

Abstract

Remote sensing and GIS was used to monitor the variation of the vegetation cover at Cu Lao Dung mangrove forest Soc Trang province from 1989 to 2016. The result showed that the mangrove forest have tended to expand to the sea. The mangrove forest developed strongly in the Southwest, but they grew up slowly in Northeast. Besides, they encroached upon the sea with an unstable speed in the central area. In the 1989 – 2016 period, the mangrove forest extended stronger than the 2002 – 2016 period. Thick and thin forest were formed a forest range along the Southeast coast of Cu Lao Dung.

CALCULATIONS OF WIND VELOCITY PROFILE AND RELATIONSHIP BETWEEN WIND AND SURFACE WAVE

Nguyen Duy Yen Duyen

Abstract

Based on data from wind speed at three height layers of 12, 17 and 25m in Binh Thuan, the wind velocity profiles can be calculated according to exponential law and logarithmic law. Weibull distribution function is applied for the distribution of wind velocities at Vung Ro - Phu Yen and Bach Ho - Vung Tau. The results show that by applying two different laws, the calculations of wind speed at different levels can give quite good agreement. If the wind data is numerous enough, the velocity distribution is approaching to Weibull distribution. Three distribution methods including SPM, JONSWAP and the Russian Federation method (RF) are used for calculating the wind waves at offshore zone (Bach Ho-Vung Tau) and in coastal area (Vung Ro - Phu Yen). The results prove that calculated data from all three methods give good correlation with measured data in Bach Ho offshore, but not suitable relations with measured data in coastal areas in Phu Yen.

CALCULATE THE WATER REQUIREMENTS FOR RICE IN CHO MOI DISTRICT, AN GIANG PROVINCE

Phan Thi Phuong Linh

Abstract

The study applied CROPWAT 8.0 model to calculate the water requirement for rice in which meteorological data from An Giang Hydro-Meteorological Forecasting Center were used to calculate reference evapotranspiration ETo. This study also used information about rice planting season at Cho Moi district, value of crop coefficient Kc in accordance to a research of Can Tho University and FAO's permanent crops and arable land to calculate the water requirements of rice in Summer-Autumn, Winter-Spring and Autumn-Winter.

The results in Winter-Spring and Autumn-Winter crops are in line with National Standard TCVN 8641: 2011. This result reflects the actual water requirement of the rice, from that provide references to generate a suitable and beneficial watering schedule.

THE IMPACT OF CLIMATE CHANGE ON MONSOON ACTIVITY TO THE SOUTH IN THE PERIOD 1984-2017

Nguyen Thi Nhut Linh

Abstract

The monsoon system adversely affects the weather and climate in VietNam, in which the South is mostly affected by the summer monsoon.Using statistical methods and data analysis helps us better understand changes of the monsoon in the period of El-Nino, La-Nina leading to the change of rain mode, temperature, sunshine, evaporation in the Southern region. The operation of Southwest monsoons starts early and ends late, which leads to longer monsoon seasons. In some years, there is a loss of crop as a result of the shortage of rain due to the late monsoon. Increasing rainfall in the rainy season causes floods and landslides in many places while it falls in dry seasons, which brings about severe droughts leading to saline intrusion, which seriously affects the provinces in the Mekong River delta. The temperature tends to rise up due to the global warming, the low temperature increases faster than the supreme temperature. The number of intensive storms has tended to move to the South.

ANALYSIS AND ASSESSMENT THE SEA SURFACE TEMPERATURE VARIABILITY IN THE SOUTH CHINA SEA USING MODIS IMAGE

Che Thi Bich Van

Abstract

The seasonal and annual variability of the sea surface temperature (SST) in the South China Sea was studied based on MODIS image on the NASA's Aqua satellite– launched in May-2002. From December-2016 to November-2017, there is a variability of the sea surface temperature between the winter (12 – 1 – 2) and the summer (6 – 7 – 8). In the winter, there is the presence of the cooling water tongue along with the southern Vietnam Coastal Zone. In the summer, the sea surface temperature field is nearly uniform in the whole South China Sea. In the period 2003– 2017, the annual average of the sea surface temperature is increasing after El Niño period 2009/2010. From the analysis, although the sea surface temperature is relative to the activity of the typhoon DAMREY (November-2017), it is not a primary factor affecting the intensity and tracks typhoon DAMREY.

HYDRODYNAMIC AND SEDIMENT TRANSPORT MODEL IN THE COASTAL ZONE

Le Duy Tu

Abstract

Along with the development of the computer technology. The hydrodynamic model is increasingly being developed and applied. This used the hydrodynamic model to calculated the flow field and the sediment transport, by the Alter rating Direction Implicit method (ADI), tri-diagonal matrix equations. The sediment transport model was compared with the mathematical solution and applied to calculating in the Dong Tranh – estuary area Can Gio, HCMC.

EFFECTS OF CLIMATE CHANGE AND URBAN HEAT ISLAND IN HO CHI MINH CITY

Huynh Thi Ngot

Abstract

Based on the results of calculating and analyzing the effects of climate change and the Urban Heat Island effect in Ho Chi Minh City, the temperature in Ho Chi Minh City is higher than in other provinces. The surrounding areas such as Dong Nai, Tay Ninh, Ba Ria - Vung Tau, Long An, Binh Phuoc ... especially in recent years, most clearly at night. The results are well described with actual observations. From the results of this study, we can see the trend of temperature rise in the coming years. Thereby, we will be better aware of the climate that we are living and find solutions that are appropriate and timely in responding to the complex climate change as today to protect our living environment.

STUDY ON CLIMATE CHANGE TRENDS IN BINH PHUOC PROVINCE

Nguyen Van Tung

Abstract

The thesis analyzes and evaluates some meteorological factors of Binh Phuoc province from 1984 to 2015, combining calculating the indexes affecting Binh Phuoc through the data of 2 meteorological stations of General Director of Dong Xoai and Phuoc Long in the context of climate change. The results show that the trend of annual average temperature increases over the years, the trend of rainfall is not changing according to the rules. In addition, the phenomenon of drought increasingly tends to affect the area. Climate change is seriously affecting the water resources, economy, life and culture of people in Binh Phuoc province.

STUDY AND THE PREPARATION FOR WAVE FORECAST IN THE SOUTH OF VIETNAM SEA AREA

Nguyen Le Thanh Tuyen

Abstract

This thesis analyzes evaluate module SW (Spectra Waves – module used to calculate the wave field in coastal water of MIKE 21 model) to calculate wave in the South of Vietnam Sea area, including the area of Dai Hung oil petroleum technical service oil-drilling equipment. The results show the highest wave height, mean wave height and minimum wave height will be provided for evaluation purposes, observing and forecasting the characteristics of the wind in this area. In addition, there should be sustainable, long-term, low-cost and cost-effective options. It is necessary to build and complete meteorological and hydrographic stations in order to accurately and timely forecast the climate situation in the region.

CALCULATING GREEN HOUSE OF ROASTED BEANS IN THE MEKONG RIVER DELTA

Pham Duc An

Abstract

Greenhouse gas emission calculation is the first step in reducing emissions that pollute the environment. Using the Agriculture and Land Use National Greenhouse Gas Inventory software (ALU) to calculate and estimate greenhouse gases because of burning of the straw. According to calculations, the amount of straw burned accounted for 54-98% of the total straw harvested at the Mekong Delta in 2015 emitted more than 900 thousand tons of CO_2 equivalent to 0,61% of total GHG emissions in the country. It is predicted that by 2030, with a yield of 23-24 million tons, an area about 3,8-3,9 million ha and a reduction in the burning rate of 50-90%, the GHG emissions will fluctuate from 450-800 thousand tons of CO_2 equivalent.

ANLYSIS OF THE WIND FIELD AND THE VORTICITY FIELD IN PREDICTING THE FORMATION AND THE ACTIVITY OF TROPICAL STORM ON THE SOUTH CHINA SEA AND WEST PACIFIC OCEAN

Bui Thi Kieu My

Abstract

In 2017, the number of tropical storm, typhoons in the South China Sea reached a record of 16 tropical cyclones and 4 tropical depressions, and even in the first few months of 2018, tropical cyclones have appeared in the South China Sea and West Pacific, even super typhoon with very unusual activity. Typhoons are devastating natural disaster, killing many people every year and causing great damage. The collection and analysis of wind fields, vortex fields, and some other dynamic fields of these storms have shown variations in these factors through the stages of formation and operation of the vortex as the different characteristics between the storms. From this we can give an early assessment of storm formation and operation in order to prevent and mitigate damage caused by storms.

THE 2017 TYPHOON SEASON AND CHARACTERISTICS OF SOME SPECIAL TYPHOONS

Nguyen Ho Phuong Trinh

Abstract

This study presents the characteristics of tropical cyclones in the western North Pacific, the East Sea and Vietnam during 1988 – 2017. In addition, this study analyzes characteristics of the 2017 typhoon season in the East Sea. The results show that the number of typhoons in the end of year 2017 is higher than the annual average. Finally, this study presents the characteristics of Typhoon Doksuri (September, 2017), Typhoon Damrey (November, 2017) and Tembin (December, 2017).

APPLYING GIS TO DIRECT RUNOFF ESTIMATION FOR SUPPORTING FLOOD PREDICTION IN TUY AN DISTRICT, PHU YEN PROVINCE

Pham Thi Ngoc Huong

Abstract

It is recorded that Tuy An district (Phu Yen province) is strongly affected by flash flood every year. In order to prevent the hazard of flash flood, combination of GIS and SCS - CN method are applied to calculate direct runoff for providing flood prediction with initial data in Tuy An district. The SCS - CN method evaluates the impact of land cover, soil type, antecedent moisture condition and rainfall on direct runoff volume. The result shows direct runoff maps with different condition of antecedent moisture and rainfall period. Areas with high direct runoff relatively match wih high risk of flash flood region in the Ky Lo river basin, Tuy An district, where suffers from annual severe floods.

APPLICATION OF THE MODIS IMAGES TO ASSESS DRYNESS INTENSITY IN THE VIETNAM SOUTHERN REGION BASED ON TVDI

Phan Thi Bich Ngoc

Abstract

The topic studied application of the MODIS images to assess dryness intensity in the Vietnam Southern Region based on Temperature Vegetation Dryness Index (TVDI). The index was calculated on the basis of the difference between the surface temperature at each pixel and the lowest surface temperature for each value of Normalized Difference Vegetation Index (NDVI). Land Surface Temperature (LST) and Normalized Difference Vegetation Index (NDVI) data were obtained from LST and NDVI products of the MODIS images in dry seasons in 2014 – 2015, 2015 – 2016 and 2016 – 2017. The result showed that the TVDI index reflected approximately dry intensity in the study area and was the potentiality to evaluate and monitor dry intensity in a large area combined with MODIS images.

MODELING OF PHOSPHORUS TRANSPORT IN STREAM USING STELLA

Vo Thi Nhu Hao

Abstract

Phosphorus is one of pollutant that effect water quality in stream system, especially eutrophication due to hight phosphorus accumulattion in the water. Therefore, phosphorus transport in stream is concerned by researchers. STELLA is applied to develop phosphorus transport modelling under simple condition which shows the spatial and temporal variations of phosphorus concentrations in stream system in order to determine influence of wastewater treatment plant on the stream heathy. To achieve in stream total phosphorus concentration below 7.0 mg/l at the point of concern, effluence concentration of wastewater treatment plant must be reduced from 2.2 mg/l to 1.0 mg/l and flow rate of the plant is at average level of 69,652 m^3/day. Therefore, phosphorus transport in stream system is a necessary scientific foundation that can answer a number of management and policy questions and assess the vulnerability of impaired streams.

ANALYSIS OF TROPICAL CYCLONE ACTIVITY IN THE "BIEN DONG" AFFECTING THE WEATHER IN HO CHI MINH CITY

Vo Ngoc Thach

Abstract

The objective of this topic is to determine the relative position of the tropical cyclone affecting the weather in Ho Chi Minh city. By analysis methods, statistic data storm and rain, 2008 to 2016, in latitude and longtitude. The results were recorded in 4 areas, where is tropical cyclone activity will affect the weather in Ho Chi Minh city. In addition, the direction of the tropical cyclone moving into these 4 areas is determined. There is a basic step to serve to forecast the effects of storm to any area to take timely measure to prevent storm.

SEASONAL SEA LEVEL VARIATIONS IN THE MEKONG DELTA

Tran Ngoc Hau

Abstract

The objective of the research is to study seasonal fluctuations of sea levels in the Mekong Delta. The spatial and temporal variations of the water level in this area are described from daily mean sea level, mean high water and mean low water data sets at Ganh Hao, Nam Can and Song Doc stations for the period 1996 – 2008. The results show that there is no significant different about the times of occurring annually maximum and minimum mean sea levels. The lowest sea levels are predominantly in June and the highest water levels are mainly in November. The average annual range between maximum and minimum values decreases from the East Sea to the West Sea in the Mekong Delta with mean values of 51, 45 and 32 cm, respectively. At Ganh Hao, the maximum and minimum water levels are always higher than 95 cm and lower than -150 cm, respectively.

INITIALLY CALCULATED THE WAVE HEIGHT DISSIPATION IN MANGROVE FOREST BY USING THE DELFT3D MODEL

Truong Thi Nhu Hao

Abstract

Delft3D model is used to calculate wave propagation in mangrove forests. The research method is based on the changes of Collins bottom coefficient (1972) and the Chezy roughness coefficient (Baptis, 2005). They depend on the characteristics of the mangrove forest as density, tree height, trunk diameter and hydrodynamic parameter. The results show that the water level and mangrove density greatly affect the wave dissipation in the mangrove forest. In particular, with 1.0m initial wave height, 1.0 tree/ m^2 forest density and 1.0m water level, significant wave height is 0.92m (8% reduction), 0.21m (21% reduction), 0.71m (29% reduction), 0.65m (35% reduction), 0.56m (44% reduction), 0.43m (57% reduction), 0.29m (71% reduction), 0.22m (78% reduction), 0.18m (82% reduction) and 0.15m (85% reduction) away from the edge forest 10m, 100m, 200m, 300m, 400m and 500m respectively.

STUDY OF THE CHARACTERISTICS HEAVY RAIN IN HO CHI MINH CITY PERIOD OF 1980 TO 2015

Le Thi Diem

Abstract

The phenomenon of heavy rains led to flooding is one of the issues in the world in General and Vietnam as well as Ho Chi Minh City in particular. In recent years, in Ho Chi Minh City, heavy rains caused much damage to the human, physical and ecological environment. In this thesis, the author has collected and processed rainy day observed data at rain gauge stations in the county People in the locality Ho Chi Minh City during the 1980-2015 and precipitation data at the interval of 60 minutes at the Tan Son Hoa stations in the period 2008-2016. Results of analysis showed that the precipitation tends to increase and the uneven distribution of rainfall, concentrated in the Central districts and part of Cu Chi district and tend to concentrate after 16 hours. Cause heavy rains often combine multiple weather patterns caused or the combination of the strong southwest monsoon.

ABSTRACTS OF GRADUATION SEMINAR

ASSESSMENT OF DRYNESS INDEX IN BINH THUAN PROVINCE FROM 2002 TO 2018 USING REMOTE SENSING AND GIS

Pham Thu Thao Nguyen

Abstract

In Vietnam, drought is natural disasters which caused the third severest damage after floods, storms and tends to occur more severe, more difficult to control due to climate change. Particularly in BinhThuan province, drought has had a profound effect on the life and economy of the region. The report presents the calculation process to determine the TVDI index based on the NDVI index and surface temperatures of the LST from 2002 to 2018. The objective of this study was to presents results of drought risk evaluation multispectral images in BinhThuan province. The results obtained in the study showed that Binh Thuan has the driest level in 2005 and 2016 compared to other years, can be used to create the drought risk map and to minimize the damage caused by drought.

ESTIMATE OF RAINFALL TRENDS IN THE LONG XUYEN QUADRANGLE AREA USING NON-PARAMETRIC TEST

Nguyen Thi Hong Tham

Abstract

This study presents the evaluation of rainfall trends in the Long Xuyen Quadrangle in the period 1984-2015. This study is constructed based on the non-parametric Mann-Kendall test with the Sen slope.

The results show that in the period 1984-2015, the trend increases in the dry season and decreases in the rainy season with slightly increases or decreases in some stations in the region. However, the trend of rainfall significantly decreases at Tri Ton and Ha Tien stations. The main cause of uneven variation precipitation in the area may be created by location at the stations and impact of climate change.

DETERMINE WATER REQUIREMENT FOR RICE CROPS IN THE DONG THAP MUOI AREA

Nguyen Thi Cam Mi

Abstract

This research for the AquaCrop model for the calculate water requirement for Winter-spring, Summer-autumn and Autumn-winter in the Dong Thap Muoi area, while determine the amount of reference crop evapotranspiration, crop evapotranspiration under the standard conditions.

The results showed that annual total reference crop evapotranspiration was estimated at 1600 mm, the highest value of ETo of 170.7 mm was observed in the middle stage of the Winter-spring in Cao Lanh, the lowest value 20.0 mm was observer in the soil preparation stage in Cao Lanh, Moc Hoa and My Tho. Crop evapotranspiration under the standard conditions highest on the middle stage of the Fall-winter in Moc Hoa 458.3 mm and the lowest was the Winter-spring all three stations 20.0-21.0 mm.

THE CORRELATION OF CONVECTIVE INSTABILITY INDICES DURING TYPHOONS

Nguyen Thi Xuan Tham

Abstract

The seminar collected data about lifetime of typhoons in Vietnam during 1998 – 2017. The study used RAOB to calculate the value of convective instability indices. Input data are the sounding data of three stations (Lang Station – Hanoi (48820), Da Nang Station (48855) and Tan Son Nhat Station – Ho Chi Minh City). Five convective instability indices K, SWEAT, CAPE, CIN and BRN are used to analysed. The results show that most of indices can represent the atmospheric instabilities, except the SWEAT index.

APPLICATION OF REMOTE SENSING AND GIS TO MONITOR URBANIZATION IN HO CHI MINH CITY

Le Thi Pha Mi

Abstract

Topic used Landsat satellite image processed based on ENVI and ArcGIS software to set up the urban space distribution map and to monitor change over time and space in Ho Chi Minh City through impervious surface. Besides, the topic also analyzed the relationship between urban and surface temperature and NDVI to assess better urban development process. The results showed that urban tended to widen from city center to suburban and tended to spread to the north, the north east and the north west of the city, focused particularly on main roads in suburban areas. In addition, the topic found the negative relationship between urban and NDVI and the positive relationship between urban and surface temperature.

SHORELINE CHANGE IN NGOC HIEN DISTRICT, CA MAU PROVINCE USING REMOTE SENSING AND GIS

Pham Minh Triet

Abstract

Shoreline change was increasingly complicated in Ngoc Hien, Ca Mau province impact on coastal forest, ecosystem and people. So the shoreline study was very necessary. The topic used ENVI and ArcGIS software to analyze qualitative and quantitative change from 1988 to 2018 at the east coast of Ngoc Hien district. Then, the DSAS tool built into ArcGIS is also used to analyze statistical values. This seminar is based on the east coast of Ngoc Hien district. The results showed that the shoreline was strongly eroded with the average erosion rate in Tam Giang Tay commune; Tan An Tay commune and Vien An Dong commune, Vien An commune respectively 34 m/yr; 29 m/yr and 20 m/yr in this period. there was erosion and accretion process with average rate of 16 m/yr and 12 m/yr respectively in Dat Mui commune.

TROPICAL STORMS – USNSEASONAL STORMS IN THE EAST SEA IN 1988 - 2017 PERIOD

Kieu Huu Toan Thang

Abstract

Tropical storms are one of the natural disasters that always threaten the life and economic, social and defense activities of our country. When storms are active and affect the mainland, beside strong wind and heavy rain, wave and storm surges threaten socio-economic structures and infrastructure in the coastal zone. This thesis presents the results of statistical analysis of the storm database for 30 years of fluctuation in number, location, duration of storms in the East Sea area, in addition to also concerned about the unseasonal storm.

REMOTE SENSING TECHNOLOGY APPLICATION TO STUDY CHANGES LAND SURFACE TEMPERATURE IN QUANG BINH PROVINCE

Nguyen Thi Thanh Dung

Abstract

Topic using remote sensing technology and ArcGIS to calculate, Landsat image processing and mapping surface temperatures in Quang Binh province. To assess the change and the distribution of surface temperature. Remote sensing application has indicated the distribution of terrain affects the temperature distribution over the period from the year 2003 – 2016 and 2016 – 2018. Research results showed the range of different surface temperatures in each region of the terrain, the temperature decreases from the coastal areas to the mountains, coastal temperatures reached the highest compared to the entire study area and background temperature tends to increase due to the process of urbanization, industrialization – modernization and ongoing climate change is increasingly powerful.

STUDY ABOUT THE FUJIWHARA EFFECT

Pham Quang Huy

Abstract

The binary interaction was described by a Japanese meteorologist, Fujiwhara (1921). Then the interaction between pairs of typhoons/hurricanes is called the Fujiwhara effect. The aim of this seminar is study about Fujiwhara effect. In addition, based on the distance of interaction, the seminar collected data about pairs of typhoons Parma – Melor (the western North Pacific, 2009) and pairs of huricanes Hilary – Irwin (the eastern North Pacific, 2017). They are two examples for the escape and merger cases.

INVESTIGATE THE CAP 2010 SOFTWARE FOR POLLUTANT QUALITY SPREAD SIMULATION IN THE AIR POLLUTION HO CHI MINH CITY

Nguyen Thi Xuan

Abstract

Process simulation and đánh giá the quality of the software with the software was saved and application is many many of the world. This request to find an one in the following samples that is not applicable in the CAP 2010, which is application to be tính for the traffic transport for quality at the source at the area of the Binh Binh in Thành phố Hồ Chí Minh . The simulation simulation is the map of the SO_2 map and the map of the area with the fatated content, results for the allocated of the quality of the distribution like the given, the given some comment about simulation CAP 2010.

TO STUDY ABOUR THE CACULATION TOOL ENERGY WIND POWER

Nguyen Van Khanh

Abstract

Wind power is now being acquired by installing wind turbines to convert wind energy into electricity. But this process will result in energy losses due to the structure of the turbine and the difference. Deviation of wind when wind speed changes resulting in loss of up to 30-40%. This seminar aims to determine the capacity when the wind speed is stable, and the wind speed changes. The results show that the wind turbine's capacity depends on the stability of the wind field and the distribution of the wind speed. When the wind speed changes with a standard deviation of 0.2 compared to the steady wind speed, the power difference is very small. As the wind speed varies with the standard deviation of 0.8 at constant wind speed, the power difference is very high.

APPLICATION OF THE WORLD OCEAN DATABASE AND OCEAN DATA VIEW TO ASSESS THE DISTRIBUTION OF DISSOLVED OXYGEN IN THE SIERRA LEONE SEA

Ton That Phu Nguyen

Abstract

Applying Ocean Ocean Database and Ocean Data View to collect and analyze data. Use data to analyze and assess the distribution of Dissolved Oxygen in seawater in the Sierra Leone sea. Understanding how to collect data from WOD and process data using the ODV model will help in scientific research as well as application to teaching.

CALCULATION OF TIDAL ENERGY IN COASTAL AREAS IN CA MAU PROVINCE

Tran Cam Nghi

Abstract

Traditional energy sources are exhausting. With the present energy demand, it is required us to search the new energy sources for replacement of traditional energy sources. Nowadays, the exploitation of renewable energy sources from the ocean including tidal energy is much more concerned. This report aims to study for the potential of tidal energy in Ca Mau province. Based on the measured data for coastal tidal evaluation in the east (Rach Goc station) and in the west (Song Doc station and Tho Chu station) of Camau, the energy capacity and tidal power will be programmed, calculated and made statistics. The results show that in the west coast (at Song Doc and Tho Chu stations) of the research area, potential for tidal energy is too low. However, in the eastern coast, specifically at Rach Goc station with 0,2 billion kWh/year, it is possible to exploit tidal energy or power with small capacity.

THE INFLUENCE OF RAINFALL ON GRAPE PRODUCTION IN NINH THUAN PROVINCE

Trinh Thi Thu Thuy

Abstract

Ninh Thuan is a poor province and is one of the regions in Vietnam. However, the dry climate of this region is suitable for grape growing well. This study's method is concentrated on data collection and analysis of the grape production and rainfall data for the 2000–2016 to identify the relationship between the rainfall and the grape production. The results of the analysis showed that the annuall rainfall higher than 750-900 mm (in 2010, 2016) is corresponding with low grape production. Low grape production value is also observed in some years of unseasonable rainfall for example in the harvest in 2009, 2012. The high grape productions such as in 2014 and 2015 are usually seen when the annual rainfall values are about 750-900 mm and no unseasonal rains. These results indicate for the effect of rainfall on grape production.

ANALYSIS A NUMBER OF WEATHER FACTOR IN SOC TRANG PROVINCE 1997 - 2017

Hoang Hoai Thuong

Abstract

This topic analyzes some meteorological factors such as temperature, precipitation and humidity in the period of 1997 - 2017 in Soc Trang province. The analysis showed that the monthly average temperature was highest in april (28,5 ^{0}C), lowest in January (25,6 ^{0}C); monthly average rainfall is highest in October (305,2 mm), lowest in February (5,8 mm); monthly humidity is highest in february, march (79%), lowest in july, august, september (88%). Trend change in 21 years, the average monthly temperature increased; monthly average precipitation and monthly humidity drops. Where temperatures and precipitation are the two most variable weather factors in the period 1997 – 2017.

VIETNAM NATIONAL UNVERSITY HO CHI MINH CITY
UNIVERSITY OF SCIENCE
FACULTY OF PHYSICS AND ENGINEERING PHYSICS
DEPARTMENT OF OCEANOLOGY, METEOROLOGY AND HYDROLOGY

ABSTRACTS OF GRADUATION THESIS AND GRADUATION SEMINAR (YEAR 2019)

Bachelor of Science in Oceanology

TABLE OF CONTENTS

ABSTRACTS OF GRADUATION THESIS

ABSTRACTS OF GRADUATION SEMINAR

ABSTRACTS OF GRADUATION THESIS

BUILDING ASI INDICATORS FOR RAISE FORECAST FOR HO CHI MINH CITY AREA

Le Quang Minh

Abstract

Heavy rain leading to flooding is one of the most worrying and urgent issues to the living environment of Vietnam in general and Ho Chi Minh City in particular. Over the past few years, heavy rain has caused great human, material and spiritual damage in Ho Chi Minh City. In this thesis, monitoring data was collected and processed at Tan Son Hoa station from 2007 to 2016. Rainy relations with meteorological factors are also very complex issues, needing objective and multi-dimensional research and evaluation. In this thesis, we conduct a study on the relationship between some meteorological components on the high floor and the precipitation, in order to give additional quantitative indicators, support for credible rain forecasting method. higher dependability.

USING GFS MODEL FROM METEOSTAR TO FORECAST MEDIUM RANGE – 16 DAYS

Nguyen Thanh Duy

Abstract

The thesis verifies accuracy from GFS model of Meteostar about pressure deviation at the same time of forecasting; compare with actual data of air pressure, precipitation, wind direction and wind speed in the research areas such as Hanoi, Da Nang, Ho Chi Minh City, Hoang Sa and Truong Sa. Analyze the changes in atmospheric pressure and precipitation in the study areas during the period from January to May 2019, thereby giving identify on weather patterns for the research areas. Predicting and analyzing some storms affected Vietnam, thereby giving the usefulness of Meteostar's GFS model in early forecasting of the formation of storms and tropical depressions. The results show that the GFS model from Meteostar has made accurate forecasts and forecast values up to 384 hours (16 days).

AN ANALYSIS OF CURRENT VELOCITY ALONG THE EASTERN COAST OF THE MEKONG DELTA IN THE SOUTHWEST MONSOON

Nguyen Thi Lan

Abstract

The Mekong Delta is the largest deltas in Viet Nam but it is adversely affected by climate change as well as human activities. To analyze the primary hydrodynamics processes affecting the Mekong Delta under the above pressures, the study of current velocity along the coast is one of the approaches aimed to better understanding the characteristics of flow in this area. This study analyzes current data at 120 short-term locations and at a mooring station at depths of 2 m and 3 m above the seabed. The results at the mooring station show an asymmetry between the velocity of flood tide (average ~ 0,8 m/s) and ebb tide (1,0 m/s). At the short-term stations, the maximum flow velocity is about 1,2 m/s. The flow velocity near the Ca Mau cape is about 0,5 m/s. The standardization velocity values at the short-term stations show the increasing trend of velocity from Go Cong to Ganh Hao.

USE OF RAINFALL INTENSITY - DURATION - FREQUENCY CURVE TO DETERMINE RAINFALL INTENSITY IN CA MAU CITY

Tran Minh Hanh

Abstract

Ca Mau city is a low-land region and the situation of flooding situation urban areas in the rainy season is increasingly serious. Therefore, the determination of maximum rainfall intensity based on rainfall intensity - duration - frequency relationships, is necessary for the area. The GEV - Generalize Extreme Value distribution is used to calculate the cumulative frequency using CumFreq software. The results show that the maximum rainfall the period of 44 years (1975 - 2018) is 189.2 mm (2015) for 41 years return period and any maximum rainfall intensity in Ca Mau can be determined from the IDF curve. This study is useful for forecasting extreme rainfall intensity with an increase of the climate change in the future at Ca Mau city.

EFFECTS OF EDDY TO THE DISTRIBUTION OF DMS(P) IN WATER IN WEST SOUTH CANADA SUMMER 2015

Le Thi Anh Thu

Abstract

Dimethysulphide (DMS) is a biogas that represents natural sulfur sources, which regulates climate and play an important ecological role in the ecosystem in the water column (Levasseur, 2013) [34]. In the Arctic study in the summer of 2015, DMS(P) concentrations and the effect of warm water mass on DMS(P) concentrations distribution on the surface water and in the water column were taken into account. Relationship between DMS(P) concentration and temperature and salinity when warm water mass appears. Results show that the concentration of DMS(P) concentrated the surface and the coastal stations, concentrations decreas with increasing gradually as in-depth. The presence of eddy does not impact the maximum concentrations of DMS(P) but does affect the temperature and salinity in the area.

THE POSSIBILITY, WARNING OF THUNDERSTORMS IN HO CHI MINH CITY AND NEIGHBORING PROVINCES BY THE CLASSIFICATION FORMULA

Tran Thi Thu Uyen

Abstract

The purpose of reseach is statistic data on thunderstorms and instability indices. Since then build a program to predicting the possibility of thunderstorms by the classification formula to forecast and warn of thunderstorms in Ho Chi Minh City and neighboring areas such as Moc Hoa, Bien Hoa, Thu Dau Mot, My Tho. The results of the reseach show that the most thunderstorms from May to October, especially in May, early rainy season accounting for 14.26% of the year. From 13h to 19h is the time of day with the highest frequency of occurrence of thunderstorms accounting for 60.13%. Probability of correct prediction of SI, KI, LI, CAPE indices with highest thunderstorm occurrence for each index is: 51.52%; 66.67%; 57.81%; 69.12%.

RESEARCH CHARACTERISTICS OF CHANGES IN TEMPERATURE AND PRECIPITATION IN THE PERIOD OF 1978 - 2018 DONG NAI PROVINCE

Pham Thi Thu Tram

Abstract

The content of this graduation thesis presents of characteristics assessment of temperature, precipitation and identify the absolute extreme values in Dong nai province based on the observation data set at Bien Hoa station on the period from 1978 - 2018. Based on the results of the analysis and calculation of the two series of temperature and precipitation data, the average annual temperature in the period of 1978 - 2018 is found by 27^{o}C; ranging from the minimum value of 25.2^{o}C to the maximum of 28.4^{o}C. The highest average monthly temperature is concentrated in April to mid-May, the lowest in January or December next year. The total average annual precipitation in the region reaches 1858.7mm; ranging from 1200 to 2700mm. The total precipitation of rainy season accounts for about 85.4% of the total annual precipitation.

ANALYSIS AND PREDICTION WATER LEVEL OSCILLATION AT CAU DA STATION, NHA TRANG

Tran Ngoc My

Abstract

This research used World Tides to analyze and predict water level oscillation at Cau Da station, Nha Trang. The data of water level oscillation is from 00:00 January 1st to 23:00 December 31st, 2010 is used to analyze water level oscillation at the reseach area. Analysis verifing result showed that resemblance phase but difference in amplitude (0-0.59 meters). From constituent's analysis result, the research used 12 main constituents to predict water level oscillation in 2011. Prediction reflected result irregular diurnal tide property at this region. Water level oscillation from 0.3 to 2.23 meters. Comparing prediction and monitoring results showed the phase is the same but there is difference in amplitude (0-0.53 meters).

EVALUATE THE EFFECTIVENESS USING THE NETHOUSE MODEL FOR TOMATO PLANTS BY AQUACROP MODEL

Ngo Thi My Linh

Abstract

Climate change is one of the main causes of extreme weather events such as drought, scarcity of water from rain and pestilent insects, high production costs and reduced crop yields. Agricultural production depends heavily on water resources and climate conditions. This study applied the AquaCrop model developed by the Food and Agriculture Organization (FAO) to evaluate the effectiveness of using a greenhouse model for tomato yield. Two experiments were carried out on two plots with the same area of 0.28 ha, the response of tomato plants in the application of drip irrigation technology and greenhouse model has a higher yield than 28.07 % for with fruit yield and 16.67 % for dry biomass productivity compared to tomato plants grown outside natural conditions by AquaCrop model.

RESEARCH DETERMINING THE RISK OF RATE LOSSES OF RICE AND GRASS PLANTS BY ENSO PHASE IN GIA LAI PROVINCE

Dam Thi Than

Abstract

The project was conducted to assess the risk of yield losses of rice and maize crops caused by ENSO phases. The thesis uses data from the US Climate Prediction Center to identify El Nino and La Nina episodes in the area of Nino 3.4 and also use two formulas for calculating SI (Severity Index) and Sazonov (Sa.I) to calculate the determination of droughts in Gia Lai province. After that, assessing the risk of yield loss of rice and corn crops according to ENSO phases based on the calculation of crop yield.

ASSESSMENT OF CLIMATE CHANGE IMPACTS ON CASSAVA IN TAY NINH PROVINCE

Nguyen Thi Luyen

Abstract

The content of this graduation thesis is a presentation on climate change and climate change impacts on cassava in Tay Ninh province from 1984 to 2018. Since then, we can evaluate and offer solutions to overcome the consequences of climate change affecting cassava productivity in the province. The project approach is to collect and analyze data on area, output and meteorological factors affecting cassava in Tay Ninh province. In this topic, the solutions are based on the assessment of the influence of meteorological factors such as temperature, rainfall and number of rainy days, number of sunny days, evaporation to cassava in Tay Ninh province from 1984 to 2018. The results show that changing temperatures and precipitation have led to droughts, inundation and pests that are growing, making cassava areas, production and productivity decrease in recent years.

STUDYING DELFT3D MODEL TO SIMULATING THE SEDIMENT TRANSPORTATION

Nguyen Minh Khang

Abstract

This thesis studied about the sediment transportation module in Delft3D model, then applied to calculate and simulate sediment transportation in Cu Lao Dung, Soc Trang province in two seasons: dry and rainy seasons. The results showed that the sediment transport process in the study area was strongly affected by the load of river and tidal. In the dry season, the sediment concentration was low and mainly distributed in the river. Whereas in the rainny season, the sediment concentration was higher, mainly distributed in the estuaries.

THE CALCULATED MODELING OF WAVE HEIGHT THRESHOLD AFFECTING ON THE CORAL BOTTOM

Nguyen Thi To Van

Abstract

Coral reefs are currently a top concern in the world in general and in Vietnam in particular because their number is decreasing due to different causes such as ocean pollution, global warming or natural disasters (storms, tornadoes, etc.). This study aims to understand the mechanical effects of waves caused by storms affecting on the coral bottom. Based on hydrodynamic mathematics of storm induced waves and corals, the model is built to calculate the thresholds of the wave height for reef-shaped individuals with ideal spherical or hemispherical shapes in different cases of long and short waves. The model is also applied in the area of Van Phong bay - Ben Goi (Khanh Hoa province) in two cases of Typhoon Mirinae (2009) and Typhoon Damrey (2017). The results show that the actual wave height caused by the storm hardly exceeds the calculated wave height threshold. These results are quite consistent with the actual conditions of the coral when facing the storm.

RESEARCH OF THE TRENDS OF TEMPERATURE AND RAINFALL AMOUNT IN HO CHI MINH CITY (PERIOD 1978 - 2018)

Huynh Ngoc Bao Tram

Abstract

This study analyzes and evaluates some factors of temperature and rainfall amount in Ho Chi Minh City in the period of 1978 - 2018 through data of Tan Son Hoa station in the context of climate change. This study reviews assess the impact and expression of climate change globally, Vietnam and Ho Chi Minh City. The results show that the temperature tends to increase over the years, the trend of changing rainfall is not in accordance with any rules. In addition, extreme events tend to affect the study area. Climate change has been seriously affecting the environment, economy and life - culture of Ho Chi Minh City people.

GRAIN-SIZE DISTRIBUTION OF SURFACE SEDIMENT ALONG THE COAST OF THE MEKONG DELTA

Tran Thi Ngoc Khuong

Abstract

The Mekong Delta is currently facing a major challenge of climate change and the decrease in sediment supply causing an increase in riverbank and shoreline erosion. The objective of the thesis is to explore the seasonal change in grain-size distribution of seabed sediment along the Mekong Delta by analyzing sediment samples in two seasons. The results show that the grain-sizes in the southwest season is smaller than in the northeast season. In the river mouth area, the changes of sediment are quite complicated, with sandy clay and sand-silt-clay types in the Southwest season replaced by sandy sediment in the northeast. The area from the south of the Hau River to Mui Ca Mau is most variated in sediment grain-sizes. While along the West coast, sediment are mainly clayey silt and silty clay types and are less changes in grain-size distribution between the seasons.

DMS FLUXES IN ARCTIC OCEAN IN 2016 SUMMER

Huynh Hong Ngoc

Abstract

DMS samples were collected from Icebreaker Research Vessel (IBRV) ARAON-07B in August 2016 with 31 stations over the Bering Strait to the Arctic Ocean (65-80oB). The highest mean DMS concentration was observed in Chukchi sea (65oB-72oB) while the lowest was observed in the Arctic Sea (76oB-78oB) with values of 2.9 and 0.24 nmol L-1, respectively. DMS flux is calculated according to the parameterizations of Liss and Merlivat. (1986), Wanninkhof. (1992) and Nightingale et al. (2000). In this study, wind speed and sea surface temperature are used to calculate gas exchange coefficients. Liss and Merlivat. (1986), Wanninkhof. (1992) and Nightingale et al. (2000) parameterizations gave atmospheric DMS flux in the study area of 0.10; 0.15 và 0.09 Tg yr-1, respectively. In addition, this study also considers the influence of sea ice on emission flux by using the formula of Loose et al. (2014) and Jarníková et al. (2018). As a result, relations between the sea ice concentration and DMS fluxes is low with the correlation coefficient (R2) of approximately 0.4 to 0.6.

SURVEY ON ORGANIC POLLUTION LEVELS IN THE SAIGON RIVER AREAS BASED ON ZOOPLANKTON

Phan Thi Kieu

Abstract

The survey was carried out at Ong Lon canal in the area of South Saigon, Tau Hu chanel and Nhieu Loc Thi Nghe Canal at three different times on March 19, 2019: net water, bad water and large water. The objective of the project is to use Animal Adventure as an indicator organism to assess water quality. The results of the study have recorded 34 species of animal plankton belonging to 5 groups (Protozoa, Rotatoria, Cladocera, Copepoda and Ostracoda). The survey shows the pollution of organic matter at the survey sites. Based on B2 (QCVN) subdivision, chemical oxygen demand (COD) exceeds the permitted standard, dissolved oxygen concentration (DO) is within the permitted limit. Based on the Shannon - Wiener and Simpson diversity indicators, the water environment at the survey sites is heavily polluted. Building a water quality assessment model, the correlation between DO, COD based on Stella model.

APPLICATION OF METI-LIS MODEL TO SIMULATE AIR QUALITY IN SEVERAL STEEL FACTORIES HOA KHANH INDUSTRIAL ZONE - DA NANG

Nguyen Le Thao Linh

Abstract

The METI - LIS model was applied to simulate the diffusion of air pollutants of steel production facilities in Hoa Khanh industrial zone in the dry and the wet seasons. The calculating scenario included: scenario (1) – the exhaust air filtration systems in steel factories did work and scenario (2) - they did not work. The results show that air quality in the dry season is higher than ones in the wet season. In case exhaust air filtration systems did not work, the pollutant concentrations exceed the limits of Vietnam's air quality standards (QCVN 05: 2013/BTNMT). In addition, this thesis collected air quality index (AQI) PM2.5 at Da Nang station to assesses the air quality at the study site.

ANALYSIS THE IMPACT OF EQUATORIAL ROSSBY WAVE ON TROPICAL CYCLONE ACTIVITY IN NORTHERN WEST PACIFIC OCEAN

Dang Dong Pha

Abstract

Equatorial Rossby wave plays a crucial role in tropical cyclone activity in the Northern West Pacific basin. The study of these equatorially trapped, tropical waves is fundamental to understand tropical dynamics, and ultimately to understand tropical cyclone genesis. In the Pacific typhoon season 2018, there were 29 tropical storms and typhoons which were investigated to evaluate the effect of equatorial Rossby wave on them by OLR maps and diagrams, synoptic charts as well as satellite images. In addition, Madden – Julian oscillation and El Nino Southern Oscillation are also used to analyze their contribution on tropical cyclones. The results could be applied to improve the quality of typhoon activity prediction.

IMPACTS ASSESSMENT OF CLIMATE CHANGE FOR USE OF BINH PHUOC PROVINCE'S FOREST

Vo Nguyen Xuan Loc

Abstract

This thesis identifies, analyzes and evaluates some meteorological factors of Binh Phuoc province in the period of 1984 - 2016. The results show the changes in average temperature and rainfall over the years, the trend of rainfall changing fluctuated and temperature rising. Combining with the climate change scenarios assess the changing trend of temperature and rainfall in the years 2025, 2030, 2050. In addition, the phenomenon of drought and flood tends to increase and difficult to predict which affects the area. Climate change is increasingly seriously affecting forest, economy, life and culture of Binh Phuoc people.

SENTINEL-1 IMAGES APPLICATION FOLLOW THE MOVEMENT OF FLOOD IN DONG THAP PROVINCE

Nguyen Chan Quoc

Abstract

Applying GIS and remote sensing technology to monitor flood receive much attention from domestic and international scientists. The topic selected Sentinel-1 image and used softwares such as SNAP, ENVI and ArcGIS to process images, to create data for the study area, to establish the inundation maps and to calculate the inundation areas caused by flood in Dong Thap province in 2017 and 2018. The results showed that flood began to appear around July, peaked in late September to mid-October, ended around late November and early December. The north of the Tien River area had low-lying topography, so it was affected by inundation heavier than the south of the Tien River area. In 2018, flood came earlier than and also drained faster than 2017.

ABSTRACTS OF GRADUATION THESIS

EMISSION BLACK CARBON ON JAPAN SEA

Huynh Thi Phuong Anh

Abstract

Reducing black carbon (BC) emissions has been recognized as an efficient way to simultaneously improve air quality and mitigate climate change. This paper discusses the source of BC emissions, the causes that affect the concentrations of BC and the correlation between atmospheric humidity and the concentrations of BC on the Japan Sea in the region between Korea and Japan. To be able to find conclusions, the paper used Matlab software and Excel tool to analyze and synthesize data from Kanomax meter and HYSPLIT model. The results show that wind was an important factor controlling BC at the site; concentrations of BC were influenced by long-range transport of air masses from northeast China and Russian, as well as the local emissions. The sudden rise BC concentrations were contaminated from the ship's exhaust; humidity did not significantly affect the concentration of BC in the region due to low correlation.

APPLYING THE EXPERIMENTAL FORMULAS TO CALCULATE THE SIGNIFICANT WAVE HEIGHT IN THE OFFSHORE AREA OF PHU QUY ISLAND, BINH THUAN PROVINCE

Nguyen Thanh Nam

Abstract

The seminar collected wind data to analyze wind regime and calculate the significant wave heights in the offshore area of Phu Quy island, Binh Thuan province in 2009. The experimental formulas SMB, Wilson and SPM were used to calculate the hourly significant wave height. The calculated and observed wave heights were compared. The results show that the SPM method correlated strongly with the observed data ($r^2 = 0,89$). In addition, the SPM and Young methods are used to calculate the wave height in the storm Usagi 2018. The average calculated value of the wave height was about 15,82 m by the SPM method and 6,46 m by Young method. Therefore, the Young method was suggested to increase the accuracy in prediction of wave height in storm.

MODELING OF NITROGEN CYCLE IN THE MARINE SEDIMENTS BY STELLA SOFTWARE

Nguyen Thi Thuan

Abstract

The thesis uses STELLA model to assess the effect of the conversion coefficients on the conversion of organic nitrogen (N_{org}), ammoniac (NH_3), nitrite (NO_2) and nitrate (NO_3) in An Thoi island (Phu Quoc) to determine the most affected nitrogen compound by the conversion coefficients. After increasing/decreasing the conversion coefficients twice, the results showed that: The ammonia excretion rate (F_A) and photosynthesis rate of ammonia (F_{PA}) much affected the N_{org} stock; The nitrification rate (F_{NT1}) and photosynthesis rate of nitrate (F_{PN}) much affected the NH_3 stock; The nitrification rate (F_{NT1}), denitrification rate (F_{DN}) and nitrification rate (F_{NT2}) much affected the NO_2 stock; The photosynthesis rate of nitrate (F_{PN}) and nitrification rate (F_{NT1}) much affected NO_3 stock.

URBAN HEAT ISLAND PHENOMENON IN BINH DUONG PROVINCE USING REMOTE SENSING AND GIS

Vo Tien Dang Bao Huy

Abstract

Today, Binh Duong province is accelerating the process of industrialization and modernization, land use structure is transformed from agricultural land to non-agricultural, many large industrial parks are formed and put into operation. The phenomenon of “urban heat island” is very common in urban and industrial areas. To monitor and evaluate the trend of this phenomenon in Binh Duong province, the topic used remote sensing and GIS to establish a map of land surface temperature distribution in 2000, 2005, 2010, 2017. The results showed that the phenomenon of “urban heat island” tended to increase with space and time, especially residential areas and industrial zones in the southern of Binh Duong province.

ANALYSIS AND PREDICTION WATER LEVEL OSCILLATION BY USING T_TIDE TOOLBOX IN MATLAB

Nguyen Thi Rin Gan

Abstract

Nowaday, Matlab have became very popular in the world and its apply to almost the majors including Oceanography. In this study, Toolbox T_Tide was adopted in order to analyze and predict a tide in Nha Trang in 1999. There are many components of tides such as K1, O1, M2, S_2, Q1, OO_1, MSF, MK3, N_2, MO_3, SK_3, MM, J_1 account for more than 99% of the total amplitude of water level fluctuation. Toolbox T_tide is used to analysis a tide elevation from January to March in 1999 give the positive result of R^2=0.87. Thus, the T_predict has been applied to predict the tide in next month with R^2 ranging 0.7 with 95% confidence intervals.

APPLICATION OF MULTISPECTRAL LANDSAT DATA TO MONITOR CHANGES IN COASTAL MANGROVES IN DONG RUI COMMUNE TIEN YEN DISTRICT, QUANG NINH PROVINCE DURING 1999 - 2018

Nguyen Duc Hoa

Abstract

Use remote sensing images to evaluate the changes in coastal mangroves forests is appropriate in consistent with this data source available and free of charge. The study shows that the mangrove forest area have decreased from 1999 to 2018, estimated at 956.52ha, Specifically, the total area of mangrove forests decreased in the two periods 1999 - 2003 and 2008-2013 about 1504.89 ha (22.5%), mainly due to people shifting the area of mangrove forests to aquaculture. The area of mangroves increased in 2 periods from 2003 to 2008 and 2013-2018 was 548.37 ha (8.99%), mainly due to the projects of planting and recovering from the chapter of the Red Cross, Japan ACTMANG.

ANALYSIS OF THE EFFECTS OF PHYSICAL FACTORS ON CORAL REEF ECOSYSTEM

Phan Thi Thanh Doan

Abstract

The geographical location and natural conditions in Vietnam are generally favorable for the development of coral reefs. The corals are distributed most widely in the Truong Sa Archipelago. This study aims to analyze and assess the effects of physical factors on coral reef ecosystem. Physical factors are considered such as sea water: temperature, salinity, turbidity, tides, waves and currents... From the collected data in some coastal areas of Vietnam such as Nha Trang Bay, Van Phong Bay, Quy Nhon, Phu Quy Island and coastal water of Eri in Outer Ambon bay (Indonesia), they prove that all physical factors are suitable for coral survival and development. The study also analyzes and evaluates the effects of physical factors on the coral reefs in Song Tu Tay (Southwest Cay) and Truong Sa Lon (Spratly Island) of the Truong Sa Archipelago. Overall, all physical factors are advantageous for the development of coral reef ecosystems in the Truong Sa Archipelago throughout the year. The southwest season is some more favorable for coral development than the northeast season.

CALCULATING AIR POLLUTANTS DISPERSION AND NOISE LEVEL AT NGUYEN VAN CU - TRAN HUNG DAO JUNCTION, HO CHI MINH CITY

Tran Huynh Long

Abstract

The goal of this seminar is calculating the air pollutants dispersion and noise level that caused by traffic at the Nguyen Van Cu - Tran Hung Dao junction, Ho Chi Minh City. First, this seminar collected the number of vehicles that passed by the junction that were mentioned in 24 hours of 02 Jun 2019, then proceed to use Sutton model to calculate the air pollutants dispersion. Compared to the QCVN 05:2013/BTNMT standard, results show that the concentration of NO_x did not exceed Vietnam's standard of air pollution, when PM_{10} did exceed throughout the day. About noise level, this seminar used the formulas from model FHWA and CRTN for estimating and evaluating. The results show that ultimately all estimated results exceed the noise level standard of Vietnam (QCVN 26:2010/BTNMT), model CRTN gave the overall higher result of noise level and the time from 16:00 to 17:00 contain the highest value among all. FHWA model have the highest value in around 23:00 to 24:00.

ANALYZING SHORELINE CHANGE IN BINH THUAN PROVINCE USING REMOTE SENSING AND GIS

Giang Thanh Nhan

Abstract

Ham Tien - Mui Ne is one of the coastlines of Binh Thuan province, where the erosion process is very complicated, affecting the socio-economic development of the province, especially tourism development. To solve this situation, Coastal structures have been built, resulting in shoreline changes in this area. The project used remote sensing and GIS to analyze and evaluate shoreline changes in 2005, 2007, 2010, 2014 and 2019. The results show that the shoreline in the period of 2005-2007 was eroded with -1.43m/month. The 2007-2010 period was accreted with 1.07m/ month.

APPLICATION CROPWAT MODEL TO CALCULATE WATER REQUIREMENT FOR MAIZE IN TANH LINH DISTRICT BINH THUAN PROVINCE IN CLIMATE CHANGE

Bui Nhu Sy

Abstract

This seminar application CROPWAT model calculate crop water requirement, irrigation scheduling and forecast water requirement in climate change in Tanh Linh District, Binh Thuan province, in order to determine the crop evapotranspiration under the standard conditions, the amount of reference crop evapotranspiration, crop water requirement and build appropriate irrigation time for maize.

Calculation results showed that annual total reference crop evapotranspiration was estimated at 1575 mm. The highest ET_O in April with a value of 163.24 mm, the smallest ET_O in November with a value of 117.6 mm. Crop water requirement of winter - spring season was highest 2038 m^3/ha, followed by summer - fall season 1426 m^3/ha and the lowest was the fall - winter 947 m^3/ha.

VIETNAM NATIONAL UNVERSITY HO CHI MINH CITY
UNIVERSITY OF SCIENCE
FACULTY OF PHYSICS AND ENGINEERING PHYSICS
DEPARTMENT OF OCEANOLOGY, METEOROLOGY AND HYDROLOGY

ABSTRACTS OF GRADUATION THESIS AND GRADUATION SEMINAR (YEAR 2020)

Bachelor of Science in Oceanology

TABLE OF CONTENTS

ABSTRACTS OF GRADUATION THESIS

ABSTRACTS OF GRADUATION SEMINAR

ABSTRACTS OF GRADUATION THESIS

CACULATION OF SUSPENDED SEDIMENT CONCENTRATION WITH TIME DURING SEDIMENT DEPOSITION

Vo Ho Nhu An

Abstract

Through data from classification of sediment samples in Cao Lanh, Dong Thap and Rach Goc, Ca Mau, the settling velocity for each class is determined by using "well-known" Stokes formula. Under steady turbulent flows, normalized suspended sediment concentration C/C_0 (ratio of instantaneous concentration and initial concentration), which is expressed based on the bed shear stress τ_b, the characteristic stress for deposition for each class τ_{ci} and the corresponding settling velocity W_{Si}, is decreased with time during deposition and gradually reached steady state after about 7 hours in Cao Lanh and 11 hours in Rach Goc. In particular, C/C_0 reaches approximately 0.6 at Rach Goc and approximately 0.9 at Cao Lanh at steady state.

.

STATISTICS OF WAVES ALONG THE COAST OF THE MEKONG DELTA INTO THE NORTHEAST MONSOON SEASON

Nguyen Thi Han Ni

Abstract

The Mekong River Delta (Mekong Delta) is currently facing with coastal erosion and damage to coastal structures. The objective of this thesis is to find out the wave direction and wave height on the coastal areas of the Mekong Delta by statisticing observed wave data measured during the northeast monsoon season. The results show the distribution of wave directions along the Mekong Delta with the wave height values depending on the region. When the northeast monsoon was strong, the wave directions clearly appears for each area along the coast of the Mekong Delta and the wave field of the northeast monsoon has a stronger impact on the East coast than in the West coast. During the gradually weakening of the northeast monsoon, the observed wave directions are scattered, and the prevailing wave directions are not clearly seen. The maximum wave height during the strong northeast monsoon is about 3.24 m and during weak northeast monsoon condition is about 0.16 m.

ASSESSING THE IMPACT OF STORM ON SOUTH-CENTRAL AREA AND EARLY FORCASTING STORM CAPABILITY OF METEOSTAR MODEL.

Ton Nu Thanh Thu

Abstract

Tropical storm is a seriously natural disaster, causing lots of damage and human life. So, the use of synoptic maps or software tools to support storm prediction for the forecast the activities of typhoon, the landing or the impact and the prevention of a storm is extremely urgent, has been a priority. With the study area limited to the South-Central Coast, this report provides an assessment of the storm's impact on this area and forecasts for a specific locality. The result of this study is using Meteostar model to early recognize the formation of cyclones, early predict of their developing, moving and severe disaster to the study area as strong winds, storm surge, heavy rain with tornadoes, thunderstorm, flooding.

WIND WAVE SPECTRAL ANALYSIS BY BLACKMAN – TUKEY AND FFT (FAST FOURIER TRANSFORM) METHODS

Vo Thanh Tuyet Hong

Abstract

Wind wave spectral analysis is to determine the energy distribution of waves in frequency and direction in the studied area. The aims of the study are to calculate and to analyze wave spectrum by Blackman - Tukey method and FFT (Fast Fourier Transform) method. Wind wave calculations are built up by Fortran. For short data series, Blackman - Tukey method is advised to be chosen because the main lobe peak does not change in the data length. In contrast, Fast Fourier Transform method requires the data series long enough and formatted in 2^n. Appyling in Cu lao Dung mangroves area (Soc Trang province), three different records in three stations (at estuary, mudflats and mangroves) were chosen. It is shown that the results in both methods gave the similar shapes. Wind wave energy was decreased significantly (c.a 50% at record 1, 56.5% at record 2 and 77% at record 3) as propagating from estuary into mangroves. Wave energy dissipation depends on offshore wave heights, topography, water level and weather conditions. Compared with Blackman - Tukey method, FFT method can give the wider spectral band, therefore less spectral leaking especially in mangrove areas with very shallow water and small waves.

ABSTRACTS OF GRADUATION SEMINAR

NUMERICAL SIMULATION OF DEBRIS FLOW IN THE ASTIFICIAL CHANNEL USING THE OPENFOAM SOFTWARE

Dang Le Khoa

Abstract

Debris flow is considered as an unstable flow of water, air and mud mixed with water, which often forms in the steep slope mountainous areas. Mass and flow velocity are probably the main causes of great loss of life and property. This study is conducted to simulate the flow velocity and its pressure in order to improve understanding of debris flow this through the OpenFOAM software.

ANALYSIS OF EROSION AND ACCRETION PROCESS IN CAN GIO, HO CHI MINH CITY

Do Minh Tuan

Abstract

The process of erosion and accretion was inceasingly complicated in the coastal estuary area of Can Gio district affecting the area of coastal mangrove forest. Facing that problem, "***Analysis of erosion and accretion process in Can Gio, Ho Chi Minh city***" analyzed of erosion and accretion process in the area from 1983 to 2017 by Digital Shoreline Analysis System (DSAS).

The results showed that erosion process occurred in most of the area. The period from 1983 to 1988 the area of the erosion process is mainly, the process of the accretion appeared at the estuary of Dong Tranh river, Can Gio cape. The period from 1988 to 2005 accretion occurs in the estuary of Soai Rap river and Dong Tranh river. The erosion process in Can Gio coastlines and the estuary of Long Tau river. From 2005 to 2015, the erosion on the area is more stable than the previous period, the process of the erosion of equal balance. The period from 2015 to 2017 erosion takes place complex and interwoven.

THE ANALYSIS OF SHORELINE CHANGE AT PHAN RI ESTUARY BEFORE AND AFTER THE JETTIES CONSTRUCTED BY LANDSATS IMAGE

Ngo Hoang Tuan

Abstract

The construction of jetties at the mouth of the Song Luy River has helped stabilize the channel for safety of ship traffics. However, the construction had also changed the seasonal sediment accumulation and erosion around the mouth creating the appearance of sandbars which affect the ship traffics to the Phan Ri Cua harbor. Using Landsats image and GIS, this study aims to analyze the coastline changes around the Song Luy river mouth. The results show that the shoreline changes of the mouth of the Song Luy River is not significant. Shoreline changes mainly occur around the river mouth with and between northeast and southwest seasons. The seasonal coastline changes after the jetties constructed has been made more obvious than previous periods without jetties.

CHANNGES IN TEMPERATURE AND PRECIPITATION DURING THE PERIOD OF 1978-2007 IN BINH DINH PROVINCE

Nguyen Thi Bong

Abstract

The seminar shows some characteristics of the changing in temperature and precipitation in Binh Dinh province based on 30-years data set (1978 - 2007) at the Quy Nhon station. The results show that temperatures had generally increased; the highest amplitudes usually occur from May to September and lowest amplitudes from November to December. Rainfall in the wet season accounted for the high proportion, at 70% of the total annual amount of precipitation. Furthermore, the observed rainfall anomaly during El Nino events show there are a rainfall shortage and the observed rainfall anomaly during La Nina events show that La Nina does not always contribute to the increase of rainfall, sometimes La Nina causes rainfall shortage.

ANALYZING OF SHORELINE CHANGE IN CUA DAI BEACH BY USING REMOTE SENSING

Tran Minh Tri

Abstract

Cua Dai Beach - Hoi An is a long and beautiful coastline, which is famous for attracting domestic and international tourism. However, over the past 20 years, it has experienced a serious erosion process with inland intrusion up about 190m over 7km of coastline at Cua Dai beach eroded. The construction of coastal projects from organizations and private enterprises exploiting beach tourism has made the coastal hydrodynamic regime become more and more complicated, causing many impacts on the development of tourism economics in the local area. This topic uses Remote Sensing and DSAS tools in ErcArGis to analyze shoreline changes in the years 2000, 2005, 2011, 2013, 2016 and 2019. The results show that the shoreline has the trend of inter-erosion. From 2000 to 2016, especially in the area adjacent to Cua Dai estuary, serious erosion occurred.

THE RELATIONSHIPS BETWEEN CHLOROPHYLL-A CONCENTRATION WITH TEMPERATURE, TURBIDITY AND DISSOLVED OXYGEN IN WATER

Pham Tran Minh Tho

Abstract

Phytoplankton plays an important role in the ecosystem of water, especially in evaluating the quality of water and climate study. Scientists usually do research on phytoplankton based on chlorophyll concentration in water. The study aims to study the correlation between chlorophyll-a concentration, turbidity, temperature and dissolved oxygen. By using multi-exciter and CTD (JFE, Japan), four factors including: chlorophyll-a concentration, turbidity, temperature and dissolved oxygen were collected in depths hourly and continuously in 24 hours from 11/1/2020 to 12/1/2020. The selected studied site was on Tien river in Ben Tre city, Ben Tre province (10.27958^{0}N–E 106.12341^{0}E). In general, chlorophyll-a concentration and turbidity were increasing with depth. Dissolved oxygen concentration got higher at the surface and decreased in depth. Temperature was almost constant and stable in depth. In 24 hours, chlorophyll-a concentration in day is higher than that in night, especially got highest at noon (12:00) on 11 January 2020. At that time, both of turbidity and chlorophyll-a concentration went to the peak and get higher value at the bottom. The result also proves that chlorophyll-a concentration is proportional to turbidity. In contrast, chlorophyll-a concentration and dissolved oxygen had inversed correlation. The stable temperature could not show obviously its influence on chlorophyll. With 1-29 µg/l of chlorophyll-a concentration, the phytoplankton amount at the study site is can estimate in medium value.

VIETNAM NATIONAL UNVERSITY HO CHI MINH CITY
UNIVERSITY OF SCIENCE
FACULTY OF PHYSICS AND ENGINEERING PHYSICS
DEPARTMENT OF OCEANOLOGY, METEOROLOGY AND HYDROLOGY

ABSTRACTS OF GRADUATION THESIS AND GRADUATION SEMINAR (YEAR 2021)

Bachelor of Science in Oceanology

TABLE OF CONTENTS

ABSTRACTS OF GRADUATION THESIS

ABSTRACTS OF GRADUATION SEMINAR

ABSTRACTS OF GRADUATION THESIS

ASSESSMENT THE IMPACT OF CLIMATE CHANGE ON BINH THUAN PROVINCE

Nguyen Thi Thuy Dung

Abstract

In recent decades, climate change impact to Vietnam with many types of disasters. This thesis shows the results of analyzing statistical meteorological data (temperature, rainfall, wind speed) in Binh Thuan province from 2000 to 2019, combining with statistics of tropical storm activity during the period 1951 – 2020. Thereby, objectively assessing the trend of meteorological elements as well as tropical storm activity in the context of clearer climate change. The analysis of the frequency and intensity of ENSO affects the variability of the above elements for purpose of giving early warning of weather abnormalities, it helps to prevent and mitigate natural disasters while climate change can not be stopped and more complex.

.

ANALYSIS OF RAINFALL AND DROUGHT IN THE MEKONG DELTA IN THE PERIOD 1978 – 2019

To Tan Thanh

Abstract

In recent decades, the Mekong Delta Area (MDA) has been continuously suffered the unprecedented drought events as part of climate variability. A comprehensive explore of the occurrence and intensity of droughts in the MDA based on the Standardized Precipitation Index (SPI) was applied to help tracking, early warnings as well as drought risk monitoring caused by change in precipitation. For this goal, precipitation data sequences in 1978-2019 at 13 national precipitation observation stations was collected. The three typical drought stages were recorded in the MDA in relation to the drought were 1989-1994, 2002-2003 and 2015-2016. Among investigated driest stages, the peak risk of the SPI-12 estimated -6.02 at Can Tho station, lasting of dry months up to 37 at Soc Trang station.

ASSESSING THE IMPACT OF STORM ON SOUTH-CENTRAL AREA AND EARLY FORCASTING STORM CAPABILITY OF METEOSTAR MODEL.

Ton Nu Thanh Thu

Abstract

Tropical storm is a seriously natural disaster, causing lots of damage and human life. So, the use of synoptic maps or software tools to support storm prediction for the forecast the activities of typhoon, the landing or the impact and the prevention of a storm is extremely urgent, has been a priority. With the study area limited to the South-Central Coast, this report provides an assessment of the storm's impact on this area and forecasts for a specific locality. The result of this study is using Meteostar model to early recognize the formation of cyclones, early predict of their developing, moving and severe disaster to the study area as strong winds, storm surge, heavy rain with tornadoes, thunderstorm, flooding.

CALCULATION OF GREENHOUSE GASES EMISSIONS (CO2, CH4) AT THE SURFACE OF TRI AN AND DAU TIENG RESERVOIRS IN THE RAINY AND DRY SEASONS

Do Hoang Minh Cuong

Abstract

Reservoirs is one of sources greenhouse gases emissions to the atmosphere. To measure theses fluxes of greenhouse gases (methane and carbon dioxide) the study carried out in situ within 24 hours chamber measurements at the surface of Tri An and Dau Tieng reservoirs in the rainy and dry seasons. At Dau Tieng reservoir the average CH4 emission rate in the dry season is 35.87 ppm/m^2/hr and in the rainy season is 13.2 ppm/m^2/hr. The average CO_2 emission rate in the dry and rainy season is 2418.83 ppm/m^2/hr and 10129.1 ppm/m^2/hr respectively, and both emission rates of gas are correlated with biochemical factors in the water (dissolved oxygen, temperature and pH). At Tri An reservoir the average CH_4 emission rate in the dry season is 18.21 ppm/m^2/hr and in the rainy season is 7.82 ppm/m^2/hr and no correlation with biochemical factors in the water. The average CO_2 absorption rate in the dry is 1131.84 ppm/m^2/hr and in the rainy season is 3835.15 ppm/m^2/hr and is correlated with dissolved oxygen, temperature.

ASSESSMENT OF SHORELINE CHANGE IN PHAN THIET CITY, BINH THUAN PROVINCE

Hoang Thi Hong Nhung

Abstract

The shoreline is the boundary between the land and the sea. In recent years, the coastal area's shoreline has become more and more complicated. Therefore, research on shoreline change is essential for the management and monitoring of the coastal area. The study used Landsat, and Sentinel-2 images to assess shoreline change in Phan Thiet city, Binh Thuan province from 1988 to 2021. The topic applied the ratio image method combined with the thresholding technique to extract shorelines from remote sensing image data. The analysis results showed that 68 percent of the shoreline was accreted, and 32 percent of the shoreline was eroded with an average erosion and accretion rate of -0.8 m/year and 1.0 m/year, respectively in the period 1988-2021. The shoreline was the most eroded with 76 percent in the period 1988-1995 and was the most accreted with 86 percent in the period 2016-2021. The percentage of accretion-erosion in 1, 2, 3, and 4 areas were 95/5, 66/34, 29/71, and 83/17, respectively, from 1988 to 2021.

ANALYSIS OF RAINFALL TRENDS IN THE LONG XUYEN QUADRANGLE IN THE CONTEXT OF CLIMATE VARIABILITY

Hoang Thi Thanh Thu

Abstract

The thesis presents the analyzed results of rainfall trends in the Long Xuyen Quadrangle in the context of climate change based on daily rainfall data series in the period 1985 - 2015. Rainfall data at all gauge stations are evaluated using the SNHT method before being used for further works. Standardized Precipitation Index (SPI) and Precipitation Anomaly Index (PAI) were applied to assess the rainfall characteristics include dry season, rainy season and annual rainfall across the study area, while Man-Kendall non-parametric test and Sen's slope estimator were applied to detect the changed trends.

During the study period from 1985 to 2015, the analyzed results of the rainfall characteristics based on the SPI and PAI showed that the weather remained stable in the state of lack of moisture (dry weather) is always higher than that of the state of wet weather (wet weather) at all observation rainfall stations across the study area. Results showed that 04 typical dry weather stages and 03 wet weather stages were detected during the study (1985-2015). Results also carried out that extremely dry weather was recorded with peak value SPI12= -3.25 at Chau Doc Station in 2002 and extremely wet weather clearly pointed out with the speak value of SPI12= 2.78 at Can Tho Station in 1999.

ESTIMATING OF GAS EMISSIONS FROM RICE STRAW IN VINH LONG PROVINCE

Nguyen Huynh Thy

Abstract

Rice cultivation is one of the main production activities of people in the Mekong Delta as well as Vinh Long province. After harvesting, rice straw is treated in many different ways but mainly by burning, which both wastes resources and emits a large amount of greenhouse gases into the environment. Our survey showed that in the Winter-Spring crop, the rate of burning straw is highest (62,16%), in the Autumn-Winter crop the rate is lowest (53.85%). The thesis uses ALU software (Agriculture and Land Use) to estimate greenhouse gas emissions caused by burning straw. The results showed that in Vinh Long in 2012, the rice straw burning emitted 75773,564 tons of CO, followed by CH_4 about 7813,639 tons, the remaining NO_x was 1875,674 tons and N_2O was about 57,034 tons. By 2019, rice production decreased by 172 thousand tons, so the estimated emissions decreased to 44032,673 tons of CO, and CH_4 also decreased to 4540,574 tons.

CALCULATION OF IRRIGATION REQUIREMENT FOR THAI JACKFRUIT TREES IN TIEN GIANG PROVINCE

Nguyen Thai Ho Phat

Abstract

The calculation of Irrigation Requirement for crops is extremely important especially in the climate change situation. Irrigation Requirement for crops and especially the Thai jackfruit depends obviously on hydro-meteorological factors. By using 10-year data (2011 - 2020) of meteorological factors such as temperature, air humidity, precipitation, wind speed and sunshine hours, the results show that the climate conditions in Tien Giang province are favorable and suitable for jackfruit tree growth. In addition, the filed measurement of some meteorological factors in one jackfruit garden in Tien Giang province during the period from April 28, 2021 to May 5, 2021 also shows that the weather here is suitable for the Thai jackfruit tree. Based on 10-year average meteorological data, the reference evapotranspiration and irrigation water for Thai jackfruit trees are calculated by using the CROPWAT 8.0 model. The results give some good agreement with the field measurement. The results reflect the actual amount of water demand for the Thai jackfruit tree irrigation should provide additional coefficients and reference for calculating the optimal and appropriate irrigation regime. Climate change scenarios which are considered in the model also affect the water demand due to the impact of temperature and rainfall increase.

ANALYSIS OF METEOROLOGICAL DATA OF VINH LONG PROVINCE FROM 2001 TO 2020

Phan Thi Kim Thanh

Abstract

This study collects and analyzes meteorological data in Vinh Long province from 2001 – 2020 to assess the change in temperature, precipitation and humidity factors. Average annual temperatures tend to drop, and average monthly temperatures range from 24.40C to 30.4^{0}C. Total annual precipitation reaches above 1000mm, tends to increase and precipitation peaks from May to November and reaches a minimum from December to April of the following year. The average annual humidity ranges from 78% to 86%, tends to increase and there are notable months because the humidity reaches a peak of 74% and peaks up to 96%. At some stage, meteorological factors are strongly influenced by El Nino and La Nina during the ENSO cycle. This makes meteorological factors volatile compared to the general trend of the whole period 2001 - 2020.

ABSTRACTS OF GRADUATION SEMINAR

SHORELINE CHANGE OF THE WESTERN SEA AREA, CA MAU PROVINCE USING REMOTE SENSING AND GIS

Huynh Thuy Thy

Abstract

Ca Mau is the only province in the country with 3 sides bordering the sea, where the erosion and accretion phenomenon are increasingly complicated, seriously affecting the ecosystem and the life of residents, especially the western sea area. Therefore, the study of shoreline change in the western sea-Ca Mau areas is very necessary. The research used remote sensing and GIS with Landsat satellite imagery in 1999, 2009, and 2019 to help monitor the shoreline quickly and accurately. The results showed that 70 percent of the shoreline was eroded and 30 percent of the shoreline was accreted with an average rate of 11.5 and 23 m / year, respectively in the period 1999-2019.

OXYGEN FLOWS IN SEA-GAS EXCHANGE IN THE SOUTHERN OCEAN

Nguyen Van Tuong

Abstract

The goal of this topic is to learn about the sea surface oxygen exchange in the Southern Arctic Ocean as well as the factors related to the gas exchange process such as temperature, salinity, dissolved oxygen concentration, oxygen saturation, ... The results obtained show the obvious changes of the above factors according to geographical latitude, in which temperature and salinity are related quite similarly while the concentration Dissolved oxygen and oxygen saturation have the opposite tendency, the above factors directly affect the uneven distribution of oxygen exchange flux. In addition, the results also show that the ocean releases oxygen in the subtropical and temperate regions, while absorbing oxygen gas in the Southern Ice Ocean.

ANALYZING AND EVALUATION OF SHORELINE CHANGE IN DONG TRANH ESTUARY –CAN GIO, HO CHI MINH CITY BY USING REMOTE SENSING AND GIS

Ton That Quy Don

Abstract

Can Gio in Ho Chi Minh City is a popular tourist attraction. However, over the years, the erosion process is very complicated with a deep penetration into the mainland at Dong Tranh estuary in Can Gio. The coastal construction projects to exploit the strengths of touris are significantly affected by the extremely serious erosion, causing many impacts on tourism and marine development. Therefore, the monitoring and research of the shoreline is an urgent task to assess the change of shoreline at Dong Tranh river door which is in the process of strong erosion. Project based on remote sensing image 2014-2019 to evaluate and analyze erosion and deposition in 5 years. The results show that the situation of erosion and accretion is always intertwined with complicated developments in the future

EXTREME RAINFALL TRENDS IN TAM KY CITY OF QUANG NAM PROVINCE IN THE PERIOD 2000-2019

Dinh Thi Y Nhi

Abstract

Tam Ky City is the capital city of Quang Nam Province, in the key economic region. In recent years, Tam Ky City has been frequently affected by heavy rainfall that cause flooding as well causing local flooding. For these reasons, this study has been conducted to assess extreme rainfall trends across the Tam Ky City area in the stage 2000-2019. The study focused on determining extreme rainfall trends applying the non- parametric Mann Kendall test and the Sen slope estimates. The results showed that annual average rainfall and number of rainfall days are recorded downward trend while monthly average rainfall of November is recorded a significant upward trend. This maybe the major cause of flooding because of heavy rainfall a crossing the study area.

APPLICATION OF REMOTE SENSING TECHNOLOGY TO DETERMINE THE SHORELINE CHANGE IN DUC PHO DISTRICT, QUANG NGAI PROVINCE

Mai Huu Khuong

Abstract

Duc Pho district is located in the south of Quang Ngai province, bordering the sea and Binh Dinh province. This area is currently undergoing a strong erosion process due to the impact of dynamic factors. This topic is based on remote sensing image technology to assess and analyze the process of erosion and accretion from 2011 to 2021. The results show that the survey area is undergoing erosion, reducing the accretion process over time and tending to continue in the future. These are important results that contribute to the rational and efficient construction of works.

SHORELINE CHANGE OF THE EASTERN SEA AREA, CA MAU PROVINCE USING REMOTE SENSING AND GIS

Nguyen Huu Sang

Abstract

Ca Mau is a province in the south of Vietnam, in the Mekong Delta, and is an area with 3 sides facing the sea, so there is a strong process of erosion and accretion. This has a great impact on the ecology and life of the people around this area, especially the East coast. The study used remote sensing and GIS images to monitor shoreline changes in the east coast of Ca Mau from Ngoc Hien area to Dam Doi area. Landsat satellite images used in the study were recorded in the years 2000, 2005, 2010, 2015, 2020. The results show that the area tends to be mainly erosion, the erosion rate is about -31.3 m/ year and the erosion process will continue to take place in the future.

STATUS ANALYSIS AND USING SUPERVISED MACHINE LEARNING IN AIR QUALITY FORECAST

Nguyen Le Gia Bao

Abstract

The thesis analyzed and evaluated PM2.5 data and Air Quality Index (AQI) collected at the monitoring stations of the US Embassy in Hanoi and the US Consulate in Ho Chi Minh City. The results show that the air quality at Hanoi station is worse than at Ho Chi Minh City in the whole period 2016-2020. In addition, the AQI is predicted by two models of Machine Learning: Linear Regression (LR) and Random Forest (RF). The thesis uses root mean square error (RMSE) and coefficient of determination (R_2) to test the training process of Supervised Machine Learning methods. The results show that the Random Forest (RF) model gives very good AQI prediction results (RMSE < 0.5 and R^2 > 0.9776) and the Linear Regression (LR) model also has relatively good results (RMSE <17 and R^2 >0.85).

STUDYING THE CHLOROPHYLL CONCETRATION AT HYDROLOGICAL STATION IN CHO LACH (BEN TRE) BY USING THE MULTI-EXCITER

Pham Van Phung

Abstract

The seminar shows some characteristics of the changing in temperature and precipitation in Binh Dinh province based on 30-years data set (1978 - 2007) at the Quy Nhon station. The results show that temperatures had generally increased; the highest amplitudes usually occur from May to September and lowest amplitudes from November to December. Rainfall in the wet season accounted for the high proportion, at 70% of the total annual amount of precipitation. Furthermore, the observed rainfall anomaly during El Nino events show there are a rainfall shortage and the observed rainfall anomaly during La Nina events show that La Nina does not always contribute to the increase of rainfall, sometimes La Nina causes rainfall shortage.

VIETNAM NATIONAL UNVERSITY HO CHI MINH CITY
UNIVERSITY OF SCIENCE
FACULTY OF PHYSICS AND ENGINEERING PHYSICS
DEPARTMENT OF OCEANOLOGY, METEOROLOGY AND HYDROLOGY

ABSTRACTS OF GRADUATION THESIS AND GRADUATION SEMINAR (YEAR 2022)

Bachelor of Science in Oceanology

TABLE OF CONTENTS

ABSTRACTS OF GRADUATION THESIS

ABSTRACTS OF GRADUATION SEMINAR

ABSTRACTS OF GRADUATION THESIS

EFFECTS OF METHODOLOGICAL FACTORS ON THE YEARLSPRING RICE FACTORY OF QUANG NAM PROVINCE

Nguyen Thi Nga

Abstract

This study uses correlation coefficient to evaluate the influence of meteorological factors (rainfall, temperature, humidity and number of sunny hours) on rice yield of winter-spring crop in Quang Nam province in the period year 2017-2021. Calculation results show that rice yield is affected by factors including rainfall, temperature, humidity and hours of sunshine. In which humidity, number of hours of sunshine has a high influence of 89 and 80, respectively. In addition, rainfall and temperature affecting rice yield are 30 and 32, respectively. Therefore, the change of climatic factors The phenomenon especially in the context of future climate change needs to be studied further because this change has a great influence on rice yield.

APPLICATION OF SENTINEL-1 SATELLITE IMAGES COMBINED WITH ORYZA2000 AND ALU MODELS TO ESTIMATE GAS EMISSIONS FROM RICE STRAW BURNING IN AN GIANG PROVINCE

Duong My Hoa

Abstract

The main agricultural production in An Giang Province is rice cultivation, and it also generates a considerable amount of straw. Straw is treated mostly by burning, which generates a large amount of gas emissions. The thesis estimates the area of rice production and rice yield, then estimates the gas emissions due to the rice straw burning in the province in the period from 2017 to 2021. According to the results obtained from the satellite Sentinel- 1 images, the area of rice cultivation was greatest in the Winter - Spring crop and lowest in the Autumn-Winter crop. Rice yield is highest in the Winter - Spring crop and fall to its lowest in the Summer-Autumn crop, according to the ORYZA2000 model. Comparing the estimated results with the statistical data shows that the difference is range from 0,21% to 12,82% , the difference in the winter-spring crop is less than in the Summer - Autumn and Autumn - Winter crops. The gas emissions calculated by ALU software are highest in Winter- Spring crop and lowest in Autumn-Winter crop. The total emissions in 2019 are the highest (350.175,53 tons), with emissions of CH4, N2O, NOx and CO are respectively 32.000,98 tons, 233,58 tons, 7.608,16 tons, and 310.332,80 tons. Total emissions are the lowest (313.241,16 tons) in 2020, with emissions of CH4, N2O, NOx and CO are 28.625,72 tons, 208,95 tons, 6.805,70 tons, and 277.600,80 tons, respectively.

FIRST STEP LEARNING AGROMETSHELL SOFTWARE CALCULATE THE DEMAND FOR USE OF WATER FOR PLANTS

Nguyen Dang Tuong Vi

Abstract

This study uses Agrometshell software to calculate favorable coefficients of agroclimatic conditions suitable for the tree, through the coefficients of rainfall, demand water use, and watering needs of crops thereby determining the appropriate planting season. Due to the current unfavorable weather conditions by climate change, it is difficult to adjust irrigation for agriculture and rice crops are also greatly affected. The relationship between watering and the development of roots, leaves, stems, and productivity is a necessary issue and should be paid attention to to increase crop yield. Through the calculation of water demand for corn in South Africa, it was found that the effective rainfall is from 67.8% to 97.4% that can meet the needs of the crop. Therefore, Agrometshell software is useful for forecasting and calculating coefficients on water demand to be able to infer a favorable system for crops.

ANALYSIS OF THE FACTORS OF WAVES, CURRENT AND WATER LEVELS IN A DAY IN NHA TRANG BAY IN 2018

Dang Pham Bao Nghi

Abstract

This research uses data collected at the continuous station, using calculation tools such as excel to process and statistics the data, and uses Ghraper 11 to represent data into graphs and charts, that gives the assessment and analysis of wave, current and water levels in Nha Trang Bay in a day and night. The results after analysis show that at Nha Trang Bay, specifically a continuous station, the waves are quite low ranging from 5 cm to 10 cm, the water level fluctuates with a difference of about 2 m between high tide and low tide. The flow in the bay during the measurement period has a velocity ranging from 0.1 m/s to 0.2 m/s and the direction is mainly southwest at low tide in all three aquifers and the velocity ranges from 0.01 m/s to 0.1 m/s, different flow direction in three aquifers at high tide..

ASSESSMENT OF pCO2 ON SEA SURFACE BY CHL–A DATA OF SATATEST IMAGES IN THE EAST SEA

Tran Kiem Khanh Linh

Abstract

The East Sea is considered as one of the CO2 reservoirs of the world ocean, contributing to the release of CO2 into the atmosphere; hence, the study of CO2 distribution in seawater is extremely essential. In addition, pCO2 correlation with seawater temperature, salinity and satellite's Chl–a concentration. Through calculations, it is found that pCO2w is negatively correlated with temperature, while it is positively correlated with both salinity and chl-a concentration. From the correlation equation of pCO2w and Chl–a concentration obtained from satellite image (pCO2w = 20 x Chl–a + 353,5, R2 = 0,7, n= 69), it is possible to estimate pCO2 in the surface seawater. Estimated pCO2 for the average of 8 days and 1 month are 359,08 µatm and 369,09 µatm, respectively. In short, the obtained results are not significantly different from other studies.

EFFECTS OF METEO-HYDROLOGICAL FACTORS ON OFF-SEASON RICE YIELD IN THE AN GIANG PROVINCE

Le Mai Anh

Abstract

The purpose of the study is to evaluate the impact of meteorological - hydrological factors on rice yield and off-season rice yield in An Giang province. The ORYZA2000 model was used in this study to simulate rice yield and offseason rice yield under different scenarios. Rice yield is simulated in 4 periods 2008 - 2009, 2015 - 2016, 2018 - 2019, and 2019 - 2020 for all 3 rice crops in the year. Off-season rice yield is simulated with weather data averaged in 2015, 2016, 2018, 2019 and 2020. The results show that the simulated Autumn-Winter crop yield is relatively stable, with little influence by weather factors. The rice yield in simulation of the Winter-Spring and Summer-Autumn crops is heavily influenced by rainfall factors. The study also analyzes the impact of climate change on rice yield in An Giang province. With the emission scenarios RCP4.5 and RCP8.5 (2021), rice yield in An Giang province in the mid-century period (2046-2065) tends to decrease.

RESEARCH FOR HOT AND SUNNY CHARACTERISTICS OF THE SOUTHEAST AREA PERIOD 2000 - 2021

Do Ngoc Anh Thu

Abstract

The content of the thesis presents the characteristics of hot and sunny weather in the Southeast area based on the highest temperature data during the day from 7 monitoring stations in the region, period 2000 - 2021. The data is collected and checked before using in all the calculation. This thesis uses statistical calculation methods to determine the number of hot, intense hot, extremely hot days and their fluctuations of the research period. The analysis results show that: From 2000 - 2021, the Southeast region has a relatively high number of hot and sunny days (except for Vung Tau Station). The average number of hot days in many years range from 40 - 80 days, the average number of hot sunny days in many years occur from 5 to 10 days. The number of particularly intense hot days only occurs to the Southeast region but is not significant, the highest are 0.4 days for the average of many years. Hot, intensely hot and extremely hot period often occurs from January to June, especially in March and April. Same as the spatial distribution of heat, the intensity of sunny and hot days in the researching area is quite high. Bien Hoa station (Dong Nai) has the highest intensity of heat, the number of hot days appears more and tends to increase. From April 10, 2020 to April 29, 2020, It was recorded as the longest and most widespread heat wave of the period 2000 - 2021.

CHARACTERISTICS OF CO2 DISTRIBUTION IN WATER MASSES IN THE SOUTHERN OCEAN

Vo Thi Nghia

Abstract

With data approximately 68,700 available number after filtered out of a total of 81987. I separate it according to each water masses basing on measured seasurface temperature (SST) and salinity (SSS). From database, we can see that the distribution of CO_2 in watermasses is different, mainly it depends on the content of SST and SSS. However, it only shows in the northern STF, SAZ, PFZ, AZ (>3℃) waters, while SZ and SSB are not clearly seen. The correlation between dissolved CO_2 concentration with SST and SSS is closed, while for pCO_2 the dependence is relatively small. In the water mass in the SAZ, north of the STF, the oceans uptake CO_2, but it releases CO_2 in the SSB. I also calculated that the Southern Ocean accounts for 2.7% of total global CO_2 emissions (11.5 ± 0.9 Gt C yr^{-1} [8]) and absorbed 12% of the total global ocean in this study.

APPLICATIONS OF WRF MODELS WITH DATA ASSEMBLY FOR FORECAST RAIN IN THE CITY. HO CHI MINH CITY FOR 3 HOURS AND 24 HOURS

Van Dinh Qui

Abstract

The location of the study area is located in the sub-equatorial monsoon area, so it is hot and humid, combined with the weather patterns, so it rains a lot. With the WRF model being increasingly upgraded and perfected, it is widely applied. This thesis describes with the model that is run at the forecast period of 24h and 3h to forecast rain for the Ho Chi Minh City area during September, October and November. After obtaining the results, conduct a comparison. with the actual measured value to evaluate the predictive quality from the model. The results show that the rain forecast model is good in the study area. The error is relatively small, the model correctly identifies the rain area and the center of the rain. The model is relatively sensitive by days with heavy rainfall. For some other cases, the error of the model is relatively high, the difference is large.

ANALYSIS AND ASSESSMENT OF THE RELATIONSHIP BETWEEN CHLOROPHYLL WITH HYDRODYNAMIC FACTORS AT RACH GOC (CA MAU)

Le Ton Nu Cuc Phuong

Abstract

Chlorophyll (CHL) can be considered as a phytoplankton biomass monitoring measurement with many applications in life. The thesis aims to evaluate and analyze the relationship between CHL and hydrodynamic factors. The data in their study is based on the survey at Rach Goc, Ngoc Hien district, Ca Mau province done by Oceanology, Meteorology and Hydrology Department – HCMUS from 13/08/2015 to 21/08/2015. Main methods are used such as data analysis of waves, currents, tides; evaluating the relationship and statistics by SPSS 16.0 software; Using Grapher 11 software for graphs. The results show the change of CHL concentration and hydrodynamic factors depend on depth and the relationship between CHL and factors. There is a inverse correlation between the CHL and the rising tide in the middle layer of water. However, CHL at the low tide keeps stable. The northeast flow gets a larger amount of CHL to the study site than the southwest flow in both the surface layer and the middle layer. Medium waves (0.2 m - 0.4 m) with sufficient energy to facilitate the increase of CHL concentration compared with weak waves (<0.2 m) and strong waves (> 0.4 m). The deeper, the weaker wave. It gets no effect on the CHL concentration in the middle and bottom layers.

CHANGE TRENDS OF THE RAINFALL CHARACTERISTICS IN THE PLAIN OF REEDS IN THE CONTEXT OF CLIMATE VARIABILITY

Ho Thi Ngoc Tram

Abstract

Climate change has severely affected production activities and people's lives in Dong Thap Muoi area in recent years. The study analyzed the rainfall trends of rainfall in the Dong Thap Muoi area in the period 1984 – 2015 using the nonparametric statistical methods namely the Mann-Kendall test and Sen's slope estimator. The analysis results show that annual rainfall trends to increase at Cao Lanh and Cai Be stations, while a decrease trend in rainfall records in Moc Hoa station. For rainfall in the rainy season an increase trend dectect in Cao Lanh and Moc Hoa stations, and decrease trend also record in Cai Be station. Based on the findings, number of rainfall days in the rainy season in El-Nino years is lower than in other years during the studied period, while La-Nina years is the opposite. In general, the annual rainfall has no significant change while rainfall in the rainy season has a significant change, and this can affect the production activities across the study area.

ANALYSIS AND ASSESSMENT OF SALTWATER INTRUSION IN DOWNSTREAM OF TIEN AND HAU RIVERS

Nguyen Thi My Ngoc

Abstract

Saltwater intrusion is becoming increasingly complicated in downstream of Tien and Hau Rivers. Therefore, the study of saltwater intrusion plays an important role in socio-economic development in this area. The study uses in situ salinity in 2010, 2014, 2016, 2019, and 2020 at 23 stations along four branches such as Cua Dai and Cua Tieu, Ham Luong, Co Chien, Hau river to analyze and evaluate the saltwater intrusion process. The results showed that the salinity tended to decrease gradually from the estuary to the inland; and the salinity gradually increased from January, peaked in February, March, or April, and then gradually decreased. According to 4ppt salinity isolines, the deepest saltwater intrusion extended approximately 80 km inland at the Ham Luong branch and the others are similar with 56km inland. Over the years, salinity penetrated the deepest at the Co Chien branch in 2016 and the others in 2020.

CALCULATION OF WATER USE DEMAND FOR RICE CROPS IN VINH LONG PROVINCE

Nguyen Thi Phuong Nhung

Abstract

Application of AquaCrop model to calculate water use demand for winter-spring, summer-autumn and autumn-winter crop seasons of rice in Vinh Long province throught calculating reference evapotranspiration (ETo) and actual evapotranspiration (ETc). Simulation results show that the total of ETo of all rice crop seasons are approximately 1567.8 mm. The maximum ETo value in the summer-autumn crop season is 617.6 mm, the smallest ETo value in the winter-spring crop is 463.9 mm. The ETc has a maximum value at the late stage of the summer autumn crop season with 63 mm and a minimum value at the begin stage of the winter-spring crop season with 3.9 mm.

USING RAOB SOFTWARE AND NHA BE DOPPLER RADAR TO FORECAST THUNDERSTORM AND RAIN IN HO CHI MINH CITY

Nguyen Thi Kim Chi

Abstract

Thunderstorms and rain are weather phenomena that directly and indirectly affect life, economy, culture and society. In recent years, these weather phenomena are becoming more and more complicated and difficult to forecast. Therefore, the use of Nha Be weather radar images in combination with RAOB software products is essential to forecast and warn of thunderstorms and rain. In this thesis, the instability indexes calculated from RAOB software are applied in order to calculate the correlation between the indexes and find out the correlation between these quantities. In addition, there is a combination with Nha Be weather radar images and a number of traditional methods such as synop maps and satellite cloud images to improve the ability to give accurate forecasts, assist in prevention and make emergency plans to minimize damage caused by thunderstorms and heavy rain.

PROGRAMING THE EARLY WARNING MODEL OF RICE CROP INSECT PESTS BASED ON THE EFFECT OF WEATHER PARAMETERS

Huynh Thi Huyen Tran

Abstract

The warning model of rice crop insect pests is programmed based on the growing stages of rice, seven differrent spieces of pests and diseases and meteorological factors (temperature, humidity, etc.) by FORTRAN software. The results show that the insects such as *thrips, brown planthoppers, rice leafrolle, scirpophaga incertulas, steneotarsonemus spinki* are growing fast in almost all stages of rice; Only rice blast disease appea in stage of flowering in winter-spring and summerautumn crops. For autumn-winter crop, there is no exist of *Bacterial leaf blight*. When increasing the temperature under climate change scenarios, the growth of thrips, brown planthoppers, *rice leafrolle*, rice blast disease decrease; the leaf scorch trends to increase; and the *steneotarsonemus spinki* and *scirpophaga incertulas* still keep developing.

PRELIMINARY ASSESSMENT OF METHANE EMISSIONS IN LANG SEN WETLAND RESERVE, LONG AN PROVINCE

Tran Ngoc Anh Thu

Abstract

Rice fields are considered the main source of CH_4 emissions in the agricultural sector. The main factors affecting CH_4 emissions in rice fields are soil temperature, water regime and fertilizers. The study area is the rice field in Lang Sen Wetland Reserve, Long An province. Methodology is used monitoring data by Eddy Covariance technique – automatic measurement and data recording. By using EddyPro software to encrypt and extract data, then use MS Excel to calculate statistics and plot graphs. In the study chosen data during autumn-winter crop in 2020 to calculate CH_4 emissions in rice fields and evaluate the influence of factors such as water level, soil temperature on CH_4 flux. From the results, it is found that most of the soil temperature have same phase with CH_4 emissions, while the alternative wetting dry regime (AWD) affects CH_4 emissions. Specifically, when water is removed from the field, the CH_4 emissions are lower than that of the field is flooded. Besides, in the dried-fields period, CH_4 emissions are about 0.008364 $mg/m^2/h$, it is higher than the rest periods

ABSTRACTS OF GRADUATION SEMINAR

INITIAL WAVE-FIELD SIMULATING USING DELFT3D WITH NESTED GRID

Pham Tran Quang Huy

Abstract

Delft3D, a third-generation wave model, was used to simulate the wave field on the Wadden Sea covering an area of more than 15,000km^2. With such a large area, using only a single computational grid can be coarse, leading to inaccurate results. Therefore, this study applied nested grid method with 03 grids. This method is suitable for a complex bathymetry representing a shallow water zone and curly coastline. The first grid is limited to the study area, with an area of 15,280km^2; the second grid is limited around two islands, with an area of 1,232km^2; the third grid is limited between the two islnds, with an area of 121km^2. The results of outer grid will be the boundary conditions of the inner grid. Initial results show that this approach to applying wave model is reasonable, with a significant wave height of 1-2 meters. The wave vectors change their directions when they meet the islands and cancel each other in the area between the two islands.

STUDYING CHARACTERISTICS OF TYPHOON ACTIVITY OVER THE EAST SEA DURING PERIOD OF 1992 - 2021

Le Nguyen Kim Hoan

Abstract

The seminar collected the number of typhoons over the East Sea during the period 1992 - 2021, calculated the descriptive statistics and provided some conclusions about typhoons activity characteristics. The results showed that there were a total of 260 typhoons in the East Sea, with the average of 8.7 typhoons in this region per year, and the number of typhoons tends to increase. In addition, the number of typhoons is also affected by ENSO, El Nino tends to reduce the number of typhoons, in contrast, La Nina tends to increase the number of typhoons. The peak of the typhoon season is July through September. Besides, the results show a majority of the typhoon activity occurs in the North of Vietnam. They reach their greatest number while located over Zone I (Quang Ninh - Ninh Binh), and Zone VII (Southern Vietnam) has the lowest number.

ANALYSIS OF RAINFALL TRENDS IN TUY HOA CITY OF PHU YEN FROVINCE IN THE FERIOD 1977-2019

Pham Ngoc Thanh

Abstract

In recent years, Tuy Hoa city has frequently affected heavy rainfall that cause flooding. Flooding occurs in many places, greatly affects many aspects of life. Therefore, study on the changing trend of heavy rains in the period 1977-2019 was conducted in this area. Within the scope of this topic, analysis the change trend of rainfall factors such as annual rainall, rainfall in the rainy season, rainfall in November and December across the study area are conducted. Calculation results from Man Kendall test and Sen's slope estimate show that the rainfall trends at Phu Lam and Tuy Hoa stations recorded slightly an increasing tend and are not statistically significant.

CALCULATE METHANE SATURATION BASING ON APPARENT OXYGEN UTILIZATION IN THE SOUTHERN OCEAN

Le Thi Thu Uyen

Abstract

Ocean absorbs about 30% of anthropogenic CO_2 in the atmosphere but releases methane into the atmosphere. Recent decades, methane has been studied extensively from seas to oceans such as the Arctic and Antarctic Ocean. However, research polar methane has many difficulties in collecting data in the farther region from the continent and has also low temperature. Therefore, using available data for calculations is very useful to understand the oceanic roles in the Southern Ocean, where is currently less study. The topic focuses on calculating methane saturation (SR) basing on apparent oxygen utilisation (AOU) to be able to see the general distribution of methane in the surface seawater whole area in the Southern Hemisphere.

USING IDV SOFTWARE TO DETERMINE THE DISTRIBUTION OF SEA SURFACE TEMPERATURE

Nguyen Thi Luyen

Abstract

Upwelling is a specific physical phenomenon in seas and oceans with one of the characteristics is the change in sea surface temperature when upwelling occurs. The thesis uses IDV software to determine the distribution of sea surface temperature (SST) in the upwelling area in South Central Vietnam and the eastern sea of Vietnam (in the East Sea) from 2003 – 2020. The results show that the distribution of SST tends to be low in the North and gradually increases when going to the South, the temperature near the coast is often lower than far away from the shore. SST is usually low in January, gradually increasing and reaching the highest around July, August, September, then gradually decreasing from October until January of the following year. In the waters of the Gulf of Tonkin, cold water tongues appear from December with low SST of only 16 – 22^0C, moving to the southern waters of the Gulf of Tonkin and the Central Central Coast in January and February, March then gradually disappears until April. In the South Central Coast, upwelling usually occurs around June to August every year. Upwelling occurs mainly in the waters of Ninh Thuan – Binh Thuan, the center of the upwelling has a sea surface temperature of about 25 – 27^0C while the surface temperature around there is about 28 – 32^0C.

RISK ANALYSIS DUE TO ALTERATION IN RAINFALL TO THE GROWTH PHASES DURING SUMMER-AUTUMN RICE SEASON IN THE TAN CHAU DOWNTOWN, AN GIANG PROVINCE

Truong Thi Phuong Uyen

Abstract

This seminar did not research rice fields, but the results used previous studies as a basic for combining the analysis and assessment of the annual mean rainfall in the Tan Chau downtown, An Giang province, 1991-2015 period. The method was using Excel to make statistics and draw graphs of the rainfall of the day for the purpose of assessing rainfall variability in place and time. From this, it is possible to risk analysis due to alteration in rainfall to the growth phases during Summer-Autumn rice season in the Tan Chau downtown, An Giang province.

ANALYSIS OF THE EFFECTS OF CHANGES IN CUA DAI RIVER WATER LEVEL IMPACTS ON SALT INTRUSION IN BEN TRE

Mai Kim Ngan

Abstract

In terms of comprehending how the water level is driving a force of salinity in Ben Tre. This seminar aims to analyze and to figure out the relationship between the salinity and water level fluctuations based on the water level and salinity data measured in 2016. In the light of aforesaid factors, we can have a clear general view of the water level and tidal level fluctuations plays an important role in affecting the salinity.

THE STORM STATISTICS IN THE WEST PACIFIC AND MADE LANDFALL IN VIETNAM DURING THE PERIOD OF 1975-2020

Le Lam Thuy Tien

Abstract

This seminar aims to recounts the number of storms that has formed in the Western Pacific region and the frequency of storms that make landfall in Vietnam in the period 1975-2020. The data resources about storms is taken from the website: Weather Underground organization and Kitamoto lab. Statistical results show that, in the period 1975-2020, there are 594 storms formed in the Western Pacific region, of which 189 storms made landfall in Vietnam. On average, there are 13.2 storms/year forming in the Western Pacific Ocean. The number of storms that hit Vietnam is unevenly distributed by region: North 26%, North Central 37%, South Central 33%, South 3%. The storms that make landfall in Vietnam are concentrated in the months of July, August, September, October and November.

APPLICATION OF REMOTE SENSING AND GIS TO MONITOR COASTAL MANGROVE FOREST CHANGE IN CU LAO DUNG DISTRICT, SOC TRANG PROVINCE

Nguyen Van Nam

ABSTRACT

Mangrove forest plays a vital role not only in the socio-economic development of our country but also in the ecosystem and environment. Therefore, it is necessary to study mangrove forest change. The topic used remote sensing and GIS with Landsat satellite images in 1987, 1996, 2005, 2014, and 2021 to monitor the change of coastal mangroves in Cu Lao Dung district, Soc Trang province. The results showed that mangroves enlarged the size of the coastal area with an increasing rate from north to south, and the average rate in the period 1987-2021 was 27.4 m/year. The average rate in each period 1987 - 1996, 1996 - 2005, 2005 - 2014, 2014 - 2021 was 29.9, 43.3, 13.3 and 24.8 m/year, respectively. Mangrove forest area over 1987, 1996, 2005, 2014, and 2021 is 810 ha, 673 ha, 1108 ha, 1147 ha, and 1376 ha, respectively.

USING CROPWAT MODEL TO CALCULATE THE WATER REQUIREMENT FOR BROCCOLI IN DA LAT

Nguyen Vu Doan Thao

The seminar calculated the amount of water demand for the main broccoli crop in Da Lat city. The approach and calculation of the Food and Agriculture Organization of United Nations (FAO) are based on the CROPWAT model applying the Penman-Monteith method. The research results determine that temperature, rainfall and crop coefficient affect actual evaporation and irrigation water demand. The actual evaporation of the broccoli is 1735 m^3/ha and the maximum evaporation is in October in the middle of the season with 273 m^3/ha. The calculated total amount of irrigation water is lower than the National standard TCVN 8611: 2011 – Irrigation works, Irrigation techniques for food and food crops, with broccoli.

VIETNAM NATIONAL UNVERSITY HO CHI MINH CITY
UNIVERSITY OF SCIENCE
FACULTY OF PHYSICS AND ENGINEERING PHYSICS
DEPARTMENT OF OCEANOLOGY, METEOROLOGY AND HYDROLOGY

ABSTRACTS OF GRADUATION THESIS AND GRADUATION SEMINAR (YEAR 2023)

Bachelor of Science in Oceanology

TABLE OF CONTENT

ABSTRACTS OF GRADUATION THESIS

ABSTRACTS OF GRADUATION SEMINAR

ABSTRACTS OF GRADUATION THESIS

ANALYSIS AND ASSESSMENT OF THE RELATIONSHIP BETWEEN CHLOROPHYLL WITH HYDRODYNAMIC FACTORS IN THE EAST AND WEST OF CA MAU

Huynh Huu Phuoc

Abstracts

Nowadays, there are many studies on relationship between Chlorophyll (CHL) with biological as well as environmental progresses. However, there are study on the relationship of CHL with physical factors such as temperature, hydrodynamics. Therefore, the study aims to analyze and evaluate the relationship between CHL and hydrodynamic factors in 2 surveys in the East Seaof Ca Mau from August 13, 2015 to August 21, 2015 and in the West Sea of Ca Mau from August 14, 2014 to August 20, 2014 Some research methods are used such as synthesizing data of tide, current, wave, wind and insolation duration; evaluating the correlations and comparing the results by SPSS 16.0; programming by Fortran and using Grapher 11 for data illustrations. As a result, CHL concentration is high at lowest tide. The concentration of CHL at the high tide is higher than that at the ebb tide in the East Sea and vice versa for the West Sea. The concentration of CHL at the in-flow is higher than that at the out-flow in the East Sea and in the West Sea. In the East Sea, in the surface layer, the CHL concentration for very strong wave is higher than that for strong wave and mean wave. However, in the West Sea, it could not identify the relationship between CHL and wave. CHL concentration tends to increase as wind gets stronger. It is not obvious for the relationship between insolation radiation and CHL during the field measurents.

GO CONG COASTAL PROTECTION SOLUTION WITH HOLLOW STRUCTURAL WAVE REDUCTION LEVEE TECHNOLOGY

Phan Nguyen Gia Huy

From the beginning of the 21st century to the present, the coastal development of the Mekong Delta has changed from accretion to erosion. Not out of the above trend, Go Cong Dong district, Tien Giang province also has aseriously eroded coastline, especially in the northeast wind season. Therefore, many coastal protection solutions have been implemented, including the solution to protect the coast of Go Fair dike to reduce the wave of hollow structure, which is a new solution and is considered suitable for this area. To assess the suitability of this project, we conducted a study of the shoreline based on satellite imagery; evaluation with existing works such as: Geotube wave reduction soft dike, roof embankment, stone wall embankment; analysis of actual measurement results at the hollow structural wave reduction levee project. As a result, in terms of coastal developments, the erosion trend continues for areas without protection works, and for areas with protected works, landslides have been controlled. In terms of the built works, it is still not possible to both protect the coast and restore the mangroves that have been lost. Regarding the measurement results achieved at the levee project, the efficiency of reducing waves, currents and sedimentation capacity to restore mangroves are clearly seen. From the results obtained as above, we can conclude that the solution to protect the Go Fair coastal dike to reduce the wave of hollow structure is appropriate.

ANALYSIS OF THE EFFECTS OF SOIL SURFACE TEMPERATURE AND WATER LEVEL ON METHANE EMISSIONS IN THE RICE FIELD

Vo Quynh Huong

Abstract

Methane is a potent greenhouse gas generated under oxygen-deficient conditions. Climate change has caused increasingly severe consequences in recent years, negatively impacting humans and the natural environment. Globally, methane emissions from rice fields account for 50% of agricultural emissions, significantly contributing to atmospheric methane levels. This study conducted data analysis from the Center for Greenhouse Gases and Climate Change to provide practical analysis and assessment. The study aimed to evaluate the correlation between methane emissions and two factors: soil surface temperature and water level, during three crops from 01/07/2020 to 30/06/2021. The results revealed that methane emissions have a positive correlation with soil surface temperature during the 8-days period after seeding. The relationship between methane emissions and the water level was closely related, although the correlation between these two factors was not clearly determined.

DETERMINATION OF IRRIGATION WATER REQUIREMENT FOR RICE CROPS IN THE DONG THAP PROVINCE UNDER IMPACT OF CLIMATE CHANGE

Nguyen Thi My Huyen

Abstract

In recent years, climate change has caused many negative impacts on many aspects of socio-economic life, in which the agricultural sector is recorded to be the most severely affected. This study applies the AquaCrop model to determine the water requirement for rice crop in Dong Thap province under the impact of climate change. Calculation results show that the total reference evapotranspiration at Cao Lanh and Hong Ngu is 1897.6 mm and 1919.6 mm, respectively. The crop evapotranspiration increases sharply during the growing period of the rice plant. Effective rainfall at Cao Lanh station is highest in the Winter-Spring crop at 348.7 mm, at Hong Ngu station the highest value is in the Summer-Autumn crop with 367.7 mm and both stations are the lowest in the Autumn-Winter season. In general, there are no major differences in irrigation water requirements between crops and between study areas.

ANALYSIS AND ASSESSMENT OF THE CHANGES OF SALINITY AND PHYSICAL FACTORS IN TIEN RIVER, BEN TRE PROVINCE

Tran Thi Quynh Nhu

Abstract

Salinity is one of the important factors in assessing water quality and issuing warnings about the impacts of saltwater intrusion. The study aims to analyze and evaluate the variations in salinity and the physical factors, including temperature, turbidity, dissolved oxygen concentration, and pH along Ham Luong and Co Chien Rivers in Ben Tre province. The analysis of salinity variation in 2023 was carried out at three stations An Thuan, My Hoa , and Chợ Lach, along Ham Luong River in 2023. The results show that the strongest saltwater intrusion occurred in March, affecting An Thuan and My Hoa stations especially highest salinity in An Thuan is 27.3‰. However, Cho Lach station was not affected by saltwater intrusion 0.1‰. Additionally, the analysis of the salinity profile and physical factors such as turbidity, dissolved oxygen concentration, and temperature in Co Chien River was conducted using the Yoda Profiler from May 19, 2015, to May 21, 2015. The measurement results during the high tide and mid-range tide showed that the dissolved oxygen concentration and temperature decreased with depth, while turbidity and salinity increased with depth. Meanwhile, during low tide, all the physical factors are evenly distributed from the surface to the bottom layer. Water quality in Ham Luong River was measured with five physical factors: temperature, turbidity, dissolved oxygen concentration, pH and salinity by WQM instrument at Cho Lach station. The data indicates that the water quality in the area is suitable for agricultural and rice cultivation purposes.

IMPACTS OF CLIMATE CHANGE ON COFFEE PRODUCTS IN DAK LAK

Nguyen Le Nhat Dan

Abstract

Climate change is a sensitive issue and strongly affects agricultural production in Vietnam, with the location near the equator, the East bordering the East Sea, and the Southwest bordering the Gulf of Thailand, Vietnam's agriculture is often affected by wind and storm activity, including the Dak Lak region (Central Highlands), where affected indirectly such as heat waves, heavy rains, floods, and droughts, with the characteristic terrain of many hills and mountains prone to landslides and flash floods. Climate change affects Dak Lak not only in terms of nature and climate but also affects the stability of the harvest, the harvest of some agricultural products such as coffee, and the time of coffee cultivation is changed, affecting the products of coffee.

MODELLING THE WAVE FIELD AT CU LAO DUNG (SOC TRANG) USING DELFT3D

Tran Mai Khang Thinh

Abstract

The studied area consists of the influxes of Dinh An and Tran De rivers and the coastal zone of Cu Lao Dung, data is taken from two measurement sessions conducted by the Department of Oceanography, Meteorology and Hydrology within the framework of the Vietnamese-United States of America cooperation project. Output from the simulation indicates the mean significant wave height during the northeast monsoon is higher than that of the southwest monsoon at the alluvial ground and the influxes of Tran De and Dinh An rivers. During southwest monsoon, mean significant wave height value is higher at Dinh An influx and wave effect range is longer compare to those at Tran De influx. During northeast monsoon, mean significant wave height value is lower at Dinh An influx but wave effect range is longer compare to those at Tran De influx.

ASSESSMENT OF THE TRENDS IN RAINFALL CHARACTERISTICS IN THE LONG XUYEN QUADRANGLE UNDER THE IMPACTS OF CLIMATE CHANGE

Nguyen Nu Kim Ngan

Abstract

The Long Xuyen Quadrangle is known as one of two large deltas in the Mekong Delta that is facing drought, saline intrusion, and sea level rise, as part of the impacts of climate change. The aim of the study is, therefore, to analyze the changing trends of rainfall characteristics to contribute to clarifying the judgments about the impact of climate change across the study area. The study used non-parametric statistical methods to analyze the changing trend of rainfall characteristics across the study area during the period 1978-2021. The results show that a slight increase/decrease trend of rainy season rainfall and a slight to a significant increase in annual rainfall occurred in Chau Doc and Rach Gia stations. The number of rainy rainfall days recorded in the range of 140-170 days and a slight increase/decrease in the number of rainy rainfall days occurred at Rach Gia and Chau Doc stations.

ANALYSIS THE ACTIVITY OF SOME TYPICAL COLD SURGES IMPACT ON THE SOUTHEAST AREA WEATHER PERIOD 2020-20212

Phan Thi Tuyet Minh

Abstract

By using analysis the synoptic charts, collecting monitor data on barometric, minimum temperature, wind at surface meteorological stations to analysis the activity of four typical cold surges impact on the Southeast area weather period 2020-2022. The goal was to find out how the weather in this area would be affected by cold surges activity. The results show that, of the four selected cold surges, there was a duration from December to February, the Southeast is mainly affected by the edge of a cold continental high pressure. Some of the main influences on the weather in this area include causing pressure increase, temperature decrease, changing wind direction and velocity. The cold surge with high pressure as well as the deepest temperature at Ta Lai Station was 14.4^0C.

APPLICATION OF REMOTE SENSING AND GIS TO MONITOR THE URBANIZATION PROCESS IN BINH DUONG PROVINCE

Pham Bao Oanh

Abstract

Binh Duong province is undergoing a rapid process of industrialization and urbanization since 1997 which has contributed to an increase in impervious surface area. This study has applied remote sensing and GIS to monitor the urbanization process in Binh Duong province in the period 1995 - 2023 through impervious surfaces. In addition, the study also analyzed the correlation between urbanization with surface temperature and normalized difference vegetation index. The results showed that urban developed strongly and gradually expanded to the North, Northeast and Northwest in Binh Duong province. The impervious surface area increased by 9.9% (26442.6 hectares) in the period 1995 - 2023. In addition, the study also found a positive correlation between urbanization and surface temperature and negative correlation between urbanization and normalized difference vegetation index.

ANALYSIS OF COASTAL WAVE REGIMES IN THE MEKONG DELTA USING WAVEWATCH III MODEL DATA

Tran Thi Ngoc Anh

Abstract

The hydrodynamic regime in the coastal waters of the Mekong Delta is strongly influenced by the tropical monsoon climate regime with two seasons of northeast and southwest winds. Studies on coastal wave regimes in the Mekong Delta are a valuable source of data for many different fields, opening up more in-depth research directions related to diverse industries. However, the source of measured data for ocean wave studies is quite limited for many reasons, so considering the source of data from automatic models is considered as an alternative to solve the problem of data for wave studies. This thesis uses data on wave direction and significant wave height at measured stations and data sources from WWIII model to evaluate and analyze wave regimes in coastal waters in the Mekong Delta. Looking at the correlation between WWIII model wave data and measured real wave data will help determine how reliable the data from the model can be for long-term wave analysis. Along with that, the study opens up a panoramic view through WWIII model of coastal wave regimes in the Mekong Delta region, comparing the difference of wave regimes between the two eastern and western coastal waters and at the same time with the seasonal variation in waves across the region.

APPLICATION OF REMOTE SENSING AND GIS TO BUILD DROUGHT MAPS IN BEN TRE PROVINCE

Phan Truc Lam

Abstract

Drought harms the habitats of plants and animals, reduces crop yields, as well as increases the risk of forest fires, soil erosion, etc. Remote sensing technology is a tool that is effectively applied in the research and monitoring of drought phenomena with advantages compared to traditional research methods. The thesis uses Landsat satellite images to calculate drought indices for the evaluation and building of drought maps for the area of Ben Tre province. The calculated drought indices include TCI, VCI, SAVI, WSVI and TVDI. The results show that the coastal area including Thanh Phu, Ba Tri and Binh Dai districts is the place with a high risk of drought in the dry season.

ABSTRACTS OF GRADUATION SEMINAR

ANALYSIS AND ASSESSMENT OF THE CHANGE OF PLANT COVER OF QUANG NINH PROVINCE BY SPECIFICATION AND GIS

Dang Minh Anh

Abstract

The use of remote sensing images to assess the change of forest vegetation cover with high accuracy and objectivity in determining the area of change, the degree of variation and somewhat the tendency of each forest object. The topic applies the method of supervised classification in combination with GIS to build a map of forest status in the period 1988 - 2022. In the period 1988 - 2000 the forest in the Southwest region lost more than the southern part. The Northeast lost about -3783791.25 hectares, the period 2000-2010 lost about -38664.9 hectares of forest, due to the large concentration of people living in this place, leading to over-exploitation of forests, imbalance of forest ecosystems, and In addition, the forest fire led to the loss of natural forests, seriously affecting the ecological balance, but then the forest was restored well thanks to the greening of bare land, contributing to the formation of forest patches. alternately in the period 2010 - 2022.

A FIRST STEP FOR IDENTIFYING MICROPLASTICS IN SURFACE SEDIMENT AT CAN GIO BEACH

Pham Van Thuyen

Abstract

The study initially identified microplastics in surface sediment at Can Gio beach. The flotation method is used to separate the microplastics from the surface sediment, then use a microscope to observe and identify the microplastics. Surface sediment samples were taken in the direction perpendicular to the shoreline (from sample CG-1 to sample CG-5) and along the shoreline (from sample CG-6 to sample CG-9). In the direction perpendicular to the shoreline, the average density of microplastics reached 6.28 ± 0.16 (microplastics/gram of sediment). The highest levels of microplastics are found in sample CG-5 (900 microplastics), and the density of microplastics reached 17.97 microplastics/gram of sediment. Microplastics components include: fragments, fibers, foams and films, in which, fragments accounted for the highest rate of 74.46%. Along the shoreline, average density reached 21.60 microplastics/gram of sediment; and microplastic density is concentrated in medium sand, coarse sand and very coarse sand.

REMOTE SENSING IMAGE ANALYSIS COMBINED WITH STORM DATA TO ASSESS EROSION AND ACCRETION IN CUA DAI AREA, QUANG NAM PROVINCE

Bui Ngoc Thang

Abstract

Coastal erosion is a common phenomenon almost throughout the country, especially in the current complex climate change situation. Quang Nam is a place where coastal erosion and accretion are more complicated. The use of remote sensing and GIS technology helps to monitor shorelines during the research period from 2019 to 2021 quickly and accurately. The study showed that the shoreline of Cua Dai area has erosion and accretion, but the erosion process on 2 banks is dominant. The results also show the speed of landslides or accretion at fluctuating shoreline locations, providing information about the landslide situation for management agencies to take timely remedies and stabilize people's lives in the region.

FIRST STEPS USING DELFT3D MODELS IN FLOW SIMULATION

Tran Thien Duong

Abstract

This report explores the Delft3D model to initially simulate the flow in the seacoast of Siu Lam (Hong Kong). The simulation time is from 12:00 on July 19, 1996 to 12:00 on July 20, 1996. The simulation results show the influence of tides on the flow in many different time points in Siu Lam Bay. The tides of the East Sea get in the calculation area from the east. During the calculation time, the highest flow velocity reached 1m/s at the ebb tide, the lowest flow velocity was about 0.05m/s at the low tide.